



Malpede, Sabrina Maria (2001) *Three-dimensional single-sail static aeroelastic analysis & design method to determine sailing loads, shapes & conditions with applications for a FINN Class sail.*

PhD thesis

<http://theses.gla.ac.uk/3744/>

Copyright and moral rights for this thesis are retained by the author

A copy can be downloaded for personal non-commercial research or study, without prior permission or charge

This thesis cannot be reproduced or quoted extensively from without first obtaining permission in writing from the Author

The content must not be changed in any way or sold commercially in any format or medium without the formal permission of the Author

When referring to this work, full bibliographic details including the author, title, awarding institution and date of the thesis must be given

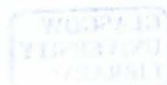
**Three-dimensional single-sail static aeroelastic analysis & design
method to determine sailing loads, shapes & conditions
with applications for a FINN Class sail**

Sabrina Maria Malpede

Thesis submitted to the Faculty of Engineering, University of Glasgow,
for the degree of Doctor of Philosophy. All aspects of the work presented
herein are original in concept except where indicated.

The research was conducted between October 1997 and February 2001 at
the Department of Aerospace Engineering, University of Glasgow.

© Sabrina Maria Malpede, 2001



Abstract

The development of modern sailing boats has been based almost entirely on the cooperative efforts of enthusiastic skippers, designers and sail-makers, with very little contribution from scientists and technologists and using just basic scientific principles. In recent times, urgent and strong requests for improved performance, mostly for racing yachts, have guided the interest and the attention of the scientific community in the optimisation of sail performance and design approach.

Sailing performance depends on the sailboat velocity, aerodynamic and hydrodynamic characteristics. This thesis focuses on the importance of the quantitative evaluation of the sail loads and how this contributes to the improvement of the performance of a sailboat through the development of a system for aiding sail design and assisting mast design.

The objective of this study is to provide an integrated design system, which supplies analysis method and design features via a user-friendly graphical interface of a single-sail configuration. The major achievement is the development of an integrating numerical method, which evaluates loads and their distribution and the consequent deformed sail-shape. It improves sail performance analyses and design of new sails.

Summarising, the major achievements are:

- efficacy of accurate performance analysis for each sail, for any given shape over all the possible sailing courses;
- critical investigation of the sail behaviour in the above-mentioned cases;
- improved approach to an integrated sail design;
- improvements in mast design from the structural and aerodynamic point of view;
- limited design costs, in terms of time consumed and computational power employed;
- efficacy of the visualisation of novel designed sail and predicted performance, which reduces the number of possible design flaws.

In conclusion, the integrated sail analysis and design system presented has important margins of improvements and diversification: extensions to non-homogeneous and anisotropic sailcloth, to two-sail configuration, windsurfs and integration of the mast.

Acknowledgements

A brief note to thank my supervisor, Dr. Marco Vezza, for his helpful advice in the completion of this thesis and his support since my initial supervisor, Dr. John Anderson, left.

I would like to thank Dr. J. Anderson who has suggested the area of this research and has helped me in the initial stages.

My gratitude is also extended to Professor Leonardo Lecce, who has encouraged and supported my research experience at University of Glasgow and Professor Ray Withford for his wise suggestions and ideas.

I would like to extend my heartfelt thanks to everyone has supported me along the way. It is impossible to list all, who I have met at the University of Glasgow, at conferences and in and around Glasgow: their smiling encouragement have led the completion of this work and mostly have strongly convinced about how important has been for me this research experience.

However, I would like to thank and to express my esteem to my special friends: Antonella, Miguel, Marcos and Alessandro. I wish you realise how much I have enjoyed your friendship and mostly our serious discussions and funny jokes, we shared and we will continue to do in the future, which I do believe are absolutely smart.

I would like to dedicate this thesis to my family who has believed in me and has been a constant source of encouragement to me throughout the years.

To my brother Giancarlo and my parents, Cristina and Gennaro Malpede

Contents

Abstract	ii
Acknowledgements	iii
Contents	iv
List of Figures and Tables	ix
Nomenclature	xv

Chapter 1: Introduction to the Sail Analysis & Design

1.1	Introduction.....	1
1.2	Conditions and Factors Driving Developments in Sail-Design	4
1.3	Fundamental Factors Governing Sailing Performance.....	7
1.3.1	Sailboat Description.....	7
1.3.1.1	The FINN Class Sailboat.....	9
1.3.2	Sailing and Trimming.....	11
1.4	Sail load calculation problem.....	15
1.4.1	Sail Performance Improvements.....	16
1.4.2	Aiding Sail Design.....	17
1.4.3	Assisting Mast Design.....	18
1.5	Research Statement.....	19
1.6	Thesis Structure.....	21

Chapter 2: State of the art of sail design

2.1	Introduction.....	23
2.2	Critical overview on sail analysis methods.....	24
2.2.1	Empirical data.....	26
2.2.2	Wind tunnel test sail loads evaluation.....	30
2.2.3	Semi-empirical methods.....	32
2.2.4	Numerical methods.....	33
2.3	Concluding remarks.....	37

Chapter 3: Analysis Method

3.1	Introduction.....	39
3.2	Geometry and physics of sailing.....	40
3.3	Aeroelastic sail behaviour.....	47
3.4	Iterative analysis process.....	48
3.5	Analysis method assumptions.....	50

Chapter 4: Initial Phase

4.1	Data acquisition.....	52
4.2	Input data G.U.I.: description and use.....	55
4.3	Development of the geometric sail surface.....	58
4.4	Geometric Phase Graphical User Interface.....	60
4.4.1	Sail section definition.....	62
4.4.2	Luff, draft and leech.....	64

4.4.3	Panel Model and Finite Element Model.....	66
4.5	Conclusions.....	69

Chapter 5: Aerodynamic Analysis

5.1	Introduction.....	70
5.2	Modified Vortex Lattice Method.....	71
5.3	The G.U.I. for the Aerodynamic Analysis Phase.....	79
5.3.1	The Wake shape.....	82
5.3.2	Flow Loads.....	83
5.4	Example of a wake evolution behind the sail.....	85
5.5	Modified Vortex Lattice Method Validation.....	92
5.5.1	Outline.....	92
5.5.2	Case flat rectangular plate with AR=4.....	93
5.5.3	Sea influence evaluated by M.V.L.M.....	96
5.5.4	Aspect ratio influence evaluated by M.V.L.M.....	97
5.1	Conclusions.....	99

Chapter 6: Structural Analysis

6.1	Observation about the sail structural behaviour.....	100
6.1.1	Materials.....	101
6.1.2	Construction methods.....	103
6.2	The structural analysis.....	105
6.2.1	The finite element model.....	107

6.2.2	The implemented finite element method.....	110
6.2.3	Loads.....	111
6.2.4	Initial and boundary conditions.....	112
6.3	The G.U.I. for the Structural Analysis phase.....	115
6.4	Conclusions.....	119

Chapter 7: Aeroelastic Analysis

7.1	Analysis Description.....	121
7.2	The Aeroelastic Analysis Graphical User Interface.....	124
7.3	Aeroelastic Analysis Validation.....	125
7.3.1	Plan, reasons and background.....	125
7.3.2	Description of the validation test.....	126

Chapter 8: Aeroelastic Analysis Results

8.1	Reasoning and planning results.....	130
8.2	Prior consideration.....	131
8.3	Results for a known sail-shape in various external conditions and trim sets..	132
8.3.1	Known sail shape in unknown sailing conditions.....	133
8.4	Results for several sail shapes in given external conditions and trim set..	142
8.4.1	Results on the flatter sail shape.....	142
8.4.2	Results on the flatter and twisted sail shape.....	147
8.5	Conclusions.....	151

Chapter 9: Design Results

9.1	Introduction.....	153
9.2	Sail Design example.....	154
9.2.1	Design process for a FINN class sail.....	154
9.2.2	Sail design from a flat surface.....	166
9.3	Mast Design example.....	172
9.3.1	Literature review.....	174
9.3.2	The application at mast design.....	175
9.3.3	Results and conclusions.....	179
9.4	Conclusions.....	183

Chapter 10: Conclusion.....185

Appendix A: Aeroelastic Sail Behaviour.....190

Appendix B: Aerodynamic Analysis.....192

Appendix C: Structural Analysis.....197

Appendix D: A Scottish sailmaker outlook.....207

Glossary.....209

References.....213

List of Figures and Tables

Chapter 1: Introduction to the sail loads evaluation problem

Figure 1.1: Typical sailboats	8
Figure 1.2: A Finn Class boat	9
Figure 1.3: Structural diagram of the FINN Class sailboat	10
Figure 1.4: Leeward side and windward side for a FINN class sailboat (top view).....	11
Figure 1.5: Brief description of the factors involved in the performance (top view).....	12
Figure 1.6: Generation of the hydrodynamic force on the hull.....	12
Figure 1.7: Possible sailing courses.....	14

Chapter 2: State of the art of sail design

Table 2.1: Gimcrack coefficients.....	27
Table 2.2: Bay-Bea coefficients.....	28

Chapter 3: Analysis Method

Figure 3.1: Global Cartesian coordinate system for the FINN.....	42
Figure 3.2: (a) Sailing angles description and (b) Velocity triangle.....	43
Figure 3.3: Forces acting on a FINN sailboat in an equilibrated configuration.....	45
Figure 3.4: Interaction between the aerodynamic and the hydrodynamic forces.....	46
Figure 3.5: Aeroelastic behaviour of a sail-plan.....	48

Figure 3.6: Aeroelastic analysis procedure.....	49
---	----

Chapter 4: Initial Phase

Figure 4.1: Typical picture taken by a masthead camera. Notable is the drawn.....	53
pattern to evaluate the geometrical characteristics.	
Figure 4.2: ‘Input Data’ Graphical User Interface.....	56
Figure 4.3: The edited ‘Input Data’ G.U.I with the data from tables 4.1 and 4.2.....	57
Figure 4.4: Local coordinate systems (x, y, z) and (X, Y, Z).....	59
Figure 4.5: ‘Menu’ G.U.I. for the geometric surface development.....	61
Figure 4.6: ‘u-Edit’ Graphical User Interface.....	62
Figure 4.7: ‘v-Edit’ Graphical User Interface.....	65
Figure 4.8: Sail surface geometry ready to be meshed.....	67
Figure 4.9: ‘3D Mesh’ G.U.I. mesh model to use in the aeroelastic analysis.....	68
Table 4.1: Chart resulting from the photograph analysis for the rig.....	54
of WB-Sails FINN	
Table 4.2: Chart resulting from the photograph analysis for the rig.....	54
of WB-Sails FINN	

Chapter 5: Aerodynamic Analysis

Figure 5.1: Flow chart description of the solution method for the aerodynamic phase.....	77
Figure 5.2: Aerodynamic Analysis Phase Graphical User Interface	80
Figure 5.3: ‘Wake’ GUI, after the first step of the aerodynamic analysis iteration.....	82
Figure 5.4: Window for Flow Load.....	83
Figure 5.5: Evolution of the wake after the third step of the analysis.....	86

Figure 5.6: Evolution of the wake after the fifth step of the analysis.....	86
Figure 5.7: External loads after the third iteration step.....	89
Figure 5.8: External loads after the fifth iteration step.....	89
Figure 5.9: Anomalous external loads distribution.....	90
Figure 5.10: Used flat plate panel model and geometric description.....	93
Figure 5.11: Circulation distribution along the span.....	94
Figure 5.12: Comparison of the total lift and induced drag coefficients..... evaluated by the M.V.L.M., for the case of AR = 4	95
Figure 5.13: Sea influence on a rectangular membrane sail (AR=4).....	96
Figure 5.14: Aspect ratio influence on the force coefficient evaluation.....	97
Figure 5.15: Force coefficients distribution for AR=4 ($\alpha=10^\circ$).....	98
Figure 5.16: Force coefficients distribution for AR=5 ($\alpha=10^\circ$).....	99

Chapter 6: Structural Analysis

Figure 6.1: Stress-Strain diagram for some of the mentioned sailcloth fabric.....	103
Figure 6.2: (a) crosscut panel layout, (b) radial panel layout.....	104
Figure 6.3: 3DL-sailmaking technology	105
Figure 6.4: Triangular finite elements in a quadrangular aerodynamic model panel.....	108
Figure 6.5: The Structural Analysis phase G.U.I.....	116

Chapter 7: Aeroelastic Analysis

Figure 3.6: Aeroelastic analysis procedure.....	122
Figure 7.1: The Aeroelastic Analysis phase G.U.I.....	124

Figure 7.2: (a) 32-panels model for Run VIII.....	128
(b) related results after 2 full iterations.	
Figure 7.3: (a) 64-panels model for Run VIII.....	129
(b) related results after 2 full iterations.	
Table 7.1: Rig measurements for test.....	127
Table 7.2: Sections geometric characteristics.....	127

Chapter 8 Aeroelastic analysis results

Figure 8.1: Aerodynamic panels model, wind and wake conditions.....	133
Figure 8.2: Finite element model and material structure properties.....	134
Figure 8.3: Total loads coefficients versus apparent attack angle β	134
Figure 8.4: Results for $\beta=22.8^\circ$	135
Figure 8.5: Results for $\beta=25.3^\circ$	135
Figure 8.6: Results for $\beta=27.8^\circ$	136
Figure 8.7: Results for $\beta=30.3^\circ$	136
Figure 8.8: Results for $\beta =10.3^\circ$	137
Figure 8.9: Results for $\beta =12.8^\circ$	137
Figure 8.10: Results for $\beta =15.3^\circ$	138
Figure 8.11: Results for $\beta=17.8^\circ$	138
Figure 8.12: Results for $\beta =20.3^\circ$	138
Figure 8.13: (a) Results after the first aerodynamic analysis.....	141
(b) Deformed shape after the first structural analysis for $\beta =32.8^\circ$	
Figure 8.14: Comparison of the total force coefficients.....	143
evaluated for two sail shapes	

Figure 8.15: Results for $\beta = 22.8^\circ$	144
Figure 8.16: Results for $\beta = 25.3^\circ$	144
Figure 8.17: Results for $\beta = 27.8^\circ$	145
Figure 8.18: Deformed sail shape at $\beta = 25.3^\circ$	146
Figure 8.19: Results for $\beta = 30.3^\circ$	146
Figure 8.20: Comparison of the total force coefficients..... evaluated for three sail shapes	148
Figure 8.21: Results for $\beta = 25.3^\circ$	149
Figure 8.22: Results for $\beta = 30.3^\circ$	150
Figure 8.23: Results for $\beta = 37.8^\circ$	150

Chapter 9: Design Results

Figure 9.1: (a) Lift and induced drag coefficients, (b) drive and heel coefficients..... on the cylindrical surface in the range of attack angle $\alpha = [0^\circ \text{ to } 40^\circ]$	156
Figure 9.2: (a) Lift and induced drag coefficients, (b) drive and heel coefficients..... on the cylindrical surface with linear twist distribution $\delta=0^\circ$ to $\delta=8^\circ$	158
Figure 9.3: (a) Lift and induced drag coefficients, (b) drive and heel coefficients..... on the cylindrical surface with linear twist distribution $\delta=0^\circ$ to $\delta=20^\circ$	158
Figure 9.4: (a) Lift and induced drag coefficients, (b) drive and heel coefficients..... on the tapered surface ($ct/cf=0.6$) with linear twist distribution $\delta=[0^\circ \text{ to } 20^\circ]$	162
Figure 9.5: (a) Lift and induced drag coefficients, (b) drive and heel coefficients..... on the tapered surface ($ct/cf=0.4$) with linear twist distribution $\delta=[0^\circ \text{ to } 20^\circ]$	163
Figure 9.6: (a) Lift and induced drag coefficients, (b) drive and heel coefficients..... on the tapered surface ($ct/cf=0.6$) with linear twist distribution $\delta=[0^\circ \text{ to } 8^\circ]$	163
Figure 9.7: (a) Lift and induced drag coefficients, (b) drive and heel coefficients..... on the tapered surface ($ct/cf=0.4$) with linear twist distribution $\delta=[0^\circ \text{ to } 8^\circ]$ and maximum camber at 45% of the chord	165

Figure 9.8: Final results for the flat sail at $\alpha=15^\circ$	168
Figure 9.9: Final results for the flat sail at $\alpha=20^\circ$	168
Figure 9.10: Final results for the flat sail with thickness=0.008m at $\alpha=35^\circ$	171
Figure 9.11: Particulars of the deformed shape assumed during..... the iterative process by the flat sail with thickness=0.008m at $\alpha=35^\circ$	171
Figure 9.12: Analysis procedure.....	176
Figure 9.13: Aeroelastic Analysis of the SAIL-MAST system.....	177
Figure 9.14: Aerodynamic Analysis of the sail shape with the viscous effects.....	178
Figure 9.15: The ‘Input Data’ G.U.I. for the analysed sail-mast system.....	179
Figure 9.16: Elaborated geometry for the FINN class sail-mast system.....	180
Figure 9.17: Sail panel model and external conditions for the aerodynamic analysis.....	180
Figure 9.18: Sail finite element model and structural properties.....	181
Figure 9.19: Results for the sail model with 320 panels.....	181
Figure 9.20: Results for the sail model with 64 panels.....	182
Table 9.1: Initial geometric characteristics of the cylindrical surface.....	155
Table 9.2: Possible sail-shape and respective sailing courses.....	166
Table 9.3:Trapezoidal sail section dimensions.....	167

Appendix A: Aeroelastic Sail Behaviour

Figure A.1: Collar Triangle.....	191
----------------------------------	-----

Nomenclature

\vec{A}_t	assembled induced velocity coefficient matrix
$\vec{A}_{ij} = (A_x, A_y, A_z)_{ij}$	induced velocity coefficient
\vec{A}_{wake}	induced coefficient matrix for the wake
\vec{A}_{sail}	induced coefficient matrix for the sail
AR	sail aspect ratio
Area _j	area j th panel
AREA _{sail}	sail surface area
α	true flow attack angle
$\alpha_{1,2,3}$	functions of the nodal co-ordinates;
β	apparent flow attack angle
CL	total lift coefficient
CL _c	lift coefficient along a sail section chord
CL _s	lift coefficient along a panel strip
CDi	total induce drag coefficient
CDi _c	induced drag coefficient along a sail section chord
CDi _s	induced drag coefficient along a panel strip
CDrive	total drive coefficient
CDrivec	drive force coefficient along a sail section chord
CHeel	total side force or heel coefficient
CHeel _c	side force or heel coefficient along a sail section chord
C _P	pressure coefficient
dV	volume differential
D	elastic material matrix
δ_m	boom sheeting angle
$\delta\varepsilon$	strain virtual increment vector

$\delta\mathbf{u}$	displacement virtual increment vector
$\Delta\mathbf{s}$	wake displacement
Δt	time step
$\Delta\tau$	non-dimensional time step
$\Delta\vec{v}$	local jump in the tangential component of the velocity
E	Young's modulus
$\boldsymbol{\varepsilon}$	strain vector
ε_x	strain component in the x-direction
ε_z	strain component in the z-direction
$\mathbf{F}_{Aerodynamic}$	aerodynamic forces
$\mathbf{F}_{Hydrodynamic}$	hydrodynamic force
\mathbf{F}_{Weight}	weight-forces
\mathbf{F}_{Drive}	driving force or thrust
F_{V-Aero}	aerodynamic vertical force
F_{Heel}	side force or heeling force
F_j	pressure force on j^{th} panel
$F_{V-Hydro}$	hydrodynamic vertical force
F_s	hydrodynamic side force
f.e.	finite element
γ_i	segment vortex strength
γ_{xz}	strain component in the xz-direction
Γ	vorticity
Γ_0	circulation in the middle of the plate
Γ_i	circulation on the i^{th} panel
Γ_j	intensity of a generic j^{th} vortex loop
Γ_{ic}	circulation acting on each panel strip in chord-wise direction
Γ_{wake}	wake vorticity
Γ_{sail}	sail vorticity
i	generic node of a finite element
i^{th}	generic panel

j	generic node of a finite element
j^{th}	generic panel
k	generic node of a finite element
l	generic node of a finite element
l_i	segment length
luff	length of the luff curve
λ	leeway angle
θ	heel angle
$M_{\text{Aerodynamic}}$	over-turning moment due to the aerodynamic forces
$M_{\text{Hydrodynamic}}$	over-turning moment due to the hydrodynamic force
M_{Weight}	over-turning moment due to the weight-forces
M_P	pitching moment due to the aerodynamic and hydrodynamic forces
M_{P-w}	pitching moment due to the helmsman and hull weight – including mast and sails
M_R	rolling moment due to the aerodynamic and hydrodynamic forces
M_{R-w}	rolling moment due to the helmsman and hull weight– including mast and sails
M_{Y-A}	yawing moment due to total aerodynamic force
M_{Y-H}	yawing moment due to the total hydrodynamic force
\vec{n}	sail surface's normal vector
n_p	total number of panels
n_{pu}	number of panels in chordwise direction
n_{pv}	number of panels in span-wise direction
n_w	number of control points on each wake's streamline
ν	Poisson modulus
p	pressure
P_∞	asymptotic flow pressure
Q_∞	asymptotic dynamic pressure
r^{th}	generic triangular finite element
R	water resistance
ρ_∞	asymptotic air density

s^{th}	generic triangular finite element
σ	stress vector in the local co-ordinate system
σ_0	stress vector correspondent to the initial sail configuration
σ_x	stress component along the x-direction
σ_z	stress component along the x-direction
τ_{xz}	stress component along the xz-direction
$u, v, z,$	translations of an internal point in the local coordinate system
(u_j, v_j, z_j)	displacement vector of the j^{th} node in the local coordinate system
$u_{i,j,l}, v_{i,j,l}, z_{i,j,l}$	translations of the $i^{\text{th}}, j^{\text{th}}$ and l^{th} nodes in the local coordinate system
V	flow velocity at a control point
\vec{V}	total flow velocity
v_i	total induced velocity by the vorticity
V_∞	asymptotic flow velocity
$V_\infty \vec{e}_\infty$	asymptotic velocity vector
V_{Apparent}	apparent flow velocity
V_{Sailing}	sailing speed
V_{True}	true wind speed
\vec{V}_∞	asymptotic flow velocity
$\vec{V}_{\text{vortices}}$	induced velocity by the vortex distribution
$\vec{V}_{\text{sail} - \text{vortices}}$	sail vortex distribution
$\vec{V}_{\text{wake} - \text{vortices}}$	wake vortex distribution,
v_d	disturbance velocity
(x, y, z)	sail section local coordinate system of axes
(x_r, y_r, z_r)	local coordinate system for the r^{th} finite element
(x_s, y_s, z_s)	local coordinate system for the s^{th} finite element
(X, Y, Z)	sail local coordinate system of axes
(X_g, Y_g, Z_g)	global coordinate system of axes
W	weight
Ω_j	average vorticity on the j^{th} panel

Chapter 1

Introduction to the Sail Analysis & Design

1.1 Introduction

The development of modern sailing boats, racers, as well as cruisers, has been based almost entirely on the co-operative efforts of enthusiastic skippers, designers and sail-makers, with very little contribution from scientists and technologists and using just basic scientific principles. Nevertheless, the entire semi-empirical procedures have led to determinate lists of rules and customs concerning sailboat design and performance optimisations.

In recent times, urgent and strong requests for more improved performances mostly for racing yachts have guided the interest and the attention of the scientific community in the optimisation of sail performance and design approach. Indeed, an important role in the development of the scientific investigation is due to the work done by Jerome Milgram in 1968, who presented and published a complete and rational method for the analytical sail-shape design [43]. His work is used today as a reference source for all the researchers in this field and has encouraged more accurate experiments and different theories.

Sailing is an ancient art. Throughout its history, enormous developments of innovative ideas have been carried out, as can be seen from the Viking ships with square sails, which

could sail only with the wind coming from behind, to the modern yacht, which is able to sail into the wind. However, the art of sailing has not benefited from the development of proper theories, models or studies, as has been done for flying. Nevertheless theories developed for flying have been used for sailing. The main reasons for the difficulties are:

- sailing is the result of a complex interaction between aerodynamic and hydrodynamic forces;
- the sailing driving force is due to the difference in pressure between the windward and leeward sides of the sail;
- sails are flexible structures;
- each sail can be used on different sailboats.

Two physical phenomena are involved in sailing: the interaction between the hull and its appendages, keel and rudder, with the water and, secondly, the air and sails and rig, which, implying a force in the direction of the course sailed, drives the boat, [41]. Thus, there are two systems of forces acting during the sailing, namely, hydrodynamic and aerodynamic systems respectively. Moreover, because each force system affects the other, a sailing condition is determined by the equilibrium of these force systems. Thus, to analyse this system is very difficult, which will be detailed in section 1.3.2. It is worth noting here that the reasons for the difficulties in analysis are due to the presence of the two force systems mutual influences, the sailing boat size, shape and type.

Sails are like thin vertical aircraft wings, [31]. In fact, the aerodynamic forces are developed on the sail by the difference in pressure between its windward and leeward sides. These forces drive the boat and determine its trim and heel configuration in association with the hydrodynamic forces.

Sails are made up of flat panels of sailcloth, [13], [20], [48]. Cutting and seaming sailcloth panels in a way where it is possible to reduce the area along the seams and to give depth to the sails produce their three-dimensional shape. Due to the sailcloth flexibility, on one-side sailors can modify the sail-shapes by using opportune controls, while on the other side sails modify their shapes under the wind forces. The final flying sail-shape is the product of the trimming actions made by sailors and the deformation due to the aerodynamic force acting on it.

Due to the fact that it is possible to use almost any sail on a sailboat, it will not assume the optimal performance in general. However, the optimal performance of the sail, although transferable, depends on the sailors' ability and the sailboat size and shape, [16], [29]. Thus, the crew, experimenting with different sail shapes or trimmed configurations in several weather conditions, develops accurate observations, which constitute the basic knowledge for improved sail shapes. The knowledge gained from this experience has driven the development of sailing and sailboats.

Indubitably, the experience gained during hundreds of years by sailors and sailmakers represents the basic knowledge for the scientific sail design. This is evident in the fact that a large number of racing sailors are either employed in sailmaking factories or have started their own business, [62]. An experienced sailor is a font of tacit and experimental knowledge, which can generate new ideas for improving the actual sail performance. One such person is Lowell North, a civil engineer and founder of North Sails, the largest sailmaking factory in the world. His strong passion for sailing drove him in starting his business, adapting his engineering insight in order to make sails with improved performance. It is not uncommon for the many established sailmaking factories to employ persons such as racing and cruising sailors, engineers and skippers, all persons with a strong passion for sailing.

Nowadays, the interest in scientific approach to the art of sailing is growing, [22]. On one side, the main evolutions in this field are due to the external pressure of racing clubs, who are willing to employ people and spend money on research in an effort to win important competitions. In fact, the established sailmaking factories publish information about new materials, new construction methods, new techniques and results concerning new analysis methods and improved performance after important and popular competitions, such as America's Cup, [25], [45], [73].

On the other side, sailing has become more popular, attracting more people of various status level and age, since the cost of participating has decreased. This fact creates on one side an increase of sailing competitions, clubs, and schools, [75], [77], while, on the other side, an increase in the demand for new improved sails, [68], [73], [76], [78], [79]. Hence small sailmaking factories are investing in research, thus opening this field to new studies.

However, the costs involved in this research are still very high because of the necessity of using powerful instruments, which will be discussed in chapter 2.

The present introductory chapter intends to illustrate the complexities in addressing research in this field, illustrating the reasons and aims of the present work. Therefore, the first part focuses on the conditions and factors, which drive the sail research. This part provides evidence of the way in which customers' preferences drive the research towards different paths of development. At the same time, it points out the need for more simplified and accurate instruments for aiding sail design, introducing in this way one of the reasons of the present research. The second part enlightens the aims and the contribution of the present research. The last section of this chapter presents the structure of this thesis.

1.2 Conditions and Factors Driving Developments in Sail-Design

Sail design research is in continuous development, guided in many directions due to the different conditions and factors acting upon it. This has resulted in the coexistence of many different sailmaking factories, which try to respond to the needs of the different customers by offering sails in different sizes, materials and shapes.

The task of the sail designer is to produce sails, which are able to respond to the sailor's adjustments with an overall goal of versatility, [21], [30], [25]. In practice, since sailing boats operate in various and unpredictable conditions there are no set rules for designing or trimming the yacht. The choice made by either a designer or a sailor is a compromise between different factors and considerations. Certainly, the sail-designer, in both cases, uses the following requirements to produce the 'optimum' sailing boat:

- speed,
- stability,
- manoeuvrability,
- easy to handle sails.

Notwithstanding these common requirements, the priority depends on the needs of each customer. For instance, a sailor requiring a sail may use the following criteria for his selection:

- 1) type of sailing;
- 2) type of boat;
- 3) simplicity.

Type of sailing

The type of sailing determines the various customers' requirements. As mentioned in the introduction (1.1), mainly it is possible to differentiate only two types of sailing: racing and cruising. However, this is only a rough differentiation. Tom Whidden [62] listed five types of sailing:

- 'Grand Prix' racing;
- 'One-Design' racing;
- racing/cruising;
- offshore cruising;
- inshore cruising.

Using the Whidden list, the first type considers all the competitors of the most important races from the America's Cup to all the Admiral's Cups. Those customers require high performance, because their aim is to win the cup. The other requirements, such as durability, price, facility in handling, are not of comparable importance.

The 'One Design' racing sailors require high performance in order to win the race. However, in this case, there are strict rules, which govern the sail design, regarding size, weight and so on. This group of racers consists of all the Olympic sailboats and generally the entire group of internationally known races, which use small sailing boats. In view of the fact that the FINN class sailboat represents the main example for the present research and belongs to this group, it is preferable to explain here what the One-Design class is, [70]. The necessity of rules for sailing races and associated boats became important from the end of the 19th century, when the races started. Today, the International Sailing Federation (ISAF) supervises all the phases of a race from the measurement of the boat structure to the particular rules and regulations governing the respective regatta. It is important to note that notwithstanding the strict rules, such as those for a One-Design class race, they have not interfered with the ongoing research pertaining to the improvements of

existing classes and the development of new projects and new classes. For instance, the Laser Class, one of the latest class, was created in 1971. In the event of a new class, the ISAF studies the rules, controls the interpretations and ensures their validity. On the other side, the strict rules influence the developments of the sailing performance. Notwithstanding the rules are formulated for performance, today however the research is aimed at the development of new ways to measure and improve performance. At present, the measurement of performance is established by the International Measurement System (I.M.S.). As the maximum vessel speed is of great importance, this has determined the development of research for its measurement. The most important research in this field has produced the Velocity Prediction Program (V.P.P.), which will be illustrated in chapter 2.

However, for the One-Design class races, the interest of big external sponsors is less compared with that of the ‘Grand Prix’ races. Thus, in this case sailors are concerned with the speed performance, considering the compromise with the costs. Consequently, the racer prefers to compete in small races with less competitive sailboats to keep the costs low.

All the sailing boats built with the dual purpose of racing and cruising belong to the third group (racing/cruising). In this case, the required qualities are high performance, tempered by the concern of keeping the costs very low, durability and possible extensive use of the sail for both purposes.

The offshore cruising sailors require sails characterised by a high level of durability and wide range of external operating condition, because their aim is to have security of navigation, whatever the weather conditions and location.

The inshore cruising sailors, which sail in the safety zone, near the land or harbours, like using sails, which are durable, reliable and can ensure all the weather conditions at an affordable price.

The above considerations demonstrate the influence of the customer requirements on the research developments in different paths. What has ensued is the adaptation of available theories, implementation of analysis methods considering different levels of approximations, invention of semi-empirical methods, development of new materials, experiments with new sail shapes and many other methodologies, which are described in chapter 2.

In conclusion, Grand Prix racing and the offshore cruising constitute the two extreme groups, whereas the first group requires high-speed performance, the latter requires durability, reliability in a wide range of weather conditions.

Type of boat.

In addition to other requirements, the sail-makers request information of the type of boat proposed for use. The type of sailing is the first determining factor for this choice. The size, the shape and the appendages of the hull determines the size of the sails, their type, the number it can carry and the weight. It is also very important to know the rig type as well as its structural and stability characteristics and how it affects the hull, [29], [41], [46], [17].

Simplicity

The driving spirit above all is the simplicity, which determines the focus on minimising number of sails, their handling and the facility in manoeuvring.

1.3 Fundamental Factors Governing Sailing Performance

In order to address the explanation of the fundamental factors governing the sailing performance, it is necessary to illustrate the physics of a generic yacht and in general the sailing phenomenology. Furthermore, the following sections introduce the particular terminology regarding the sailboat and sailing, specified in the glossary of this thesis.

1.3.1 Sailboat Description

A standard sailboat configuration, as figure 1.1 shows in a race, presents a hull, sails and rig, [29], [62], [79].

On a hull, there are the keel, rudder and sometimes a trim-tab. Each of the above components can be built in different shapes and materials, and they can be assembled in various configurations. These characteristics depend upon the required performance, the boat size, the class and the destined use, racing or cruising.

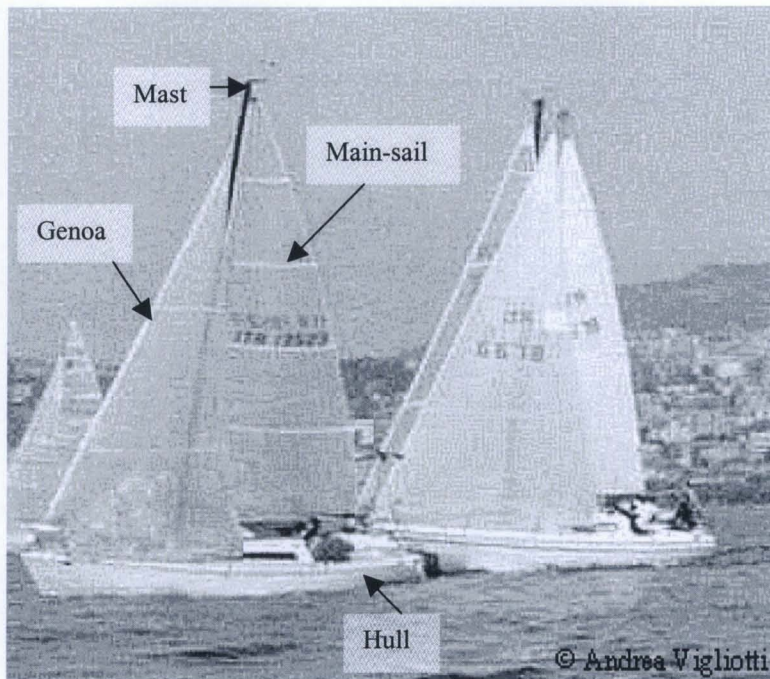


Figure 1.1: Typical sailboats

Considering the sail plan, usually there are three sails on a boat: the mainsail, the jib or genoa and the spinnaker. In most of the sailing conditions, described in the next section 1.3.2, usually only the first two sails are used, trimmed in order to form a unique and continuing lifting surface to produce the sailing forces.

The mainsail is the largest regular sail on a sailboat, it has triangular form and stretches aft from the mast. Its foot curve is fastened to the boom.

The jib is also a triangular sail but it stretches in front of the mast. The jib is called genoa when it overlaps in part of the mainsail forming a slot.

The spinnaker is a large sail, used only in acceleration when the boat is broad reaching or running. Because it is not fundamental in sailing, it can be built in different shapes: nowadays the trend consists of using an asymmetric shape, in order to make it usable for a wider range of sailing conditions around the running one. It should be noted that if there is a spinnaker, usually the jib or genoa is taken away to help the sailboat stability and spinnaker set.

1.3.1.1 The FINN Class Sailboat

The present work focuses particular attention on the case of a FINN class sailboat. Thus, this paragraph briefly describes this particular sailboat configuration. The information are taken from the FINN class web site [70].



Figure 1.2: A FINN Class boat, [70].

Figure 1.2 plots a Finn Class sailboat in working conditions. Figure 1.3 plots the structural scheme of this boat. It is a dinghy with a very simple rig, as it has a mast and a boom. The mast is unstayed and the boom can be considered fixed to its end point. In the same figure, the table illustrates the dimensions for rig and sail, defined by the rules.

In the January 1949, the Finnish Yachting Association organised a design competition for single-handed dinghy to be used in the Olympic Games at Helsinki in 1952. Rickard Sarby produced the full-size drawings of what has become the FINN as well as built the first prototype. The first FINN was launched in May of the same year. The project did not win the design competition, however, it started to participate in small race competitions, which made it popular because of its performance in light and in heavy weather conditions. In 1952 the FINN Class was first used in the Olympic Games, held in Helsinki, Finland. Four years later, the FINN Gold Cup was presented and the International FINN Association

(I.F.A.) was founded. Since then, several changes were made to improve the performance of the FINN with I.S.A.F authorising the use of synthetic cloth for the sails, reinforced polyester for the hulls and aluminium alloy and reinforced polyester for spars. Finally in 1974, building materials for hulls were unrestricted and a minimum weight was fixed for booms and rudders. Ten years later any flexible material was authorised for making sails. Nowadays, the minimum weight for the mast is fixed at 8 Kg, and the structure can be entirely built in carbon fibres.

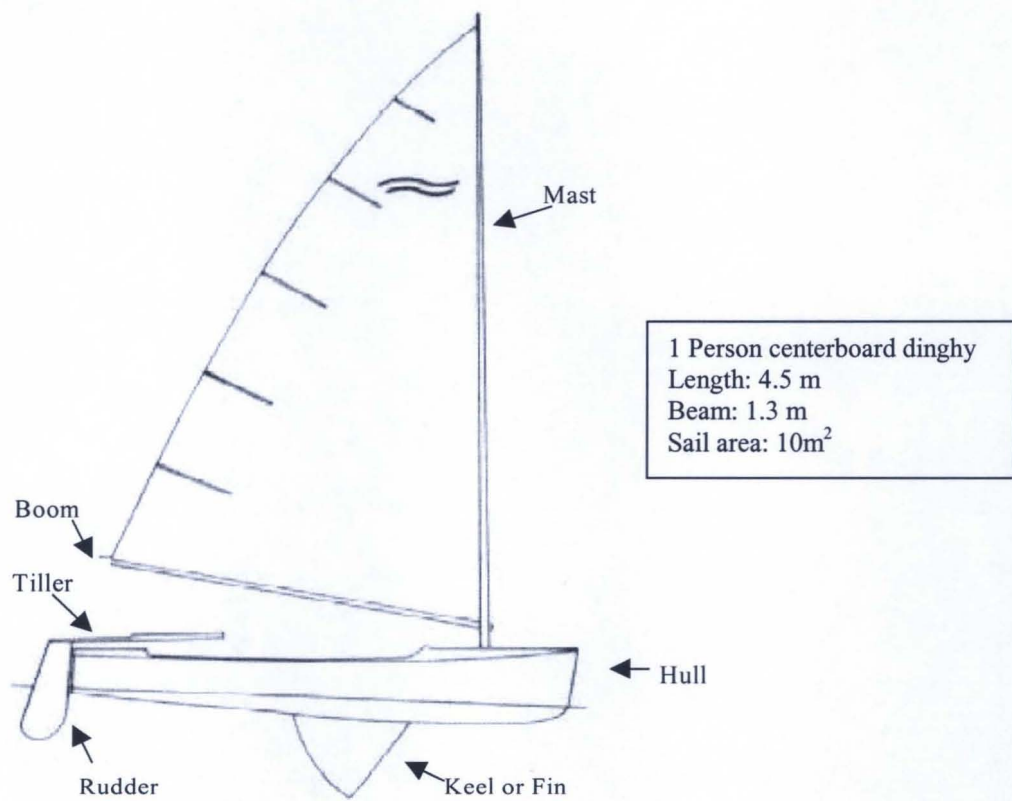


Figure 1.3: Structural diagram of the FINN Class sailboat

For this kind of boat, the sailing forces derive from the use of one sail, whose shape is formed from the combined action of the mast bend and the kicking strap forces. The crew is composed of one person, named helmsman, who steers the tiller, moves the boom and bends the mast. His or her position on the boat and posture, which is called hiking, contrasting the pressure loads, makes sailing stable.

1.3.2 Sailing and Trimming

A stable sailing condition is the result of an equilibrium condition between the hydrodynamic forces, due to the interaction between the hull and its appendages, keel and rudder, with the water and the aerodynamic forces, developed by the interaction of the air flow with the sail plan and rig, [41].

This paragraph addresses the description of the physics of sailing, in order to identify the main variables involved. As previously mentioned all the descriptions considered the particular case of the FINN class sailing boat. However, the following description and considerations are extendable to any sailing yacht.

Sails are yacht engines, because they develop the thrust force. In fact, a sail is a lifting surface, whereby the air travels faster on the leeward side than on the windward, as figure 1.4 shows. Consequently, this difference in pressure originates the aerodynamic force, which depends upon the geometry of the sail-shape, the trimmed configuration of the boat and the external conditions, in terms of wind and sea.

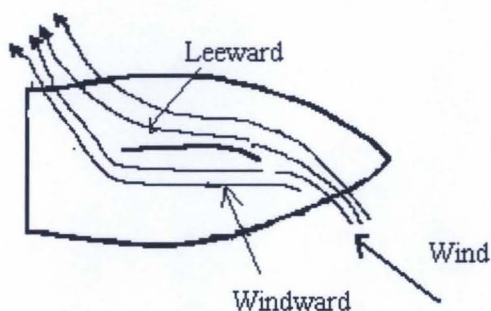


Figure 1.4: Leeward side and windward side for a FINN class sailboat (top view)

Considering a windward sailing condition, as figure 1.5 shows, the total aerodynamic force generated has a component in the sailing course direction, which is the thrust force and a lateral component, which is usually bigger than the thrust force. It is expected that this side force heels and turns the boat.

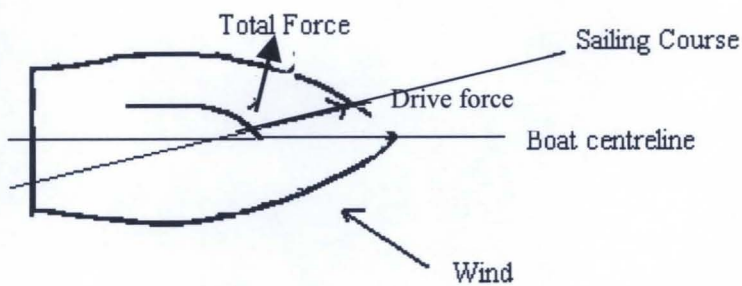


Figure 1.5: Brief description of the factors involved in the performance (top view)

Then, as the sailboat moves through the water, hydrodynamic forces are generated, as it is shown in figure 1.6. Their magnitudes and direction depend on the hull shape and the position assumed by the boat in the water. As explained above, the hull and its appendage are like symmetric wings – but only in the upright condition.

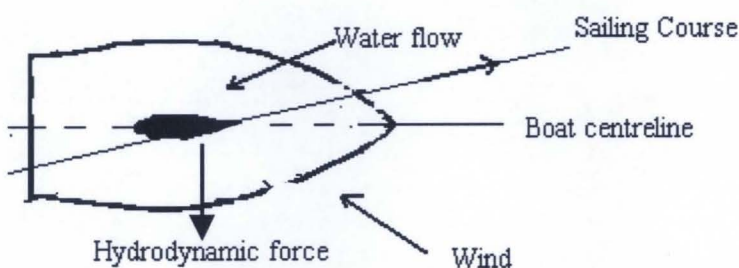


Figure 1.6: Generation of the hydrodynamic force on the hull.

A stable sailing condition appears when the wind force is equal in magnitude and exactly opposite in direction to the water force. This condition is achieved by several adjustments made by the crew during a transition period. In fact, consider a FINN class boat sailing windward, with a speed V_{Sailing} and keeping a determined sailing course. In the event that the wind intensity increases or its direction changes, this causes an increment and

deflection of the total wind force acting on the sail plan. In the events described above, the boat accelerates and the side force increases, causing heeling and turning of the boat.

When the boat presents a bigger heel angle and a turned position, the hull surface in contact with the sea-water increases and considering that the velocity has increased, the hydrodynamic force changes intensity and direction with respect to the previous condition. This increment affects the position of the sailboat. In fact, a bigger hydrodynamic force means an overturning moment, which decreases the boat heeling. As the angle between the sailing course and the boat centreline has increased, this moves the total hydrodynamic force to the back. This displacement will push the boat to reduce the angle mentioned above. As the sailing boat configuration has changed again with respect to the airflow, the boat accelerates. As a result, new sets of aerodynamic forces and consequently hydrodynamic forces are generated until a new equilibrated condition is established. From this description, it is clear that a stable sailing condition is characterised by the equality in intensity and direction of the two systems of forces. At the same time, the aerodynamic and hydrodynamic forces depend upon:

- wind speed and direction,
- sea condition,
- boat velocity and
- decided sailing course.

Further and accurate details concerning the system of equations governing this phenomenon are explained in chapter 4. This further clarifies the difficulty experienced in discussions pertaining to sailboat performance. High performance always implies a compromise between those two force systems. High sailing performance does not mean maximum velocity to windward, it means the understanding of how to maximise the velocity and the stability of the boat in all the possible external conditions for any sailing course. This results in yacht and sail designers trying to achieve versatile sailing boat design.

Once the sailing boat is delivered to the customer, the crew plays an important role in getting the maximum designed performance. The entire actions for adjusting sails and rudder for any weather condition and in any given sailing condition is called trimming.

Specialised magazines dedicate articles to describe the ‘best’ trimming conditions or how to obtain them, which diffuses the belief in the existence of an ideal trim setting for every given sailing situation. This is theoretically true, but involves balancing of many factors according to conditions and performance goals. The constant change in wind and sea, the relative disturbance of the air and even the tactical position in a race can affect the sail trimmer’s goal at any one time.

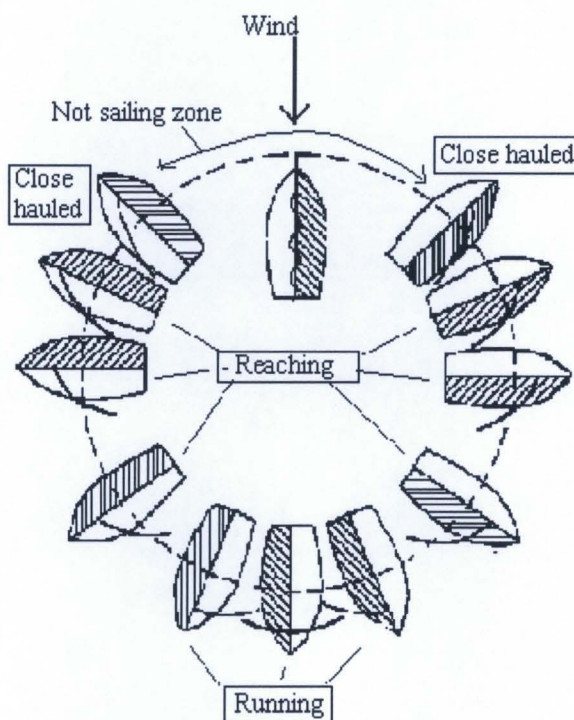


Figure 1.7: Possible sailing courses

Figure 1.7 plots all the different possible sailing courses. It is evident that there is a no-sailing zone, which represents the range of angles, in which the aerodynamic force drags and heels the sailing boat, in a way which makes it impossible to move forward. The sailing course, called close hauled, corresponds to the minimum possible angle for sailing to windward. When the wind is coming from behind the boat, the sails are opened in a way that develops the maximum aerodynamic drag possible, which actually drives the boat. The entire sailing courses between the two mentioned extremes are called reaching. These configurations, including the close-hauled, have to be assumed by the sailboat to move towards the wind in a zigzag course.

The crew decides which sailing course to maintain. The decision is the result of considerations about available boat and sail wardrobe and about wind and sea conditions. The crew then sets the sail plan and takes a sailing course, which will be kept. Thus, to trim means to adjust sails, rig and hull, according to different wind strengths in order to make the sails work across the maximum wind range possible, maintaining a sufficient level of performance.

1.4 Sail Load Calculation Problem

Considering the simple case of a sailboat sailing to windward, the performance depends on the sailing velocity, aerodynamic and hydrodynamic characteristics. Marchaj [41] identifies four groups of characteristics, which are listed below and influence the sailing performance:

- the hydrodynamics of the hull,
- the aerodynamics of the sails,
- the geometry of sailing,
- the mutual interaction between the two force systems.

Naturally, every group of these characteristics depends upon variables, which can be in part controlled by the crew and are partly independent of the crew.

In particular, the crew can act on the hull hydrodynamic characteristics by moving the trim-tab, if it exists, and steering the rudder. These manoeuvres depend on the sail speed $V_{Sailing}$, and the sailing course. However, for any boat, these characteristics are fixed and well known by the crew, who are aware of their use.

The geometry of sailing depends on the sailing velocity $V_{Sailing}$, the wind velocity and its attack angle, as seen by the boat, known respectively as the apparent wind velocity $V_{Apparent}$ and the apparent wind velocity angle β or course angle.

The mutual interaction between the two force systems depends upon the chosen trimmed configuration, sailing course and weather condition. As explained in the previous section, the crew regulates this kind of interaction.

The sail aerodynamic characteristics depend on the apparent flow velocity V_{Apparent} and its attack angle β and on the trimmed sail configuration established by the boom sheeting angle δ_m and the heel angle θ . These, in turn, depend on sail geometry, sail shape and structural material properties. In addition, it is important to consider the influence of the mast and its structural properties, such as section, material and geometry. However, given the characteristic sail flexibility and the usual presence of a wide selection of sails on a boat, the crew can largely change the aerodynamic characteristics.

The evaluation of sail loads is one of the subjects of the current research. The discussion hitherto has highlighted the qualitative importance of this aspect and the main factors associated, which can be ascertained from the identified factors influencing the performance. The particular sail aerodynamic characteristics play an important role in the determination of the sailing performance. Therefore, any action, which improves the aerodynamic characteristics, automatically improves the sailing boat performance.

Henceforth, the discussion focuses on the importance of the quantitative evaluation of the sail loads and how this contributes to the improvement of the performance of a sailboat. There are several ways of deducing sail forces and of investigating the influence of essential factors on which these forces depend. Chapter 2 illustrates the variety of techniques available, illustrating limitations in reliability and accuracy.

Herein, an integrating numerical method is presented, which evaluates the sail loads and their distribution in the chord-wise as well as span-wise direction. A brief description is given in the latter part of the present chapter. The following sections describe the other motivations of a sail load evaluation, namely improvements in sail performance, aiding sail design and assisting mast design.

1.4.1 Sail Performance Improvements

Techniques for sail performance improvements encompass all the actions, which enhance a given sail, its durability and stability of the structural properties.

Consider a stable sailing condition for a FINN class sailing boat, as shown in figure 1.2. Consider the sail with its geometry, shape and trimmed configuration in a known wind

condition. Regarding the loads acting on the sail and their distribution, it is possible to take a critical view of the chosen shape and even the trimmed configuration.

In fact, since the sailing condition observed is stable, this means that the hydrodynamic force must be equal in intensity and opposite in direction to the aerodynamic force. In the event the crew wants to maintain this configuration, a sail load analysis in this case enables an evaluation of the sailing forces and their direction.

In the eventuality that the crew and/or the sail designer are aware of the aerodynamic loads, the deformed shape of the sail and the stress distributions, it is possible to criticise the chosen shape. For example, the following observations can be made:

- keeping the same sail, it is possible to determine if the same aerodynamic loads can be obtained by using different sail-shapes or trimmed configurations, while maintaining or improving the stress distributions;
- if the sail can be changed, the structural properties of the new sail can be evaluated;
- in the event of lateral gusts, the loads can be determined and consequently the best sail configuration obtained.

These observations do not exhaust the kind of actions, which can be taken, with knowledge of the external loads. They illustrate the importance of load determination and how this can affect the sail performance.

1.4.2 Aiding Sail Design

Several numerical methods, using high computational power and full scale as well as wind tunnel experimental tests done on sails have been developed in order to aid sail design.

The most important problem for sail-designers and/or sail-makers is not to define a sail shape they wish to achieve, rather it is to understand if, [19], [21], [25], [27], [58], [62]:

- in real sailing conditions, the designed shape can be obtained and maintained by the crew;
- the considered shape corresponds to the shape designed for the assumed set of external conditions.

In order to clarify how knowledge of sail loads is an aid to design, it is important to mention the following facts.

Firstly, sail shapes change continuously as the weather changes, due to their flexibility. This means that the same sail, built from two different materials, assumes two different shapes for the same external condition, boat and rig. Knowledge of sail behaviour, in terms of deformations and loads for a particular set of external conditions, improves and hastens the design phase. In addition, since it generates awareness of all the possible material and shape implications, the design phase becomes more efficient.

Secondly, once a sail is fixed, it is important to map its behaviour. In fact, the design obtained does not give the best sail in all conditions. A good design project gives a versatile sail as a product, whose performance can be optimised over a known range of external conditions.

Concluding, it is clear that sail design is an interdisciplinary subject, not restricted only to the shape of the sail. It involves research in materials, sail cutting techniques, control devices and trimming solutions. A good sail design is the achievement of a compromise between different aims and it is the result of improvements in all of the above mentioned research fields.

1.4.3 Assisting Mast Design

A very important issue involved in the sail load analysis focuses on the design of the mast and its rig, [5], [8], [35], [44], [47], [55], [64]. In a generic sailing boat, either cruising or racing, the mast is an element of the rig. This structure holds the sails and drives the sailing boat, due to the combination of the boat's trimmed configuration and the particular sail shapes required, moulded using the rig's elements.

Since the mast structure and its position on the deck affect the resistance and the driving force of a sailing boat, a poor mast design decreases the sailing performance, particularly for racing boats. Properties such as low weight, high flexibility and high fracture loads are required from the structural point of view, whilst from the aerodynamic point of view, section shape is important for reducing the drag and the influence on the sails, [44], [64].

An efficient mast design achieves the best possible combination of the above structural and aerodynamic properties through a correct evaluation of the acting loads. Distinguishing three main categories: sail loads, tuning loads and dynamic loads, within the static analysis, the first two classes are considered, [5]. In given external conditions, the crew will adopt a particular sail shape and rig configuration, in order to reach maximum sailing performance. Thus, the sail loads are properly due to the sail shape, whilst the tuning loads are developed for keeping the sail shape and consequently their value is influenced by the sail loads. Therefore, a realistic evaluation of the external loads acting on the sail is an important factor in mast design.

1.5 Research Statement

The objective of this study is to provide an integrated design system, which provides an analysis method and design features via a user-friendly graphical interface.

The analysis enables the following predictions to be made on a single-sail configuration in stable sailing conditions:

- the aerodynamic loads acting in given external condition for any shape;
- the corresponding deformed shape;
- the stress distribution.

As previously mentioned and in the view of the design demands, the system has been created with proper design features. The list below describes some of the possible actions, which the system facilitates, given the fact that the design field is open.

The sail designer can:

- start the project of a new sail shape with few initial design parameters;
- improve a designed sail-shape, by the easy results review features;
- test structural sail behaviour;

- evaluate if the designed sail shape is maintained in the prescribed external conditions;
- aid mast design.

The problem has been approached in three broad areas:

- development of a static aeroelastic algorithm;
- development of a graphical user interface;
- tests on existent sails and new geometry.

The static aeroelastic algorithm permits the analysis of a sail shape to be made in given external condition. This analysis gives the aerodynamic loads in terms of pressure distributions or sailing loads acting over the sail shape, the corresponding deformed sail shape and stress distribution.

The implemented method, which will be fully explained in chapters 3, 4, 5, 6, 7, consists of three main parts:

- geometric sail surface generation,
- aerodynamic analysis,
- structural analysis.

The development of a graphical user interface (G.U.I.) aids the use of this method, including by those with no proper skills in engineering, such as sailmakers. Descriptions of the interfaces, created for any analysis phase, are in the latter sections of chapters 4, 5, 6, and 7, and they have been designed with proper features in order to:

- build data-files interactively for existent sail geometry or new design project;
- make decisions about how to perform the aerodynamic and structural analyses;
- display the results.

The tests on existent sails and new geometry, detailed in chapters 8 and 9, illustrate the power of this instrument and how the results can be used, providing the base for general design concepts. The anticipated reduction in experimental tests required and a more focused design process before the full construction of the sail should lead to lower costs for sail-makers and mast-makers.

Therefore, the objective of this study is:

to provide a full static aeroelastic method of analysis and design of a single-sail configuration supported by a user-friendly graphical interface. The emphasis shall be on providing a practical application of the sail analysis, which will allow further developments in sail design.

1.6 Thesis Structure

Chapter 2 describes the state of the art with regard to the sail load evaluation problem. A critical outline of the actual methods commonly used by sailmakers is given. An overview of the historical background and how the research field has been developed up to the present is given. A detailed literature review on this subject is provided which outlines the development of interest in this topic, and the difficulties and applied methods for tackling the sail design and loads evaluation problems.

Chapter 3 describes in detail the structure of the implemented analysis method. A full static aeroelastic analysis has been performed, complemented by data pre-processing and post-processing. It does not only perform an analysis of the loads acting on a sail-shape, but is a simple and user-friendly integrated sail design system. It is a customised system, whose achievements respond to the actual requirements of sail designers. The analysis focuses the attention on the Olympic FINN Class sailboat, however it can be performed for a single sail configuration. The theoretical background of the analysis is explained and the limitations and rationale are discussed.

Chapter 4 describes the technique utilised for constructing the sail surface from the introduction of the input data to the complete development of models, which are to be used for the subsequent analyses. In parallel, it illustrates the related graphical user interfaces. The object accomplishes the issue of building the geometry of a sail shape, which corresponds to the first phase of the method implemented and presented in chapter 3.

Chapter 5 illustrates the modalities for carrying out the calculation of the aerodynamic loads acting on the sail surface. Initially it describes the method applied to perform the

aerodynamic analysis, which is the Modified Vortex Lattice Method and how it has been integrated for running the full sail aeroelastic investigation. It also shows how the method is integrated into the designed graphical user interfaces. This chapter concludes with the validation of the implemented code.

Chapter 6 illustrates the accomplishment of the calculation of the deformed sail shape. It focuses on the structural behaviour of a sail, analysing materials and construction methods used for them, which determine difficulties in tackling the structural analysis. It, then, outlines the applied method and how it is implemented in the graphical user interface. The chapter ends with the validation of this part of the code.

Chapter 7 demonstrates how the system automates the aeroelastic analysis loop, explained in chapter 3. It, then, illustrates the features of the graphical user interface designed for it, whilst the ending part of this chapter examines a validation process for the entire analysis system.

Chapter 8 displays and criticises the results obtained with the implemented numerical method through the created graphical user interface, as presented in the previous chapters. The results concern the general sail behaviour and the corresponding loads acting upon it, in the case of several external conditions, or in a fixed external condition and several trim settings or for fixed external conditions and for a trimmed set and several sail shapes.

Chapter 9 describes the design features of the system presented in this thesis by presenting results concerning improvements in sail design and mast design. Various possible design actions are condensed in three examples: the design of a FINN class sail shape, the definition of the final shape for a flat trapezoidal sail and the design of a FINN class mast, which focuses the attention on the interference between sail and mast.

Chapter 10 summarises the accomplishments of the designed goals, identifying the results obtained in terms of analysis and design. In addition, possible improvements and further developments of the system are suggested.

A wide *Glossary* of the terminology is furnished at the end of this work.

Chapter 2

State of the art of sail design

2.1 Introduction

This chapter describes and reviews the evolution and the state of the art of the research concerning methods for loads evaluations and sail design. This section outlines the main reasons which have characterised this research field.

Notwithstanding the fact that the interest in improving the ‘art of sailing’ is very ancient, a scientific approach is modern, [62], [61]. The corroboration is in the fact that the expression ‘art of sailing’ is nowadays normally used, since the evidence that most of the main improvements in this subject are the result of a complex combination of experience, clever observations and tests conducted by sailors. Therefore, the ‘maker’ of improvements in sail design is seen as an artist, as he is able to determine, with his hands, strategies for winning races, exploiting his experience and inventive capacity.

This fact is very important in order to understand the particular evolution of the scientific approach to this subject, [62]. Indeed, it has determined two typical characteristics of this research field.

On one side, the main international sailmaking factories recognise the importance of the expertise sailors contribute to research developments, [62], [29]. Consequently, what is notable is the number of expert sailors employed and their principal role within small and large sailmaking factories and clubs, developed for building yachts for important races, notwithstanding the actual availability of powerful computational techniques, [77].

Secondly, this fact has delayed the development of the scientific approach to sail analysis and design. In reality, researchers have been utilising techniques and methods, developed for other fields, to the sail research. For instance, they have adopted methods developed for lifting surface and for tension membrane structures, in order to calculate the aerodynamic loads and stress distribution on the overall sail, [43], [41], [31]. Therefore, there is no autonomous development of the scientific approach to this subject. Furthermore, a belief in the efficiency of the new techniques is weak and has continued to be criticised by experts in the field, who are normally old sailors and winners of important competitions.

Hence, the present chapter analyses the principal methods developed, considering the important role still played today by expert advisers. Furthermore, the continuous effort in developing full theoretical methods is described, which will aid the design and consequently decrease the cost of experimental tests.

2.2 Critical overview of sail analysis methods

As outlined above and in chapter 1, most of the improvements in sailing performance are due to the experience of sailors. Sailmaking factories employ them, since they are a font of unwritten knowledge about what realistically happens in sailing. It is common that sailors and sailmakers have used their experience and observations in order to create empirical methods for sail design. In 1962, a first complete scientific approach was realised by Milgram, and since this work there have been more studies. Notwithstanding the techniques developed, the state of the art in sail design and performance analysis is still connected to empirical approaches.

It is the intention of the following subsections to present a critical overview of the large number of methodologies for sail load evaluation and design.

Prior to the start of this review, it is important to mention the performance prediction process most widely utilised at the present, mainly because the current studies for improving the sail loads evaluation are done in order to achieve more accurate results with those methods.

The common achievement of these methodologies is the improvement of the sailing performances. They are commonly named Velocity Performance Prediction or V.P.P. due to the fact that their aim is the maximisation of the yacht speed. At present, there are several developments of those methods, which undergo continuous improvements: the most popular in the academic field are the ones implemented at Southampton University, [12], in Europe or at the Massachusetts Institute of Technology in the United States, [45].

The V.P.P.s, [49], [34], [24], are created for predicting sailboat speed in any prescribed wind condition and apparent wind angle. As seen in chapter 1, particularly section 1.3.2, this prediction requires the solution of the equilibrium between the aerodynamic and hydrodynamic forces and moments acting on the yacht. Since the solution of this non-linear system of equations for the equilibrium is complex, the efforts of the known V.P.P. is to build up sets of routines which provide a solution through iterative loops, and give a realistic velocity prediction. Thus, all V.P.P.s have common aims and structure. Their differences are in the data used and in the routines implemented. A generic V.P.P. method solves the non-linear system of equations by an iterative solution process, which requires information about the stability properties of the yacht, which the designer can provide, and the value of the hydrodynamic as well as aerodynamic force coefficients for the entire range of possible external conditions.

With regard to the hydrodynamic forces, they can be calculated from towing tank tests, numerical prediction or semi-empirical relations. Notwithstanding these above methodologies, these data are not difficult to obtain, unlike the aerodynamic coefficients, principally because the hull and appendages can be considered rigid and have almost the same characteristic coefficients, especially if they belong to the racer class, [45].

The concern of obtaining reliable sail load coefficients is more difficult, [7]. Currently, V.P.P. methods use three forms of evaluations, these are:

- empirical data,
- wind tunnel tests results,

- numerical results.

Together the three methodologies do not ensure accurate aerodynamic data, furthermore they are difficult to find and, above all, the last two items in the list are very rarely obtained [34]. For this reason, a realistic sail load evaluation constitutes the most difficult part in developing a V.P.P.. At present, these methods use simple aerodynamic theory or data derived from a combination of model tests and empirical full scale tests, related to some rigs and sailplane, which could be completely different from the actual sail yacht analysed. Both approaches make the results of the V.P.P. very approximate.

The following subsections 2.2.1-2.2.3 describe in detail how the above listed data are obtained. This introductory discussion intends to point out the main applications for the sail load coefficients and to highlight the importance of implementing methods for accurate evaluation of the aerodynamic forces, which is one of the main aims of the present thesis. Euerle and Greeley, [24], believe that the development of a theoretical method for calculating the sail force coefficients will improve the efficiency of the V.P.P.. In view of this fact, they have implemented a method for generating sail force coefficients for V.P.P., requiring a minor amount of empirical data concerning mainly the viscous effects.

2.2.1 Empirical Data

Empirical sail load evaluations are derived by experiments carried out on full-scale sails, employing several methodologies. Full-scale sail load measurements mean the determination of the forces on a sail while it is sailing on a boat in normal conditions. Indeed this method is the logical procedure for getting optimal estimations of those forces. However, it is difficult and expensive to realise, [36], [39]. There have been a few serious attempts, and this section attends to describe the most popular.

Indubitable, in the majority of the sailmaker factories the technique commonly used for calculating the aerodynamic loads consists of consulting force coefficients tables, which are obtained from experimental tests on full-scale sails and transformed with empirical relations in order to make them adaptable to different sails.

Indeed, the most popular table, [41], still in use today, is the Gimcrack coefficients table, due to the work of Professor Davidson at the Stevens Institute of Technology, Hoboken, U.S.A., published in the paper ‘Experimental Studies of the Sailing Yacht’ in 1936, [80]. These coefficients are the product of a correlation between results obtained from tests done on the full-scale yacht Gimcrack and on a hull model towed in a tank.

The adopted methodology calculated the aerodynamic forces by measuring the forces acting on a hull towed in a tank, due to the fact that in steady conditions aerodynamic forces have to be equal in modulus and acting in opposite direction to the hydrodynamic forces. Therefore, the tank test was required to be realistic. Thus, sailing speed V_{Sailing} , apparent wind velocity and angle V_{Apparent} and β coincided with those measured on the 6m Gimcrack yacht, sailed by an experienced sailor in a range of heel angles $\theta=[0^\circ, 35^\circ]$, when the sailing conditions were considered optimal. In those conditions a towed model was tested and the measured hydrodynamic force, in terms of components along and orthogonal to the sailing direction, were considered as the aerodynamic thrust and heel force.

Table 2.1, adapted from Marchaj, [41] (page 528), lists the Gimcrack coefficients. Today, the calculation for the aerodynamic forces of similar sailplans are obtained by multiplying by the actual sail area and a selected dynamic pressure of the apparent winds $0.00119 V_{\text{apparent}}^2$.

Heel Angle θ	0°	5°	10°	15°	20°	25°	30°	35°
Apparent wind V_{apparent} (knots)		6.22	9.33	11.87	14.33	16.97	19.70	22.50
Apparent wind angle β	25.8°	26.1°	26.5°	27.0°	27.6°	28.6°	29.7°	31.0°
Sailing speed V_{sailing} (knots)		3.32	4.50	5.18	6.60	5.87	5.97	5.97
Driving coefficient CDrive		0.457	0.417	0.378	0.341	0.307	0.269	0.234
Heel Coefficient CHeel		1.54	1.345	1.195	1.045	0.902	0.778	0.666

Table 2.1: Gimcrack coefficients.

For many years, the Gimcrack coefficients, evaluated in 1936 were the only sail load coefficients available and they have been applied with success, notwithstanding the obvious limitations. Undoubtedly, the first limitation concerns the fact that the external conditions

were roughly calculated due to the poor instrumentation available on the yacht, as admitted by the same author, Professor Davidson. Two further approximations regard firstly the fact that sailing velocity depends on the wind speed, which changes in magnitude and direction with altitude, and secondly that an experienced sailor determined the conditions.

Other full-scale data have been obtained by the tests carried out on two ocean racers Standfast and Bay Bea. Table 2.2 lists those coefficients, adapted from Boote, [5].

These two coefficient tables have been reported to demonstrate the scattered values of the force coefficients for this kind of measurement and the different values derived from them for the similar sailing conditions. Therefore, notwithstanding the fact the obtained coefficients are the results of experiments on real sailboats, when applied to similar sail plans, built with different material, predicted values are very approximate.

Heel Angle θ	$\beta = 40^\circ$	$\beta = 60^\circ$	$\beta = 120^\circ$
0°	$C_{\text{Drive}} = 1.3 \quad C_{\text{Heel}} = 3.5$	$C_{\text{Drive}} = 2.0 \quad C_{\text{Heel}} = 4.3$	$C_{\text{Drive}} = 2.6 \quad C_{\text{Heel}} = 2.1$
20°	$C_{\text{Drive}} = 1.0 \quad C_{\text{Heel}} = 2.25$	$C_{\text{Drive}} = 1.5 \quad C_{\text{Heel}} = 2.9$	$C_{\text{Drive}} = 1.1 \quad C_{\text{Heel}} = 2.0$
30°	$C_{\text{Drive}} = 0.85 \quad C_{\text{Heel}} = 1.7$	$C_{\text{Drive}} = 1.25 \quad C_{\text{Heel}} = 2.18$	$C_{\text{Drive}} = 1.7 \quad C_{\text{Heel}} = 0.9$

Table 2.2: Bay-Bea coefficients.

As a point of interest, Marchaj [41] mentions the case of Sir Geoffrey Taylor, where the technique used measures the strain in the rig. Consequently, the sail loads were obtained as the transverse component of the tension to the mast. Notwithstanding the progress in the instrumentation, this method was not very successful. In fact, these measures were subjected to different weather conditions and the complexity of the rig geometry. However, Marchaj [41] clarifies that this method for calculating aerodynamic loads was successfully used in different occasion, as by Robb for the 12m boat Norsaga in 1961.

Today, the trend for empirical evaluation of aerodynamic force coefficients consists of measuring the forces required to balance the aerodynamic loads, by a dynamometer fixed on the boat attached to the mast rig, as this ensures reliable sail loads. There are several known dynamometers, [49], developed mainly for America's Cup Challengers for two

main reasons: the required high performance and the consequent high cost for building this device; maintenance of the device and the experiments themselves, in terms of time and people employed. Notable published works are due to Mutnick, [6], who built a dynamometer device for use by dinghy rigs, such as the Laser, or on scaled offshore racers. A contemporaneous publication is due to Fukasawa and Masuyama, [39], who developed another dynamometer fitted on the rig of a 10.3m yacht, with a complex system of cameras in order to record the sail shapes. In both these latest trials, the authors are confident in the high quality of the results, despite in the first case they are compared with the BayBea coefficients, whereas in the second case a comparison is made with results obtained from an in-house numerical method.

The most important problem for a full sail test concerns the extremely unsteady nature and unpredictability of the wind conditions. Therefore, the same techniques for full-scale tests were used on the boat towed in a tank in the real wind condition. However, in this case the unpredictability of the wind condition incurs additional expenses in terms of time, people employed and money in instrumentation, without being sure that the map of the load would be completed in a few days for all the possible sailing conditions, [8], [27].

With reference to the experimental techniques applied for sail load evaluation, but mostly for testing directly the sail performance, the latest technology consists of a video camera at the masthead, which records sail shapes in real sailing conditions, [78]. The most important feature is the possibility of verifying the sailing performance of several shapes for the same sail, repeating the experiment for the same sail conditions [8]. This technique is usually applied in the development of the America's Cup yachts and it is very expensive. In fact, the time to build them is considerably long and the realisation has high costs. The tests need two boats and need time, people, expertise, upkeep and maintenance of the equipment, despite the awareness that it does not ensure the fact that the entire range of sailing conditions has been analysed.

Concluding remarks concern the following facts. Naturally, the scientific community agrees with the fact that only experimental tests on a yacht gives reliable evaluations of sail loads because of the high number of variables involved: from the structural properties of sails and rigs to the various possible sailing conditions.

However, the certainty of a reliable evaluation of the sail loads is possible only when a yacht is already designed, built and almost ready for sailing. Therefore, from the design point of view, these tests permit one to verify the performance and improve the sailing trimmed configuration, preventing design flaws and the related expenses. The initial design phases utilise results from previous experiments on similar yachts and are successively corrected using empirical formulas, described in section 2.2.3.

The latter consideration emphasises once more the extremely expensive nature of those experiments and their use in very important projects.

2.2.2 Wind tunnel test sail load evaluation

Wind tunnel tests are conducted on scaled models of rigs and sails in order to have results under controlled external conditions allowing the effect of systematic variations of the geometrical and physical factors. Latest published work reports the results of a series of wind tunnel tests conducted in 1997 at the Glenn L. Martin Wind Tunnel, University of Maryland by R. Ranzerbach and his group for the Quantum Sail, [51], [52]. The tests comprised the observation of the performance in terms of the driving force of twenty-three different sails in three styles of running and in three styles of reaching with various design shapes and sizes. This work appears to be important as it defines the state of the art of the wind tunnel test features, which the following considerations describe.

One of the most important features of wind tunnel tests is undoubtedly the possibility of recording and reviewing them, in order to improve the trimmed configuration in particular wind conditions. Further, they permit testing of the sail model over a full range of conditions of wind, whereas full-scale tests cannot ensure the complete map of the sail behaviour in all the possible wind conditions. The investigation of the behaviour of a given trimmed sail configuration over a known range of conditions enables both a quantitative comparison to be made of aerodynamic performance of various designs of the same type of sail and on different geometry shapes in order to improve the design performance, [7].

Summarising, the intrinsic worth of testing is the possibility of getting data in terms of performance, sail design and materials. Notwithstanding the high costs due to the

realisations of the wind tunnel, the device for monitoring the sails under working conditions and the sail, they have proved to be cheaper and easier to conduct than full-scale measurements. Although the design of new shapes and the realisation of more sails might be needed, working with smaller models makes the realisation cheaper and easier when compared to the case of a full-scale sail. Furthermore, the comparison among a range of tested sails proves it is less expensive and simpler in terms of time and people involved.

Wind tunnel tests enable the measurements of sail forces without any reference to the performance of the yacht. However, given that hydrodynamic characteristics of the yacht are known or fixed by rules – as in the case of One Design Class – this allows debate on the expected sailboat performance, [7], [12].

In the wind tunnel it is impossible to introduce the effect of leeway angle and heeling angle therefore the results are not realistic in terms of sail behaviour. The first effect is not taken into account because in the wind tunnel it is impossible to simulate the interaction between the hydrodynamic forces, while the latter effect could be simulated in cases where the wind tunnel allows twisted flow, like the one built by Flay in 1995, [7].

Since wind tunnel tests are carried out on scaled models of sails, despite the use of the same material, the results are not accurate since the evidence shows that on small scale models stretch as well as other structural properties are different. Published and popular tests were conducted at Southampton University, on a 2/5-scaled model of a Finn class sail, at 8.9m/sec and at a constant true attack angle of 25°. Notwithstanding the approximations due to the fact that the tests were conducted on a model, they highlighted the main factors affecting the sail force and the boat performance, by analysing several trimmed and geometrical configurations. The results are in Marchaj [41], (from page 548 onward), which are used in this thesis for validating the implemented analysis system in section 7.3. Ian Campbell, [7], has continued the work started by Marchaj at the same University, mostly for getting useful data for the IMS, as explained in the next section. The work of Campbell adds the possibility of analysing a complete model of mast rig, hull and sails in different wind profiles.

In conclusion, the scientific community recognises that wind tunnel tests are effective for estimating sail performance for downwind and upwind conditions, [41], [45], [46].

An accurate scaled sail model, similar to a real sail, ensures regard for the reliability of the results. However, the obtained results are affected by the fact that scaled sail models have different structural properties, [41].

Despite the difficulties in setting up the tests and the limitations due to the wind tunnel features and the limited validity of the results, they are less expensive than full-scale sail tests and ensure an investigation over the entire range of possible wind conditions.

2.2.3 Semi-empirical methods

The most common approach for sail force modelling and measurements is the development of semi-empirical coefficients, by exploiting the basic theories governing sail analysis. Several techniques have been developed. Marchaj, [40], [41], mentions the most popular methods. One determines the aerodynamic coefficients by a combination of the wind tunnel tests results made by Marchaj and the lifting line theory of Milgram, whilst the other compiles data from various sources including the Bay Bea - Standfast results.

The current system of coefficients used are in tables recognised by the international sailing association, which provides standards about loads to use for design, known as the International Measurements System (I.M.S.). I.M.S. is a handicapping system [12], which regulates the sailboat measurements for any race or for cruising. According to the fact that the main concern regards the sail load calculation, it is important to underline that from the designer's outlook, the system provides aerodynamic force coefficients for given hull and rig configurations, to be used as V.P.P. inputs. Further details are in the Offshore Racing Council publication (O.R.C.). However, here it is important to recall the existence of internationally recognised rules for loads acting on sails as functions of the apparent wind angle. In practice, designers take lift and drag coefficients for a given apparent attack angle and, through the use of empirical relations, calculate the coefficients corresponding to their case. Therefore, these initial values are used for starting V.P.P. calculations or for beginning an optimal yacht design, [34].

2.2.4 Numerical methods

As mentioned in chapter 1, the first scientific approach to sail design was due to Milgram, who, since his thesis in 1962, had been aware of the lack in studies concerning sails.

The paper ‘The Analytical Design of Yacht Sails’, published in 1968, is believed to be the fundamental stone in the development of sail research which has brought forth the new ideas and has driven subsequent developments. Today, Professor Milgram continuously improves techniques for the aerodynamic load evaluation, particularly for V.P.P. methods, currently used at the MIT University. The major innovation, in the above-mentioned paper, [43], was the assertion of the possibility of an analytical approach to sail design within the existing framework of the aerodynamic theory. Exploiting the lifting line theory he calculated the sail shape corresponding to a predicted optimal pressure distribution on the sail surface, without evaluating if this could be obtained in reality. Furthermore, Milgram realised that the lifting line theory is efficient for calculating the sail load, whereas it is not satisfactory for designing the pressure distribution and the related sail shape, and hence the vortex lattice method has become fundamental, [46].

Inspired by the work of Milgram, the lectures of Jackson [31], [32], improved the theoretical basis for sail analysis. His main contribution was in asserting the difference between tackling the analysis of a sail and of a lifting surface. In fact, he has observed that sails are built from materials which, under pressure loads, react with large displacements and small strains relative to their unloaded shape. Therefore, the analysis problem consists in predicting the sail shape, which is in equilibrium with an unknown pressure distribution to be evaluated.

Thus, the solution necessitates the simultaneous calculation of the aerodynamic loads and the deformed sail shape, which determines the contemporaneous solution for the aerodynamic and the structural problem.

All successive studies have been in agreement with the observations made by Jackson regarding how to carry out a complete sail analysis, [32].

The main difference consists of the techniques utilised: several methods have been applied to address this problem. However, today the scientific community agrees with the

necessity of developing more accurate analytic methodologies, which can evaluate the behaviour of sails, treated as flexible structures, in realistic working conditions. This trend has coexisted with the continuous development of computational power on one side, and high costs of experimental tests, either on full-scale or scaled sail models, on the other side.

The first studies concerned two-dimensional sails, emphasising the sail membrane characteristic and its reaction under pressure. The initial models for three-dimensional sail analysis were entirely an extension of two-dimensional models. For instance, sail were modelled likewise a series of sail sections, linked together by cables at the leading and trailing edges. Subsequently, other models have been developed following the same idea of correlating solutions on sail sections to a three-dimensional model. The limitation of those models consists in the fact that each section works independently, therefore the three-dimensionality cannot be reproduced. For instance, the Ormiston analysis method calculates the aerodynamic loads by the lifting line theory, whilst, since a sail is considered as a rectangular membrane composed of a net of cables kept together by spars, the tension evaluated chord-wise is independent of that evaluated span-wise, [31].

Two main characteristics are common to this group of theories: they have stronger restrictions on the membrane structural behaviour, as it is strongly non-linear, but quite advanced aerodynamic modelling is employed for calculating the external loads, due to the employment of wing aerodynamic theories. Commonly, sails are considered as vertical wings, which has justified the direct applications of the results obtained for similar wings.

In 1987, Jackson and Christie, [33], published a full analysis method by splitting the problem into two phases. Firstly, the aerodynamic loads are evaluated by a vortex lattice method using triangular panels. Secondly, those loads are applied to a structural membrane model for sails, implementing the formulation of Oden and Sato for solving the structural problem. The main accomplishment was the determination of the deformed shape for a triangular flat sail for different attack angles, which overcomes the limitation of the Milgram theoretical approach, as described above.

Contemporaneous and later works have followed the same methodology, using different instruments for the calculations. Undoubtedly, it is important to mention the work of Professor Caponetto and Boote, [8], which implemented a complete numerical calculation.

The evaluation of the aerodynamic loads are done by a vortex lattice method with a fixed wake shape, where the structural analysis has been carried out solving the tension in a sail section. Notwithstanding the fact that their methodology is quite approximate, the importance is in the fact that it brings out the urgency of a better understanding of the sail loads and their distribution, as well as their connection with the mast and generally the yacht design. Studies carried out for the yacht FAST2000, [9], made clear that competitive design can be enhanced by the use of computed sail loads, which replace the previously employed empirical data.

Other important work is due to Schoop and Hansel, [54], who implemented a method for structural and aerodynamic analysis. Deformed sail shape and stress distribution was calculated by a non-linear finite element method, using Oden and Sato triangular finite elements and Haug and Powell quadrilateral finite elements. Aerodynamic loads were evaluated by a non-linear vortex lattice method, with the correction of the wake and inclusion of viscous effect. The main contribution was the effort of improving the methodology, notwithstanding the difficulty of available data.

With regard to the sail design problem, certainly the contribution of Milgram, [43], [46], Jackson, [31], and Greeley [30], are relevant for the development of modern trends. However, this section omits the review of the entire collection of published works, considering the large number of design techniques and the numerous variables connected with sailing performance. Therefore, only some of the most important works, which have driven subsequent studies and connected with the subject of this thesis, are reviewed. Particular attention on studies concerning the implication of the sail loads evaluation on mast design is considered in chapters 8 and 9.

Sail design is indeed crucial for high sailing performance. Sails produce driving force therefore they are sailboat engines. As a result, another important discussion in the scientific community concerns the definition of sailing performance and which are the main variables involved. The majority of scientists agree with the basic fact that sailboats have to travel as fast as possible without capsizing, [65], therefore the way they perform this aim is different. Early works approached the problem by defining the optimal pressure distribution acting on the sail and building the correspondent sail shape. As mentioned above in this

section, Milgram [43] predicted a wide variety of sail plans, without verifying their feasibility. Jackson, [32], [33] stated two different approaches to obtain better sails: develop direct sail analysis methods, which yield information about the performance of particular sails, or predict the optimum sail under a given set of conditions. Further works intended to develop general design trends, without achieving convincing results. However, it is commonly believed that to analyse directly a particular sail shape, given the variety and high number of variables involved, does not ease the development of general principles governing sail performance. Therefore, since Milgram, who suggested the definition of models (idealistic and simpler) in order to get more general results, although the accuracy of the results becomes questionable, it is currently believed that the best way to improve performance is to analyse the specific case.

Therefore, a notable contribution is due to Haarstick, [21] who focussed on the design of the best sail in known given conditions and how to cut the panel to build it up. In the paper ‘Scientific Sail Shape Design’, [30], Greeley and others reported the principal problems involved in sail design and proposed a method. They believed that the main question in designing a sail shape concerns the distribution of sail loads along the luff, in order to generate high drive force and maintain its stability, which means lower heel force or even better heel force equal to the side force generated by the hull. Of course, this determines the decision of choosing sail plan-form shape, twist and camber distribution in the span-wise direction. They realised a sequence of aerodynamic calculations for obtaining the sail shape from a pressure distribution, which was retained as optimal. Indeed, this work constitutes the driven guide for all subsequent techniques developed for sail design, [25], [30]. Similarly, Day, [17], [18], [19], believed in this method for optimising the yacht speed by using the lifting line theory. He introduced the effects due to yacht configuration and wind gradient in the calculations for the lifting distribution along the span-wise direction.

Summarising, the above mentioned contributions bring forth the necessity of developing instruments of analysis which are easy to use and less expensive, since it has been recognised that remarkable differences exist among single cases.

In the event that the design goal is to win the race, as in the case of America’s Cup challengers, powerful as well as expensive computing instruments are applied. In recent years, Computational Fluid Dynamic packages (C.F.D.) have been aiding sail yacht

designers and, usually after the end of the race, results of any C.F.D. analysis are published, [14], [15], [50], [45], [25], not only for calculating sail loads but for the entire yacht. Once again methods developed and used extensively in the design and analysis for air and spacecraft have been extended to yachting design. The high computational power of those techniques facilitates reliable flow solutions around the yacht, as full-scale tests can be simulated without building the prototype. A C.F.D. analysis provides visual and numerical feedback of the potential flow around a model built by a grid generation phase. Currently, as C.F.D. techniques are applied in a very large number of problems, new improvements have been made for making the generation of grid faster and easier. Notwithstanding the numerous existent commercial packages based on C.F.D. techniques, this method is still very expensive in terms of time and power of employed machine. The consequence of these high costs is that normal sailmaking factories are unable to buy one of these similar software packages. Therefore they are only applied for America's Cup yachts, [50], [45].

2.3 Concluding remarks

The first chapter highlighted the need for accurate evaluation of the loads acting on the sails, in order to improve sail design and generally sailing performance.

This chapter has assessed critically the evolution and the state of the art of investigative methodologies and techniques for calculating the loads. High relevance has been given to the passionate development of the ‘art of sailing’, always connected with the efforts of winning the race. At the same time, new design trends have been described.

From published literature, it has been recognised that the large number of variables connected with the improvements in sail design determines the necessity of particular studies for any single design case in order to get better results. However, all the analysis techniques either full-scale test, wind tunnel tests or C.F.D. calculations are very expensive in terms of time, technology and people involved. The corroboration is in the fact that nowadays studies and results for single classes of sailing are available, whilst in the past there have been investigations about generic sails, achieving essential information about

sail behaviour. Furthermore, the above works denounce the poor availability of sail loads data to validate the results.

However, it is important to clarify that the above sections do not report all methods implemented for sail loads evaluations. With respect to the main aim of the thesis, the mentioned works are the most important references. In reality, other important references are mentioned and reviewed where appropriate in the remainder of the thesis, in order to avoid repetition.

In conclusion, since every technique has qualities and defects, none has been recognised as entirely appropriate. However, the importance of predicting and mapping the sail behaviour over the entire range of possible external conditions has been commonly recognised. Therefore, the current trend is addressed by putting efforts into developing computational instruments for generating sail geometric shapes and analysing them as flexible membranes under adaptable loads.

According to the above discussion, the integrated sail design and analysis system, presented in this thesis, responds to this need. Furthermore, the features described in the following chapters allow inexperienced persons to use the application on a simple personal computer. As a result the added value of this integrated system is in making sail design actions cheaper and easier than the currently available techniques.

The value of the integrated system presented in this thesis and the considerations referred to in this chapter have been substantiated by the opinions of John Highcock, who is co-founder and owner of one of the bigger U.K. sailmaker factories. He was interviewed by the author of this thesis, who believes that the history and the opinions expressed by him constitute indubitably the reality of the state of the art for the majority of sailmaking factories. In view of the fact that there is no existing integrated design system, which goes through all the sail design phases, permitting the visualisation of the geometry and results on the market, John Highcock considers positive its development and its marketing. Furthermore, he believes that if the cost of this system is sustainable and it is not very difficult to use, this system will make an important step ahead in sail design techniques currently used in the majority of the sailmaker companies. Reports on the important facts brought out during this interview are given in Appendix D.

Chapter 3

Analysis Method

3.1 Introduction

Sailboats sail through the sailing course under the aerodynamic propulsion developed by the interaction between wind and sails. As mentioned in chapter 1, the crew chooses the geometric sail shape for any given set of wind and sea conditions, boat speed and sailing course, in order to achieve an optimum sailing condition.

In order to ease these actions, every sail is required to be flexible and, at the same time, able to keep the assumed configuration. Therefore, sails are made with thin cloth, characterised by particular structural properties, which are better explained in section 6.1.1 and using proper constructive methods, illustrated in section 6.1.2. Briefly, opportune combinations of material and constructive methods entail flexible sails, which means besides versatile, adjustable, durable and usable over a wide range of wind.

The chosen sail-shape enables modulated intensity and direction of aerodynamic loads. The primary role played by the sails explains the significant interests of researchers and sailors regarding sails and their performance.

In operative conditions sails acquire aeroelastic behaviour. The flow generates a particular pressure distribution causing a deformation due to the sail flexibility. Therefore, it is necessary to consider the aeroelastic interaction when performing the sail analysis and evaluating the sail loads, [32].

This chapter presents the structure of the implemented analysis method. A full static aeroelastic analysis has been performed, complemented by data pre-processing and post-processing. In order to explain the reasons behind the assumptions and the choices made about the structure of the method, the emphasis has been put on the geometry and the physics of a sailing boat, focusing on a FINN class boat. The additional information constitutes an implementation of the description done in section 1.3. It is important to repeat here that the attention on the FINN class sailing boat is justified by the fact that the analysis is performed for a single sail system. Therefore, any other sailboat presenting a sail plane, with one sail, can be analysed. For example, this analysis system can be applied to the sail of a Laser. In this thesis, the FINN class sailboat has been preferred as it is an Olympic class sailboat and there are more published data available.

From the description provided, it is clear that the method presented does not only perform an analysis of the loads acting on a sail-shape, but is a simple and user-friendly integrated sail design system. Therefore, on one side, this integrated system increases the accuracy of the evaluation of sail loads, which is still a problem for sailboat designers. On the other side, through the possibility of reviewing and criticising the results, it permits the manipulation of the input data for further analyses in order to improve the sail design or to map the behaviour of a fixed sail shape at little cost.

These achievements respond to the actual requirements of sail designers, who currently use, for the external load evaluations, force coefficient tables extrapolated from wind tunnel tests or semi-empirical formula, as it was announced in the second chapter.

3.2 Geometry and physics of sailing

Consider a FINN class boat sailing to windward in smooth water, (figure 1.2 and 1.3).

In this case, sailing forces derive from the one sail, whose shape is formed from the combined action of the mast bend and the kicking strap forces and it depends on the initial isolated sail shape. The crew is composed of one helms-person, [70], who steers the tiller, moves the boom, bends the mast and helps the stability of the sailing moving his or her weight with a manoeuvre called hiking, [4].

The force systems acting on the boat are as follows, [41]:

- aerodynamic forces, $F_{Aerodynamic}$, due to the interaction between wind, sail and part of the hull, as plotted in figure 1.5;
- hydrodynamic force, $F_{Hydrodynamic}$, due to the interaction between the sea waves and the hull, as plotted in figure 1.6;
- weight-forces, F_{Weight} , due to the sail, the hull, spars, lines and the helms person.

To remain at constant speed in a given sailing course, the resultant of the forces and of the moments must be zero, (consider figure 3.3):

$$F_{Aerodynamic} + F_{Hydrodynamic} + F_{weight} = 0 \quad (3.1)$$

$$M_{Aerodynamic} + M_{Hydrodynamic} + M_{weight} = 0 \quad (3.2)$$

Consider a global coordinate system of axes (X_g , Y_g , Z_g), plotted in figure 3.1, with:

- X_g coincident with the centreline of the boat directed from aft to forward of the boat,
- Z_g coincident with the mast axes, positive in the upper direction, in its initial resting configuration, without bending,
- Y_g is orthogonal to the plane (X_g , Z_g), forming a right hand Cartesian coordinate system.

Considering all the possible sailing courses of a sailing boat (figure 1.7), it is evident that a part of the running configuration, overall the range between the close hauled course to the reaching, there is always a non-zero angle between the sailing course and the boat centreline. This angle is called *leeway angle* and it is indicated by the symbol λ , as figure 3.2-(a) shows.

As the boat moves along the chosen sailing course, the vector of the sailing speed V_{Sailing} has that direction. As a result of this motion, the wind velocity vector, seen by the boat, is not the real one, V_{True} , but is given by the sum of the vectors V_{True} and the sailing speed V_{Sailing} . This vector is called the apparent wind velocity V_{Apparent} and it is the result of the velocity triangle, as plotted in figure 3.2-(b). The angle formed between the apparent wind velocity V_{Apparent} and the sailing course is called *apparent wind angle* or *course angle* and is symbolised by β , plotted in figure 3.2-(a).

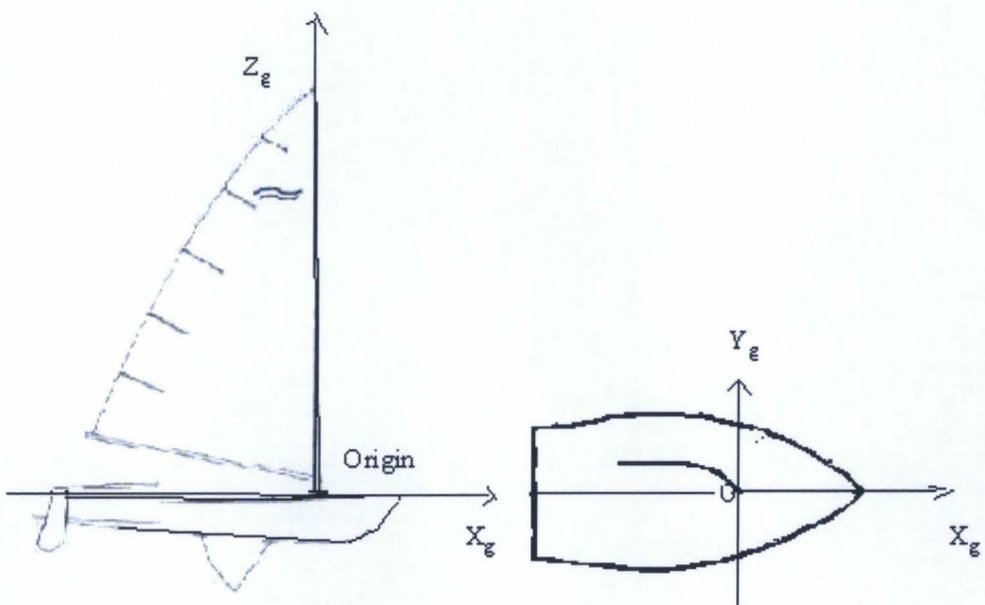


Figure 3.1: Global Cartesian coordinate system for the FINN.

Finally, as mentioned above, in a usual sailing condition, the crewmember ‘kicks’ the boom. The angle that the boom forms with the X_g axes is called *boom-sheeting angle* and is symbolised by δ_m , (figure 3.2-(a)).

In addition, usually the mast is bent and forms a non-zero angle with the initial configuration, which coincide with the Z_g axes. This angle is called *heel angle* and it is symbolised by θ , which does not include the bending of the mast in the fore-aft direction.

In order to explain the physical reasons behind this boat configuration described above, it is convenient to consider the vector components of the total forces along the sailing

course direction, the Z_g axes and along the orthogonal direction to the plane formed by these axes.

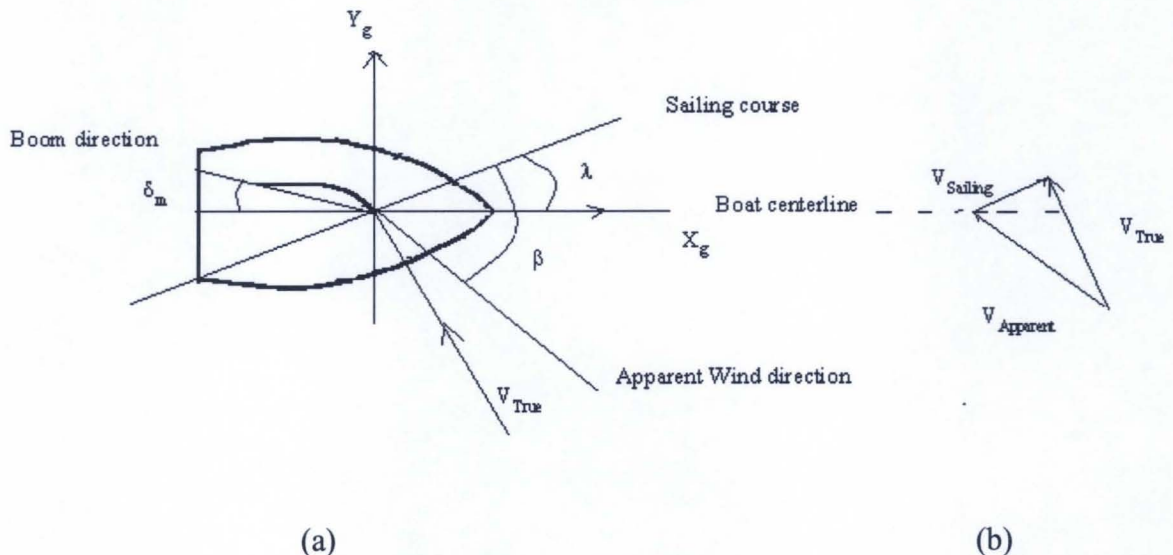


Figure 3.2: (a) Sailing angles description and (b) velocity triangle.

The vector components of the total aerodynamic force $F_{Aerodynamic}$ are, respectively:

- driving force, F_{Drive} (or thrust),
- aerodynamic vertical force, F_{V-Aero} ,
- side force or heeling force, F_{Heel} , which is not necessarily orthogonal to the Z_g axes.

Equally, the vector components of the total hydrodynamic force $F_{Hydrodynamic}$, are:

- water resistance, R
- hydrodynamic vertical force, $F_{V-Hydro}$,
- hydrodynamic side force, F_S which is not necessarily orthogonal to the Z_g axes.

It should be kept in mind that weight forces W act along Z_g when the boat configuration is not heeled, like it is considered in the present work.

Since the above groups of forces do not act along the same axes and they have different application points, given the first is applied on the sail and the second on the hull, they produce moments, which are:

- pitching moment M_p due to the driving force F_{Drive} and water resistance R ,
- rolling moment M_R due to the side forces F_{Heel} and F_s ,
- yawing moment due the total aerodynamic force M_{Y-A} , and the total hydrodynamic force, M_{Y-H} .

The helmsman needs to find a proper sail-shape, a trimmed boat configuration and an opportune position for his weight, in order to produce a system of forces, which satisfy the equilibrium equations 3.1 and 3.2. Those equations can be written in the form below that follows the decomposition described above.

$$F_{Drive} + R = 0 \quad (3.3)$$

$$F_{Heel} + F_s = 0 \quad (3.4)$$

$$W_{Sail} + W_{Hull} + W_{crew} + F_{V-Aero} + F_{V-Hydro} = 0 \quad (3.5)$$

$$M_p + M_{p-w} = 0 \quad (3.6)$$

$$M_R + M_{R-w} = 0 \quad (3.7)$$

$$M_{Y-A} + M_{Y-H} = 0 \quad (3.8)$$

In reality, the effect of the turning moments arising from the presence of the aerodynamic and the hydrodynamic side forces produce a tendency, known as weather helm, to turn the boat toward the wind, which the helmsman is aware of as he/she moves the tiller to turn to leeward. Thus, the sailboat leans to leeward and the mast forms a heel angle, θ , from its initial position.

Therefore, in the case of a FINN class sailboat, in order to establish a stable condition the sailor reacts by leaning over the opposite side of the boat to counteract the heel. Clearly, in order to satisfy the equations 3.5, 3.6 and 3.7, the helmsman hikes in order to produce, with his weight as well as the hull weight, two moments, named M_{p-w} and M_{R-w} , which

counteract the pitching and the rolling tendency of the boat. Thus, usually, the corresponding stable configuration to pitch and roll requires a non-zero heel angle, θ .

Considering that equations 3.5, 3.6 and 3.7 are satisfied, the remaining equations involve only the force components acting in the plane (X_g , Y_g), as figure 3.3 shows.

Specifically, they are:

$$F_{Drive} = -R \quad (3.3)$$

$$F_{Heel} = -F_s \quad (3.4)$$

$$M_{Y-A} = -M_{Y-H} \quad (3.8)$$

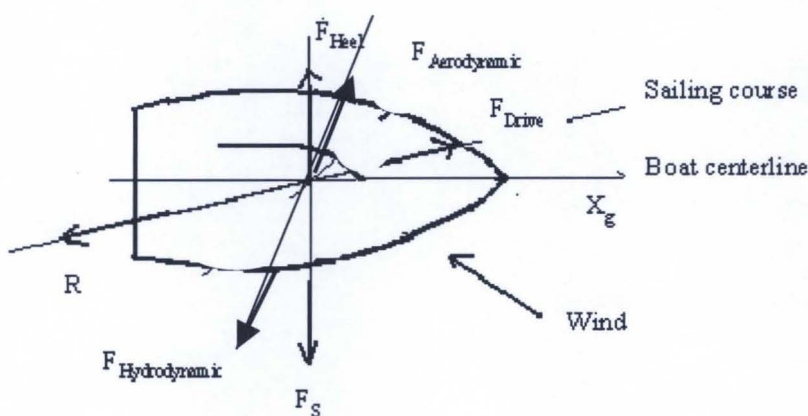


Figure 3.3: Forces acting on a FINN sailboat in an equilibrated configuration

From figure 3.3 and the equations 3.3, 3.4 and 3.8, it is clear that in order to achieve a stable sailing condition, the helmsman has to shape the sail and trim the boat to establish the equilibrium between the total aerodynamic force $F_{Aerodynamic}$ and the total hydrodynamic force $F_{Hydrodynamic}$. In addition, it justifies the fact that a trimmed sailboat configuration is characterised by the presence of the leeway angle λ , the boom sheeting angle δ_m and the mast bend. For the same reasons, the sail presents a particular shape, whose geometry will be presented in the next chapter.

Summarising, in the hypothesis that by hiking the helmsman balances the vertical forces as well as the roll and pitch tendency of the boat, for given external conditions, the solution of the three remaining equations gives a stable sailing configuration.

The equations system establishes the equilibrium between the following two systems of forces:

- aerodynamic forces, F_{Drive} and F_{Heel} , which depend upon the apparent wind velocity vector, $V_{Apparent}$ and β ,
- hydrodynamic forces, R and F_S , which depend upon the sailing boat velocity, $V_{Sailing}$ and λ .

Thus, there are further unknown variables, which are the leeway angle λ , the boom sheeting angle δ_m , the sailing velocity $V_{Sailing}$, described by the triangle of the velocity.

Therefore, the configuration corresponding to the equilibrium is the result of a compromise among the entire nine unknown variables mentioned above.

Furthermore, it is important to underline that there is a strong interaction between the two systems of forces, as the block scheme in figure 3.4 shows, which causes a transition period for adjusting the configuration.

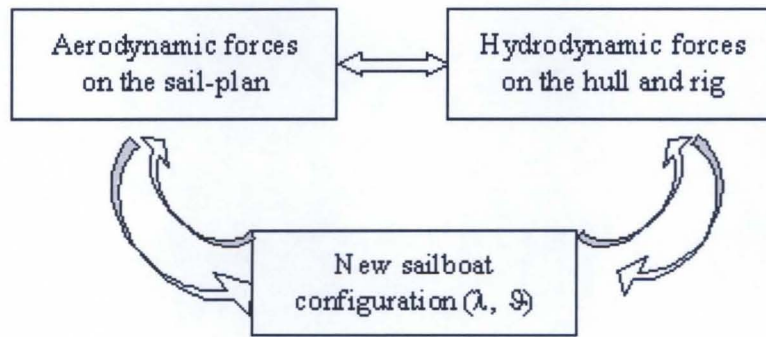


Figure 3.4: Interaction between the aerodynamic forces and the hydrodynamic forces

As mentioned in chapter 1, the chosen course sailed as well as the configuration achieved by the adjustments of the helmsman as described in this section, do not correspond to the optimum in terms of sailing performance. In fact, in the event that a

sailboat is starting to move towards the wind, the aerodynamic forces, generated by the sailplane, determine the angles of leeway and heel. The hydrodynamic forces produce a variation on both the angles, determining an unstable configuration. Thus, the sailor, hiking, steering the tiller and kicking the boom, tries to find the stable configuration, which usually is an optimum compromise between these tendencies.

3.3 Aeroelastic sail behaviour

The solution of the equation system 3.3 - 3.8, is more complicated than described above, because of the aeroelastic behaviour of the sail, which this section illustrates.

For the duration of the transition period due to the interaction between the hull and sail, as described in the previous section and plotted in figure 3.4, another important phenomenon is present. Considering only the generation phase of the aerodynamic forces for a chosen sail-shape, the flow around the sail plan generates a particular pressure distribution, which depends upon the geometric characteristics of the sail shape. By virtue of its flexibility, the aerodynamic pressure generated can deform its shape. Then, again, on the new sail-shape, the same flow will cause different aerodynamic forces and so on.

This iterative process, which figure 3.5 represents, continues until the sail-plan assumes a particular shape, characterised by an internal stress distribution, which is in equilibrium with the external force configuration. For each of these sail loads set, there will be a corresponding new set of hydrodynamic forces. Further details are in Appendix A.

Then, aeroelasticity is essential in this context, [33]. In fact, on one hand the flow around the sail depends upon its shape, but, on the other hand, the pressure resulting from the flow determines the shape of the sail. Naturally, the incidence of this phenomenon depends upon the sail cloth material properties and the external conditions (figure 3.5). Appendix A provides more details regarding the definition of the sail behaviour seen as aeroelastic.

As a direct consequence of this characteristic behaviour, the evaluation of the aerodynamic loads acting on a single-sail requires that the structural and aerodynamic analyses must be solved simultaneously.

For given set of external condition: $V_{Apparent}$, $V_{Sailing}$, β
and for a given structural sail cloth properties

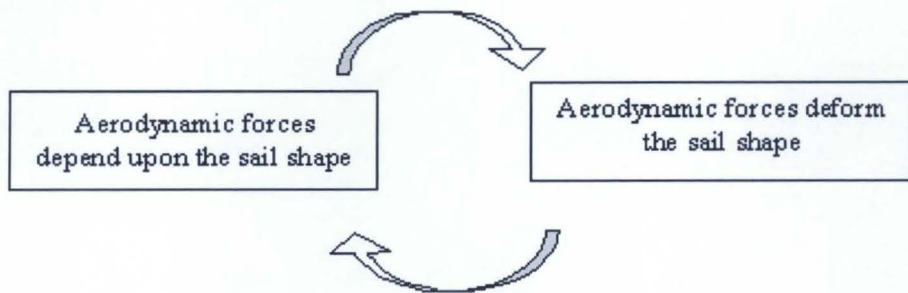


Figure 3.5: Aeroelastic behaviour of a sail-plan.

3.4 Iterative analysis process

It is useful to state here that the area covered by this work consists of calculating the active loads on a sail, when the transition period has finished. Then, the object of the analysis is the sail-shape corresponding to the equilibrated configuration for a sailboat. Further details about the assumptions made are stated in the next section.

This paragraph illustrates the structure of the iterative analysis implemented to calculate the loads acting on the sail, in an equilibrated configuration, taking into consideration its aeroelastic behaviour.

As suggested by Jackson [31], [33], the obvious as well as popular approach to this problem consists of splitting the problem into two. Firstly, the aerodynamic loads acting over a known sail-shape are computed. Since their action deforms the sail shape and the new sail configuration depends on its structural properties, a structural analysis is performed to give the new sail shape. For this new configuration, the aerodynamic loads are calculated again. The final solution is obtained by using an iterative analysis process, which involves both aerodynamic and the structural analysis solutions.

Figure 3.6 displays the approach employed for the aeroelastic analysis of a sail shape in a real sailing condition. As shown, the method provides:

- 1) a data acquisition phase, concerning the sail-shape geometry and the trimmed boat configuration,
- 2) the automatic generation of the sail geometric shape and the possibility of interactive adjustments,
- 3) the definition of a panel model and the aerodynamic analysis;
- 4) the definition of the finite element model and the structural analysis under the external loads, evaluated from the previous aerodynamic phase,
- 5) the iterative process between the two analyses until convergence is achieved;
- 6) the visualisation of the results.

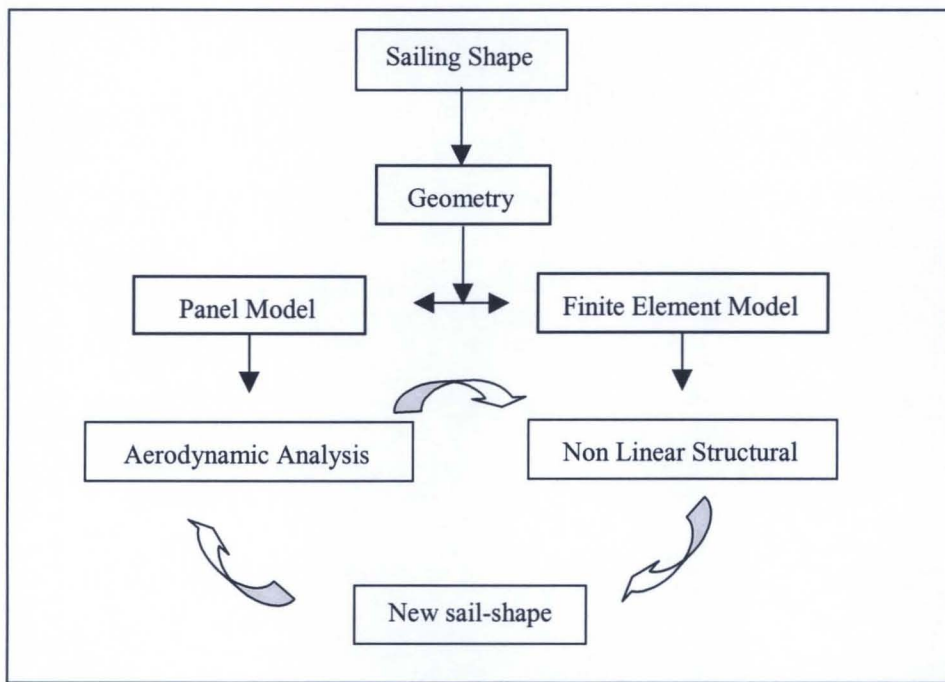


Figure 3.6: Aeroelastic analysis procedure.

This iterative process calculates the pressure distribution for the given sail, as a result of the aerodynamic analysis. It then performs the structural analysis, applying the evaluated external loads, estimating the stress distributions and the deformed sail-shape. On this obtained sail geometry, the aerodynamic analysis is performed again until the equilibrium between the evaluated external loads and the corresponding deformed sail shape is

obtained. The systematic and versatile graphical user interface has been developed in order to provide the user with a tool that facilitates the performing of all these actions. This G.U.I. provides important design features, as it enables reviewing the results and re-designing a test case.

The following chapters explain how the above phases have been developed following the listed sequence. In addition, they describe the graphical user interfaces implemented.

3.5 Analysis method assumptions

The assumptions made in the analysis method are:

- absence of hull influence;
- absence of the mast and boom influence;
- fixed equilibrated rig configuration: heel angle θ , boom sheeting angle δ_m , course angle β , leeway angle λ .

The first assumption confirms that the aerodynamic forces developed around the part of the hull out of the seawater are ignored. Thus, the only influence on the sail is due to the deck and the sea surface, which are considered belonging to the same plane orthogonal to the mast in its initial configuration.

The second assumption comprises the following double hypotheses: the presence of mast and boom do not affect sail-shapes as well as the sail aerodynamic force.

As it will be described in detail in chapter 9, masts are flexible structures, which under normal working conditions, are bent. The assumption made here implies that the mast bent configuration is constant and it does not change during the entire iterative process, otherwise, the curvature of sail luff curve has to change, due to the fact that it coincides with the mast axes. However, in view of the fact that the object of the sail load analysis is equilibrated, the mast configuration is supposed to be in equilibrium with the loads transmitted by the boom and sail. Thus, if this hypothesis is not very restrictive for the structural point of view, it omits the aerodynamic flow implications of the influence of the presence of the mast on the flow field generated on the sail.

In addition, confirming that the mast and boom presence does not affect the aerodynamic forces is more restrictive. In fact, in the majority of sailing conditions behind the mast separation bubbles are formed and both the spars induce turbulence.

The third assumption, which means that the trimmed as well as the sailing configuration are fixed, considers that only the sail geometry can undergo deformations. Thus, the analysis method, henceforth used, does not consider the influence of the loads acting on the sail on the sailboat configuration.

In conclusion, it is important to clarify the versatile use of the loads calculated by the routine presented in this work. In fact, they can be used by external codes in order to overtake the restrictions described above in the following ways:

- external loads to apply at mast structural analysis solver, in order to evaluate the deformation of the mast;
- external potential solution, in terms of velocity distribution, for calculating the boundary layer solution and introducing the mast presence effect on the loads distributions;
- sail loads for V.P.P. methods or other solvers in order to appraise the influence on the boat trimmed configuration.

An example of the feasibility of the first two listed operations has been carried out and the results are shown in section 9.3. The demonstrated versatility of the present system is believed to be one of its most valuable features.

Chapter 4

Initial Phase

4.1 Data acquisition

The proposed integrated design system brings forth the issue of building the geometry of a sail shape. This chapter describes the technique utilised for constructing the sail surface from the introduction of the input data to the complete development of models, which are to be used for the subsequent analyses. In parallel, it illustrates the related graphical user interfaces.

In view of the fact that the integrated design system allows:

- analyses for existent sail-shapes,
- modifications of their geometry to test further performance,
- creations of new sail-shapes,

the first problem encountered consists of developing the geometry of the sail-shape and proper models, for subsequent aerodynamic and the structural analyses.

Therefore, in both cases of analysis or geometrical modifications of a known shape, the major complication concerns the collection of useful available geometric data for developing the geometry as close as possible to the actual sail shape.

In the eventuality the tool is used to design a new sail shape the problem is to input the geometric data in a manner which enables shape development.

However, in order to develop the sail geometric shape, firstly the selection and organisation of the input-data has to be addressed. Thus, the question concerns the choice of which data are necessary, how to obtain and structure them. Naturally, the relevance of these questions pertains more to the analysis of existent sail-shapes, as the search for suitable data on known shapes is not straightforward. However, after several searches on the current data available, the type of data and its organisation have been standardised for use within the system. The developed system for the geometry remains, however, very versatile, as it permits data modification and enhancements in the geometric generation phase, as described later in this chapter. The reasoning and presentation of the systematic organisation for the input-data is presented below.

The capture of geometric data for a sail-shape in working condition has been a problem tackled by several and diverse methods. The latest sail development system, [78], which is considered in this work, is the photographic technique. This consists of taking pictures of the sail-shape and the rig, when the crew considers that the sailboat is sailing at maximum efficiency in an equilibrated configuration. In brief, a camera, fixed at the top of the mast, photographs the sail (see photograph in figure 4.1).

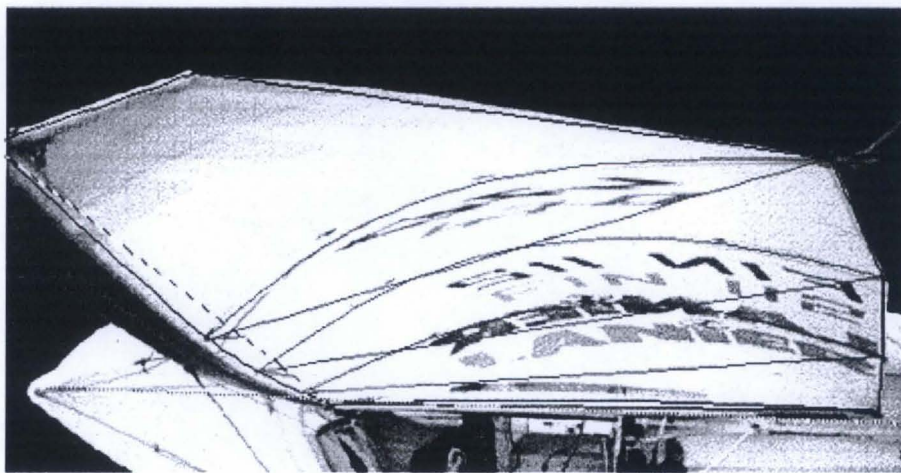


Figure 4.1: Typical picture taken by a masthead camera. Notable is the drawn pattern to evaluate the geometrical characteristics.

The most important feature of this photographic technique is the possibility of capturing the real sail shape, when the performance is considered optimal. A computer program analyses the photographs to determine the shape parameters. Tables 4.1 and 4.2 pictures a typical chart result of the sail-shape analysis. Nowadays, this method is very popular, mainly because it is possible to obtain information about the geometric parameters of the real sail surface, and the errors are negligible. For instance, the sail-maker factory WB-Sails use this technique and their web site, [78], provides the result of an example of a sail shape description, given in tables 4.1, 4.2.

Sail name:	Finn	Photo date:	6/95
Model: WB light			
Rig measurements			
Mainsail luff:	5,750 m	Foot:	3,270 m
J-measurement:	2,050 m	Mast rake at	0,550 m
		I-measurement	4,100 m
		Boom height	0,500 m

Table 4.1: Chart resulting from the photograph analysis for the rig of WB-Sails FINN, [78].

	Sheeting angle: 10,3°	Foot depth: 7,3%	Twist at head 11,5°			(ref. to boom)	
	Max depth	Position of max depth	Twist referred to boom	Twist ref. boat centerline	Entry angle ref. to local chord	Exit angle ref. to local chord	Mast bend
Lower draft stripe 25% from bottom	12,7%	45,1%	2,3°	12,6°	31,7°	-22,9°	114 mm
Middle draft stripe 50% from bottom	13,5%	47,5%	3,8°	14,0°	26,2°	-19,9°	146 mm
Upper draft stripe 75% from bottom	-13,6%	148,1%	6,7°	17,0°	23,3°	-21,2°	104 mm

Table 4.2: Chart resulting from the photograph analysis for the sail of WB-Sails FINN [78].

Considering table 4.1, the available lengths of the luff, foot and mast, and the boom height on the mast are the rig descriptive data.

Table 4.2 provides the boom sheeting angle, δ_m , the foot curve curvature and the twist angle between the head section chord and the boom. Regarding the sail, the acquired data

are related only to a few sections, three or four. Usually, the considered sections are at the 25% (lower), 50% (middle) and 75% (upper) of the luff curve. Reading the table from the left to the right, for each of these positions, the acquired data are in sequence, namely:

- camber, or maximum depth, in percentage of the sail section chord;
- draft, or position of maximum depth, in percentage of the sail section chord;
- twist referred to the boom, which is the angle between the section chord and the boom, or commonly called local twist;
- twist referred to the boat centreline, which is the angle between the section chord and the boat centreline, equal to the local twist plus the boom sheeting angle, δ_m ;
- entry angle referred to the local chord, which is the angle between the section leading edge tangent and the local chord;
- exit angle referred to the local chord, which is the angle between the section trailing edge tangent and the local chord;
- mast bend.

Summarising, data are available usually for three sail sections. Further, each section is described by camber and draft and the angles formed by the tangents at the starting and ending point with the boom direction. Regarding the position of each sail section in the global system of coordinate, it is defined by the twist angle of the chord relative to the boom and the boom-sheeting angle.

4.2 Input data G.U.I.: description and use

In view of the fact that the above listed data are commonly available, the graphical user interface, implemented for this phase, follows the scheme suggested by the tables 4.1 and 4.2. Figure 4.2 plots the Input data G.U.I..

Briefly, looking at the top-right section of this figure, there are editing spaces concerning the external geometric shape of the sail, defining lengths of luff, foot and leech, as well as some rig measurements, such as lengths of mast, boom and the maximum deflection of the mast at the tip. At the bottom of this section, there are spaces for the angles defining the

configuration of the rig on the boat, the boom sheeting angle, the heel and the leeway angle, which define the boat sailing course. Furthermore, along the bottom of the G.U.I., there are the editing spaces for the previously listed five entries, usually known for the lower, middle and upper sections.

In order to analyse an existent sail-shape for the first time, once the data are available, it is possible to type them in the input interface (figure 4.2) and save to a file, by clicking on the ‘Save’ button.

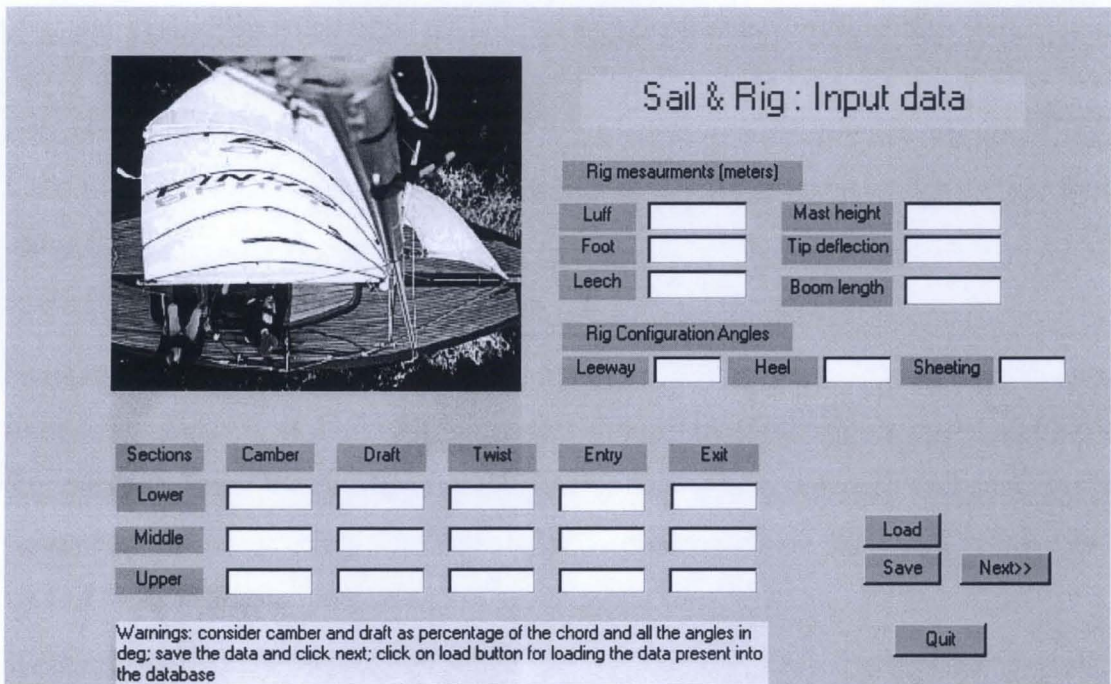


Figure 4.2: ‘Input Data’ Graphical User Interface.

In the event of designer actions, it can happen that the data for a particular sail-shape have been already saved once and the designer might use them again, for example, to analyse the same sail-shape for different external conditions and/or changing material properties. In this case, it is possible to review those data on the screen, by using the ‘Load’ button, perform any editing and save the new data set, by clicking on the ‘Save’ button.

Figure 4.3 shows the Input data G.U.I., in the case where the data listed in tables 4.1 and 4.2 have been inserted. Once this Input data interface has been completely edited, as figure

4.3 shows, the process for the development of the geometry starts, by clicking on the 'Next' button. The 'Quit' button naturally permits closure of the work session.

Before illustrating the next step, it is important to clarify some points. Firstly, the data are saved in a mat-file called *inputdata*, where the data related to the sail are organised in column vector format.

Then, as the next paragraph describes, the sail geometry process needs five sections. Therefore, the foot and the head sections have been added, using the data for the lower and upper sections, respectively. However, it has to be clarified that these initial approximations allow starting the calculations for the sail-surface geometry and that they may be edited in the geometric phase. Obviously, this happens for the entire data set apart from the foot length chord, which is taken directly from the input-data G.U.I., and the twist angle, which is set to zero, as the other twist angle inserted for the remaining sections are referred to the boom.

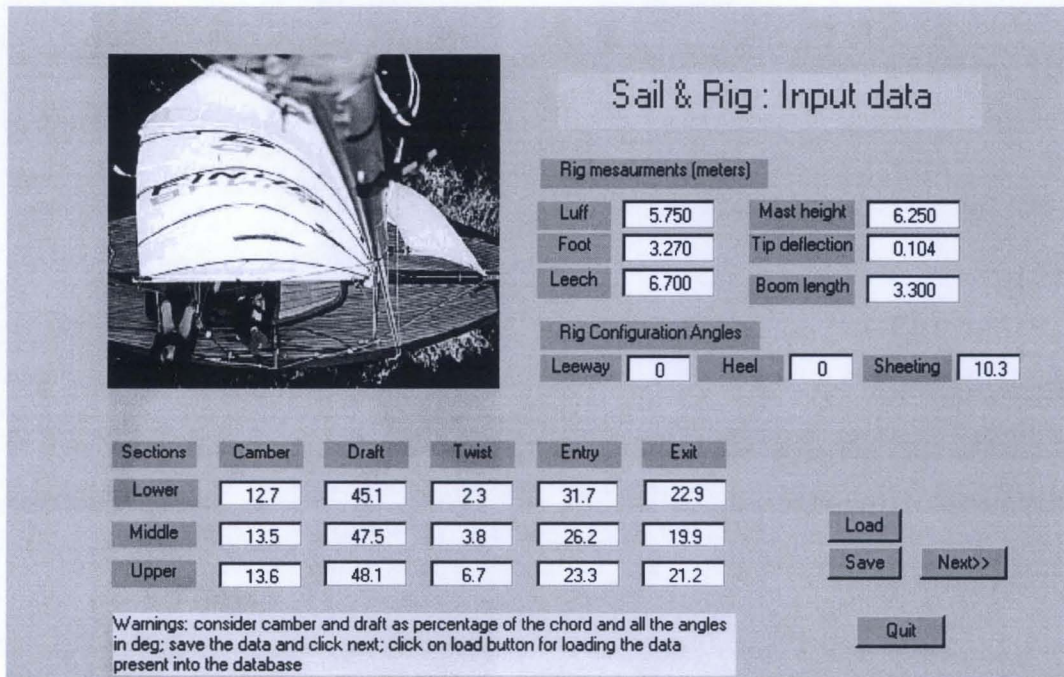


Figure 4.3: The edited 'Input Data' G.U.I with the data from tables 4.1 and 4.2.

In addition, the mat-file *inputdata* has to be located in the same directory of the running package.

When finished, the new saved set of data is written to the same mat-file, deleting the previous version. In the eventuality that a data item is changed in the following G.U.I.s, this change will not affect this data file. Only changes made in this present interface affects the initial *inputdata* file.

4.3 Development of the geometric sail surface

This section describes the method applied to construct the geometry of the sail surface as close as possible to the real sail. The associated graphical user interface is described in the following section.

Briefly, the geometrical data for the external dimensions of the sail, as well as the data for five sections, are stored in a file.

In order to tackle the generation of the sail geometric surface optimising the use of these data, two further coordinate systems have been introduced with respect to the global system, as defined in figure 3.1. Considering figure 4.4, there are two local coordinate systems: one is indicated by (o, x, y, z) defined as:

- the origin, o , coincident with the intersection between the plane containing the considered section and the luff curve;
- the x -axes, x , coincident with the local chord,
- the y -axes, y , belonging to the section plane and orthogonal to x
- z coincident with Z_g .

The second has:

- the origin, O , coincident with the origin, o , of the above-described coordinates system,
- the x -axes, X , coincident with the boat centreline,
- the y -axes, Y , orthogonal to the boat centreline,
- Z coincident with Z_g .

Therefore, the angle between these two coordinate systems is equal to the boom sheeting angle, δ_m , and with respect to the global system the latter by the height translated of the quote of the section considered, indicated by Z_o .

Each section is then developed in the coordinate system (o, x, y, z) using the Bezier method, [26]. In fact, in this system the section belongs to the plane (o, x, y), which eases the definition of positions and tangents to the starting point, the point of maximum curvature and the ending point. Once a sail section has been calculated, it is convenient to transform the entire sections in the system (O, X, Y, Z) and finally into the global system.

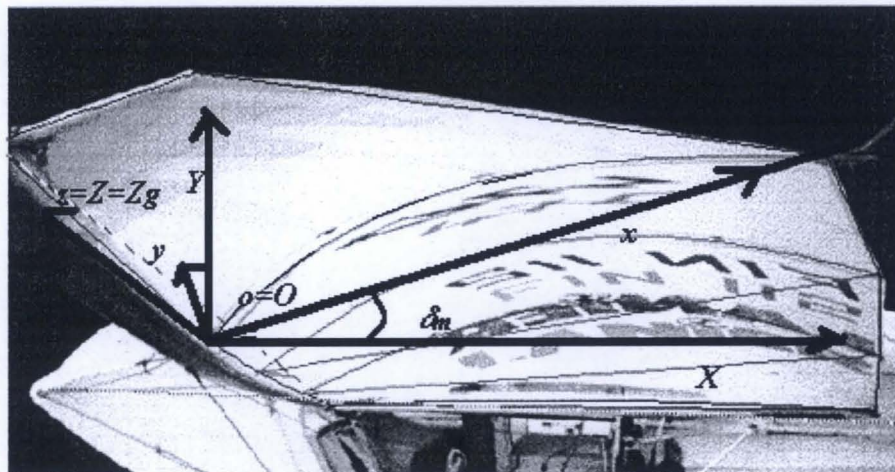


Figure 4.4: Local coordinate systems (x, y, z) and (X, Y, Z)

However, the main issue is the development of the geometry of a complete sail. The method applied in the present work is due to Byoung, Ha-Yong and Woo, [3], which permits the development of a three-dimensional surface. The reasons behind this choice are associated with the capabilities of this method in developing a smooth surface using only the few data available, avoiding local flatness and bulge. This is illustrated in the brief description of the method, given below.

This method enables the construction of the sail surface by combining patches of surface, drawn between the sections, where the data are known. Thus, as aforementioned, each section is built as a cubic Bezier curve. Then, it is transformed into a sextic Bezier curve. At this point, to develop a patch between two successive sections, sets of ‘off-boundary’ and of ‘internal’ control points must be found. The first set gives a condition of continuity between two patches. This condition makes the tangent planes to the two patches coincident. The ‘internal’ set of control points permits the development of the considered patch with more points. These points are located on the curve orthogonal to the two

following sections. Therefore, each patch of the surface is built between two sections and three curves, which links the starting points, the maximum curvature points and the ending points. These curves in the orthogonal direction are also Bezier curves. By interpolating the entire set of points, it is possible to describe a three-dimensional surface. Further details are in the reference paper. Here, the interest is in pointing out how the method has been implemented and its integration with the graphical user interface developed. Therefore, the descriptions of the G.U.I.s related to this phase follow in the next section.

4.4 Geometric Phase Graphical User Interface

As mentioned at the end of paragraph 4.2, clicking on the ‘Next’ button of the Input Data G.U.I. opens the window for the graphical user interface for developing the three-dimensional sail surface geometry.

As figure 4.5 shows, a geometric sail surface is generated automatically, which does not appear regular and smooth as predicted. Nonetheless, the fact that this geometry is the result of the code implemented using the given data, the distortions are due to three main approximations. In fact, in order to start the calculation, the data for the foot and head sections are automatically generated, as mentioned in paragraph 4.2. In addition, default values have been established for the positions of the Bezier control points along the tangents for each section and for the tangent directions at the luff, draft and leech curves for developing the surface patches. However, looking at the G.U.I. developed for this step, it is important to note its features. On the bottom of the graph, which plots the current state of development of the sail surface geometry, there are two slider buttons, ‘Azimuth’ and ‘Elevation’. Clicking on these changes the point of view of the graph. In this way the designer can verify if the geometry is satisfactory.

On the right of the G.U.I., there is a column of ‘push’ buttons. Each button opens a graphical user interface. In order, from the top to the bottom:

- ‘u Edit’ opens the G.U.I. which allows editing of each sail section, as section 4.4.1 describes;

- ‘v Edit’ opens the G.U.I. which enables editing of the luff, draft and leech curves, as section 4.4.2 illustrates;
- ‘3D Mesh’ opens the G.U.I. which permits decisions to be made about the distribution of the nodal points for building up the models for the aerodynamic and structural analyses, as section 4.4.3 demonstrates;
- ‘Aerodynamic Analysis’ opens the G.U.I. for performing the aerodynamic analysis, as chapter 5 explains;
- ‘Structural Analysis’ open the G.U.I. for performing the structural analysis, described in chapter 6;
- ‘Back’ button allows reviewing Input Data G.U.I.,
- ‘Quit’ button abandons the analysis.

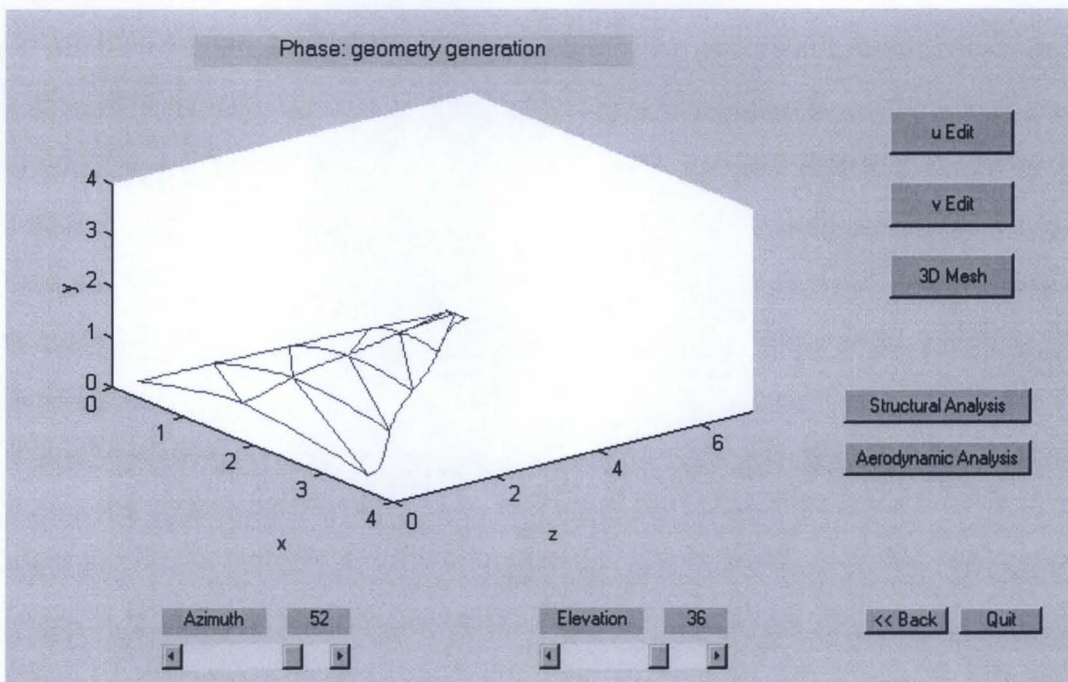


Figure 4.5: ‘Menu’ G.U.I. for the geometric surface development.

4.4.1 Sail section definition

As aforementioned, clicking on the ‘u-Edit’ button opens the G.U.I., which allows interactive modifications of the sail sections. Figure 4.6 shows this interface, as it appears after pushing the ‘u Edit’ button. The graph plots the foot section in the plane (o, x, y).

Since the geometric method develops the full sail surface among five sail sections, this interface permits operations on the sections, one after another from the foot section, which correspond to section number 1 up to the head section. Therefore, looking at the top of the list on the right side of the G.U.I., the number related to ‘section’ indicates which section is currently edited, (in this case, the graph plots the foot section) and all operations carried out in this phase affect only this section.

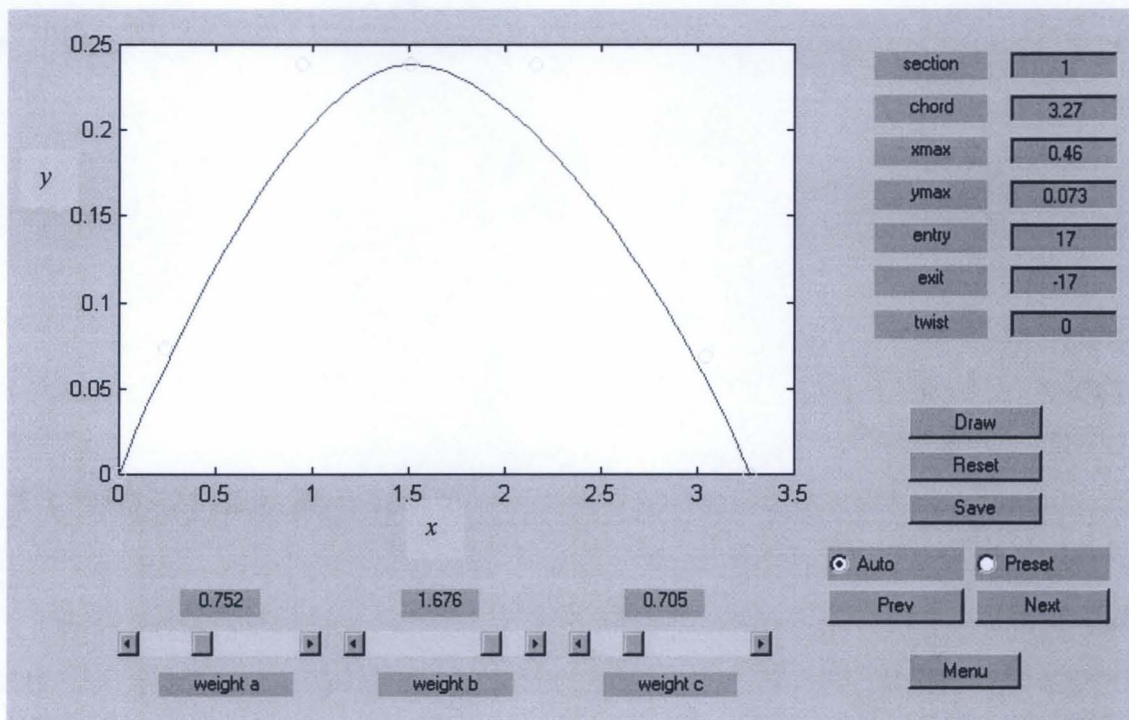


Figure 4.6: ‘u-Edit’ Graphical User Interface.

As can be seen, the column of editing buttons on the right side displays the data related to the foot section, as they have been introduced in the ‘Input Data’ G.U.I. (see figure 4.3). In this phase, it is possible to make adjustments interactively for all the entry parameters.

In accordance with the design system features, as listed in section 4.1, and those of the related G.U.I., this phase allows improvements to be made to geometrical description of the sail sections in several ways, which are described below.

In the event that the design requires the analysis of an existent sail-shape, since the foot and the head section data have been almost generated automatically, as mentioned in section 4.2, this phase allows adjustments which introduce the real available data. Furthermore, as each section has been drawn using default data for the positions of the control points on the tangent at the starting, middle and ending points, by moving the slide buttons for ‘weight a’, ‘weight b’ and ‘weight c’, they can respectively be changed. Naturally, these interactive changes continue until the section shapes seem better defined. Clicking on the ‘Save’ button saves the shape, when it seems to be optimised.

In the event the designer wishes to check modifications in the geometry, in order to test the new performance, or to optimise the invented geometry, this G.U.I. allows changes to the entire set of parameters, as they have been introduced in the Input Data G.U.I..

Furthermore, the G.U.I. provides the possibility of:

- verifying the section shape corresponding to any change in the parameters, by clicking on the ‘Draw’ button;
- reviewing the previous saved shape by clicking on the ‘Reset’ button, which undoes the entire set of changes made, but not saved;
- saving the best drawn shape and its set of parameters by clicking on the ‘Save’ button;
- screening how the changes have affected the full geometrical surface, by clicking the ‘Menu’ button, which, returning to the geometric phase interface, pictured in figure 4.5, plots the sail surface with the current set of saved section shapes;
- plotting the section in the local co-ordinate system (O, X, Y):
 - by clicking the ‘Preset’ button,
 - or zooming it, by clicking on ‘Auto’;
- re-evaluating the previous section, by clicking on the ‘Prev’ button;
- continuing with the next section, by clicking on the ‘Next’ button.

Concluding, it is important to state that the entire set of changes saved in this interface do not affect the initial data entered in the Input data interface of figure 4.2, as well as the inputdata file. In this way, the designer can re-load the initial geometrical data.

4.4.2 Luff, draft and leech

Through the ‘Menu’ G.U.I. (figure 4.5), the geometry of the vertical curve of the sail surface can be improved by entering the ‘v Edit’ G.U.I.. Figure 4.7 shows this interface as it appears after pushing the aforementioned button. From the left, the two graphs plot the view of the luff curve, which is the sail leading edge in the coordinate planes (O, X_g, Z_g) and in (O, Y_g, Z_g), respectively. The plots allow accurate examinations to be made of the geometric definitions of these vertical curves, as they are three-dimensional.

In order to construct a set of control points for the employed geometric method, two surface patches are built between any two subsequent sections:

- one between the luff and draft, which joins the points of maximum curvature of the five sail sections,
- one between the draft and the leech, which is the sail trailing edge curve.

A consequence of the fact that there are four patches in the vertical direction on the sail is that each curve, for instance the luff, is formed from the assembly of four curves, built between the starting points of two subsequent sail sections using the Bezier technique. The unification of these four parts of the curve implements the condition of tangent continuity at the joints, which maintain smoothness.

Notable is the fact that, as for the starting input data, little information is available regarding the above-mentioned curves, apart from the position of the trailing, draft and leading edges of the sail sections. The first plotted curves are therefore more approximate than the sail sections for the same state. In view of the fact that these curves are three-dimensional and considering the lack of the initial information, extra effort has to be spent in this phase to improve the initial geometric definitions.

This interface allows improvement to be made to the geometry of the luff, draft and leech curves, by operating interactively on their defining parameters. To start the calculation the code provides a set of default values for the inclination of the tangent and the control point positions for the sail section, which can be changed appropriately.

Looking at the top of the list of the editing buttons on the right side of this G.U.I., figure 4.7, the ‘location’ field indicates the curve which is currently being edited. Then, there are four fields for editing the azimuth (‘azim’) and the elevations (‘elev’) of the tangents for the current curve at the ‘top’ (corresponding to the head section) and bottom (meaning the foot section). Further, the shape of each sail curve, luff, draft and leech, can be improved by repositioning the control points at the bottom and top, by moving respectively the ‘weight bott’ and ‘weight top’ sliders. Apart from the aforementioned buttons, this G.U.I presents a set of buttons on the bottom right, which operate like those in the ‘u-Edit’ interface (see for the relevant descriptions section 4.4.1).

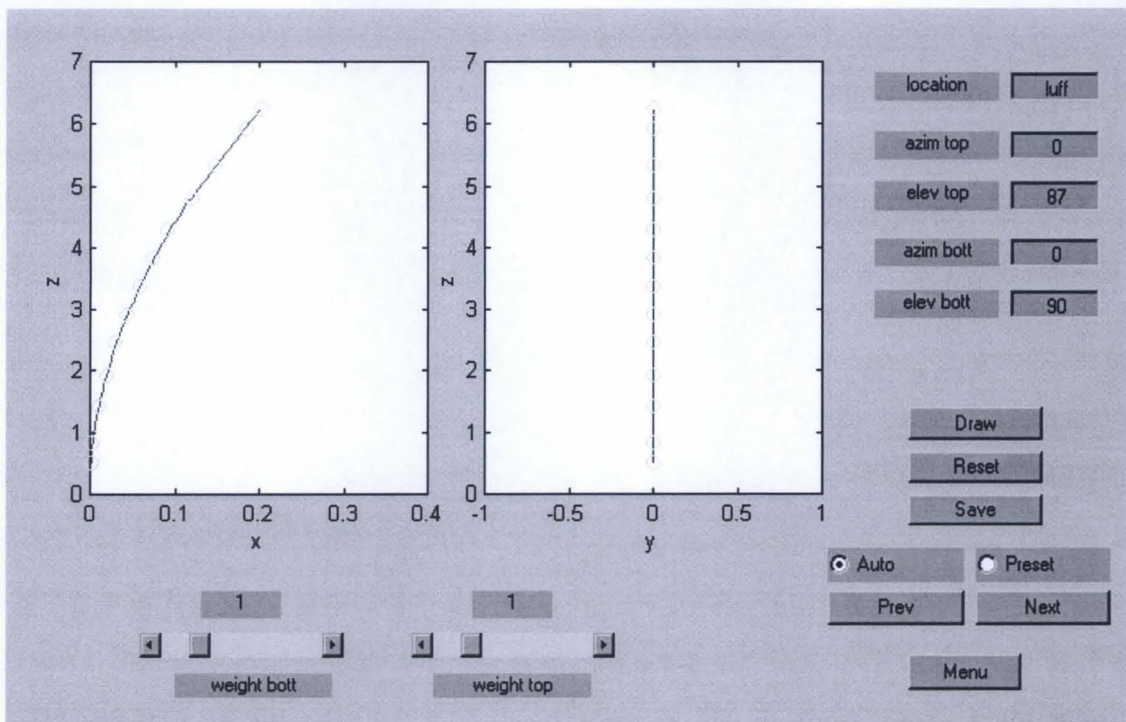


Figure 4.7: ‘v-Edit’ Graphical User Interface

For clarity, figure 4.7 plots the optimal luff curve shape, in case of fore-aft mast bend. However, this geometric method and G.U.I allows the possibility of lateral mast bend.

There are two final considerations related to this phase. The first pertains to the fact that the shapes of these curves depend on the sail section shapes, therefore they have to be edited once the sail sections have been well defined. This means that at this stage of the geometric definition, the particular intent of the sail-designer does not matter.

Secondly, as for the sections generation phase, the current data saved in this stage, illustrated in the ‘Menu’ G.U.I., whether it does not change the initial input data.

4.4.3 Panel Model and Finite Element Model

The ‘Menu’ button in the ‘u Edit’ and in the ‘v Edit’ G.U.I.s recall the interface, which plots the full geometric surface, with the current changes made in the previous interfaces. Therefore, when the designer considers that the geometry is satisfactory, the geometrical generation phase is concluded.

Consider the geometry of the sail surface plotted in figure 4.8 and the sail surface in the same G.U.I., shown in figure 4.5. Both the graphs draw the geometry of the sail surface derived from the input data of figure 4.3. The difference is in the fact that the former is obtained by working on the sail sections and the luff, draft and leech curves, as described in the previous sections. In the same figure, a Bezier patch is highlighted.

Henceforth, since the methods employed for performing the aeroelastic analysis are numerical, the next step consists of creating the surface mesh. Therefore, from the ‘Menu’ G.U.I., as plotted in figure 4.8, by clicking the ‘3D Mesh’ button opens a new window, plotted in figure 4.9, for this purpose.

Once this G.U.I. is opened, the graph plots already an initial mesh for the current sail surface, which can be opportunely changed, since the main feature of this G.U.I. is the possibility of choosing the distribution and number of nodal points. In fact, in the upper-right area of the window, there are two fields for specifying the number of parts into which every Bezier patch, highlighted in figure 4.8, should be subdivided. Thus, ‘ustep’ and ‘vstep’ indicate the coefficients, which specify the subdivision of each part of the section and vertical curve respectively. For instance, in the case illustrated in figure 4.8, u-step equal to 0.25 means that the each part of the section is divided into four. Therefore, the number of nodal points in the horizontal direction is 9. The v-step value works in the same

way for each part of a vertical curve. Thus v-step equal at 0.25 means 17 nodal points along the vertical direction.

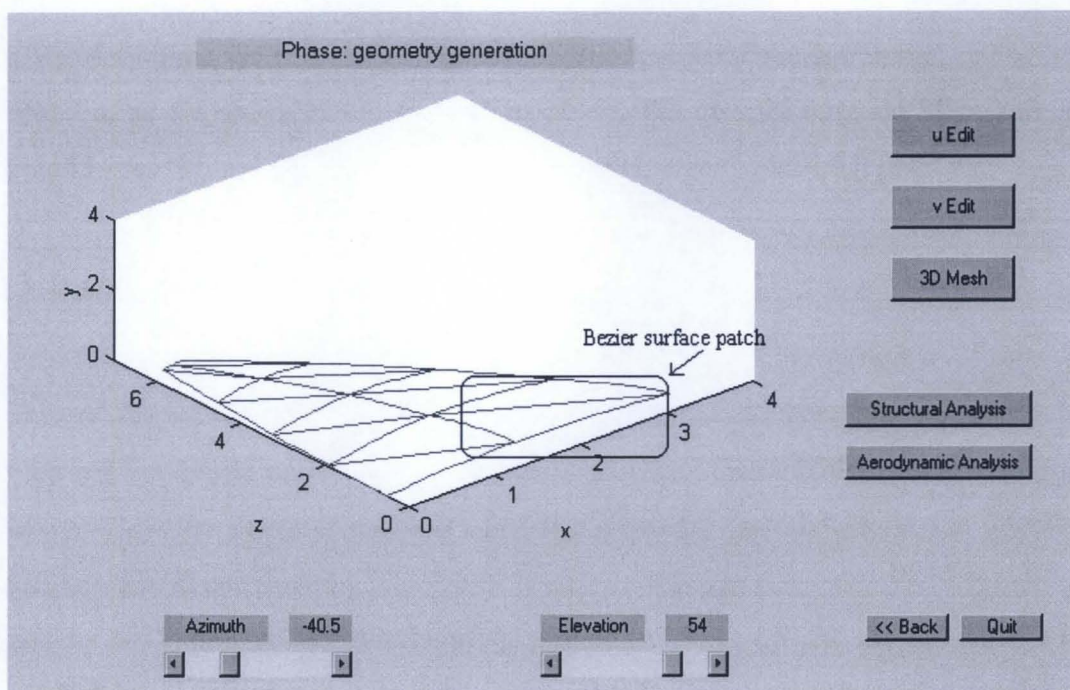


Figure 4.8: Sail surface geometry ready to be meshed.

On completion, clicking on the ‘Draw’ button enables the model to be visualised. Then, clicking on the ‘Save’ and ‘Save grid’ buttons saves the model and the nodal points. Finally, the ‘Menu’ button brings back the main interface, which presents the option of selecting the aerodynamic analysis or the structural analysis, respectively described in chapter 5 and 6. As for every interface concerned with the three dimensional sail model, this G.U.I furnishes two slider buttons, ‘Azimuth’ and ‘Elevation’, which permit interactive movement of view point and facilitate checking the model. In addition, the ‘Rotate’ button allows viewing the model with the Z_g axes vertical.

Some concluding remarks can be made regarding the link with the analysis phase.

The aerodynamic model, which will be used for the aerodynamic analysis, is formed by creating a series of quadrilateral panels defined by four nodal points, which essentially coincide with the mesh plotted in figure 4.9. The finite element model, which is used for the structural analysis, requires triangular panels. Therefore, each quadrilateral panel is subdivided in order to form two triangular finite elements for each panel.

This procedure satisfies the priority of building up easily related models with a simple connection between nodes of the finite element model and the aerodynamic loads acting on them.

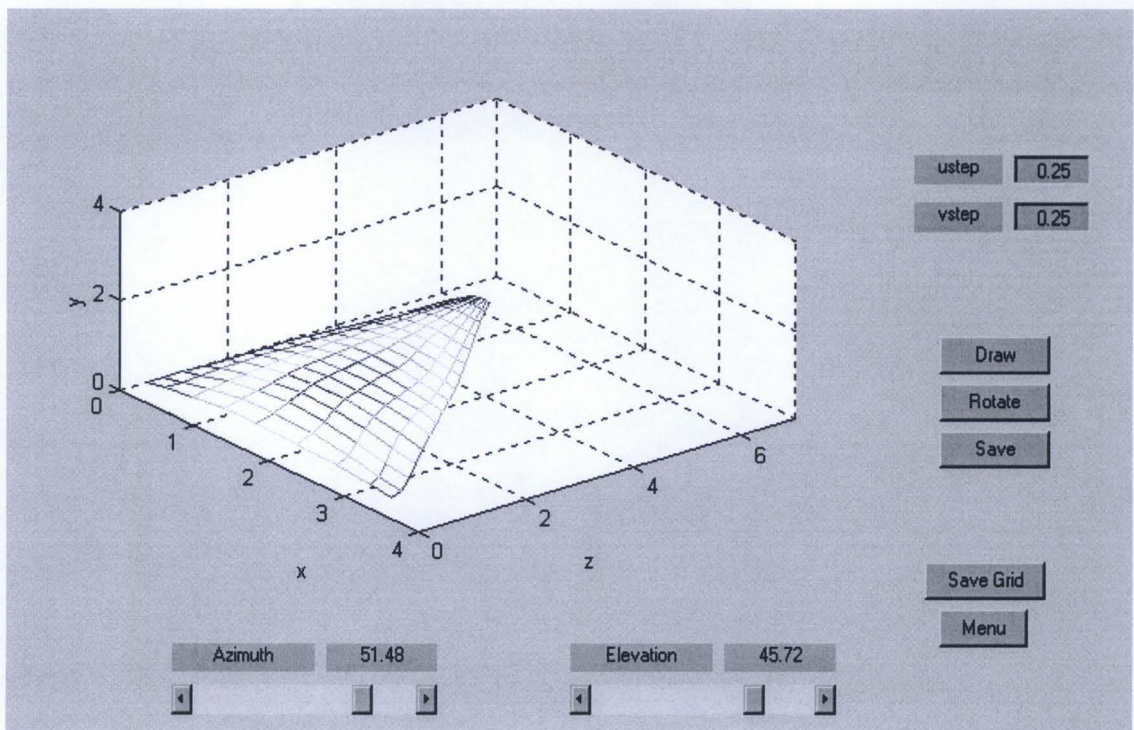


Figure 4.9: '3D Mesh' G.U.I. mesh model to use in the aeroelastic analysis

With reference to the distribution of the nodes in both the directions, it is worth stating that this is strictly linked to the position of the control points used for developing the curves. For instance, the meshed model plotted in figure 4.9 shows a relatively uniform distribution of the nodal points. Generally, homogeneous models, which are characterised by regularity in the dimension and distribution of the panels, have better numerical behaviour, [53], [57], [66]. Therefore, since uniformity is a preferred characteristic, the above mesh is the result of a relatively uniform distribution of control points. However, if the sail designer is particularly interested in the aerodynamic as well as the structural behaviour of the sail at the leading edge, for example, he can modify the distribution of the control points at the leading edge of each section by making them closer to each other. Naturally, this option increases the versatility of the mesh tool.

4.5 Conclusions

This chapter has described the main features of the geometric method and the integrated graphical user interfaces used to develop, from the few initial input data, the mesh of nodal points for use by the subsequent aeroelastic analysis.

Particular attention has been given to the features of all the initial phases, in order to respond to the three main requirements for optimal sail design, listed in section 4.1. In fact, all the phases presented allow building sail surface models for:

- existent sails,
- modified shapes of existent sails
- novel sail-shapes.

Further details about the features concerning the ‘design actions’ phase as well as the development of new sail shapes are presented in chapters 8 and 9.

Chapter 5

Aerodynamic Analysis

5.1 Introduction

In order to perform the aeroelastic analysis, the design system requires the calculation of the aerodynamic loads acting on the sail surface. Therefore, the next section 5.2 describes the method applied to perform the aerodynamic analysis and how it has been integrated for running the full sail aeroelastic investigation. Sections 5.3 and 5.4 illustrate how the method is incorporated into the designed graphical user interfaces. Section 5.5 demonstrates various examples for validating the implemented methodology.

The aerodynamic analysis has been tackled using the Modified Vortex Lattice Method, [54]. This method is a modified version of the Vortex Lattice Method, which represents the most widely used technique for solving the sail aerodynamic problem. In 1968, Milgram, [43], started to apply this method to the sail aerodynamic analysis. After his basic development, most of the researchers involved in this field have used it in several ways. However, it has been demonstrated that the V.L.M. is an effective tool for sail analysis, [8], [27], [28]. In section 2.2.4, there is a wide-ranging discussion of the different numerical methods used in the past and how the V.L.M is considered the most popular method. In

particular, low costs in terms of time, money and people involved make this method still more popular than other CFD techniques and wind tunnel tests.

5.2 Modified Vortex Lattice Method

The purpose of this section is to outline the Modified Vortex Lattice Method (M.V.L.M.) applied, detailing the hypotheses and the major implications. Further particulars about the theoretical background of the presented methodology are given in the appendix B and in the references [1], [8], [27], [28], [42], [54], [60].

The Modified Vortex Lattice Method is capable only of predicting the potential flow over the sail, and hence the fluid viscosity effects are ignored. This method turns the sail surface into a vortex sheet, which means that the surface has zero thickness and the jump in velocity across it is equal to the local strength of the vortex sheet. The local vorticity is evaluated by imposing the condition that there is no flow through the surface of the sail and, hence, the velocity field is tangent to the surface. Furthermore, to obtain a unique solution, it is assumed that the flow separates from the sail surface at the trailing edge.

Therefore, at the base of this method, there are the following assumptions:

- the flow-field is irrotational everywhere: all the vorticity is assumed to be concentrated in the boundary layer and in the wake leaving the trailing edge;
- there are no flow separations on the sail surface.

The first condition can be considered satisfied for high values of Reynolds number, based on the chord dimension. Usually, the analysis involves large sails and strong wind conditions, and hence high wind-speed, [8].

The second assumption is more problematic and derives from the hypothesis that the viscous effects are ignored. With regard to the fact that a sail is a highly cambered lifting surface, working at high attack angle, even if the external conditions are not so strong, a wrong trim can generate leading edge separation. Although, today, the telltales help the crew in trimming the sail, the flow is separated in a conventional sailing condition, [8], [11], [64].

Consequently, the vortex lattice method evaluates approximately the aerodynamic forces by predicting the pressure distribution and the induced drag, as described below. However, some studies have estimated the effects of ignoring the viscosity.

In view of the fact that the potential flow is known, it can be used as the external solution for the boundary layer solution. Newman, [11], verified that the skin friction does not affect the final shape of a bi-dimensional membrane and they consider a similar behaviour can be extended to a three-dimensional membrane. Haarstick, [21], calculated that the induced drag on a sail yacht is four times greater than the remaining drag component. Furthermore, the author of the thesis [38] verified that viscous effects are not dominant on FINN class sail sections and masts, for high average Reynolds number and in the absence of separation.

The Vortex Lattice Method considers the sail and the wake as surfaces over which there is a distributed vorticity. The vorticity intensity is variable and unknown, and must satisfy the flow field described by the following equations:

- mass conservation for an incompressible flow:

$$\vec{\nabla} \cdot \vec{V} = 0 \quad (5.1)$$

where \vec{V} is the total velocity;

- the sailcloth is considered impermeable:

$$\vec{V} \cdot \vec{n} = 0 \quad (5.2)$$

where \vec{n} is the sail surface's normal vector;

- in the wake, the pressure is continuous: from the Kelvin-Helmholtz theorems, the vorticity is carried with the fluid particles and the discrete lines of vorticity are parallel to the streamlines;
- the disturbance velocity must vanish far from the sail:

$$v_d \rightarrow 0 \quad (5.3)$$

as a sail is a lifting surface, the flow leaves the trailing edge smoothly and so must satisfy the Kutta condition.

As aforementioned, this method considers the sail surface as a vortex sheet. This continuous vortex distribution is replaced by a discrete distribution of vortex loops. Briefly, as the sail surface has been modelled with ' n_p ' panels, with a vortex loop on each panel, then there are ' n_p ' vortex loops.

Considering a vortex loop of intensity Γ_j acting on the $j^{th} \in (1, n_p)$ panel.

Its intensity is unknown, thus there are ' n_p ' unknown variables Γ_j , which requires a system of ' n_p ' equations for solutions. As mentioned above the problem is solved by imposing that the flow is tangent to the sail surface, and the discrete formulation verifies this condition at n_p points on the sail surface, called 'control points'.

In the present formulation, the method has been applied with the following considerations:

- each control point is positioned at the centre of each sail panel;
- since each panel is quadrilateral, the vortex loop acting on it has the same shape;
- in order to satisfy the Kutta condition, the vortex lines placed on the trailing edge are deleted;
- in order to respect the Kelvin-Helmholtz theorems, free vortex lines leave the corners lying on the trailing edge, following the direction of the streamlines;
- in order to respect again the Kelvin-Helmholtz theorems and the fourth condition, the streamlines will assume the asymptotic flow direction, far from the sails.

Henceforth, the only remaining condition to verify is with regard the impermeability of the sailcloth, which is equal to the condition that the normal component of the total velocity at each control point is zero. In this way the ' n_p ' equations are generated.

Considering the total flow velocity V as the sum of the asymptotic flow velocity \vec{V}_∞ and the induced velocity by the vortex distribution $\vec{V}_{vortices}$, the equation (5.2) is expressed as:

$$\vec{V}_{vortices} \cdot \vec{n} + \vec{V}_\infty \cdot \vec{n} = 0 \quad (5.4)$$

Taking into account that $\vec{V}_{vortices}$ has contributions from the sail vortex distribution $\vec{V}_{sail-vortices}$ as well as the wake vortex distribution $\vec{V}_{wake-vortices}$, equation (5.4) becomes:

$$(\vec{V}_{wake} + \vec{V}_{sail})_{vortices} \cdot \vec{n} + \vec{V}_\infty \cdot \vec{n} = 0 \quad (5.5)$$

Equation (5.5) must be true at every point on the sail surface. As the M.V.L.M. considers the continuous circulation distribution described by ' n_p ' vortex loops, this equation must be satisfied at every control point. Hence, the condition (5.5) corresponds to a system of ' n_p ' equations.

The induced velocity by a vortex lying on the $j^{th} \in (1, np)$ panel on the control point of the i^{th} panel, can be expressed as:

$$\vec{V}_{ij} = \vec{A}_{ij} \cdot \Gamma_j \quad (5.6)$$

where $\vec{A}_{ij} = (A_x, A_y, A_z)_{ij}$ is called an 'induced velocity coefficient' and represents the induced velocity in the i^{th} control point by a vortex of unity intensity ($\Gamma=1$) acting on the $j^{th} \in (1, np)$ panel.

Hence, in matrix form, the equation (5.5), with the relation (5.6), is expressed as:

$$(\vec{A}_{wake} \cdot \Gamma_{wake} + \vec{A}_{sail} \cdot \Gamma_{sail}) \cdot \vec{n} + \vec{V}_\infty \cdot \vec{n} = 0 \quad (5.7)$$

where \vec{A}_{wake} and \vec{A}_{sail} are called respectively the induced coefficient matrix for the wake and for the sail. Assembling the two induced velocity coefficient matrices and considering the Kelvin-Helmholtz theory for the vortex intensity in the wake, the equation system (5.7) can be written as:

$$(\vec{A}_t \cdot \Gamma) \cdot \vec{n} + \vec{V}_\infty \cdot \vec{n} = 0 \quad (5.8)$$

where \vec{A}_t is called the assembled induced velocity coefficient matrix.

The equation system (5.8) is composed of ' n_p ' equations in the ' n_p ' unknown Γ intensities. According to the fact that the coefficients of the matrix \vec{A}_t are unknown, the problem is non-linear. Thus, the next problem is to calculate the induced velocity coefficients and consequently to solve for vector Γ .

Considering the expression (5.7), the total induced velocity coefficient at one control point is the sum of two contributions:

- one due to the vortex distribution on the sail;
- one due to the vortex distribution on the wake.

The coefficients are calculated using the Biot-Savart law for vortex segments, therefore, the calculation process assumes known the geometric shape of the inductor vortices.

Then, in order to carry out the calculations for the first contribution to the induced velocity, the method considers the sail-shape taken rigid for the entire aerodynamic phase, which means that the geometry of each of the n_p vortex loops on the sail is always known. In detail, for the first step of the analysis, the sail shape is known and coincides with the surface generated by the previous geometric phase. In the successive step of the aeroelastic analysis, it is the known deformed shape, obtained from the solution of the previous structural phase. Consequently, the induced velocity due to the ' n_p ' vortex loops over the sail at the ' n_p ' sail control points is constant for the duration of the aerodynamic phase.

Concerning the prediction of the second contribution to the induced velocity, \vec{A}_{wake} , the M.V.L.M. requires the implementation of an iterative process for estimating the wake geometry. Then, the iterative procedure presumes, for the first iteration, that the wake is a semi-infinite vortex sheet leaving the trailing edge in the direction of the asymptotic flow. For this assumed geometry, it is possible to calculate the total influence matrix \vec{A}_t . In fact, knowing the positions of ' n_w ' control points on each streamline and the wake geometry, the sail-wake, wake-sail and wake-wake induced velocity contributions are known.

As \vec{A}_t is known, the equation system (5.8) provides a first distribution of Γ .

This first evaluation of the vorticity enables calculation of the induced velocity at the ' n_w ' of control points distributed on each streamline. Every control point in the wake is given a displacement equal to

$$\Delta s = v_i \cdot \Delta t \quad (5.9)$$

where Δt is the time step and v_i is the sum of the induced velocity by the vortex distribution on the sail and on the wake.

Evaluating the displacement Δs for each control point on the wake, and successively adding it to its initial position in the wake, deforms the initial wake geometry. For this new wake geometry, it is possible to evaluate the current influence coefficient matrix, as described above (see figure 5.1). This process is repeated until the current wake geometry stabilises or until the difference between two successive wake shapes is smaller than a prescribed value ϵ . The wake shape corresponds to the convergence criteria and, for the related distribution of vorticity, it is possible to evaluate the aerodynamic forces, as described below. The flow-chart in figure 5.1 shows the scheme of this procedure. Section 5.4 describes in detail how the iterative process works for estimating the wake geometry.

Summarising, for each of the above steps the wake assumes a new geometry. Thus, the contribution to the induced velocity on the wake control points due to the vorticity on the sail and wake has to be evaluated at each step. Equally, the contribution of the wake vorticity on the sail control points is calculated. Only the contribution on the sail control points by the sail vorticity does not change during the entire process.

Heretofore, the described M.V.L.M. is valid for a free body. In the case of a sail aerodynamic analysis, the sea as well as the deck influence must be evaluated. This effect has been introduced by considering the image-method.

The described procedure does not change, but all the calculations are extended to incorporate a panel model of the real sail and wake plus their images. Further details about how the method has been extended are in the appendix B. After convergence, the evaluation of the aerodynamic loads is performed. This uses the Bernoulli principle for calculating the pressure coefficient distribution:

$$C_p = \frac{p - p_\infty}{\frac{1}{2} \rho_\infty V_\infty^2} = 1 - \left(\frac{V}{V_\infty} \right)^2 \quad (5.10)$$

where C_p, p, V are, respectively, the pressure coefficient, the pressure and the velocity at a control point, while $p_\infty, \rho_\infty, V_\infty$ are the pressure, air density and velocity of the asymptotic flow.

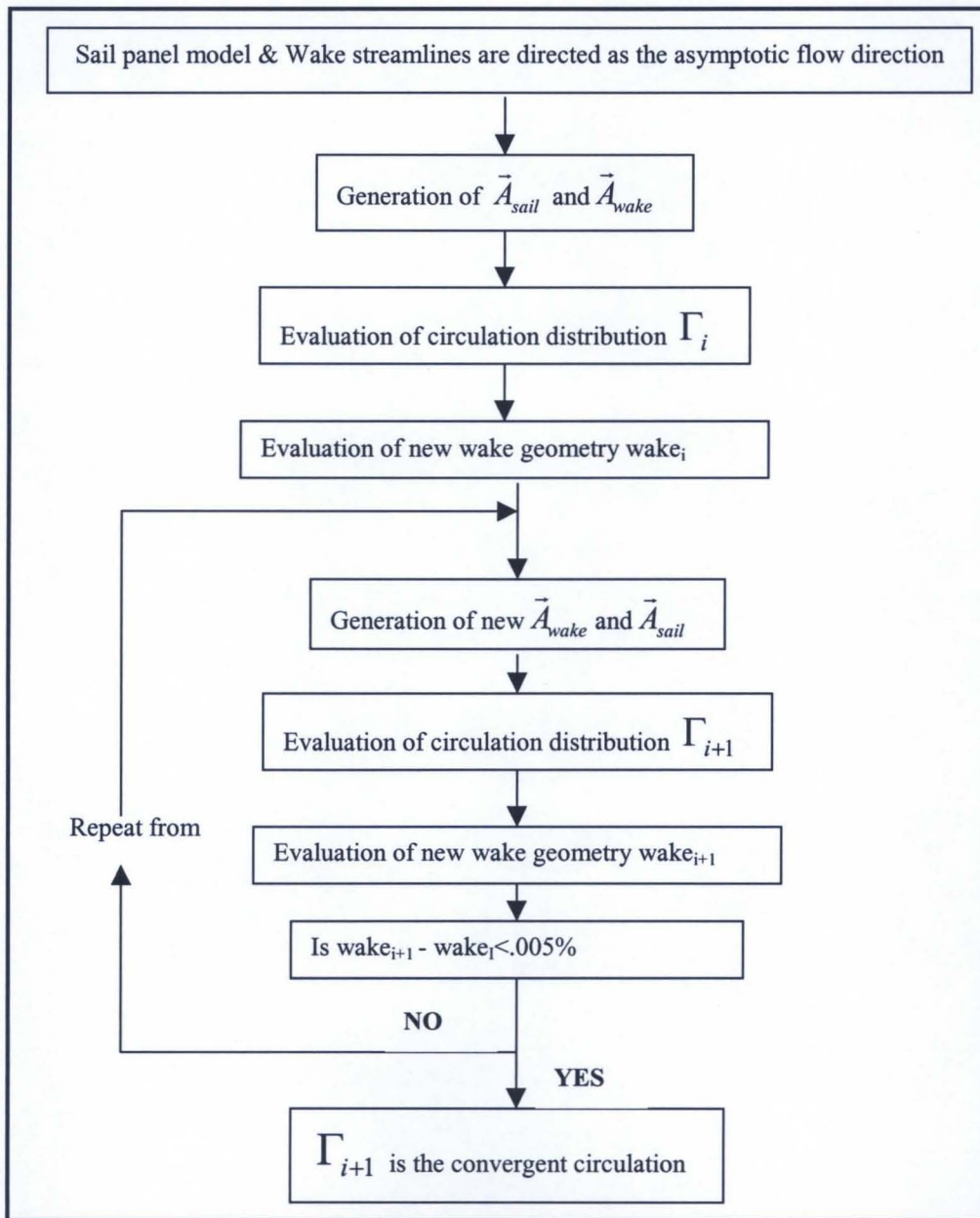


Figure 5.1: Flow chart description of the solution method for the aerodynamic phase

The velocity at each control point can be expressed as follows:

$$\vec{V} = V_\infty \vec{e}_\infty + \vec{v}_d \mp \Delta \vec{v} \quad (5.11)$$

- where $V_\infty \vec{e}_\infty$ is the asymptotic velocity,
- \vec{v}_d is the disturbance velocity, and
- $2\Delta \vec{v}$ is the local jump in the tangential component of the velocity, due to the vortex distribution.

An average vorticity on the j^{th} panel is calculated using the formulation:

$$\bar{\Omega}_j = \frac{1}{Area_j} \sum_{i=1}^4 (\gamma_i \vec{l}_i) \quad (5.12)$$

where the γ_i, \vec{l}_i are, respectively, the effective vortex strength and edge vector of each segment.

The jump in the tangential component is given by:

$$\Delta \vec{v} = \frac{1}{2} \vec{n} \times \bar{\Omega} \quad (5.13)$$

Using the expression (5.13), the force acting on j^{th} element of surface equal to $Area_j$ is expressed by:

$$F_j = -\rho_\infty V_\infty^2 Area_j [\vec{e}_\infty \cdot (\vec{n} \times \bar{\Omega})] \vec{n} \quad (5.14)$$

The lift and induced drag forces, acting on j^{th} element, are evaluated as the components of the force F_j normal and parallel to the asymptotic flow direction. As a result, the distributions along the luff direction of these coefficients are the component of the sum of the pressure force acting on each panel strip along this direction.

Since the interest is in evaluating the sailing forces, the drive force coefficient is calculated as the sum of these components along the sailing course direction, while the heeling force, as the sum of the components in the orthogonal direction to the sailing course.

5.3 The G.U.I. for the Aerodynamic Analysis phase

This section describes the graphical user interface for running the phase of the aerodynamic analysis, as described in the previous section 5.2. The principle, which has driven the design of this G.U.I., shown in figure 5.2, is to develop it with appropriate features in order to aid the approach of any user when performing the analysis without requiring knowledge about the implemented method. Therefore, the intent of this section is to illustrate the features of this interface and how it works in conjunction with the modified vortex lattice method.

Briefly, the sail surface geometrical generation phase ends when the user has decided on the number and the distribution of a set of nodal points, belonging to the sail surface generated, which are to be used for building the panel model for the aerodynamic analysis. The co-ordinates are saved in a data file, as seen at the end of section 4.4.3. Then, by clicking on the ‘Aerodynamic Analysis’ button in the ‘Menu’ interface (figure 4.8), the G.U.I. related to this phase appears. On the left of the interface, the graph plots the panel model, as it is expected from the previous meshing phase.

For the sail shown, the latter mentioned button starts calculation of the following matrices:

- panel node co-ordinates
- control point co-ordinates
- connectivity for nodes belonging to more than one panel
- connectivity for edges belonging to more than one panel
- induced velocity coefficient of the sail vorticity on the sail control points, $A_{\text{sail-sail}}$.

The elaboration of the listed matrices makes opening this G.U.I. window slower, if it is compared with other window open times.

Notwithstanding the fact that the calculations before the analysis delays the opening of the G.U.I. for the aerodynamic analysis, they constitute a set of operations which test the chosen set of nodal points and the panel model. Indeed, the certainty that the connectivity matrices are well compiled ensures that the model is well defined and in the event problems appear later in the calculation, they do not depend on the created model, which has been verified. In addition, the evidence that the above-mentioned influence matrix, which is

fixed for the entire phase calculations, does not present complications, guarantees about the correct functionality of the same created connectivity matrices.

The meaning of the above considerations is that the panel model and the control points set have been correctly created and moreover they work properly. This avoids the possibility of stops during the analysis runs due to an improper definition of the problem, and at the same time, it is guaranteed that if the analysis stops, the problem does not concern the panel model. Finally, it speeds up the start of the analysis and allows faster results to be obtained.

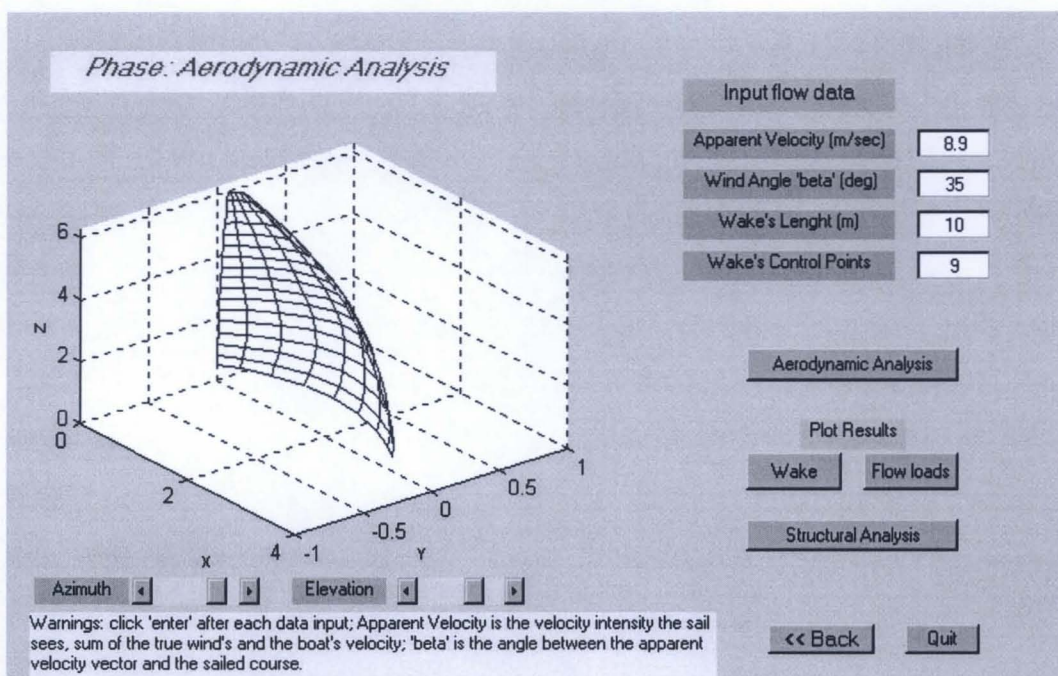


Figure 5.2: Aerodynamic Analysis Phase Graphical User Interface

Aware of these introductory considerations, the description of the features of this G.U.I. follows. Looking at figure 5.2, firstly, the ‘Azimuth’ and the ‘Elevation’ sliding buttons help to visualise the model from different points of view. On the right, from top to bottom, there is a list of editable spaces, which are:

- asymptotic apparent wind velocity intensity (m/sec);
- apparent wind angle β (deg);
- length of the wake;

- d) number of control points on each streamline.

Naturally, the values required in a) and b) are the external conditions.

The values used in c) and d) depend upon the accuracy required by the designer in doing the aerodynamic calculation. However, concerning the data in c), the influence of a wake of length at least equal to ten times the length of the mean sail chord is considered appropriate. Further, regarding the data in d), if the sail panel model has many control points along the chord direction, a good description of the wake is desirable. Since considering a similar degree of accuracy for the sail and the wake is advisable, the same chordwise distribution of control points on the sail can be used for the related wake streamline. Adapting the iterative calculations in this way avoids discrepancies in the evaluation of the reciprocal influence between the wake and the sail.

Once these parameters are fixed, it is possible to start the aerodynamic analysis, by clicking on the associated button. This button activates the code of the method described in section 5.2. The duration of the calculations varies upon the number of control points in the model. For example, running the code on a Pentium with 32MB RAM, each iteration step lasts two minutes long, in the case of a 32-panel sail model and with a total of 40 control points on the wake. The time increases as the accuracy of the panel model increases. In fact, on the same p.c., for a 122-panels model, each step lasts almost 30 minutes.

On the bottom right, there are other push buttons. Naturally, 'Quit' permits abandoning the analysis and 'Back' permits return to the 'Menu' G.U.I.. This latter button has an important role, where initial compiling problems concerning the panel model exist, as described in the first part of this section. Allowing review of the phase of saving the nodal points permits immediate correction of any errors.

In addition, there are two push buttons in the group of 'Plot Results', 'Wake' and 'Flow loads', which open two new windows plotting the results in terms of the wake evolution and loads distribution over the sail. A better description of these operations is given in the following two sections, respectively 5.3.1 and 5.3.2.

When this phase is concluded, the loads acting on the sail panel model are known. Then, clicking on the push button 'Structural Analysis' allows opening the window for starting this analysis. Detailed description of this phase is in the following chapter 6.

5.3.1 The wake shape

With regard to the ‘Wake’ push-button, this section illustrates the graphical user interface, which allows visualising the wake shape behind the sail, as it is when the iterative loop, comprising figure 5.1, achieves the convergence. This plot covers an important role in measuring the accuracy of the results. In fact, in a case where the wake possesses a non-physical structure, which is nonetheless converged, the solution is not physically valid.

Therefore, this G.U.I., as plotted in figure 5.3, has only the features aiding an optimum visualisation of the three-dimensional wake plus panel model shape, using the two sliding buttons ‘Azimuth’ and ‘Elevations’. In addition, it has the ‘Quit’ button, which permits abandoning the current investigation of the results and the ‘Back’ button, which enables the return to the ‘Aerodynamic phase’ G.U.I., plotted in figure 5.2, for proceeding with the analysis. In particular, in the case where the wake has a physically correct shape, the designer can start the structural analysis, as described at the end of section 5.3. Whilst, in the case where the solution does not appear correct, the designer has the possibility of restarting changing either the analysis edited inputs or going back to the ‘Menu’ interface and modifying the panel model geometry.

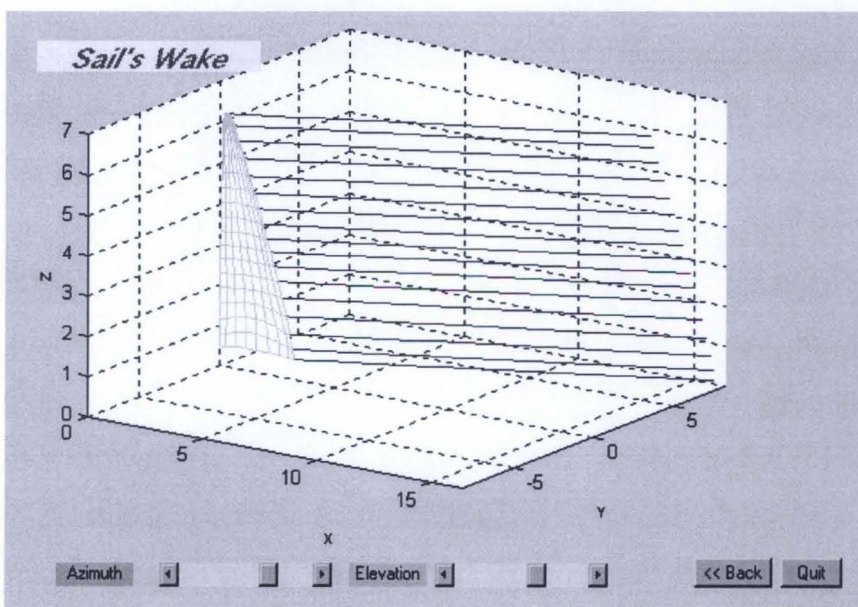


Figure 5.3: ‘Wake’ GUI, after the first step of the aerodynamic analysis iteration.

5.3.2 Flow Loads

With reference to the ‘Flow Loads’ push-button, this section illustrates the graphical user interface, which allows visualising the results in terms of pressure distribution and evaluation of the aerodynamic loads acting on the sail-shape, when the iterative loop, plotted in figure 5.1, achieves the convergence.

As figure 5.4 shows, this interface does not allow interactive operation. Basically, clicking on the aforementioned button opens a new window, which plots the loads resulting from the previous analysis without closing the G.U.I. related to the aerodynamic analysis phase (figure 5.2).

Looking at figure 5.4, there are four plots.

On the top left there is the plot of the opposite value of the difference between the pressure coefficient on the leeward and windward surface, along the section with maximum curvature, which is usually between the lower and the middle section.

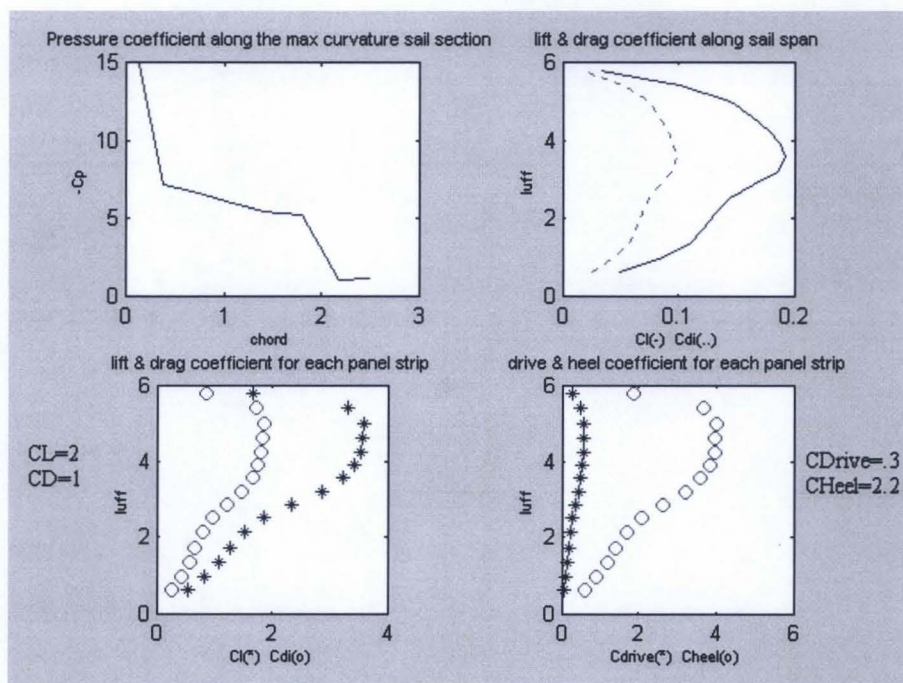


Figure 5.4: Window for Flow Load

The top right graph plots the lift and the induced drag coefficients along the luff curve, evaluated as follows. Considering for the asymptotic dynamic pressure, the expression:

$$Q_{\infty} = \frac{1}{2} \rho_{\infty} V_{\infty}^2 \quad (5.15)$$

these coefficients are evaluated as:

$$CL_s = \frac{Lift_c}{Q_{\infty} AREA_{sail}} \quad (5.16)$$

$$CDi_s = \frac{Drag_c}{Q_{\infty} AREA_{sail}} \quad (5.17)$$

where the subscript symbol c , which is for chord, indicates that the values refer to the total calculated along the strip of panels.

The graph on the bottom left plots the same coefficients along the luff, but referred to the total area covered by the panels of any strip. Briefly, the related expressions are:

$$CL_c = \frac{Lift_c}{Q_{\infty} AREA_{strip}} \quad (5.18)$$

$$CDi_c = \frac{Drag_c}{Q_{\infty} AREA_{strip}} \quad (5.19)$$

On the bottom right the plot is related to the components of the aerodynamic load coefficients along the sailing course, drive force coefficient, and in the orthogonal direction, heel force coefficient, evaluated as follows:

$$CDrive_c = CL_c \sin \beta - CDi_c \cos \beta \quad (5.20)$$

$$CHheel_c = CL_c \cos \beta + CDi_c \sin \beta \quad (5.21)$$

Finally, the plot gives the total values of all four coefficients.

Concluding, as the aerodynamic analysis solves the potential flow, the drag is the induced aerodynamic value.

5.4 Example of a wake evolution behind the sail

Using the features of the ‘Wake’ and ‘Flow Loads’ interfaces, the present section shows how the wake evolves behind the sail and how its evolution affects the loads and their distributions along the luff curve. The purpose is to understand the meaning and the consequences of the iterative loop solution proposed in section 5.2 as well as in the flow chart of figure 5.1.

As asserted in the section 5.2, the first iteration for the aerodynamic analysis presumes that the wake shape is a vortex plane leaving the sail trailing edge in the direction of the asymptotic flow. Therefore, considering as an example the panel model and the condition for the analysis, illustrated in figure 5.2, figure 5.3 plots the wake shape corresponding to the first step of the iterative loop for guessing the wake shape and figure 5.4 plots the related external loads. Noticeably, as the asymptotic direction of the flow is $\beta=35^\circ$ and considering that the leeway angle is $\lambda=0^\circ$ and the boom sheeting angle is $\delta_m=10.3^\circ$ (compare with the ‘Input data’ G.U.I., figure 4.3) the true attack angle is $\alpha=24.7^\circ$ and the stream follows the asymptotic flow direction.

In order to demonstrate the wake evolution through the sequence of the iterations, the analysis has been carried out with a larger time step with respect to the one normally used. In fact, following the expression 5.9 for the wake control point displacement, in this way the deformation of the wake is significant. Therefore, for this example, the time step used is $\Delta t = 0.1$ sec, and as a reference length the luff length, the non-dimensional time step is $\Delta\tau=\Delta t(V_\infty/L)$ is equal $\Delta\tau = 0.15$. For normal calculation the value used is two orders smaller than this, ($\Delta\tau = 0.001$). The following figures 5.5 and 5.6 provide the wake shape after the third and fifth steps of the iteration process.

With reference to figure 5.5, the third iteration step wake shape leads to some important considerations. Visibly, the effect of the downwash causes the deformation of the wake mostly in the middle of the luff-wise direction, than at the sail tips. In view of the facts that the asymptotic flow is uniform along the luff and the sea and the deck influence is at distance of 0.5m, which is like the extension of the body of the sail, this locates the major deformations in the upper part of the sail.

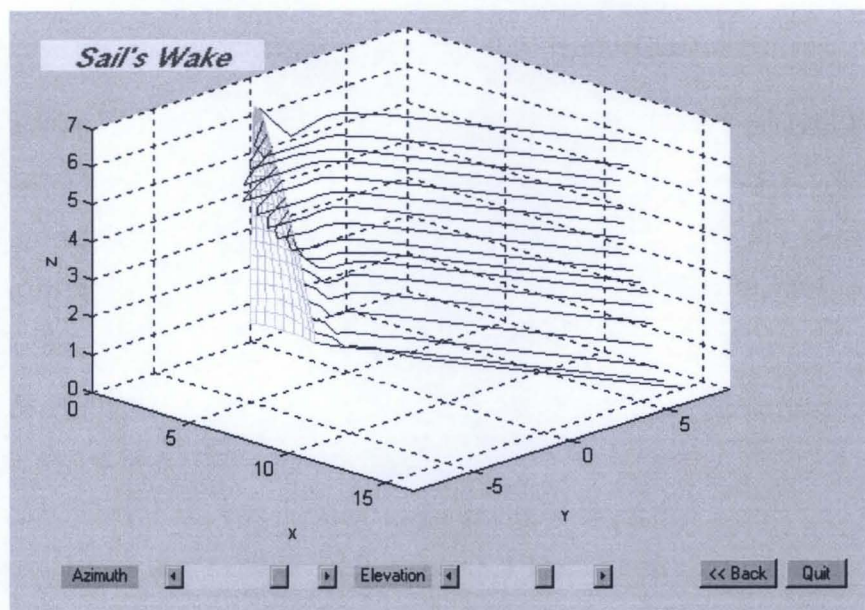


Figure 5.5: Evolution of the wake after the third step of the analysis.

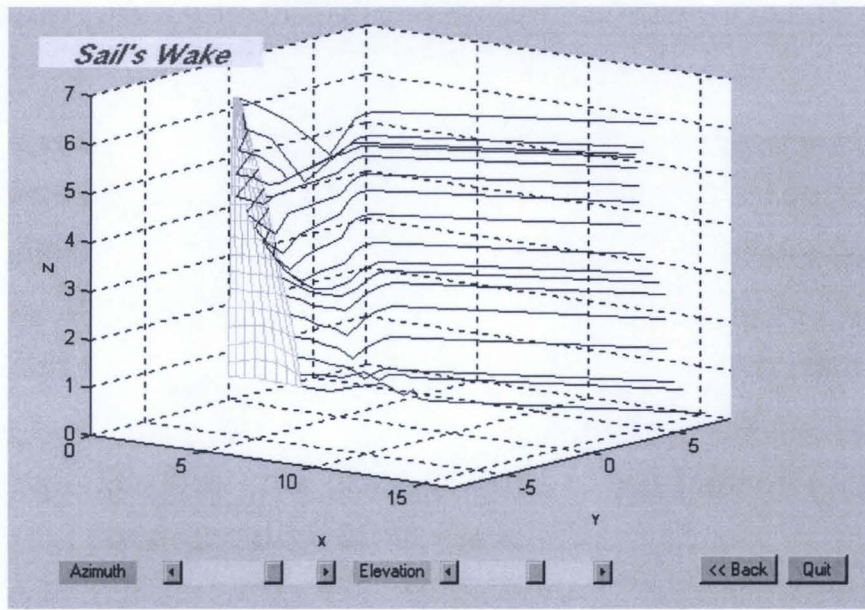


Figure 5.6: Evolution of the wake after the fifth step of the analysis.

In detail, looking at the streamlines leaving respectively the foot and the head sections, they show smaller displacement if compared with their adjacent streamlines. In particular the foot streamline is less deformed than the one leaving from the tip section, which

undergoes a stronger deformation as the upper part of the sail is twisted and tapered. Furthermore, considering figure 5.6, which plots the wake after the fifth step, the tendency of the tip rolling vortices is more evident.

In both the latter figures, it is evident that part of the wake is not affected by deformation and follows the asymptotic flow direction. This depends upon the number of the control points ' n_w ' chosen and upon the way they have been distributed on each streamline, which is explained above:

- the first control point coincides with the node on the sail leech curve;
- the following $n_{w1} = [(n_w - 1)/2 - 1]$ control points are equally displaced of a distance equal to the 25% of the length l_w , which is equal to the n_w^{th} part of the total streamline length;
- the remaining $n_{w2} = (n_w - n_{w1})$ control points are equally displaced of a distance equal to the 50% of the same length l_w .

In essence, the purpose of this choice responds to the expectation of more significant deformations of the wake closer to the trailing edge than farther downstream. In order to reduce the degree of error, it is desirable to have a more accurate description of the wake closer to the leech.

Taking into account that for this example $n_w = 9$ for each streamline of length 10m, the first control point coincides with the node at the leech, the following three are fixed at an increment of 0.28m and the last five at an increment of 0.55m. Thus, for the first iteration, the wake length covered by control points is equal to 3.6m.

By the calculations, a non-zero displacement ought to result for the point coincident with the node belonging to the leech. As for physical meaning the control point on the leech cannot move, at the end of each step the node at the trailing edge is the new first control point on each streamline. Since this operation ought to add a new control point each step, in order to operate with the same number of wake control points, the last control point on each streamline is deleted. Consequently, going ahead with the steps of the process, the control points move closer to the leech.

Considering the example here proposed, this means that after five iterations, the latter five control points are deleted. Nonetheless given the displacements, which the control points can undergo, the deformation affects roughly the first 2.2m of the wake.

Furthermore, the implemented code for guessing the wake shape supposes that from the last control point on each streamline, the wake assumes the asymptotic flow direction.

Concluding, in the view of the wake correction method, as it has been described in this section, the wake disturbance becomes closer to the sail as the number of the iteration steps increases. Therefore, many streamline control points enable a better wake description.

As aforementioned in section 5.2 and implied in figure 5.1, when the wake shape indicates a stable geometry, the aerodynamic analysis is convergent. It is important to clarify that the method has been tested many times for different sail shapes in several external conditions, and changing the number of control points on the wake. Variables such as computational time, workspace employed and hard memory utilised versus quality of the results have been estimated, for different numbers of control points used. From these tests, it has been concluded that the best set-up is to stop the iteration process for the aerodynamic analysis after the fifth step for a number of control points on each streamline in the range 7 to 11. In this case, the solution is already convergent, and the pressure distribution over the sail does not change significantly.

Thus, the entirety of the tests presented in this chapter, as well as the tests in subsequent chapters, employ the above set-up. The calculated pressure distributions have to be interpreted taking into account this procedure. In order to show how the loads evolve after each iteration step, consider figures 5.4, 5.7 and 5.8, which plot the external loads respectively after the first, third and fifth iteration steps.

In particular, figure 5.4 plots the loads for the wake geometry of figure 5.3, whose shape has been imposed. For this step, the numerical evaluation of the loads is not very accurate, although the shape of their distribution is a good representation of their shape at the converged state. In fact, comparing with the loads in figure 5.7, related to the third iteration step, the shape of the pressure distribution along the maximum curvature sail section, as well as the lift and drag forces, show similar behaviour. With respect to the total force coefficients, there is a significant difference. The total lift coefficient CL decreases from the value of 2 to 1.6. Further, considering the figure 5.8, plotting the external loads at the fifth iteration step, it is more evident that the shape of the load distributions are similar to the previous one, as are the total value of the force coefficients. In fact, CL is equal to 1.56 and the induced drag coefficient is again equal to 0.8. This is in accordance with the

previous decision to stop the iterative process after five steps. This simple example is a corroboration of the validity of this restriction, as the solution at this point is stable.

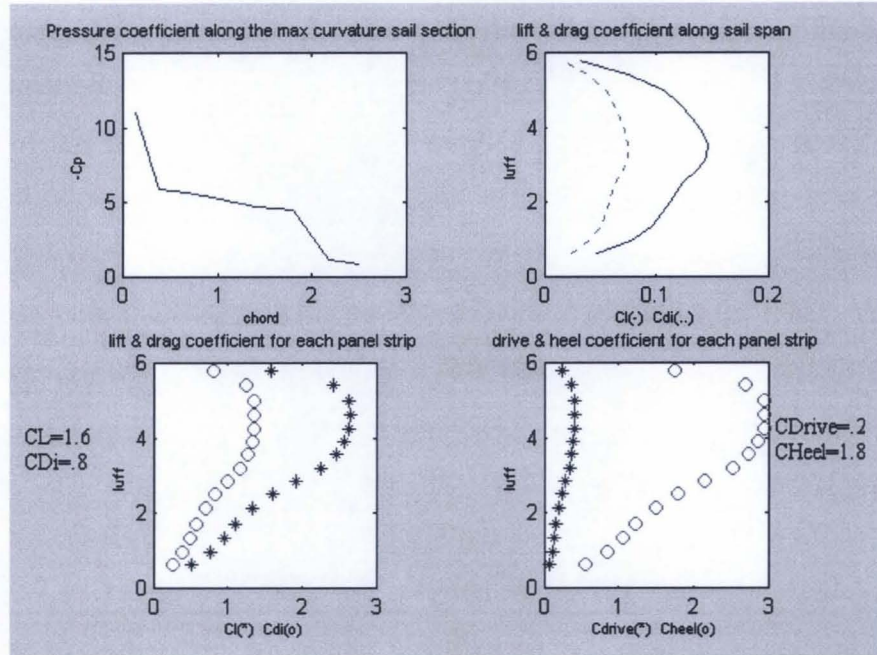


Figure 5.7: External loads after the third iteration step

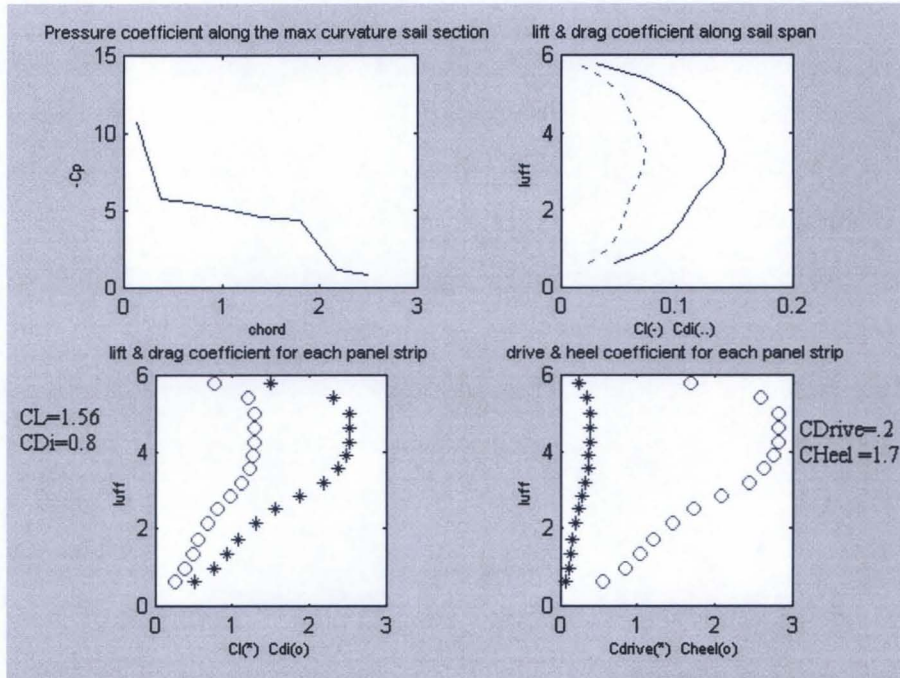


Figure 5.8: External loads after the fifth iteration step

The above lift and induced drag force distributions lead to other considerations. Inasmuch as the aerodynamic solution, plotted in figure 5.8, is related to the sail shape considered as a rigid wing, this step of the aeroelastic solution measures the quality of the initial sail geometry as well as the chosen sail panel model. Undeniably, a ‘strange’ result, as figure 5.9 plots, which ought to include the entire range of possible non-continuous distributions for whatever reasons, indicates the existence of problems within the model and the way the analysis has been performed.

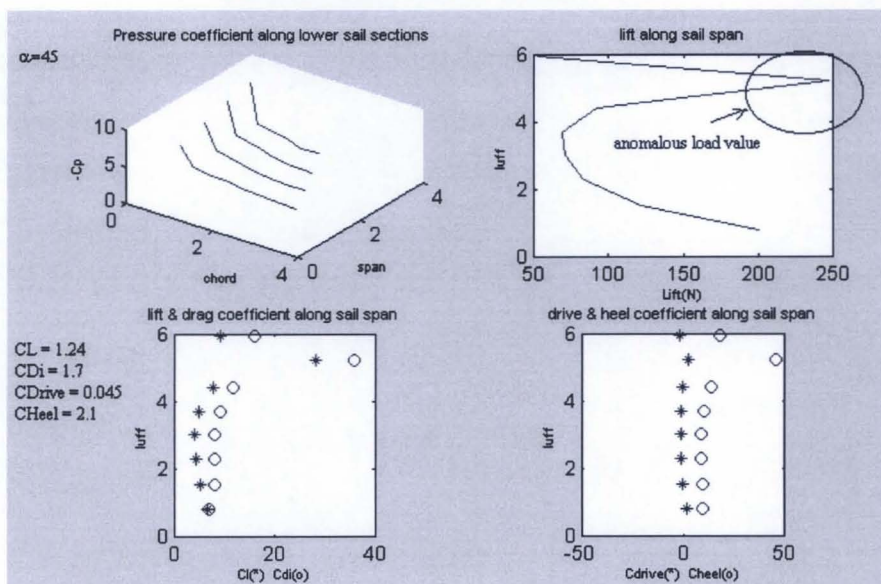


Figure 5.9: Anomalous external loads distribution.

With reference to the loads plotted in figure 5.9, in the circle is highlighted an anomalous behaviour of the load distribution along the luff curve, the probable causes of which are described below.

Considering that the pressure profiles on the lower sections are regular, the unexpected value can be caused from a non-optimised geometry or panel model generation.

The consequence of an inaccurate geometric phase is an unsmooth surface, which produces a panel model with sharp edges. These edges, or rather the points of discontinuity in the tangents along the curve, might also be due to the panel model used. For example, the actual panel model has 32-panels (4 along the chord direction and 8 along the luff direction) and every panel area is around 0.3m^2 . The small number of panels used causes an

incorrect description of the initial geometry, and when following the curvature there could develop a sharp angle between two contiguous panels. This unexpected situation becomes worse when the surface presents a high value of the twist angles (for instance in correspondence with the head sections for the actual case).

In both cases, however, the common problem relates to the presence of sharp edges between two contiguous panels. From the numerical point of view, taking into consideration the Biot-Savart laws, expressed in appendix B, this means a large difference between the evaluated influence coefficient. The reasons for these differences are that the influence coefficient values depend upon the distances between the control points and the considered vortex segment as well as upon the angles between the vortex filament and the segment linking the control point and the vortex filament edges.

In order to improve the solution, there are two steps, which can be taken:

- 1) check the geometry, which means verifying whether:
 - a) there is any bulge or hollow over the sail surface,
 - b) the twist angle distribution is discontinuous,
 - c) the entry or exit angles are not forming a curved trailing or leading edge;
- 2) verify if the chosen panel model is adequate for describing the geometry.

Acting in the above way, the model has been ‘corrected’, and the analysis has been carried out. An accurate analysis of the geometry and the panel model determined that the twist angle distribution was not continuous and therefore the angle at the fourth section was decreased by two degrees. In addition, the number of panels for the model has been increased to 64: 4 along the x-axes and 16 along the y-axes. Chapter 7 displays the results for all the aeroelastic analyses conducted on the ‘corrected’ panel model.

Concluding, in the event the aerodynamic analysis produces good results, as it has been described in section 5.3, it is possible to proceed with the aeroelastic analysis, clicking on the ‘Structural Analysis’ button in the G.U.I. plotted in figure 5.2.

5.5 Modified Vortex Lattice Method Validation

5.5.1 Outline

The main purpose of this section is to validate the code written for the Modified Vortex Lattice Method (M.V.L.M.), described in section 2 of this chapter.

All the examples, which the following parts describe, address the question of the validation considering the case of the simple geometry of a rectangular sail membrane, considered as a rigid body. The purpose of this section is the validation of only the part of the code solving the aerodynamic field.

Since there are few experimental data available for not well described geometry, as it has been seen in chapter 2, the first problem was the choice of the case study to consider for proving the validity of the results, obtained by the implemented code.

Consequently, the corroboration has been accomplished by comparing the aerodynamic flow field solution obtained by the calculations made using the implemented code with the ‘lifting line’ theory, in terms of total force coefficients. This choice is justified by the fact that Prandtl theory is very well known and, nowadays, it is still used for preliminary calculations for finite wings. Furthermore, Prandtl theory solves the flow field over a rectangular plate and the comparison considers the particular solution of Prandtl for an elliptical distribution of the circulation, [1]. In this case, the expressions for the lift and induced drag coefficients are:

$$C_L = \pi \cdot AR \cdot \alpha_i = \pi \cdot AR \cdot \frac{\Gamma_0}{2 \cdot luff \cdot V_\infty} \quad (5.22)$$

$$C_{D_i} = \frac{C_L^2}{\pi \cdot AR}. \quad (5.23)$$

where:

- Γ_0 is the maximum value assumed by the Prandtl elliptical circulation distribution;
- AR is the aspect ratio, calculated as $AR = \frac{luff^2}{AREA_{sail}}$;

- V_∞ is the asymptotic flow velocity.

Henceforth, these formulas calculate the force coefficients that, in the next paragraphs, will be compared with those calculated with the modified vortex lattice method.

5.5.2 Case flat rectangular plate with AR=4

Figure 5.10 plots, through the G.U.I. for the Aerodynamic Analysis phase, the rectangular sail panel model used for the experiment, the geometry of which is defined in the side table.

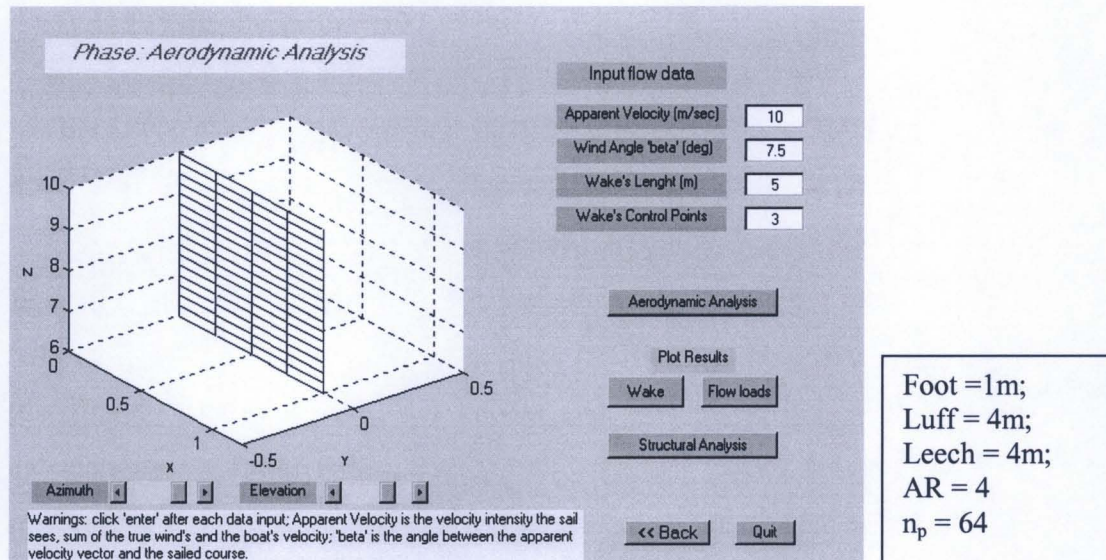


Figure 5.10: Used flat plate panel model and geometric description

In light of the fact that Prandtl theory does not include the wake influence on the plate circulation distribution, in order to minimise this effect, which is taken into account in the M.V.L.M, the aerodynamic solution considers only 3 control points on the 5m long wake. In order to make the implemented M.V.L.M. codes work as similar as possible to the Prandtl solution, the iterative process has been stopped after the first iteration, when the M.V.L.M. considers the wake as a flat vortex sheet. Furthermore, the wake direction has been taken coincident with the plate chord, in lieu of the usual direction of the asymptotic flow V_∞ .

To accomplish this comparison, then, the main problem was to evaluate the value of the circulation to use in formula (5.22), Γ_0 from the distribution of the circulation on the panel model. In fact, the M.V.L.M. solution gives a distribution of the circulation, which is elliptical on each panel strip parallel to the span-wise direction of the plate, but it changes in intensity at each chordwise position. Therefore, the comparisons have been carried out by calculating the distribution of the circulation along the span, taken as the average values assumed by the circulation acting on each panel strip in the chord-wise direction (formula 5.24). Figure 5.11 plots the circulation distribution obtained for the case considered in figure 5.10:

$$\Gamma_{i_s} = \frac{\sum_{i=1}^{n_{pu}} \Gamma_i}{n_{pu}} \quad (5.24)$$

where:

- Γ_i is the circulation acting on the i -th panel;
- n_{pu} is the number of panels in chordwise direction.

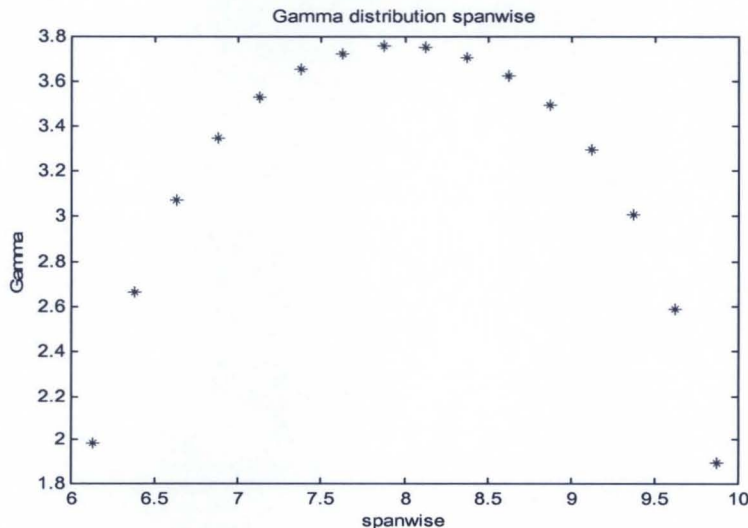


Figure 5.11: Circulation distribution along the span

The maximum value Γ_0 of this distribution seen in figure 5.11 has been considered for the comparisons. In particular from those above values of the circulation:

$$\Gamma_o = \max(\Gamma_{i_s}) \quad (5.25)$$

The calculations have been carried out through the range between $\alpha=0^\circ$ and $\alpha=12.5^\circ$. Using the maximum value of the circulation, Γ_0 , the results of the comparison between the evaluated coefficients with formulas 5.22 and 5.23 and with those resulting from the M.V.L.M are excellent. Considering figure 5.12, which plots on the left the total lift coefficients and on the right the induced drag coefficients, it is notable that for small attack angle the two solution are in perfect accordance, as the maximum observed difference is about 1%. For attack angle $\alpha>10^\circ$ the difference starts to increase.

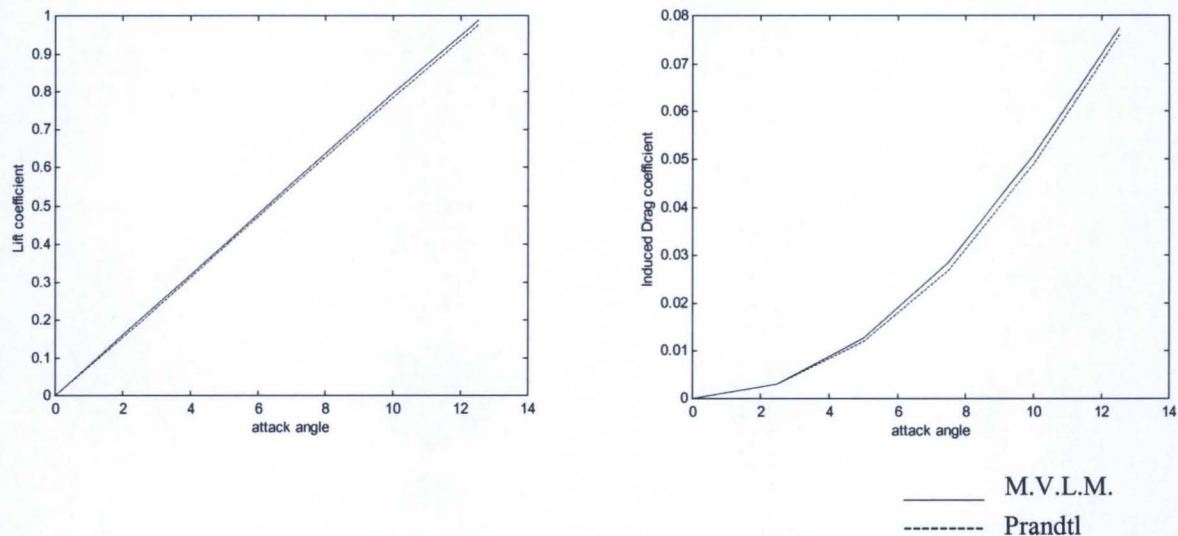


Figure 5.12: Comparison for total lift and induced drag coefficients evaluated by the M.V.L.M, for the case AR=4.

The explanation of this behaviour is that the used coefficient formulas are evaluated as a solution of the Prandtl theory, assuming that the circulation distribution is elliptical, with the maximum value of the circulation in the middle of the span and zero at the edges. It is well known that, for this distribution, the Prandtl solution gives a constant downwash all along the span. The solution obtained from the elaborated M.V.L.M. codes is different because the evaluated circulation distribution assumes the average value of the circulation on the panels distributed along the foot and the tip of the sail, as figure 5.11 shows. This no-zero value at the edges induces, consequently, a non-optimal down-wash distribution, which is not taken into account due to the fact that the iteration stops at the first step, by the M.V.L.M. solution. This fact is believed to be the main reason for the perfect coincidence

of the results for small attack angles, in the light of the fact that the influence of the induced attack angle is small. Thus, the increment in the difference between the two solutions with the attack angle is clarified.

Therefore, the M.V.L.M. code provides reliable results, and, as it was foreseen, a more accurate estimation of the force coefficients.

5.5.3 Sea influence evaluated by the M.V.L.M.

Figure 5.13 plots a direct comparison between the calculated force coefficients for the rectangular membrane sail considered above, in the case of the presence of the sea and/or deck alternatively as a free body. Both the total lift coefficient, on the left, and the induced drag coefficient, on the right, in the presence of the sea and deck influence are lower than those calculated for the sail considered as a free body. Their behaviour derives from the following consideration: around the lower zone of the sail, in the presence of the sea, the deflection of the wake is weaker than that in the case of a free body.

In accordance with this phenomenology, there are two direct consequences. The first is the generation of lower induced angles and, consequently, a lower induced drag coefficient. The second consists of an asymmetric and non-elliptic distribution of the circulation, which yields lower lift coefficients. The estimated difference is a maximum of 3% for the lift coefficients and is a little bigger for the induced drag (~4%).

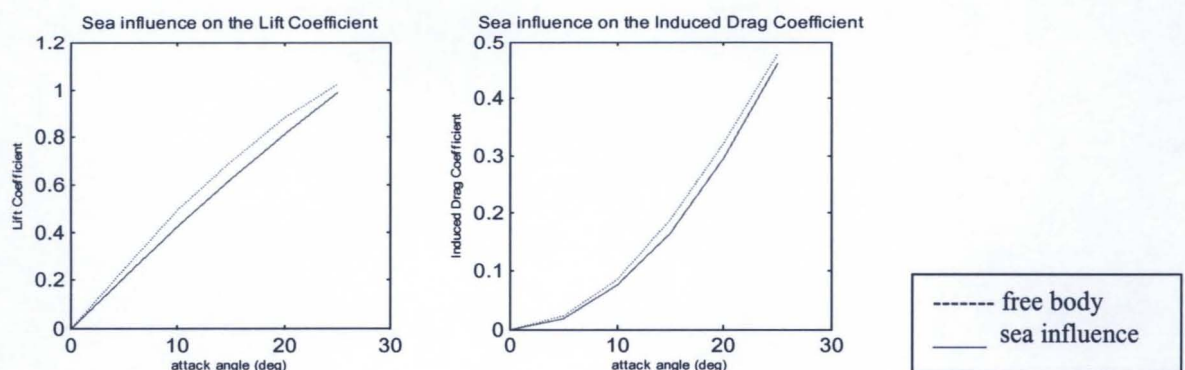


Figure 5.13: Sea influence on a rectangular membrane sail (AR=4)

One other important reason for this result is the low value of the aspect ratio ($AR=4$), because in this case the effects of the finite wing are more intense.

5.5.4 Aspect ratio influence evaluated by the M.V.L.M.

Tests concerning the influence of aspect ratio on the coefficient values have been carried out. They consisted of evaluating and comparing the force coefficients in the same range of attack angle ($\alpha=0^\circ$ to 25°) on two flat rectangular membrane sails, considered rigid, in the presence of the sea and deck effect, located at 1m below the foot curve. The $AR=4$ sail panel model is that analysed above, while the $AR=5$ sail is characterised by lengths of the foot and luff of 1m and 5m respectively.

From figure 5.14 on the left, as the aspect ratio increases, the lift coefficient increases mainly because it becomes more similar to a 2-dimensional plane. On the right, the polar diagram shows that the difference becomes significant for attack angles $\alpha>10^\circ$.

Figure 5.15 and 5.16 show respectively the distribution of the forces acting in the spanwise direction, for the two above mentioned rectangular flat membrane sails in the case of an external flow, characterised by an asymptotic velocity of $V_\infty=10\text{m/sec}$ and $\alpha=10^\circ$.

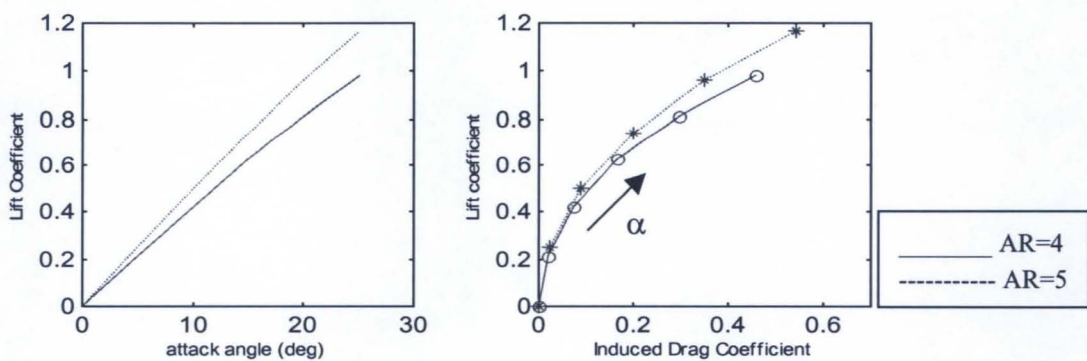


Figure 5.14: Aspect ratio influence on the force coefficient evaluation

Considering both figures 5.15 and 5.16, the pressure coefficient distribution along the middle section, upper left graphs, does not change. Whilst, looking at the lift and induced drag distribution along the span, the AR affects the values and the distribution shape (upper right and lower left diagrams). The lift is almost following an elliptical law distribution along the sail span on the sail with AR=4. The maximum lift coefficient is achieved at 66% of the sail-span and its value is around $C_L=0.53$.

Then, the lower aspect ratio influences the force distributions in terms that the finite wing effects are more evident. In fact, considering what happens on the sail with AR=5, the lift force does not follow a symmetric distribution, the maximum value is around almost the 84% of the sail-span, reaching the maximum value of 0.6.

The concurrence of a higher aspect ratio and the sea presence bears three main consequences:

- lift coefficient maximum value shifted in the upper direction along the span
- bigger value of the maximum coefficient
- bigger value of the induced drag coefficient.

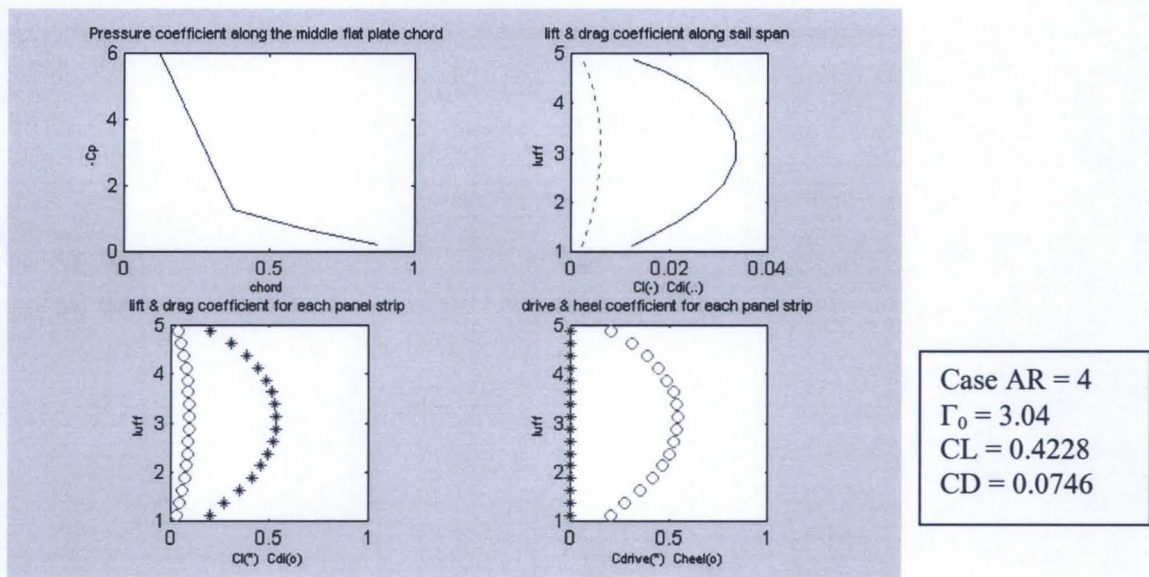


Figure 5.15: Force coefficients distribution for AR=4 ($\alpha=10^\circ$)

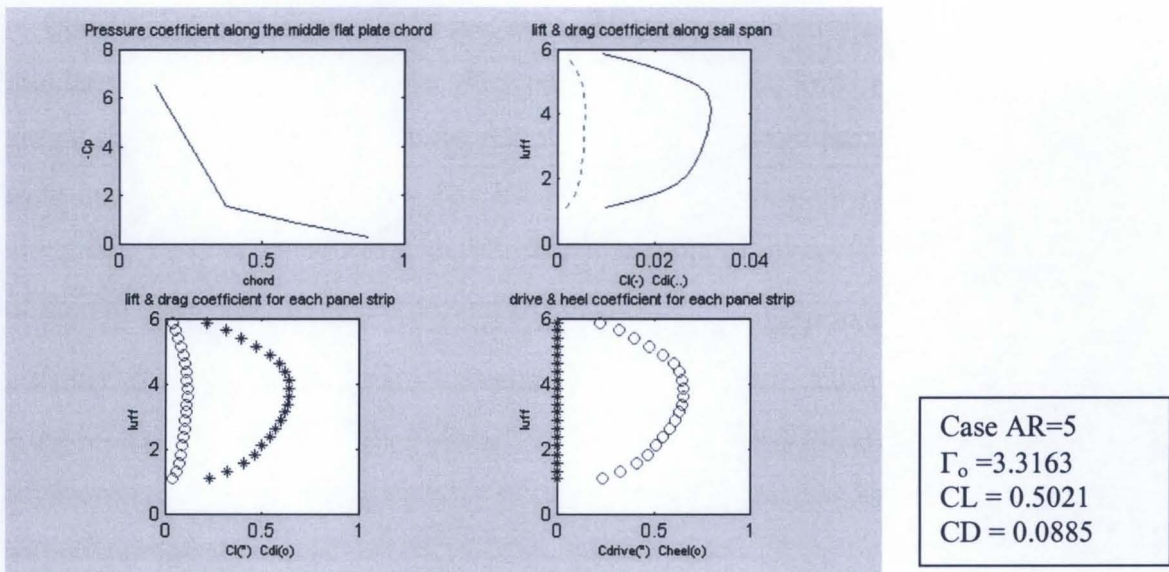


Figure 5.16: Force coefficients distribution for AR=5 ($\alpha=10^\circ$)

5.6 Conclusions

This chapter has illustrated the reasoning and modalities used to accomplish the calculation of the aerodynamic loads on the sail surface.

General aspects of the Modified Vortex Lattice method have been described, since the indicated literature and section B furnish further accurate details. In addition, the graphical user interfaces for performing the aerodynamic analysis, visualising the wake geometry and the aerodynamic loads obtained at the end of the first iteration have been illustrated in their functionality. Debate about critical aspects concerning the solution method used and the suggested actions integrate the descriptions.

It has been considered opportune to investigate the coherence with Prandtl theory, in order to validate the model. The results for a flat plate are very positive.

Further the influence of the aspect ratio and of the sea surface are shown.

Those investigations affirm the validity of the implemented M.V.L.M. for analysing three-dimensional high cambered lifting surfaces, like sails, ensuring the quality and the reliability of the results obtained.

Chapter 6

Structural Analysis

6.1 Observation about the sail structural behaviour

A typical flying sailboat configuration, like figure 1.2 illustrates for a FINN class sailing boat, presents the rig in tension due to the necessity of keeping a particular sail-shape, obtained by bending and twisting the mast and a full sail. The final sail configuration is usually indicated as loaded.

Consider the same sail in the following described conditions.

For example, considering the case of wind absence ($V_{True} = 0\text{m/sec}$) and considering the boat standing in the harbour ($V_{Sailing}=0\text{m/sec}$), no aerodynamic force can be developed by the sail. The configuration adopted in this case is habitually identified as unloaded: the sail wrinkles, seeing that the material folds on itself in particular zones, due to the fact that the sail is not built flat, as it needs to assume a particular curved shape during the sailing.

An additional example concerns the eventuality of changes in the external conditions, which determine modifications in loads and their distribution and consequently changes in the sail shape, which will adapt its shape to the new load conditions. In any of the above circumstances, the common consequence is that large displacements have occurred.

Reconsidering the above-described facts, common behaviour can be observed, [48]:

- sail undergoes large displacements;
- displacements do not increase linearly with the applied loads;
- material behaviour may not be always linear elastic;
- boundary conditions may change during the application of the loads.

The explanation of these sail structural behaviour aspects is in three main factors:

- adopted material,
- construction methods,
- applied loads.

Hereafter, the influence of the adopted material and construction methods are reviewed in sections 6.1.1 and 6.1.2, while details concerning the applied loads is widely developed in the previous chapter 5 and in the following chapter 7.

The purpose of this section is to describe the structural behaviour of a sail, in order to explain the difficulty in tackling the structural analysis.

The rest of this chapter illustrates the applied method and how it is implemented in the graphical user interface, developed to accomplish this phase. The chapter ends with the validation of the implemented code.

6.1.1 Materials

According to the fact that sailcloth are inhomogeneous, orthotropic membranes with non-linear behavior, their main characteristic is the high flexibility that causes sails to assume the typical aeroelastic behaviour, as seen in chapter 3, [31].

These characteristics result from researches in developing materials for sailcloth, [61], [62], [68], [72], in order to achieve the most required structural properties, which are:

- low stretching,
- high strength,
- light weight, which allows sailing boats to go faster because they carry smaller loads.
- sunlight resistance, porosity, damage resistance, which strongly influence the sail life length.

Most of the new materials, which satisfy these requirements, have been available for ten years and are new woven and laminated sailcloth. In reality, until the end of the 1980s, woven polyester, known as Dacron[®], was the only sailcloth in use. Nowadays, sailcloth includes not only the dacrons and nylons in various weights and finishes, but laminates using Kevlar, Technora, PBO Zylon, Pentex and Spectra yarns. Hence a brief description of these materials follows, for the purpose of outlining their principal structural properties, which are determinant factors in the sailmakers decision, [20], [30], [68], [79].

Dacron[®] is a woven polyester extremely durable and relatively inexpensive. It has been used since the middle of the 1950s and hence sail-makers are aware of its performance characteristics. It is still used when durability is the primary concern. According to the fact that the material can be created with added strength by orienting stronger or more yarns in the warp or fill direction, it can be considered:

- homogeneous, in the case the yarns have equal strength in both warp and fill directions,
- "warp-oriented" in the event the yarns are oriented in the warp direction,
- "fill-oriented", when the yarns are mostly oriented in the fill direction.

Laminated sailcloth is composed of some cloth or yarns, which are glued to one or more layers of Mylar[®] film. While the strength of woven cloth lies in the direction of the yarns only, the Mylar[®] film reinforces in all directions because it has strength in all directions. Then varying thickness from fractions of one millimetre to three or even four millimetres, it is possible to improve or define particular laminate structural properties. Yarns such as Nylon[®], Kevlar[®], Vectran[®], Spectra[®], Technora and other polyester fibres can be used. Therefore, the kind of yarns and orientation chosen and the reinforced thickness of Mylar determine the structural properties of the particular laminate. However, they are built to be lighter and able to hold the sail shape for an equal value of the Dacron[®] strength.

For instance, Vectran[®] has similar flex fatigue characteristics to Spectra[®], but unlike Spectra[®] has high heat resistance. This allows it to be woven with polyester. Then, through a special patented process, it achieves a very low stretch, which allows a reduction in the true weight of the sailcloth compared with other sailcloth under the same loads, as figure 6.1 shows. Notwithstanding Spectra[®] yarns are lighter, more flexible than Kevlar[®] and Technora and it doesn't break down from folding, it gets softer with use and it is also more expensive. This means, eventually, that under high loads, Spectra[®] yarns elongate.

Thus, it is not used for predicted loads, which are high enough to cause significant elongation. The entire aforementioned products are registered trademarks by Dupont. For this paragraph and for the figures 6.1 and 6.2, refer to the UK sailmaker factory encyclopedia at: <http://www.ukhamble.com>.

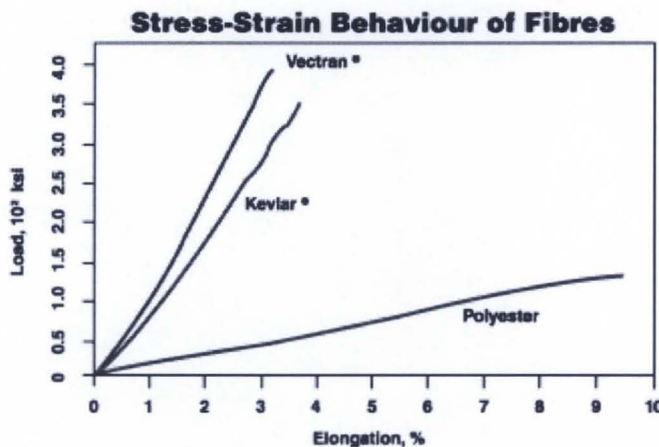


Figure 6.1: Stress-Strain diagram for some of the mentioned sailcloth fabric.

In conclusion, indeed other sailcloth manufacturers have developments underway with a goal of providing enhanced durability. The trend for sailcloth and sail making will depend on the demands of sailboat owners. For instance, in the eventuality that the hydrodynamic loads increase because of a bigger yacht, sailing loads are higher and as a consequence sailcloth manufacturers will need to continue developments that provide increased durability.

6.1.2 Construction Methods

In view of the fact that one of the design goals is to manufacture a sail, which is able to keep its designed shape when it will sail, nowadays, several computer codes aid the entire process involved. One of the steps produces a stress map on the sail. This is very important, due to the fact that sailcloth is most resistant to stretch when the yarns are in line with the stress. In fact, being aware of the stress distribution over all the sail, the construction methods tend to use more sailcloth panels seamed together in order to align stronger thread-

line with the loads. Therefore, there are considerable variations in how panels are arranged in modern sails. The most popular ways to seam together the panels are:

- cross-cut panel layout, and
- radial panel layout.

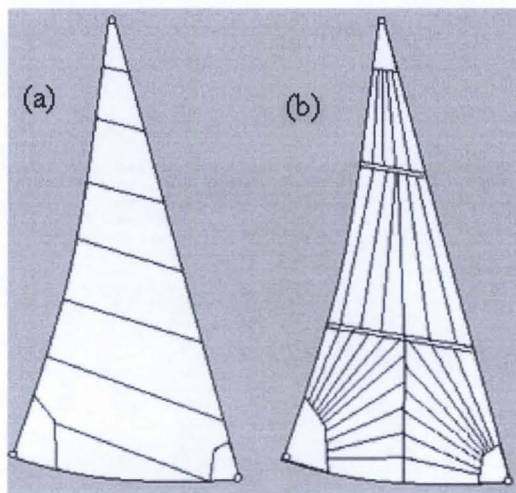


Figure 6.2: (a) crosscut panel layout, (b) radial panel layout

The first technique, plotted on the left side of figure 6.2 in case of a jib sail, places all panel cloths parallel to each other and perpendicular to the sail-leech. Due to the fact that the technique is simple, does not waste cloth and permits the sail shape control through the seams, sail-makers prefer the cross cut layout for large area sails, such as a main sail and genoa. The purpose of this layout is to reinforce the leech, which is particularly loaded. In order to achieve this requirement, the panel cloths are ‘fill-oriented’, because the fill direction will be parallel to the leech curve.

Radial cut layout, plotted on the right side of figure 6.2 in case of a jib sail, uses long narrow triangular laminate panels, called gores. Generally, they have more strength in the warp direction. The main characteristic of this layout is the possibility of using more than one laminated fabric in a sail, which leads to building a lighter sail that has strength where it is needed. Thus, wide gores in light cloth are used in low load areas. Then, in high load areas like the leech and tack, narrow and stronger gores permit making the warp-threads parallel to the loads in the sail. This construction method allows using lighter cloth in the

less loaded sail luff and a third fabric, heavy and resistant, can be used in the foot panels. Considering all loads start from a corner and then run in arcs through the sail and end at the other two corners, the gores radiate from the sail corners.

The newest sailmaking technology introduced in 1994 by North Sail is called 3DL, [73], which is nowadays very popular. It is a three-dimensional laminate: different types of material are laminated together as figure 6.3 shows. It moulds sails three-dimensionally in a single, seamless piece.

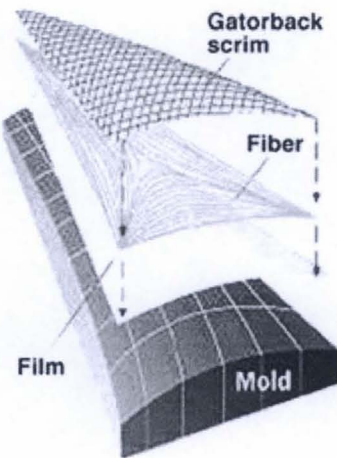


Figure 6.3: 3DL-sailmaking technology (picture taken from www.americascup.org)

The entirety of the above issues necessitates a simplified structural model in order to accomplish the analysis.

6.2 The structural analysis

With reference to section 6.1, the described sailcloth properties determine particular difficulties in tackling the structural analysis. Jackson [32] observes that the corroboration of this latter observation is in the fact that all of the published studies concerning the sail

aeroelastic analysis are characterised by strong assumptions concerning the sailcloth structural behaviour.

As mentioned previously, these structural sailcloth characteristics generate a non-linear geometrical structural behaviour, which require a non-linear structural analysis, [48]. For the purpose of clarifying this question, consider that the result of a well-performed structural analysis is to find an equilibrium condition between the stress distribution over the sail and the external applied loads. Due to the fact that sailcloth undergoes deformation under the aerodynamic loads, finding this equilibrium condition requires an iterative procedure. Therefore, the non-linearity of the structural analysis determines the necessity of making restrictive assumptions regarding the following listed possible problems:

- define the stress distribution of a known loaded sail-shape,
- determine the sail-shape, beginning from the unloaded sail structure.

The structural analysis has been tackled using the Finite Element Method (F.E.M.). In order to perform it, the representative model has been built utilising a finite element characterised by structural behaviour as close as possible to the real structural behaviour.

Considering that the aims of the presented integrated sail design system are the following, as announced in section 4.1, page 52:

- analyses for existent sail-shapes,
- modifications of their geometry to test further performance,
- creations of new sail-shapes;

the first two aims refer to the case of a known loaded sail shape, while the third aim is the concern of a designed sail. Due to the fact that in all situations, the sail shape is well described at the time $t=0$, the present problem formulation uses the Total Lagrangian Formulation.

The F.E.M. formulation adopted derives its procedures through the following steps:

- (i) define the constitutive relations for the finite element adopted;
- (ii) obtain the governing F.E. equations through the principle of virtual work;
- (iii) assemble the equations and solve with the Newton Raphson iterative solution method.

Henceforth, the following sections describe firstly the used finite element model and secondly the assumptions made and the method applied for tackling the structural analysis.

6.2.1 The finite element model

The accomplishment of the first step (i), mentioned in section 6.2, has considered the observation that sails are membrane structures, due to the following facts, [8], [33], [48]:

- typical sailcloth is very thin, the thickness is usually around 0.005m, with respect to sail size, noting that usually luff, leech and foot are of the order of a few meters
- sailcloth are flexible.

With this assumption the variation of the mechanical quantities, such as the displacement, stress and strain fields are neglected through the thickness.

Supplementary, since the fact that sailcloth allows large displacements and small strains, the stress-strain relation, in the present formulation, is linear, [53], [66], [57].

Consequently, these assumptions indicate that a membrane element would be suitable to build the finite element model. Apart from the aforementioned characteristic, the element has, as the sailcloth, in plane, but not flexural stiffness, which means that it can only resist transverse loads by virtue of its curvature, [59].

Summarising, the adopted element has to have the following characteristics:

- each node has the three translation degrees of freedom,
- each node can assume large displacements,
- each point within a single finite element follows the node displacements and its resulting displacement is a linear combination of the nodal displacements;
- large displacements within the finite element cause a non-linear relation between strain and displacement, because of dependence on the new assumed sail geometry;
- sailcloth are built for keeping their flexibility, notwithstanding the large sail displacements, which corresponds to a linear stress-strain relation.

The triangular membrane element, described by Tabarrok and Qin [59], has been chosen, because it satisfies all of the above points and moreover it allows structural analysis

in case of loaded sail-shape as well as finding the final shape, in given external condition, from the unloaded flat shape. Henceforth this section describes how the formulation for the finite element model, due to Tabarrok and Qin [59], has been applied in this work. Further details are described in the Appendix C.

The ‘Mesh’ stage of the geometric generation phase, as section 4.4.3 and figure 4.9 illustrate, ends after fixing a set of nodal points, which are used for building up the aerodynamic panel model, as section 5.3 describes. The finite element model is built up with triangular elements among the same set of nodal points, considering that in each panel of the aerodynamic model, there are two triangular finite elements for the structural model.

In order to clarify this statement, the intent of figure 6.4 is to plot how two finite elements (f.e.) are built in one of the n_p quadrangular aerodynamic model panels. Namely, the r^{th} f.e. is built among the nodes i, j and l whilst the s^{th} f.e. among j, k , l . Figure 6.4 displays also the local coordinate system for each finite elements, respectively (x_r, y_r, z_r) and (x_s, y_s, z_s) , as well as the global coordinate system (X_g, Y_g, Z_g) , as described in section 3.2 and plotted in figure 3.1.

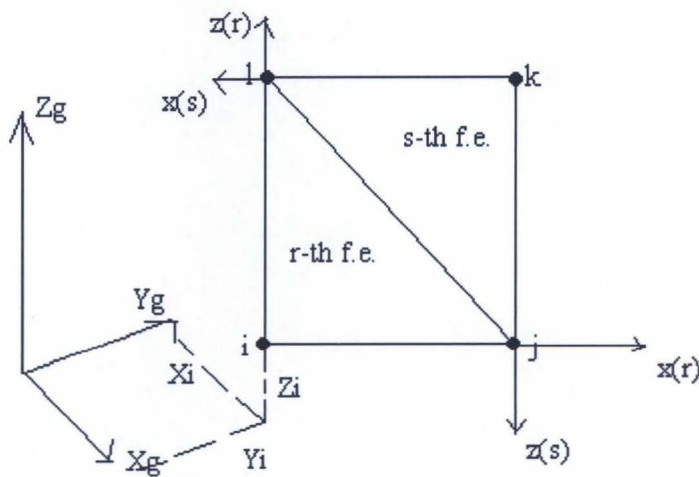


Figure 6.4: Triangular finite elements in a quadrangular aerodynamic model panel.

The reasons for this particular subdivision are in the fact that it:

- eases the connectivity matrix calculations between the node co-ordinates of the aerodynamic model and the degrees of freedom of the triangular elements nodes,

- facilitates the transformation matrix evaluation between the local and the global coordinate systems, as the local z axes is always vertical, and
- permits to apply directly the aerodynamic loads on each f.e. node.

According with the above considerations, the relations governing the structural problems are listed below:

- since any node has three degrees of freedom, for instance node j, belonging to rth f.e., can translate along the three directions of the Cartesian space (x_r, y_r, z_r) and the corresponding displacements are indicated as u_j, v_j, z_j;
- due to the fact that any f.e. is plane, all the points within each of them have the coordinate y=0, the shape functions which link the displacement of an internal point to the node are linear and they can be written as follows, in the case of the rth f.e.:

$$\begin{cases} u(x, z) = \alpha_1 u_i + \alpha_2 u_j + \alpha_3 u_l \\ v(x, z) = \alpha_1 v_i + \alpha_2 v_j + \alpha_3 v_l \\ w(x, z) = \alpha_1 w_i + \alpha_2 w_j + \alpha_3 w_l \end{cases} \quad (6.1)$$

where u, v, z, and u_{i,j,l}, v_{i,j,l}, z_{i,j,l}, are, respectively, the translations of an internal point and nodes, while α_{1,2,3} are functions of the nodal co-ordinates;

- the displacement-strain relations are non linear, for instance the expression for the strain in the x direction is expressed by the following expression:

$$\varepsilon_x = \frac{\partial u}{\partial x} + \frac{1}{2} \left[\left(\frac{\partial u}{\partial x} \right)^2 + \left(\frac{\partial v}{\partial x} \right)^2 + \left(\frac{\partial w}{\partial x} \right)^2 \right] \quad (6.2)$$

Taking into account that the membrane finite element has in-plane stress, analogous expressions exist for ε_z and γ_{xz}, therefore through the derivative, the deformations vector is expressed by:

$$\boldsymbol{\varepsilon} = (B + \frac{1}{2} AG) \boldsymbol{u} \quad (6.3)$$

where ε , the (3x1) strain components vector, is the sum of a linear part, which depends on the displacement vector u and a non linear part, which is dependent on the square of displacement derivatives;

- the strain-stress relations are linear:

$$\sigma = D \cdot \varepsilon + \sigma_0. \quad (6.4)$$

where σ is the (3x1) stress component vector ($\sigma_x, \sigma_z, \tau_{xz}$), according with the in-plane stress stiffness, D is the elastic matrix depending on the Young's modulus E , the Poisson ratio ν , while σ_0 is the stress vector corresponding to the stress distribution over the initial sail shape at the time $t=0$.

The relations (6.1) to (6.4) describe the structural laws for each finite element. Appendix C furnishes further details about the mathematical developments of those expressions. Thus, as the step (i) is completed, it is possible to pass to the employed method description.

6.2.2 The implemented finite element method

This section describes the completion of the phases indicated by the points (i) and (ii) in section 6.2.

In order to define the equations governing the equilibrium of a single finite element the principle of virtual work has been utilised. Therefore, considering the r^{th} f.e. in the local coordinate system (x_r, y_r, z_r), it is expressed as follows:

$$\int_{V_r^{\text{th}}} \delta \varepsilon^T \sigma dV - \delta u^T p = 0 \quad (6.5)$$

where the first term represents the virtual work due to the internal forces, whilst the second term is the virtual work due to the external loads, acting on the nodes in the local coordinate system, due to the body force vector, such as the sail weight, and the surface forces, due to the pressure distribution calculated in the previous aerodynamic phase and V_r^{th} is the volume of the r^{th} finite element.

Substituting (6.3) and (6.4) into (6.5), the equilibrium equation for the r^{th} f.e. is expressed as follows:

$$\int_{r^{\text{th}}} \left[[(B + AG)\delta u]^T \cdot \left[D \cdot \left(B + \frac{1}{2}AG \right) u + \sigma_0 \right] \right] dV - \delta u^T p = 0 \quad (6.6)$$

Summarising, the equation (6.5) expresses the equilibrium in the local coordinate system (x_r, y_r, z_r) of the r^{th} f.e.. In view of the fact that it is possible to write this expression for any finite element, there are $2 \cdot n_p$ equations (6.5), which, in order to be assembled, have to be transformed into the sail coordinate system (X, Y, Z) .

Once the $2 \cdot n_p$ equations (6.5) are expressed in the common sail coordinate system, they constitute an non linear equilibrium equations system, which may be solved iteratively through the Newton-Raphson iterative procedure. From the physical point of view, it asserts the fact that the sail membrane is affected by a geometrical non-linearity.

It is important to repeat here that the developed code for solving the structural analysis follows the method developed by Tabarrok and Qin, [59] and the iterative solution applies Newton-Raphson, as in Muttin, [48], where details can be founded, while some important mathematical aspects are developed in Appendix C.

Henceforth, this section addresses two fundamental questions:

- how the loads have been applied and distributed,
- definition of the initial conditions and constraints used for running the code.

6.2.3 Loads

The equilibrium equation (6.6) is written for any finite element in the respective local coordinate system. Therefore, the sum of the loads applied over the sail has to be calculated before and in the sail coordinate system (X, Y, Z) and then transformed into the local coordinate system (x_r, y_r, z_r) .

With reference to the loads acting on the sail, this formulation presumes two types:

- body loads,
- aerodynamic loads.

The body loads are due to the weight of the sailcloth. Therefore, knowing the specific weight of the particular material used and the finite element volume, since the thickness is known and considered constant for all the process steps whilst the area is evaluated step by step, it is possible to calculate the weight of any single finite element. Once the weight is transformed into force, it is divided in three equal parts and applied on the three nodes of a finite element. Further, due to the connectivity matrix of the elements, in any node the total weight force acting is the sum of the weight forces due to the finite elements to which it connects. It is notable that, since for this formulation the heel angle is always equal to zero degrees, the weight force acts along the Z-axes of the sail coordinate system (X, Y, Z).

The aerodynamic loads are those resulting from the aerodynamic phase, as seen in chapter 5. According to the fact that the pressure force is known on each panel and it is considered constant over a single panel, the value of the pressure force acting on each panel is also constant. Further, thanks to the connectivity matrix for the fluid-dynamic model, the pressure force acting in each node is the sum of the pressure force acting on the panels to which the node is connected.

As announced at the start of this section, these two force systems are added in the sail coordinate system (X, Y, Z). Then, in order to write the equation for a single finite element, they are transformed into the element coordinate system. Finally, when the entire equations are obtained, they are assembled in the sail coordinate system and the solution process starts.

6.2.4 Initial and boundary conditions

This section illustrates the way the implemented code determines the initial conditions. In its latter part the used boundary conditions are described.

In view of the fact that the implemented code considers the Total Lagrangian Formulation, whereby the entire static and kinematic variables are referred to the initial configuration, corresponding to the time $t=0$, the initial sail-shape and the variables involved have to be known at the instant $t=0$.

As the used formulation allows the structural analysis in these three cases:

- known flying sail-shape
- unknown flying sail-shape and due external condition
- known flying sail-shape and unknown external conditions

a variable, called *direct*, is introduced which enables switching among three ways of introducing the initial conditions for any of the aforementioned cases. In each of those three cases, the boundary conditions are equal.

Considering the solution of the equations system, in the eventuality that the iterative solution starts from a configuration of equilibrium, where the displacement field is always zero, the calculated stiffness matrix is singular at the first iteration.

In order to start the iterative process, it has been necessary to calculate by linear analysis the force and stress fields for a possible small-deformed shape of the structure. Subsequently, the non-linear analysis could start, considering this assumed deformed configuration and the related field of stress and displacements. In this way the stiffness matrix is not singular, but badly conditioned. In fact, the convergence results are sensitive to the following factors:

- the chosen initial deformed shape;
- the evaluated initial stress for this shape;
- how the load is applied.

In the eventuality of a loaded sail-shape analysis, looking at the formulation of the equilibrium equations for this problem (6.6), the start of the iterative process needs, apart from the sail geometry and loads distribution, the initial stress σ_0 and the deformed shape. In view of the fact that the latter variables are unknown, the first problem in solving the structural analysis consisted in deciding how to calculate them. Therefore the decision was to estimate the initial stress distribution σ_0 as the solution of the linear structural solution for the finite element model, as derived from the geometric generation. This solution enables the evaluation of the initial stress σ_0 , initial vector for the displacements and loads, which are to be used for starting the non-linear solution.

The decision to evaluate these vectors through a linear analysis, in lieu of inserting an imposed initial value for them, has been driven by the consideration that the analysed sail-shape is in equilibrium under certain loads. Therefore, the displacements from its initial

configuration are expected to be small. Notwithstanding the fact the linear solution does not provide the final deformed shape and stress distribution because the solution is affected by the initial hypothesis that the displacements are small, it provides an approximate solution, which can be improved by the successive non-linear solution.

This previous calculation is saved in the mat file named structure. In this initial linear solution, the considered loads acting on the sail are the weight forces due to the sailcloth, which are added to those evaluated by the previous aerodynamic phase, introduced as section 6.4.3 describes. According with the fact that the non-linear code considers all small strains, the relation between stress-strain continues to be expressed by the (6.4). However, the σ on the left is going to be the σ_0 , sought for the non-linear solution and the σ_0 on the right is considered a zero vector.

However the solution is accomplished by an iterative loop similar to the one used for the non-linear solution, as it is described above. The principal difference is in evaluating the stiffness matrix, which relate the displacements to the strain. In this case, it is formed only by the linear part, as the small displacements hypothesis implies that in the expression (6.2), the squared value of the cross derivative can be ignored. When compared with the first term on the right.

Then, the equation (6.3) becomes:

$$\varepsilon = Bu \quad (6.7)$$

The iteration process will stop when the solution for the deformed sail-shape becomes stable. The final solution provides an initial vector for the displacements, initial stress and total loads applied. It is important to report that the computational time on the same p.c. basis is a few seconds.

In the eventuality that the loaded sail shape is unknown, the input is a flat sail membrane shape, characterised by no initial stress, and the external condition. In this case, the loads evaluated by the initial aerodynamic solution are related to a rigid flat sail. From the structural point of view, these loads with the weight forces are applied on the flat membrane. To start the solution, the procedure is similar to the one for the known loaded sail-shape. In this case, the solution process requires longer iterations and sometimes the

solution yields by a non-uniform displacement distribution due to an incorrect evaluation of the initial stress distribution.

In the eventuality that the shape is known and the design goal consists of verifying the external conditions, which produce it, the previous linear analysis considers only the weight as loads.

With reference to the boundary conditions, the chosen constraint equations aim to reproduce the real behaviour of a FINN class sail configuration. In view of the fact that the sail is linked to the mast and the boom, in the way it can slide along them, whilst the leech is free, the boundary condition are:

- nodes along the foot section can move only along the boom axes, which coincides with the X-axes of the sail coordinate system;
- nodes along the luff curve can move only along the mast
- nodes along the head section are fixed;
- nodes along the leech are free.

6.3 The G.U.I. for the Structural Analysis phase

This section describes the graphical user interface for running the phase of the structural analysis, as described in the previous section 6.2. As assumed in the chapter 5 for the aerodynamic analysis phase G.U.I., the principle driving the design of the present G.U.I., shown in figure 6.5, is to customise it with proper features for facilitating the approach by any user when performing the analysis without requiring knowledge about the implemented method. Therefore, this section illustrates the features of this interface and how it works, in the view of the non-linear structural analysis method.

It is important to remember that the finite element model is built using the nodal points, decided at the end of the geometrical phase by the designer, as described in section 4.4. Those nodal points coincide with the nodes of the quadrangular panels for the aerodynamic analysis. In order to ease the connectivity between the two models, in view of the fact that the structural analysis is carried on with triangular elements, each quadrangular panel is

divided into two triangular elements, as section 6.2 explains. Therefore, the nodal points saved in the meshing phase are nodes for the aerodynamic panel model as well as for the finite element model.

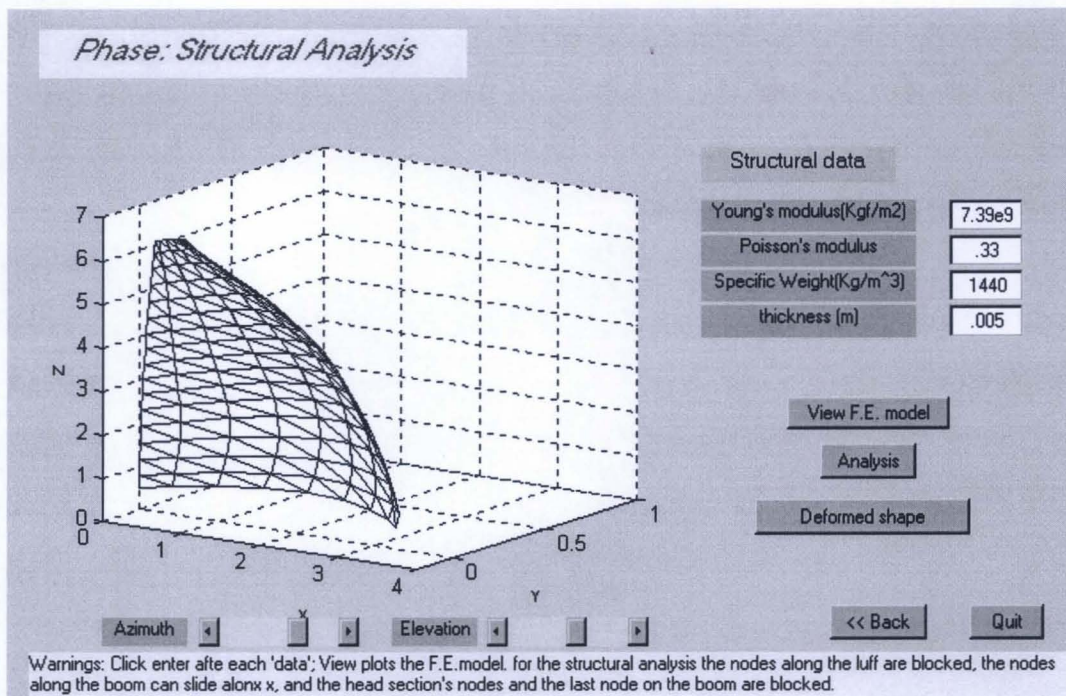


Figure 6.5: The Structural Analysis phase G.U.I.

Looking at figure 6.5, on the left of the interface, the graph plots the finite element model, as it is expected from the previous meshing phase. For the sail shown, the opening of this interface calculates the following matrices:

- finite elements matrix;
- connectivity for the degrees of freedom of nodes belonging to more than one element;
- boundary conditions.

The elaboration of the above listed matrices does not imply long computational time, as happens in the case of opening the Aerodynamic G.U.I., if the code runs on the same p.c. As well it constitutes a set of test operations for the finite element model. Indeed, a correct visualisation of the finite element model in the G.U.I., as figure 6.5 shows, ensures due regard for the proper compilation of the matrices for the elements and for the connectivity.

Therefore, in the event that problems appear later in the calculation, they do not depend on the created model or on the boundary conditions, which is verified as being correctly built.

Aware of these introductory considerations, the description of the features of this G.U.I. follows. Considering figure 6.5, as usual the ‘Azimuth’ and the ‘Elevation’ sliding buttons ease visualising the model from different points of view.

Then, on the right, from top to bottom, there is a list of editable spaces for defining the properties of the chosen material, which are:

- Young’s modulus (Kgf/m^2);
- modulus of Poisson ν ;
- specific weight (Kg/m^3);
- thickness (m).

On the left, hence, there are a series of push buttons.

The ‘View F.E. Model’ button plots on the graph the actual finite element model. When the designer has typed the material properties and believes in the correct definition of the model, clicking on the ‘Analysis’ button starts the non-linear structural analysis.

In the eventuality the model has to be improved, the ‘Back’ button allows opening the ‘Menu’ interface for a variety of changes, as chapter 4 describes.

Considering the fact that the analysis has finished successfully, the button ‘Deformed Shape’ opens another G.U.I., which plots the deformed shape, derived by the structural analysis. The next section 6.4 illustrates the features of this latter announced G.U.I..

As usual, the ‘Quit’ button closes the analysis session.

It is important to explain that the present G.U.I., figure 6.5, can be opened by clicking on the button ‘Structural Analysis’, which appears in the ‘Aerodynamic Analysis’ G.U.I., as figure 5.2 shows, and in the ‘Menu’ G.U.I., as figure 4.8 shows. This double link to this kind of analysis is justified by the following considerations.

The first link is the obvious continuation of the aeroelastic analysis procedure implemented, as explained in chapter 3. In fact, the Structural Analysis phase allows inserting the structural material properties.

The latter link adds an important feature to the entire G.U.I.. Indeed, as it is a design system, in this way it is possible to follow a different approach to the particular sail structure analysed. In fact, with the button in the ‘Menu’ interface it is possible to perform directly the structural analysis, avoiding the aerodynamic analysis phase. This direct link aids the design for two different strategies. On one side, it aids the test of new materials for known aerodynamic loads and sail shape. On the other side, it allows the investigation of new sail shapes, built with the same material, under known external loads. Naturally, it is possible to combine these two strategies in order to find the best combination of sail shape and material, under given aerodynamic loads.

This double link feature has been performed creating a new binary variable, called *direct*. This variable allows switching between two different ways to perform the structural analysis. Thus, clicking on the button ‘Structural Analysis’ in the Aerodynamic Analysis phase G.U.I., the variable *direct* assumes the value 0 (zero) and the non-linear structural analysis starts, as it has been described in the first two sections of this chapter. This performs the calculation of the deformed sail shape and stress distribution all over the sail under the external aerodynamic loads calculated in the previous phase.

Clicking on the button in the ‘Menu’ interface (figure 4.8) opens the structural analysis phase G.U.I. and the variable *direct* assumes value equal to 1. Notwithstanding the fact that the interface is the same, the analysis that is going to start assumes particular design characteristics. Two design purposes can be identified in having a structural analysis without the aerodynamic analysis phase.

For instance, consider the eventuality that the designer has chosen the sail shape, for a given set of external conditions and for a determined trimmed configuration. Then, in a previous shape design investigation, the designer gets for the given external condition the geometric sail shape and first evaluation of the aerodynamic analysis. At this point, the main interest is to build up a sail with structural properties and thickness, which permit maintaining the decided shape. The definition of a material, which better suits this shape, might need a sequence of tests for the same shape under the same aerodynamic loads. Then, bearing in mind that the first aerodynamic load evaluation on the sail depends upon its initial shape considered rigid, this can be calculated once. Hence, in order to avoid the repetition of this operation for any combination of material and thickness, by locating this

button in the ‘Menu’ interface, the structural analysis using the same set of external loads can be directly performed. It is notable that when a material suits the designer’s condition, the entire aeroelastic analysis converges in maximum two iterations. This is expected by the initial design condition, which requires that two subsequent deformed sail shapes are very similar.

Indeed, this feature works due to the introduction of another binary variable, called *phase-number*, which indicates the phase of the analysis. In fact, for the case above described, it is important that the set of loads evaluated once is available and used every time this kind of analysis would be done. Therefore, in order to start the analysis using the calculated loads, the *phase-number* variable assumes the value 1.

In the eventuality that the previous aerodynamic analysis has not been carried out for the actual sail shape, the *phase-number* variable assumes value 0. This indicates that external aerodynamic loads are not available and it is the first time that the structure is to be analysed. In this case, the sail structure is analysed only under the weight loads and it represents the second feature of this link. Mostly in the first design phases, sail designers might be interested in the evaluation of the influence of the weight of the sail on the entire deformed shape.

A conclusive consideration regards the duration of the calculations, which depends upon the number of finite elements used. However, the system converges in less than 120 seconds for 64-finite element model, in the case where the code runs on a Pentium processor with 32MB RAM. Naturally, the time increases almost linearly with the number of elements.

6.4 Conclusions

Summarising, this chapter has described the features of the implemented structural analysis, illustrating the membrane element characteristics and the definition of the structural equilibrium equations. Further, section 6.3 has described the features of the integrated graphical user interface and the reason behind the choices made.

Conclusive consideration regards the G.U.I. built in the present case. In fact, particular attention has been given to the implementation of a versatile G.U.I., which allows different design approaches. For instance, the possibility of using this G.U.I. for deepening investigations for testing or choosing material and/or sail shape has been discussed. However, further details about the features concerning 'design actions' phase as well as 'development of new sail shapes' will be presented in chapters 8 and 9.

Chapter 7

Aeroelastic Analysis

7.1 Analysis Description

In accordance with the analysis method implemented, as described in chapter 3 and in particular in section 3.3, this section demonstrates how the system automates the aeroelastic analysis loop. The next section illustrates the features of the graphical user interface designed for this phase, whilst the final part of this chapter examines a validation process for the entire analysis system.

In order to facilitate the description of the routines for the aeroelastic analysis, consider the figure 3.6, repeated in the next page for convenience. The subject of this section is the loop plotted in the bottom of the picture. It is completely automatic and there are no interactive actions made by the user.

Recapitulating, chapter 4 has described the phases for the definition of the geometric sail shape in order to have a set of distributed nodal points over the sail surface for building up the panel model and the finite element model for respectively the aerodynamic and structural analysis.

Afterwards, chapter 5 has illustrated the modalities for building the panel model and setting the aerodynamic analysis, defining which operations are automated and which are due to the user. Similarly, chapter 6 has described the implemented system for the sail structural analysis, clarifying the typology of considered loads for the analysis. In fact, as figure 3.6 shows and according with the system design features mentioned in section 6.3, in the case that the aerodynamic analysis is the first done, the loads considered for the structural analysis coincide with the one calculated in this phase. This procedure is not unique or suggested, it corresponds to the purpose of analysing a known sail shape.

In any event, the user in part conducts the first loop between the aerodynamic and structural analysis since it is necessary to define the accuracy of the aerodynamic analysis, the external condition and the structural material properties. This first iterative process ends with the calculation of the deformed sail shape in static equilibrium with the previous evaluated aerodynamic loads.

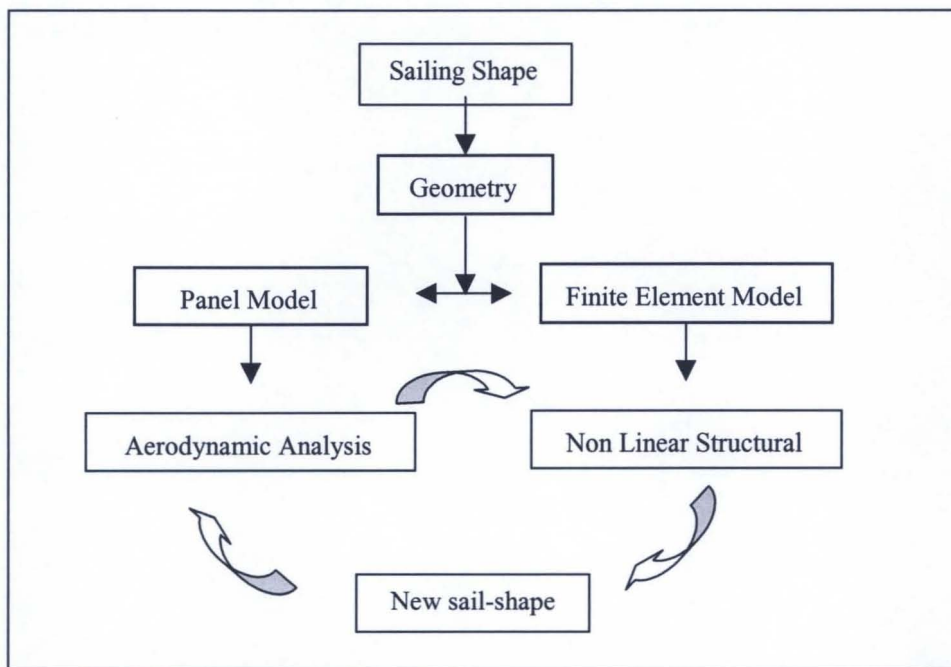


Figure 3.6: Aeroelastic analysis procedure

This deformed shape might not correspond with the final solution for the analysis intended. In fact, in the eventuality that the difference between the initial sail shape and the

current, in terms of modulus of the maximum displacement among the nodal points, is less than 0.001m, the solution is believed to be the conclusive one. For a different result, the analysis continues, until the convergence criteria is verified.

Therefore, in the second eventuality, as the sail shape is different from the initial, the same external conditions will produce a different pressure distribution.

Thus, the ‘aeroelastic analysis’ code automatically performs the following actions:

- 1) generates a new panel model, among the same nodal points, displaced on the actual deformed sail shape,
- 2) proceeds with the aerodynamic analysis in the same external condition and with the same wake geometry feature previously established by the user,
- 3) generates the corresponding finite element model,
- 4) applies the external loads, evaluated in 2), on the current finite element model, pretensioned by the stress distribution calculated at the previous time,
- 5) proceeds with the structural analysis, utilising the same material properties previously defined by the user,
- 6) evaluates the modulus of the maximum displacement between the current deformed shape and the previous one,
- 7) in the eventuality that the difference, evaluated in 6), is less than 0.001m, the iteration stops,
- 8) in the eventuality that the difference, evaluated in 6), is greater than or equal to 0.001m, the iterative process continues, starting from the operation described in point 1), until the convergence described in point 7) is verified.

Summarising, the result of this iterative process is the sail shape, with given structural properties, which is in static equilibrium with the known external condition. Further, it gives the aerodynamic loads and their distribution over all the deformed sail shape, which are fundamental in the design application, as explained in chapters 1 and 2.

Results of these analyses and their application are shown in the next chapters, 8 and 9.

7.2 The Aeroelastic Analysis Graphical User Interface

The present section illustrates the features of the graphical user interface, shown in figure 7.1, for performing the aeroelastic analysis automatically, as described in the previous section. This G.U.I. is opened by clicking the push button ‘Deformed Shape’, in the structural analysis G.U.I., as mentioned in section 6.3.

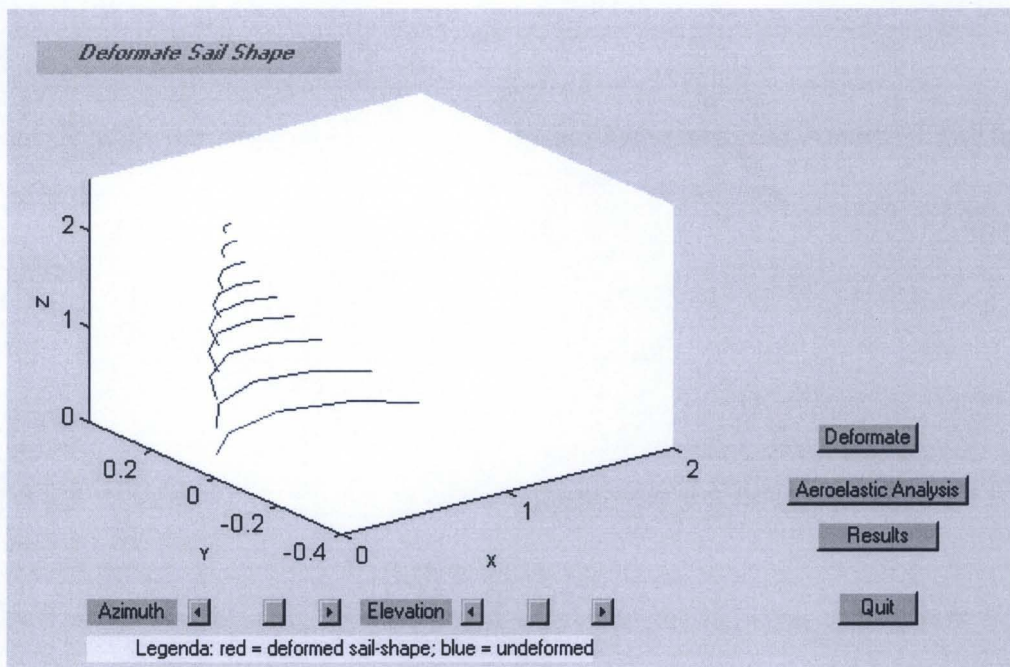


Figure 7.1: The Aeroelastic Analysis phase G.U.I.

Looking at figure 7.1, the graph of this G.U.I. plots the deformed sail sections, solution of the first structural analysis. Similarly to other interfaces, the two sliding buttons ‘Azimuth’ and ‘Elevation’ ease the view of the deformed shape, whilst the push button ‘Quit’ closes the actual analysis phase.

The push button ‘Deformate’ plots the current sail deformed shape.

The reason for viewing the obtained sail shape from the first full iteration is in the possibility of verifying the state of the aeroelastic analysis. In fact, in the eventuality that the first loop achieves the convergence, in this G.U.I. the graph plots the solution in terms of deformed shape and allows seeing the loads, by clicking on the ‘Results’ push button. In

the event that the first iterative loop does not converge the view helps in optimising the rest of the automated aeroelastic analysis. By visualising this first deformed shape, the designer decides if it is convenient that the analysis continues. It has been proved that in cases above the deformed sail-shape at this stage is irregular in someway, the successive analysis, if it converges, does not give a physically correct result.

In the event that the first iterative loop did not converge and the deformed sail shape appears physically correct, the button ‘Aeroelastic Analysis’ allows starting the automated analysis loop, as described in the previous section following the listed operations from points 1 to 8, page 123.

This solution process can last for a long period and, as mentioned in chapter 5, the aerodynamic phase consumes the majority of the entire computational time. When the process converges, pushing the button ‘Results’ plots the results in terms of pressure distribution, aerodynamic loads and deformed shape. As mentioned above, a large number of these kinds of plots are shown in the next chapters, 8 and 9.

7.3 Aeroelastic Analysis Validation

7.3.1 Plan, reasons and background

The main intent of this phase consists of establishing a comparison between the numerical results obtained from the developed package and the experimentally available results. From this comparison, the developed numerical package can be validated.

Prior to discussing the tests carried out, it is important to explain the difficulty in planning them. In fact, the existent literature is poorly provided, for several reasons.

Certainly, the first reason is the high cost of each experiment, either on a full-scale sail or on a scaled model in wind tunnel tests.

Another common reason concerns the fact that scientific studies in that field are young. Only recently more efforts have been applied to research in that field, involving universities

or research groups. Most of the racing teams push the research in that direction, because they have the dual motivation of the desire for victory and availability of sponsorship.

A further reason depends properly on the fact that the main research is done by race teams. Of course, they want to keep their developments secret, and so works carried out often do not appear in the literature. Published works are usually related to test cases done several years ago, and most of these give results calculated for a poorly described geometric sail surface or with an insufficient number of parameters. Moreover, most of the time there is not a clear description about how the force coefficients have been evaluated: for example, the way in which the forces are non-dimensionalised is usually omitted.

Being aware of the above-described difficulties met in tackling this delicate phase, the accomplishment of the work has been a considerable effort.

With reference to the main object of the present work, the plan has been to compare the numerical results obtained from the numerical package with the data available in Marchaj, [41], related to FINN class sails.

7.3.2 Description of the validation test

In order to validate the full implemented aeroelastic method, several tests have been carried out comparing the numerical results with the wind tunnel tests, made by Marchaj, [41], at the University of Southampton on a FINN sail model of 2/5scale. Consider Part III of the reference book, in particular pages 542-556, where the author, analysing the factor affecting the sail forces, illustrated their effects on the boat performance. The intent of the investigation was to look at the effect on the aerodynamics of the sail of the kicking strap tension and associated mast flexure, the effects of the sea influence and the influence of the wind speed and its direction on the sail shape (camber and twist distribution). Thus, no detailed description of the method and the sail used for those tests is given, ensuring that the results do not pretend to be accurate.

Given the above situation, it is obvious that the geometry realised from the available data cannot be equal to the sail used by Marchaj in his tests because of the lack of information.

Bearing this in mind, the published data described, in particular from pages 552 and 553, have been considered for extrapolating the data to insert in the ‘Input’ G. U. I.. From them, it is possible to deduce roughly the geometric description of some shape adopted by the same sail, for several conditions of kicking strap tensions. In fact, the available data are related to the sail shape assumed for an unknown kicking strap tension in a flow coming with a velocity of $V_\infty=8.9\text{m/sec}$ at $\alpha=25^\circ$. The test case considered is named as Run VIII in the reference. Then, further data available to construct the geometry are listed in table 7.1. Summarising, a rational comparison provides the results only for the above-described external conditions.

Notwithstanding this restriction, the behaviour of the force coefficients for the range of true wind attack angle $\alpha=[5^\circ \text{ to } 60^\circ]$ has been evaluated, considering the same sail shape. In view of the above discussion, it is believable that the errors in the evaluation of these force coefficient results has to be consistent with the approximations made in the geometry and in the extension of this shape to a larger range of conditions.

Table 7.1: Rig measurements for test.

Sail Area	SA	1.61 m ²
Aspect Ratio	AR	3.1
Tip deflection		0.216 m
Boom attach		0.25 m
Luff length		2.29 m

Table 7.2: Sections geometric characteristics

Section	Camber (local chord %)	Twist (deg)
I	9.7	1.7
II	9.9	2.0
III	8.2	2.2
IV	6.5	4.2
V	4.7	7.0
VI	3.8	9.8

Table 7.1 and 7.2: Geometric data available for the test case, derived from Marchaj [41].

Once the geometric data had been extrapolated and adapted in order to type them in the input interface, the phase related to the development of the geometric surface followed, trying to get a smooth surface. The approximations made concerned:

- position of the maximum camber,
- section chord lengths.

Both of the questions were solved considering the available photographs. Then, the camber was put at 50% of the local chord and the chord distribution was taken to be linearly decreasing. With these features, when the geometry seemed well defined, the aeroelastic analysis was started.

The validation test began considering a 32 panel-model, which figure 7.2 (a) shows. To reproduce a similar test case to the one described in Marchaj, the used external conditions are $V_{\text{apparent}} = 8.9 \text{ m/sec}$, $\beta = 25^\circ$. The wake length influencing the potential solution is 7m and the number of control points is 7. Figure 7.2 (b) plots the results of this first test case. For this particular case, the evaluated error is high due both to the small number of panels used and the error incurred in developing the geometric surface. In fact, the aspect ratio is equal to 2.3, as opposed to 3.1 in the test case adopted for the comparison. The calculated errors are around the 20% for both the force coefficients, lift and induced drag.

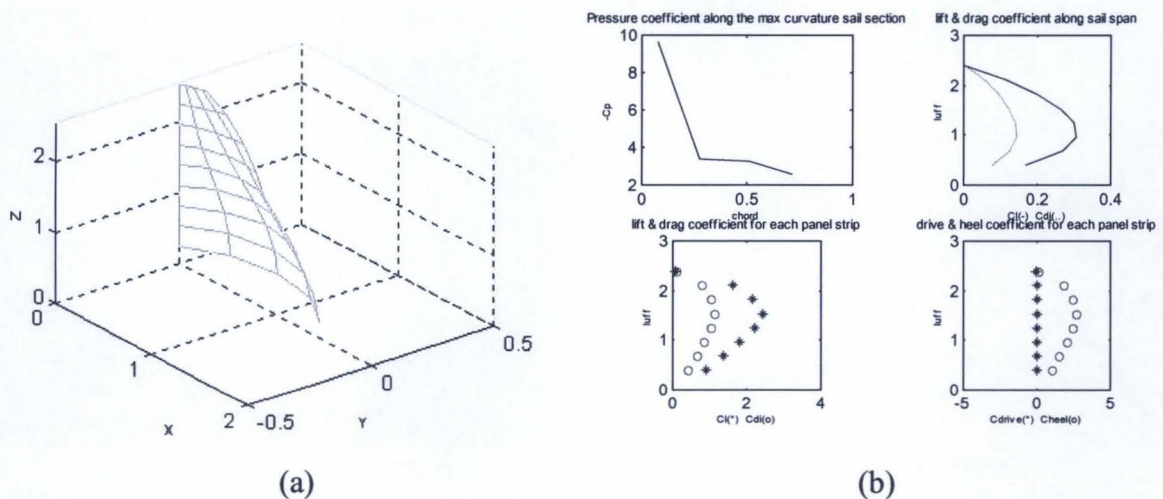


Figure 7.2: (a) 32-panels model for Run VIII; (b) related results after 2 full iterations.

Despite the fact of the quantitative error and considering the good quality of the obtained force distributions, the analysis on a 64-panels model (figure 7.3 (a)), using the same approximated geometry, was carried out. For this experiment the apparent wind angle is $\beta=45^\circ$ and in the light of the fact that the leeway angle was set at $\lambda=10^\circ$ and the boom

sheeting angle at $\delta_m=10^\circ$, thus the sail surface sees a true attack angle, $\alpha=\beta-(\lambda + \delta_m)=25^\circ$. Like in the previous experiment, the wake length is 7m, whilst the number of control points is 11. The apparent flow intensity is $V_{\text{apparent}} = 8.9\text{m/sec}$.

Figure 7.3-(b) shows the results for the test case presented in figure 7.3-(a). The lift coefficient is underestimated by 1%, in fact the estimated value by the calculation is $CL=1.34$, against Marchaj evaluation of $CL=1.22$.

Concerning the induced drag coefficient, this is overestimated, with the calculated value of $CD_i=0.67$, while Marchaj gives $CD_i=0.42$. The discrepancy is due to the panel aspect ratio, which is $AR=2.5$ in the calculations.

According to these tests, the results are encouraging bearing in mind the following points. Firstly, as aforementioned, the geometry could not have been realised better, due to the lack of information. Additionally, the structural analysis phase has been carried out without knowing the tension applied to the luff curve and the foot. Concerning this question, as the chosen run had strong applied tension, the chosen sail shape was the one presenting the minor deformation. Further, there is no description of the position of the sensors and how the given coefficients are calculated. These investigations and considerations make the obtained results positive, notwithstanding that the same author declares that the results do not pretend to be accurate. However, he achieved his main aim, which was outlining to sailors what happens in certain sailing circumstances and then how to react. Thus, the given information is sufficient.

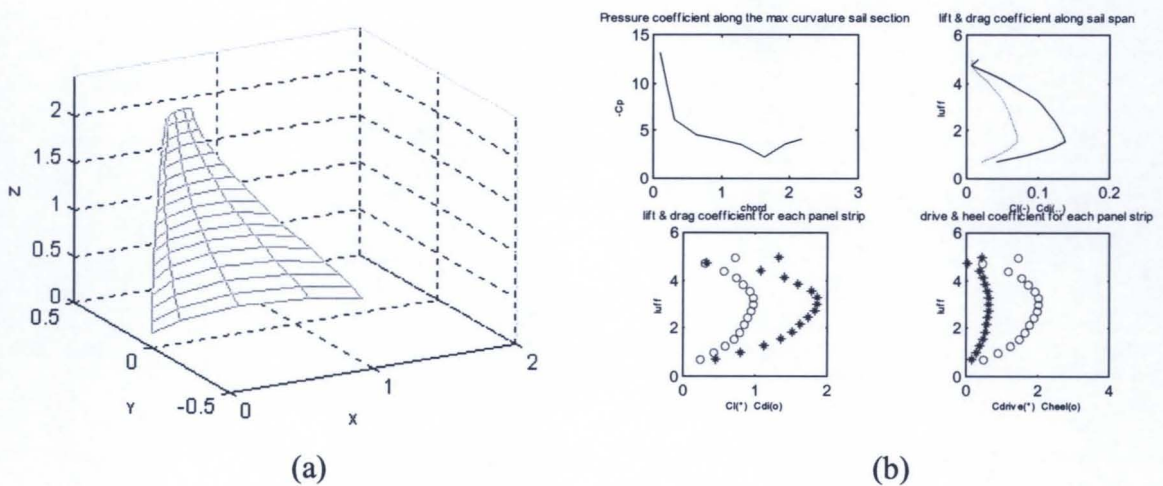


Figure 7.3: (a) 64-panels model for Run VIII; (b) related results after 2 full iterations.

Chapter 8

Aeroelastic analysis results

8.1 Reasoning and planning results

The intent of this chapter is to display the results obtained from applying the implemented aeroelastic analysis method for the sail shape through the created graphical user interface, as presented in the previous chapters. Given the dual function of the implemented system, as it enables numerical analysis and design actions, it has been considered appropriate to divide the presentation of results into two sets. Therefore, this chapter focuses on the results of the aeroelastic analysis of a known sail shape, whilst chapter 9 concentrates on the sail and mast design results.

Since this work is intended to create both a user-friendly integrated sail analysis design package and a basic knowledge about the general behaviour of the external loads acting over the sail, a considerable number of differentiated experiments have been carried out. The necessity of providing these results is corroborated by the demanding interest of sailors and sailmakers on one side and the lack of reliable scientific approach on the other side, as chapter 1 has described. Chapter 2 overviewed the variety of experimental, empirical and numerical techniques in use today for calculating the sail loads and for approaching sail

design. Experimental tests, on scaled or full sail models, evaluate external loads and their distributions in limited conditions, without guaranteeing reliability. This fact is due to the lack of accuracy of the used instrumentation, despite the high costs in terms of time, technologies and expertise involved. Equally expensive are current numerical analyses, due to the high-powered computational methods used.

The results presented in this chapter are expected to describe the behaviour of a known FINN Class sail, or whatever single-sail configuration, from the qualitative and quantitative point of view. In purpose, this section shows the evaluation and distribution of the loads on a FINN class sail and the corresponding sail behaviour, in the following cases:

- in various external conditions and several trim settings;
- for fixed external conditions and for a trimmed set and several sail shapes.

The results calculated for each one of the above groups of experiments are plotted and criticised in the following paragraphs.

8.2 Prior considerations

This section illustrates two important considerations about the method assumptions, described in section 3.5, and the limits of the sail analysis method implemented, specified through the validation tests in section 7.3, which have to be kept in mind in criticising the results presented in this chapter.

The first consideration regards the external condition. In reality, the wind velocity profile increases from zero at the sea level, with an almost parabolic law up to its maximum value at the tip sail section. Considering, then, the velocity triangle plotted in figure 3.2(b), being the sailing velocity V_{Sailing} constant, while the true wind speed V_{True} increases with the height from the sea level, the resulting apparent velocity V_{Apparent} , and attack angle β increase. This effect, known as wind twist, is not taken into account in the following calculation. In fact, the considered apparent velocity intensity V_{Apparent} and the apparent attack angles β are assumed constant along the luff and their values coincide with the average value assumed along the luff in reality. Due to the fact that the wind twist effect

increases the load at the head section, usually the sail shape is twisted at the head in order to decrease the loads. Therefore, a realistic quantitative evaluation of the twist influence at the sections is likely to be hazardous, due to this limitation.

The other important consideration concerns the trim set, which is kept constant for the duration of the analysis, as explained in section 3.5. This means that the load distribution deforms the sail shape, but does not influence the configuration. The aeroelastic analysis is static and its object is already a sail and rig configuration, which actually sails to windward. Therefore, the influence of the trim setting can be evaluated considering the expression for the apparent wind angle, which is $\beta = \alpha + (\delta_m + \lambda)$. Given the trim setting angle is constant, the variation in setting becomes a variation of the apparent wind attack angle. Therefore, having the map of sail behaviour for all the β angles automatically enables an assessment to be made about the influence of different trim sets.

8.3 Results for a known sail-shape in various external conditions and trim sets

This section illustrates the results obtained analysing the same known sail-shape in several external conditions and for different trim sets. External conditions mean apparent wind velocity V_{Apparent} and direction defined by the apparent wind angle β . Trim set consists of the position of the rig and sail into the airflow, defined by the three angles: leeway λ , boom sheeting angle δ_m and heel angle θ .

In the light of the observations described in section 8.2 and considering the fact that the analysed sail geometry reproduces, in the shape and in its trimmed set, a realistic sailing configuration, two kinds of results are expected through the aeroelastic analysis. The output depends upon the typology of problem input.

One eventuality is that the sail shape is known, whereas the external conditions enabling that shape sailing are unknown. Thus, by analysing the same input sail shape in different conditions and possible trimmed sets, the condition which produces the minimised deformed shape corresponds to the sought solution.

In the event that the sail shape, wind conditions and trim set are known, the same kind of analysis produces other sets of possible sailing conditions for the same shape.

Apart from this information, in both the above situations the analysis evaluates the external load distribution and the deformed sail shape, from which conclusions can be drawn regarding the general sail shape behaviour and its performance.

8.3.1 Known sail shape in unknown sailing conditions

In this section, the used sail shape coincides with the one used for explaining the G.U.I. features in chapter 4. The analyses furnish wind condition and trim set, which enable sailing the sail shape. In brief, the geometric data and the trimmed configuration are shown in figure 4.3, page 59, while the final geometric surface and the chosen set of nodal points are shown respectively in figures 4.8, page 67, and 4.9, page 68. It has been analysed for the range of apparent wind angle $\beta=[10.3^\circ, 35.3^\circ]$, with a step of $\beta=2.5^\circ$, which in terms of true attack angle is $\alpha=[0^\circ, 25^\circ]$, since $\alpha=\beta-(\delta_m+\lambda)$. Figure 8.1 plots the aerodynamic panel model and the used wake condition and figure 8.2 the finite element model and the used material properties.

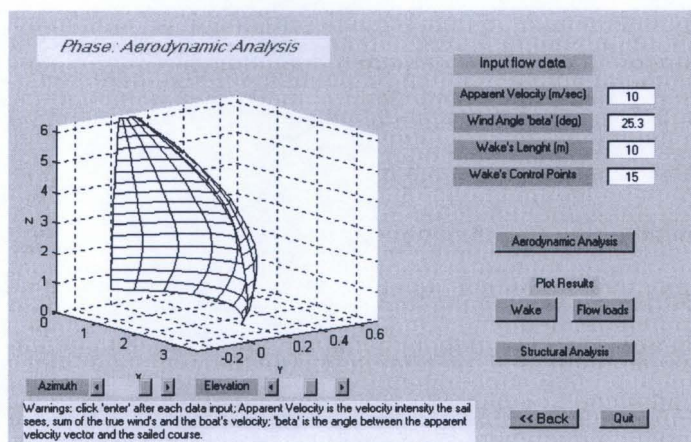


Figure 8.1: Aerodynamic panels model, wind and wake conditions

The intent is to look for the minimised deformed configuration, as it coincides with the initial drawn geometrical shape and gives the external condition and the corresponding

loads. Considering the graphs in figure 8.3, summarising the results in terms of total values of the load coefficients over the range of external conditions, it is notable that:

- the total lift coefficient increases almost linearly until $\beta=32.8^\circ$;
- the total induced drag increases for all the apparent attack angle range;
- the total drive coefficient is almost constant around an average value of $C_{Drive} = 0.25$;
- the total heel coefficient increases.

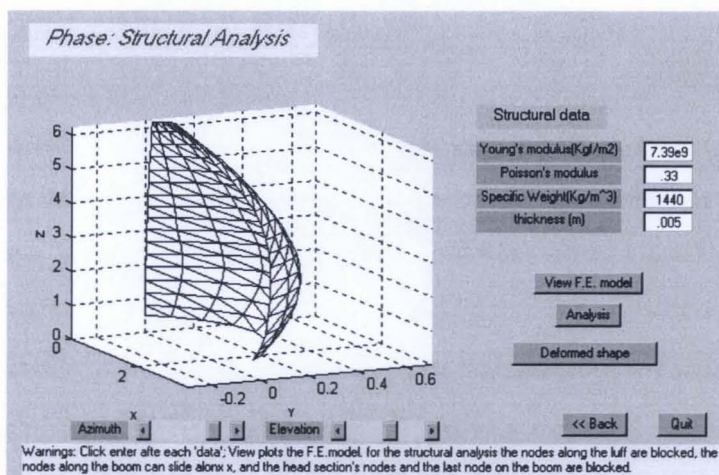


Figure 8.2: Finite element model and material structure properties

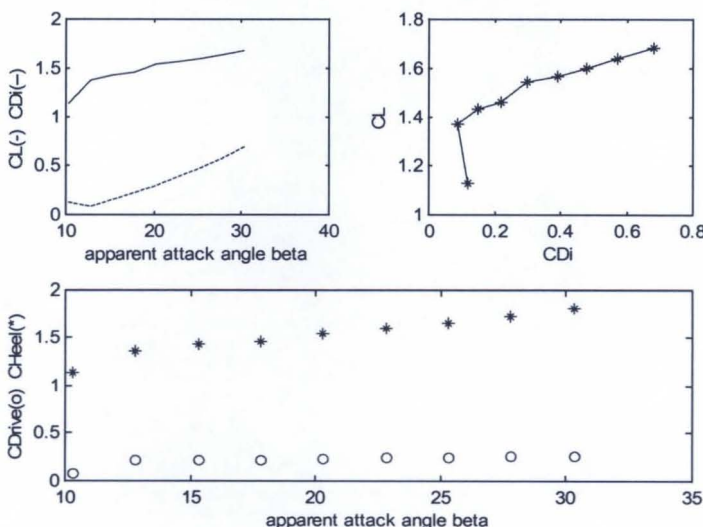


Figure 8.3: Total loads coefficients versus apparent attack angle β

Looking at the polar diagram for the lift versus the induced drag at the top right of figure 8.3, it is possible to note that the tangent to the curve, which means the aerodynamic

performance, is almost constant in the range $\beta=[22.8,32.8^\circ]$. In the same range, the drive coefficient is almost constant ($C_{\text{Drive}} = 0.25$), whilst by the graph for lift and drag, the best performance is indicated at $\beta=12.8^\circ$.

In conclusion, by looking at the graphs related to the total coefficient values, possible optimal sailing conditions have been identified, without having been verified. Therefore, in order to decide which is the optimal wind condition, which maximises the sailing performance and minimises the deformed shape, it is necessary to look at the results concerning deformed shape and load distributions.

Figures 8.4 to 8.7 plot the complete set of results in the range $\beta=[22.8^\circ, 30.5^\circ]$, leading to possible considerations of optimal conditions.

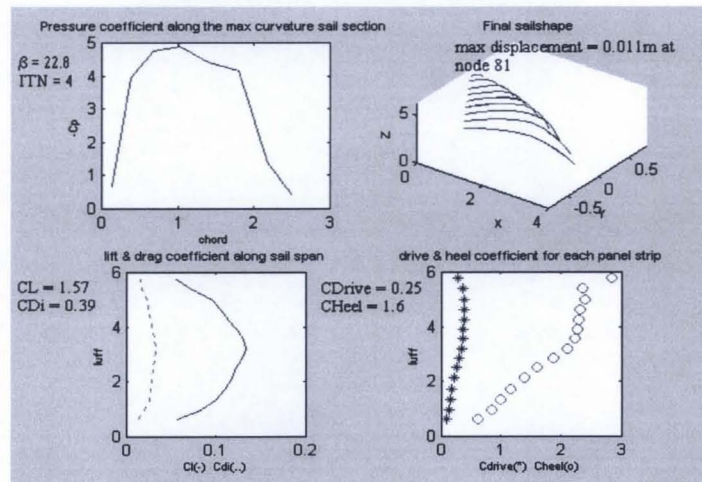


Figure 8.4: Results for $\beta = 22.8^\circ$

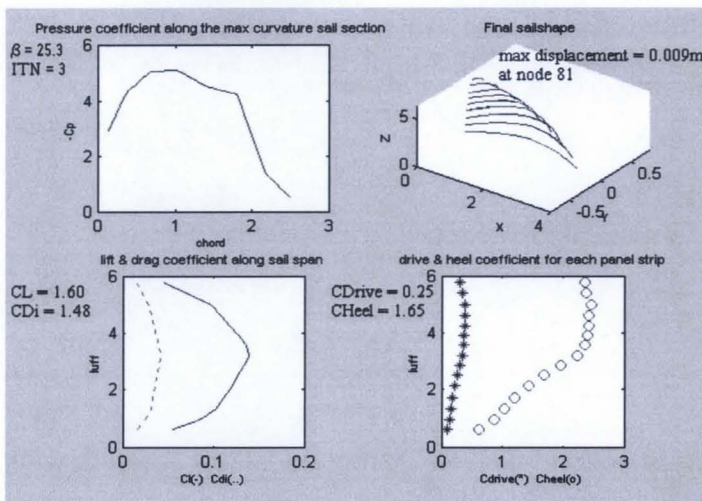
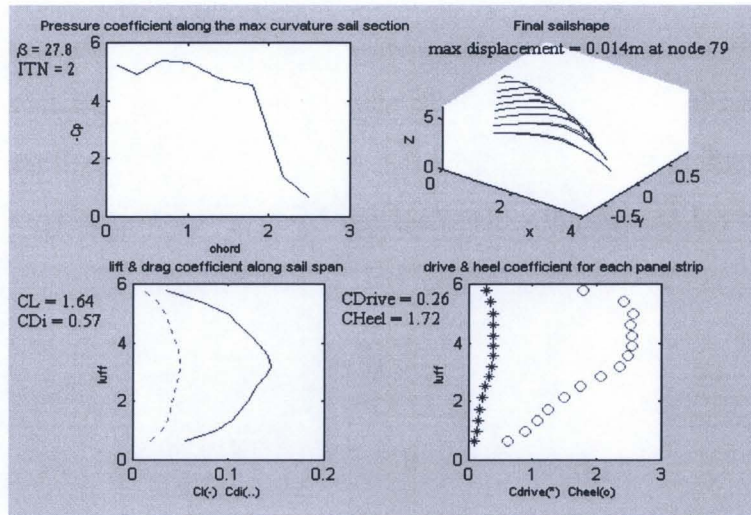
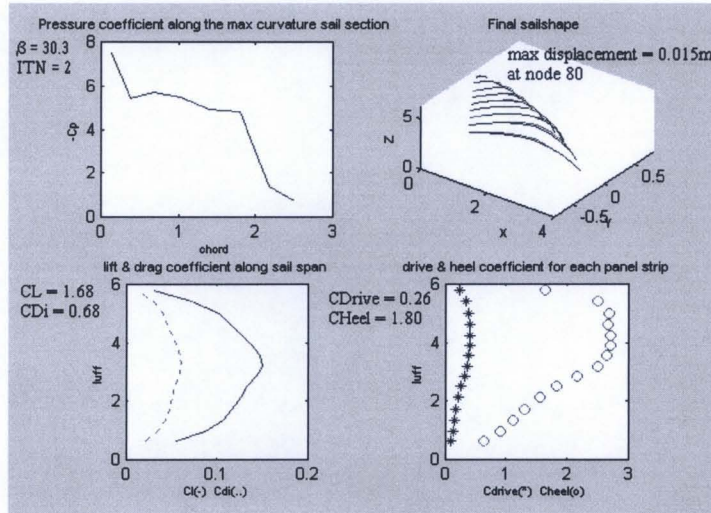


Figure 8.5: Results for $\beta = 25.3^\circ$

Figure 8.6: Results for $\beta = 27.8^\circ$ Figure 8.7: Results for $\beta = 30.5^\circ$

By looking at the deformed sail shape, plotted with the maximum displacement and its location in the upper-right graphs in each of the above figures, the solution obtained for $\beta = 25.3^\circ$, plotted in figure 8.5, corresponds to the sought result, as the deformed shape is the closest to the initial shape. In fact, the maximum displacements resulting for $\beta = 22.8^\circ$ (figure 8.4) and for angles bigger than $\beta = 25.3^\circ$ occur on the same node and are only a few millimetres bigger, showing a tendency in increasing their maximum value with β .

Therefore, it can be concluded that this shape can be kept for the indicated external and trimmed conditions.

In order to investigate the maximum range of feasibility of this shape, as it cannot be deduced by the graphs, plotted in figure 8.3, it is important to look at the final solutions for the analyses done in the range $\beta = [10.3^\circ, 20.3^\circ]$, shown in the figures 8.8 to 8.12.

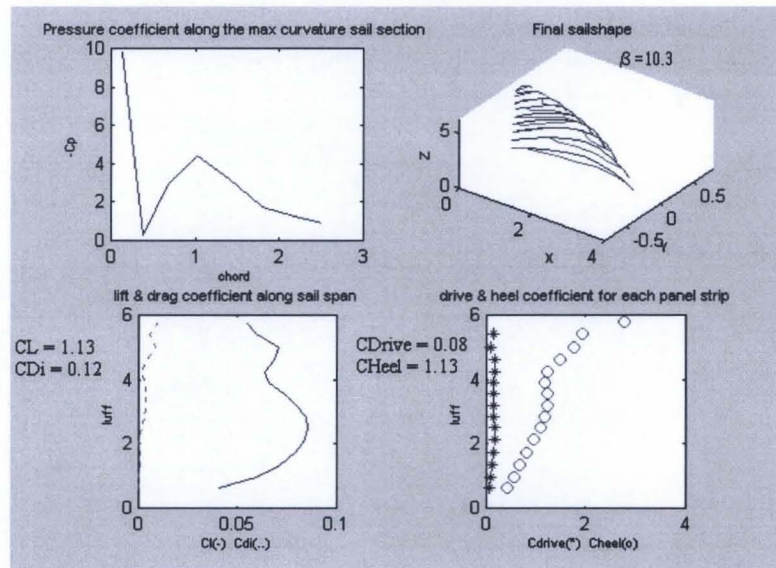


Figure 8.8: Results for $\beta = 10.3^\circ$

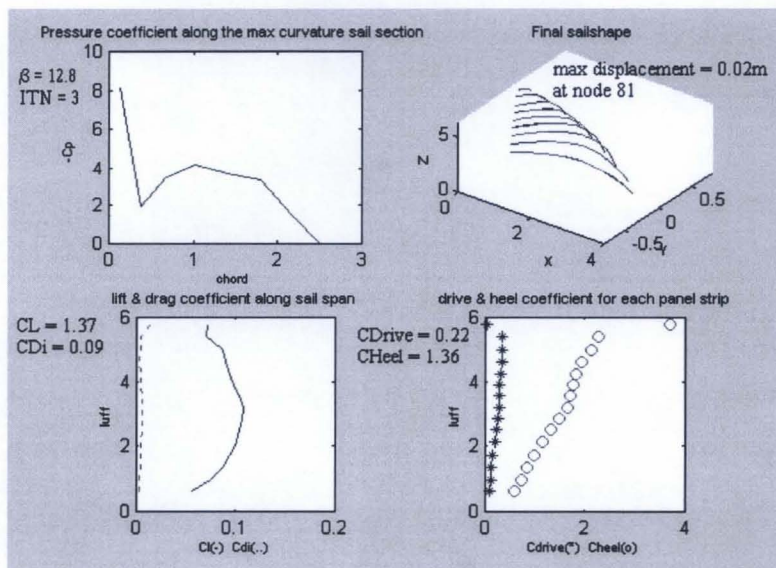


Figure 8.9: Results for $\beta = 12.8^\circ$

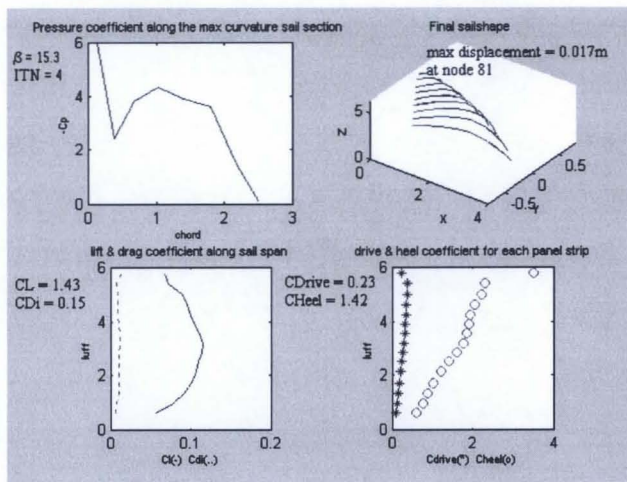


Figure 8.10: Results for $\beta = 15.3^\circ$

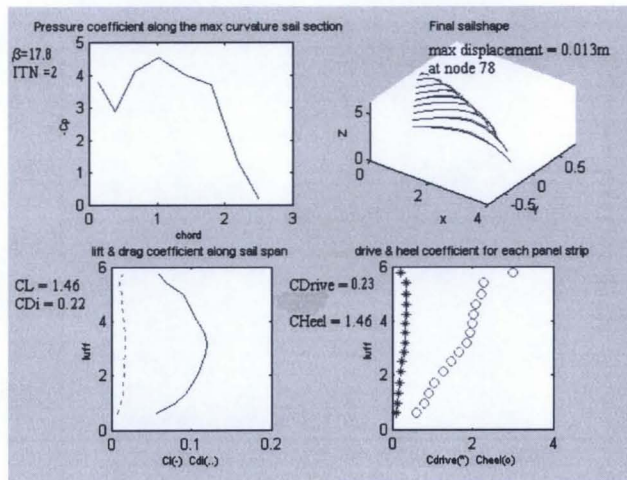


Figure 8.11: Results for $\beta = 17.8^\circ$

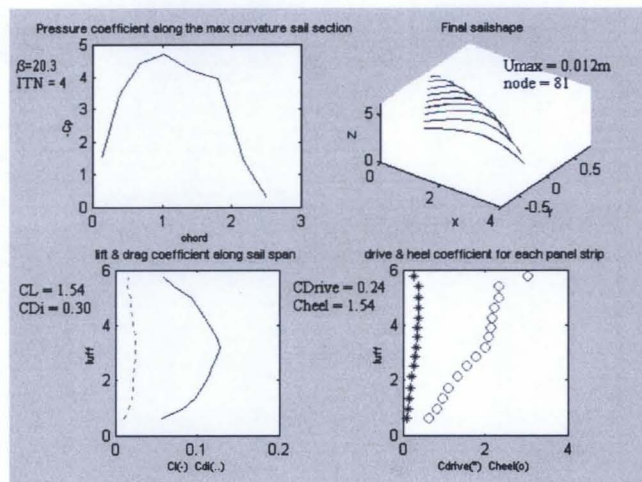


Figure 8.12: Results for $\beta = 20.3^\circ$

It is possible to conclude that the deformed shape for $\beta = 20.3^\circ$ (figure 8.12) has similar behaviour with the one realised for $\beta = 25.3^\circ$ (figure 8.5). Notwithstanding the fact that small displacements occur for a smaller apparent attack angle, at this point the distribution of loads becomes fundamental for evaluating performance and, finally, the optimal configuration.

In view of the external load distributions, the optimal sail configuration is within the range of apparent attack angles $\beta = [20.3^\circ, 25.3^\circ]$. In fact, consider the aerodynamic load distributions along the luff, displayed in the bottom left graphs in figures 8.12, 8.4 and 8.5 respectively. For these three mentioned cases, the luff-wise lift distribution is evidently elliptical, with its maximum load values located in the middle sail section. Consequently, this characteristic distribution maximises the aerodynamic and sailing efficiency and determines the maximum sail deformation displaced in that section. In fact, node 81, located at the leech of the middle sail section, experiences the maximum displacement.

The top-left graphs of the above-told figures plot the pressure profile along the maximum curvature section, located just below the middle section. These pressure profiles are characterised by a smoother peak of pressure and further by an average value kept constant for almost the entire section. Similar profiles are common for almost the entire sail area between the lower and upper sections. Two observations can be made about this typical pressure profile.

From the aerodynamic point of view, this characteristic pressure profile avoids the risk of separation and ensures the tendency of having a full sail. Further, it has been observed that for any convergence step, the deformed shapes are fuller than the solution obtained for the previous step. This means that the aerodynamic loads evaluated at the previous iteration stretch the sail, making it fuller. Then, the new set of loads are bigger, due to the fact the actual sail shape is more curved.

From the structural point of view, this pressure distribution makes an equal distribution of tension along the section, which maximises the structural performance of the used homogeneous material. Indeed, the highest average value and the largest area covered by this value is realised for $\beta = 25.3^\circ$, which ensures this as the best configuration for the given external conditions.

With reference to the total drive and heel coefficient distributions, consider the graphs at the bottom-right in the above-mentioned figures. The displayed values do not take into account the effect of the wind twist, explained in section 8.2. Therefore, since they have been calculated by the formulas 5.20 and 5.21, their values depend upon β , which is taken constant along the luff. The drive coefficient slightly increases along the luff from the foot section up to the middle section where it assumes its maximum value and smoothly decreases up to the head section.

In view of the wind twist effect, this profile ensures a stable configuration heading towards the wind. The same effect will produce more side force, than the one plotted here, whereas the distribution is believed to be very similar. The centre for the application of the overturning moment is almost around the upper sail-section and its low total value ensures the lateral stability of the FINN sail. Nonetheless it cannot be realistically assessed.

Besides all the above observations, it is important to remember that the configuration analysed is a product of a geometrical construction, which means that it is similar to the real flying shape but they are not guaranteed to coincide. Therefore, as the results suggest, the real configuration is expected to sail in the range of observed apparent attack angle. Hence, bearing in mind that this configuration, photographed and analysed in its geometric characteristics by WB-Sails, corresponds to the sail shape flying at its optimum performance, the obtained results give information about when optimum performance is achieved. Moreover, this result is in perfect accord with the Marchaj conclusion about the effects of sail shape on boat performance from the wind tunnel test [41], as he calculated that a FINN class sailboat sailing to windward in similar condition has its optimum performance around $\beta=25^\circ$. In addition, according with the hypothesis regarding the trimmed configuration, any combination of true attack angle α , boom sheeting angle δ_m and leeway λ , which results in an apparent wind angle in the above range, furnishes the same sail shape, optimising the sailing performance.

Concluding, for the chosen sail shape in the given trimmed configuration, the analysis accomplished the optimal sailing performance in the eventuality that the apparent wind angle is within the range $\beta =[20.3^\circ, 25.3^\circ]$. The corroboration is given by the fact that:

- the deformation is minimal,
- the aerodynamic load distribution is elliptical.

Finally, consider the result obtained for $\beta=[10.3^\circ, 17.8^\circ]$ in figures 8.8 to 8.11, page 137 and 138. Notwithstanding the small deformations of the final sail shape, the pressure profiles on the maximum curvature section indicate the possibility of separations, where the aerodynamic loads distributions along the luff show the tendency to become elliptical, as β increases.

Apart from the range of possible sailing course seen in the previous paragraphs, the behaviour of the same sail shape has been investigated for a larger sailing course. Results related to the sailing course for $\beta=32.8^\circ$ are reported. Figure 8.13(a) plots the aerodynamic loads evaluated at the first step, when the sail shape is considered rigid. Figure 8.13(b) plots the deformed shape obtained after applying the above loads. As the maximum displacement is too high and the deformed shape exceeds the structural limits, it is evident that in this condition the sail shape, built with the above-described material cannot sustain the loads. Therefore, continuing the analysis has no physical meaning. This example corroborates the importance of considering the sail as a membrane. In fact, both the load distributions and their total values obtained after the first iteration are possible, whereas their application induces the sail shape crisis, making clear that this condition of sailing is not sustainable by this sail.

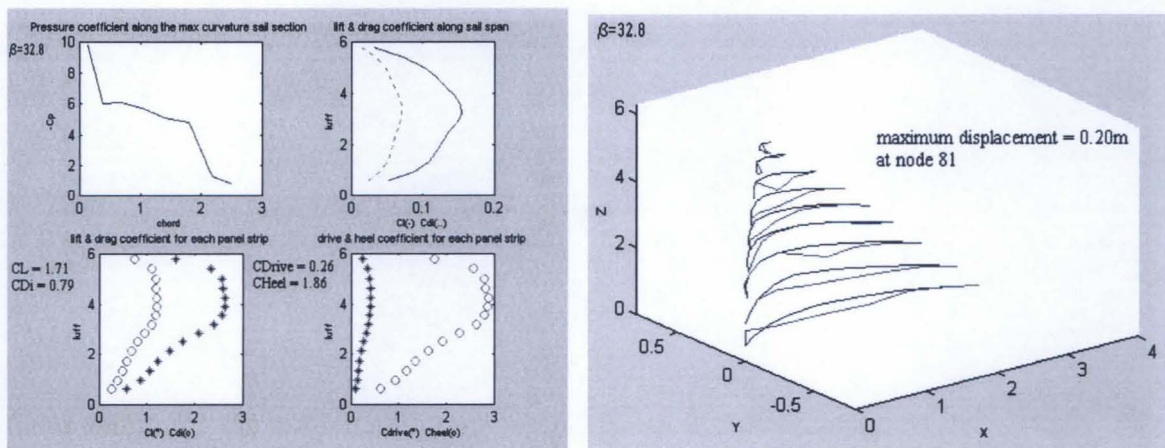


Figure 8.13: (a) Results after the first aerodynamic analysis; (b) Deformed shape after the first structural analysis for $\beta = 32.8^\circ$

8.4 Results for several sail shapes in given external conditions and trim set

This section presents the results obtained by analysing several sail shapes in identical external conditions and for the same trimmed configuration. In particular, with reference to the results obtained on the sail shape seen in section 8.3, this section focuses on investigating the behaviour of the same sail, when different shapes are assumed.

The results of the aeroelastic analyses carried out in this section, compared with the results obtained in the previous section, will make evident how small changes in the shape can enlarge the sailing wind range and modify the aerodynamic forces, corroborating the necessity of this kind of analyses and the reasons behind this thesis.

Two sail shapes are considered, which are differentiated with respect to the sail input, seen in section 8.3:

- 1) the section camber has been decreased by 3%;
- 2) on the sail shape obtained in point 1, the twist has been increased by $\Delta\delta=3^\circ$;

The reasoning for these choices and results are explained in the following subsections.

8.4.1 Results on the flatter sail shape.

Due to the fact that the sail shape analysed in section 8.3 can sail in the range of apparent attack angle $\beta = [20.3^\circ, 25.3^\circ]$ and for bigger apparent wind angles the obtained deformed shape is unstable under large aerodynamic loads, it has been considered interesting to investigate the behaviour of the same sail, when the helmsman shapes it to a flatter form.

Thus, analyses have been carried out on the same sail, considered in section 8.3, with the value of the camber reduced by 3% of the local chord, for any section apart from the foot, for the range of apparent attack angle $\beta=[22.8^\circ, 37.8^\circ]$.

Briefly, apart from the camber values, both the structural properties and the aerodynamic solution characteristics have been kept equal to the previous example in order to facilitate the comparisons. This is valid for the further analyses, except where indicated.

Primarily, it is important to announce that these above described analyses have determined that this shape can sail in the range $\beta = [22.8^\circ, 27.8^\circ]$, considering that the maximum node displacement is 0.009m. Figure 8.14 plots the total aerodynamic and sailing force coefficients, evaluated in this case, as well as the total force coefficient curves obtained for the previous example, in order to facilitate the comparisons.

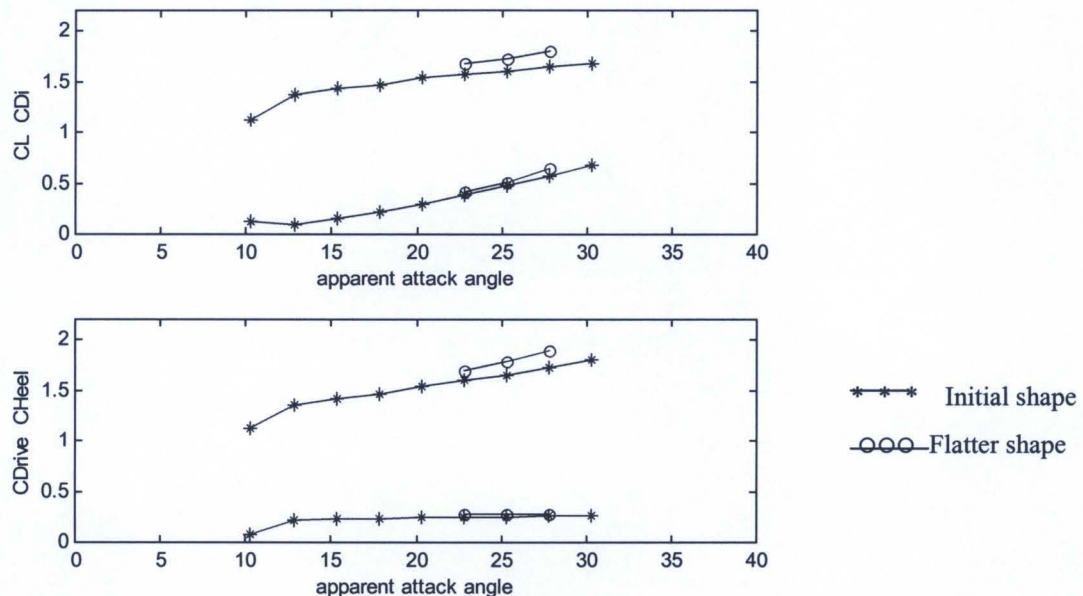


Figure 8.14: Comparison of the total force coefficients evaluated for two sail shapes.

Looking at these curves the following facts are evident for each apparent attack angle β :

- the total lift and induced drag coefficients are bigger;
- in percentage, the total lift is bigger than the total induced drag, determining a bigger aerodynamic as well as sailing efficiency , due to a bigger CL/Cdi ratio;
- the total drive coefficients are almost constant and equal to the same value evaluated on the previous sail shape, which is around 0.25;
- the lateral force coefficient is increased, nonetheless the value of the coefficient is $CHeel=1.89$ at $\beta=27.8^\circ$, which ensures regard for the lateral stability.

Concluding, a flatter shape can sail over all the apparent wind angle range $\beta=[22.8^\circ, 27.8^\circ]$, as the resulting deformations are small, the total drive force is constant and the increment in the lateral force does not affect the lateral stability.

Now, consider the influence of the changed sail shape on the force distributions, plotted for the three apparent attack angles $\beta = [22.8^\circ, 25.3^\circ, 27.8^\circ]$ respectively in figures 8.15, 8.16 and 8.17. In order to consider the differences keep in mind the plots of the results in the same external conditions and for the same trim set, plotted in figures 8.4, page135, and figure 8.5 and 8.6, page 136.

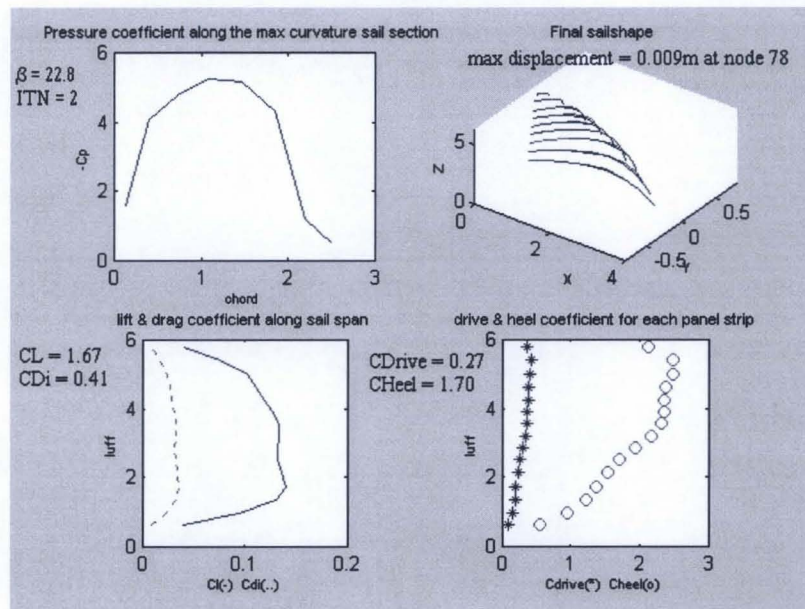


Figure 8.15: Results for $\beta = 22.8^\circ$

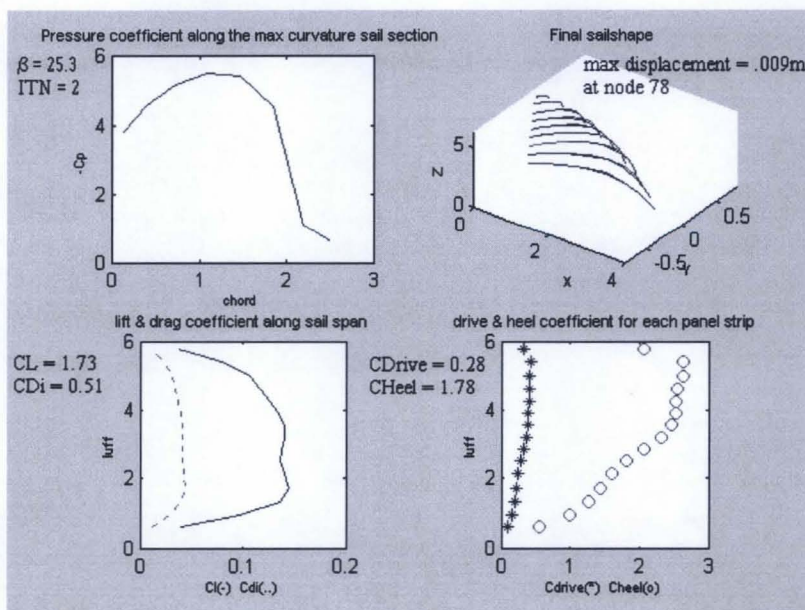


Figure 8.16: Results for $\beta = 25.3^\circ$

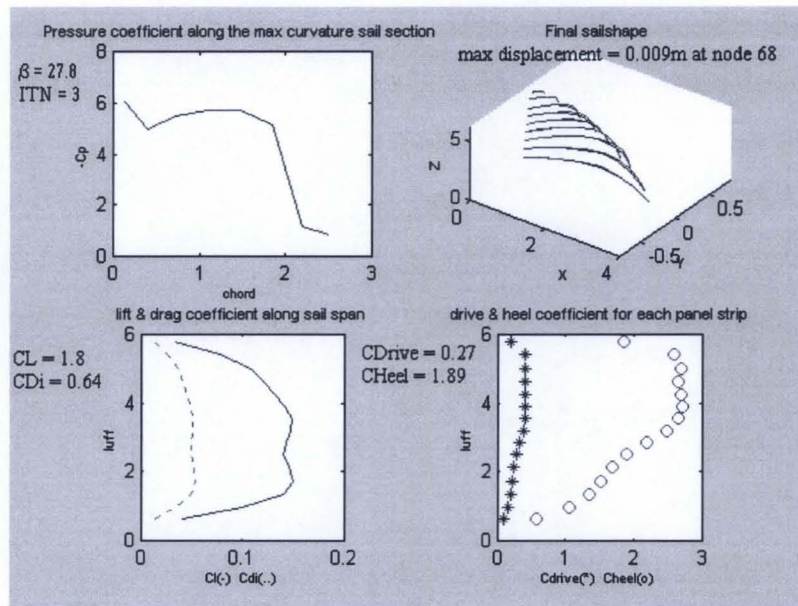


Figure 8.17: Results for $\beta = 27.8^\circ$

The first important and immediate consideration regards the fact that although the value of the total forces are only slightly different, the load distributions are dissimilar. This is the first important evidence of the importance of the results of this research. These simple examples illustrate how significant is knowing the total force coefficients and, moreover, their distribution over the sail. Since the majority of the sailmaking factories assume that the aerodynamic loads acting on the sail are uniform and constant, or equal to loads calculated for different shapes of the same sail or for different sails, the improvements brought out by applying this integrated methodology in estimating the aerodynamic loads are evident.

In particular, two main observations derive from the above graphs.

While the lift distribution of the sail shape, seen in section 8.3 for the same external conditions and trim set, is almost elliptical and assumes its maximum value in the middle sail section, in the present case the load distribution has an oval shape, with, however, its maximum values assumed between the lower and the middle sections.

While in the previous case the sail section pressure profile is almost constant at its maximum value, in the current case, while the maximum pressure coefficient is similar, the leading edge is less loaded.

Both the above described load distributions determine two important facts. The higher and more distributed loads displace the position of the maximum deformation at a node, to a more central and lower position with respect to the position obtained before. Furthermore, the lateral force, notwithstanding its increment, has its application point at a lower position with respect to the previous example, ensuring the maintainance of the lateral sailing stability.

However, just flattening the sail shape has not increased the range of possible sailing courses. Indeed, analysis for bigger apparent attack angle has been done, but the resultant deformed shape, even after the first iteration, demonstrated its instability, as the shape looked fuller. For instance, figure 8.18 plots the sections of the input sail shape and the deformed sail shapes solution of the first and the last iteration in the case of $\beta = 30.3^\circ$.

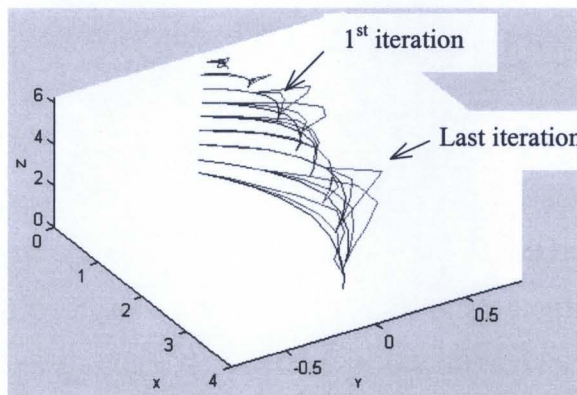


Figure 8.18: Deformed sail shapes at $\beta = 30.3^\circ$

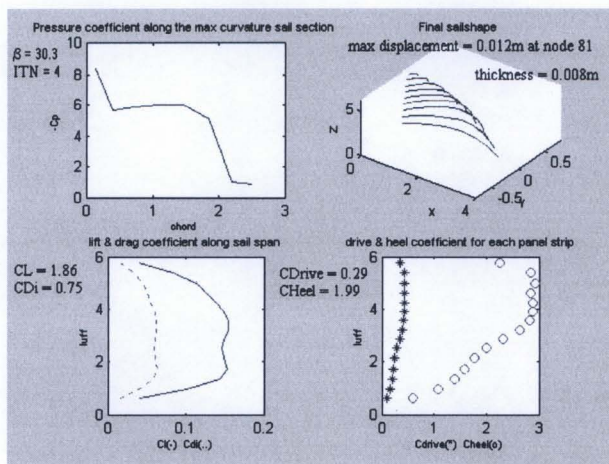


Figure 8.19: Results for $\beta = 30.3^\circ$.

Then, considering that the deformed shapes are fuller and not unstable, due to the lack in elasticity, the same sail shape has been analysed considering the sailcloth thickness equal to 0.008m. Figure 8.19 plots the results for this case.

Successive analyses report that the flatter sail shape increases its possible sailing course up to $\beta = 37.8^\circ$, which means an enlargement of 10° . In the range $\beta = [30.3^\circ, 37.8^\circ]$, the behaviour of the load distribution is the same as that reported in figure 8.19. Naturally, the total load values increase. As figure 8.19 shows, the maximum load value is assumed for almost the entire luff curve, which causes higher displacements located in the middle sail section. Furthermore, as the lateral force coefficient increases and its application point is displaced around the upper section, the configuration stability has to be verified.

Concluding, the maximum pressure coefficient is higher at the trailing edge and its profile indicates a possible separation before the middle section. Therefore, as the method permits calculations given the hypothesis of unseparated flow, the analysis stops with this sailing course.

8.4.2 Results on the flatter and twisted sail shape

Summarising the conclusive results obtained on the sail shapes seen in section 8.3, page 132, and 8.4.1, page 142, the maximum sailing course is at $\beta = 27.8^\circ$. For bigger apparent attack angles, it has been verified that the loads cause large deformation and the sail appears fuller. Therefore, the next suggested shape is one that reduces the loads in every section and in particular, considering figure 8.19 at the tip and lower sections. Thus, on the flatter sail shape seen in section 8.4.1, the twist angle of each section chord, apart from the foot chord to avoid changing the trimmed configuration, has been increased by $\Delta\delta=3^\circ$. Hence, the obtained sail shape is flatter and twisted with respect to the initial one, seen in section 8.3. This action is meant to reflect the fact that increasing the twist section angle decreases the local section apparent attack angle.

The analyses have been carried out over all the apparent attack angle range $\beta=[25.8^\circ, 37.8^\circ]$, where the sail shape, as above described, has been verified able to sail. However, the analyses have been stopped at $\beta = 37.8^\circ$, due to the fact that for bigger sailing

courses large separated flow zones can appear, which the Modified Vortex Lattice Method cannot represent. Figure 8.20 plots the calculated total force coefficients along with the data, seen for the previous sail shape. The following observations are evident:

- the total lift coefficient result is bigger by a maximum of 3%, if compared with the initial shape and smaller by a maximum of 4 % with respect to the flatter sail shape;
- the total induced drag coefficients are a maximum of 2% bigger compared with the initial shape and smaller with respect to the flatter sail shape;
- the total drive coefficient remains constant around $C_{Drive} = 0.25$;
- the total heel force coefficient increases up to $C_{Heel} = 2.17$;
- the aerodynamic efficiency decreases with the apparent attack angle.

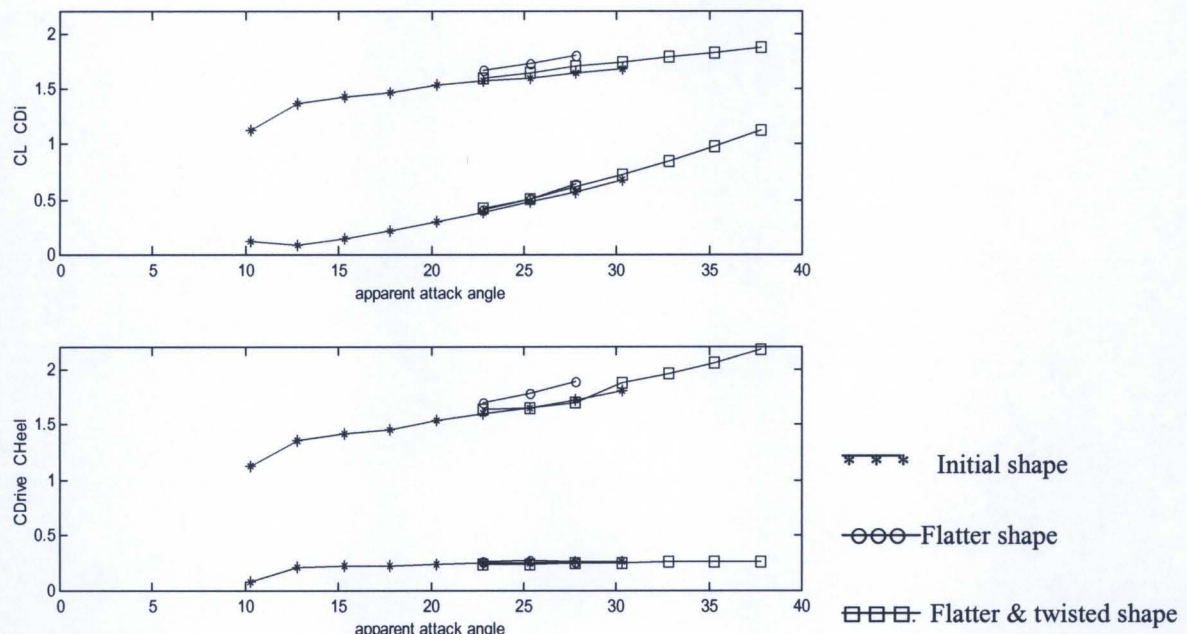


Figure 8.20: Comparison of the total force coefficients evaluated for three sail shapes.

In order to detail the above observations and the differences in the load distributions, consider figure 8.22, which plots the final results obtained with the flatter and twisted sail shape for $\beta = 25.3^\circ$ and compare it with figures 8.5 and 8.16, related respectively to the initial and the flatter sail shape.

Looking at the graphs for the total lift distribution along the luff curve, as expected the added twist has decreased the load acting in every section, where the distribution profile

continues to assume the oval-shape seen for the flatter shape. However, in this case, the higher lift values are assumed mostly around the lower section. Then, the aerodynamic efficiency decreases. Further, as the application point of the total heel force is around the middle section, notwithstanding its bigger value with respect to the initial shape, it is more stable to the heel moment. Finally, considering the pressure coefficient profile on the same section, it is similar to that for the one over the flatter shape, as it depends upon the camber distribution, showing lower values at the leading and trailing edges.

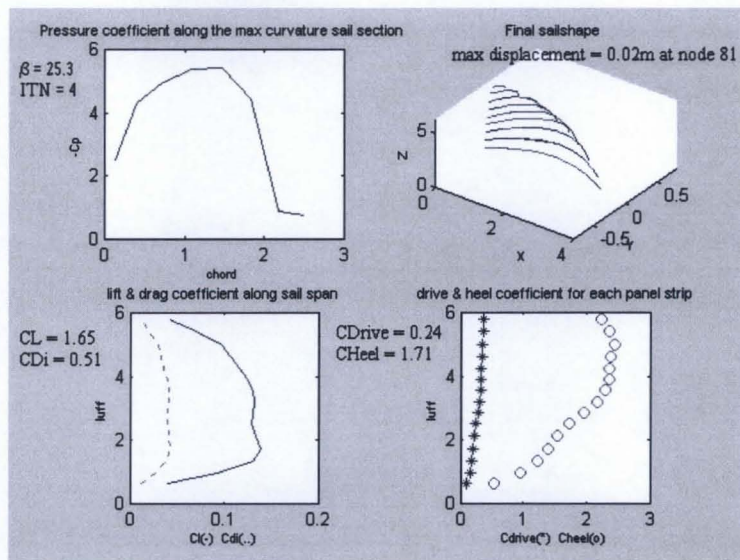


Figure 8.21: Results for $\beta = 25.3^\circ$

A conclusive consideration has to be given to the deformed sail shape. The maximum displacement is located on the middle section node located on the leading edge and its value is bigger than that evaluated in the previous tests. Thus, this result indicates that the optimal shape in terms of aerodynamic efficiency, for the same driving and lateral force values, is the initial one.

However, considering the entire group of deformed sail shapes obtained over all the range of apparent attack angles, the flatter and twisted sail shape optimises the sailing course corresponding to $\beta=30.3^\circ$, as figure 8.22 plots. In fact, despite the smaller deformation with respect to the input shape, the lift distribution tends to be more elliptical and the application point of the heel force is displaced down the middle section, which maintains the lateral stability. The pressure coefficient shows a high value at the trailing

edge and indicates the absence of possible flow separation, as it does not present a large reduction.

Concluding, the behaviour in terms of load distributions are kept until $\beta = 37.3^\circ$. Indeed the only differences are in the deformed shape and pressure profile. In fact, the maximum displacement are of the order of a few centimetres and the pressure profile assumes almost the same value, as seen for $\beta = 25.3^\circ$, up to $\beta = 27.8^\circ$. Successively, the deformations become smaller, whilst the pressure profile with the attack angle shows a larger negative slope, indicating a higher possibility of flow separation under the influence of the adverse pressure gradient (see figure 8.23).

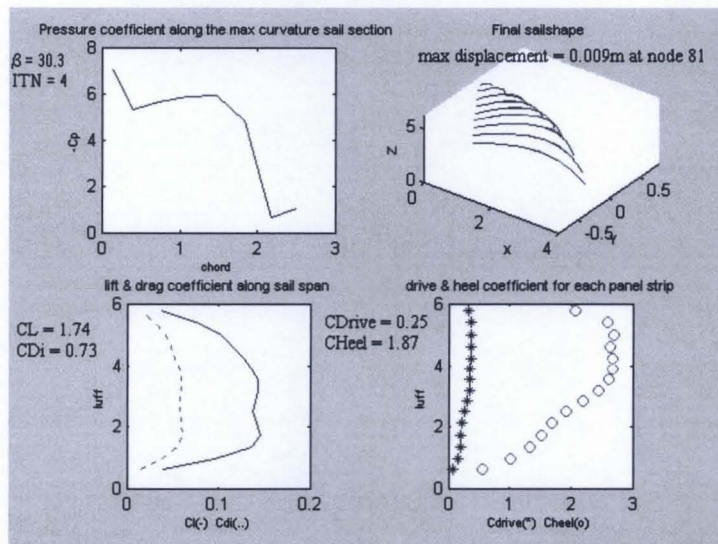


Figure 8.22: Results for $\beta = 30.3^\circ$

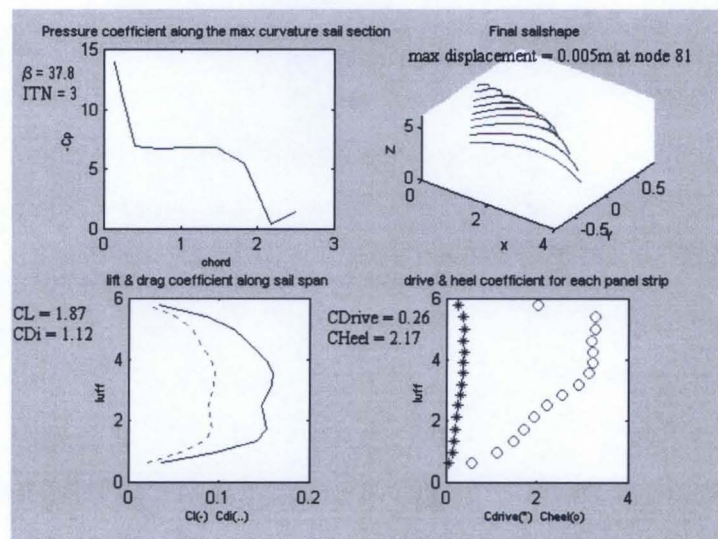


Figure 8.23: Results for $\beta = 37.8^\circ$

A consequence of the observations is the use of a cambered surface for lower attack angles. In the event the same trimmed configuration has to be kept and the wind changes direction, flattening the sail shape is not enough, as seen in section 8.4.1. It has to be twisted. This analysis has accomplished not only this obvious result, but it has shown how the amount of camber and twist influence the sailing performance.

8.5 Conclusions

This chapter has shown the result of aeroelastic analyses for the evaluation and loads distribution for a FINN Class sail in different shapes and in different sailing courses.

This section aims to summarise and generalise the results obtained.

The first important result is undoubtedly the necessity of accurate performance analysis for each sail, for any possible shape over the entire range of possible sailing courses. This chapter has focused the attention on just one sail shaped in a few possible ways. The general conclusion is that the general sailing behaviour of a determined shape can be forecasted, in view of the basic aerodynamic and structural principles. The unpredictable fact regards the interaction between the aerodynamic loads and the structural properties of the sails. Therefore, the necessity of the aeroelastic static analysis is incontestable.

The second general conclusion regards the load distributions. It has been verified through these analyses that the initial shape optimises the sailing around the apparent attack angle $\beta = 25.3^\circ$, which was the condition used by the designers of the WB-Sails, as the lift distribution along the luff has an elliptical shape. The analyses for a few degrees more have demonstrated that the deformed shape becomes unstable, and just flattening and twisting it, the sail shape is optimised for larger sailing courses. However, the amount of camber and twist and their distribution, influence not only the total force coefficient values but also mainly the load distribution. The analysis permits evaluation of those values. It has been demonstrated that knowing only the total force coefficient values does not ensure regard for the effective sailing possibility of the given sail, and moreover does not ensure regard for its lateral stability nor the possible appearance of separated flow.

The above observations and the results seen in this chapter corroborate the improvements brought out in the sail load evaluation by the methodology presented in this thesis. These results shed light on regarding the significant approximations made when the sail loads are believed constant and uniform or even when loads evaluated by experiments on other sails are adapted for new sail designed shapes. This is the reason for most design flaws, which are reviewed after the construction and tests of an initial shape. Knowing the behaviour is the only way to cut initial design flaws and related costs. This model of analysis does not achieve perfect numerical results, due to its limitations. This analysis system, however, gives important information regarding the general behaviour of sail shapes and a good estimation of the effective load distributions for possible windward sailing courses.

Chapter 9

Design Results

9.1 Introduction

This chapter describes the design features of the system presented in this thesis by presenting results concerning improvements in:

- sail design
- mast design.

Three examples have been chosen in order to condense the variety of the possible design actions, as mentioned in section 5.1. However, they do not presume to cover the entire range of possible design actions, which can be carried out with this tool or otherwise.

In particular, with reference to sail design, section 9.2 explains details of the design of a FINN class sail shape, starting from a curved surface and the definition of the final shape of a flat trapezoidal sail, in known external conditions.

Section 9.3 describes an example of a FINN class mast design, focusing the attention on the interference between sail and mast. The example illustrates how the system improves mast design, by accurate evaluations of the load distributions over the sail and how these

results can be integrated with a boundary layer solver in order to evaluate the influence of the presence of the mast on the flow regime overall the sail.

Concluding, given the fact that design is a complex topic, characterised by technological trends, availability of particular materials, practical necessities and many other restrictions, the conclusions arisen in this chapter are not expect to be indisputable statements. Indeed, they are open to further discussions in light of more direct sail manufacture experience.

9.2 Sail Design example

The following subsections describe two examples of sail design, which accomplish:

- drawing a new sail shape, starting from few project data,
- improving a known sail-shape,
- determining the final shape of a flat sail, under given external conditions.

However, these examples do not represent the unique way of using the system as a design tool. Moreover, they are not the description of the only way of approaching the design and improvements of a sail shape. Thus, these examples intend to:

- demonstrate how the presented methodology and the G.U.I. aid a sail design project,
- show how the decisions of the sail designer are eased as a consequence of an iterative analysis on different sail-shapes until an optimum design is obtained.

9.2.1 Design process for a FINN class sail

This section describes the design process for a FINN Class sail shape, starting from a cylindrical surface. The characteristics of this boat and sail are described in section 1.3.1.1. Keeping in mind that it is a One-Design Class (see part of the section 1.2, *Type of sailing*), the federation (I.S.A.F.) imposes restrictive requirements regarding the design of the sail, which are used for starting the new project.

Abiding by I.S.A.F. requirements, in order to explain easily a possible design process, consider the case in which the sail-designer knows the following information regarding the project:

- the sail will fly on a mast of length 5 metres,
- the boom length is not more than 1.20 metres,
- the gap between the sea surface and the sail foot curve is 1 metre,
- the Finn is designed to sail windward,
- the material is not specified apriori.

The normal design procedure consists in starting the project with a known sail shape within the database available at the sailmaker factory and making adjustments, in order to satisfy the listed requirements. The initial chosen sail shape is the most similar to the project requirements. This starting action accomplishes other design aims. For example, in the event the designer aims to extend the utilisation of a known sail shape in different sailing conditions, it is achieved by verifying the improvements by modifying the initial sail shape.

In this case, it is assumed that there is no database. Therefore, the design must start from building up the first sail surface, which will subsequently be deformed and reshaped until it satisfies the listed requirements. Thus, as a first shape, a cylindrical surface has been chosen. The geometric characteristics are listed in table 9.1.

Foot chord length	1 metre
Luff length	4 metres
Gap	1 metres
Camber	10% of foot chord
Draft	50% of foot chord

Table 9.1: Initial geometric characteristics of the cylindrical surface

The sail designer types the above information into the ‘Input Data’ G.U.I., displayed in figure 4.2, specifying that the twist and all the trimming angles, leeway, heel and boom sheeting, are equal to zero degrees. Adjusting the geometry in the appropriate G.U.I.s,

shown in figure 4.5, 4.6 and 4.7, the designer defines a particular panel model, thanks to the '3D-Mesh' interface, as figure 4.9 plots. The adopted total number of panels is 128, consisting of 16 along the span-wise direction and 8 along the chord. The chosen distribution of nodal points over the sail is homogeneous and in addition facilitates the construction of regular quadrilateral panels. On completion of this geometry, the aerodynamic analysis in the range of attack angle $\alpha=0^\circ$ to $\alpha=40^\circ$ is performed. Figure 9.1 summarises the obtained results in terms of force coefficient distributions.

As repeated several times in this section, this is only a simple design example. Current design trends require the optimisation of the drive force, maintaining the heel force under opportune limits, while avoiding the capsizing of the sailboat, [65]. Therefore, the common sail design procedure draws a sail shape corresponding to the required distribution of pressure profile, which satisfies the project performance. This design exercise shows that this system aids the design procedure illustrated, by verifying the pressure distribution for a designed sail surface and subsequent improvements.

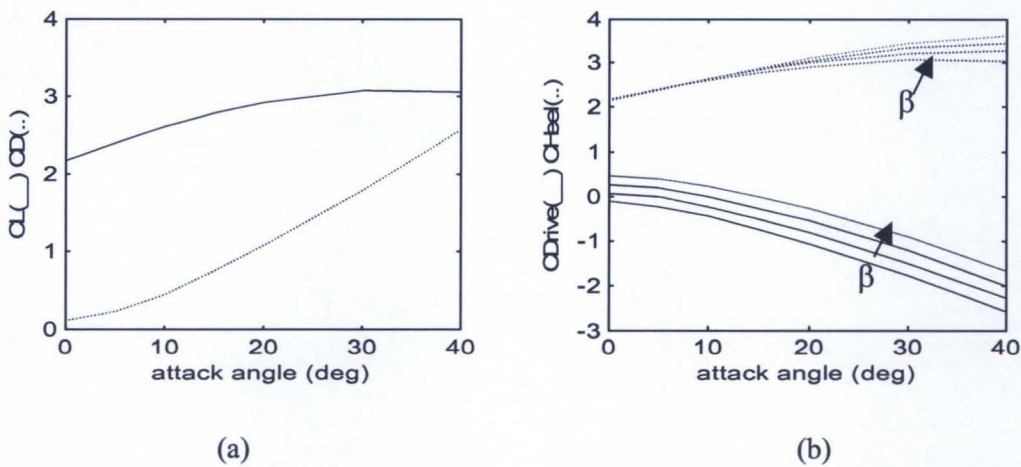


Figure 9.1: (a) Lift and induced drag coefficients, (b) drive and heel coefficients on the cylindrical surface in the range of attack angle $\alpha = [0^\circ \text{ to } 40^\circ]$

The aerodynamic analysis of the cylindrical sail surface has been carried out over the range of attack angle of $\alpha = [0^\circ \text{ to } 40^\circ]$, for the following reasons outlined below.

The first reason depends on the fact that the maximum lift coefficient is around $\alpha=30^\circ$ (figure 9.1(a)) and the maximum efficiency occurs around the same value of attack angle.

Secondly, considering the fact that a sail surface can fly to windward for a positive drive force coefficient, it is useful to plot the drive and heel coefficients for the apparent wind angles $\beta=[0^\circ, 5^\circ, 10^\circ, 15^\circ]$. From drive coefficient curves in figure 9.1(b), it is clear that the possible sail configurations are obtained for all the combinations of leeway angle and boom sheeting angle that make:

- $\beta > 5^\circ$ for a true attack angle $0^\circ < \alpha < 5^\circ$ and
- $\beta = 15^\circ$ for $0^\circ < \alpha < 17^\circ$.

For the entire range of possible configurations associated with these limits, the heel coefficient force is already quite high, being always higher than two. Hence, these observations justify the absence of interest in continuing the analysis for $\alpha > 40^\circ$.

In order to improve the performance of this surface, assuming as a strict requirement that the camber value and the external geometry cannot be changed, there are three geometric characteristics, which can be used to vary the sail shape:

- distribution of twist angle along the span;
- taper ratio;
- position of maximum camber.

Thus, following the idea that one of the most important requirements for an optimum sail is the possibility of using it in a large range of attack angle, the first idea was to slightly twist the cylindrical surface. Therefore, a linear twist angle distribution has been adopted with a twist angle $\delta=8^\circ$ at the tip section relative to the foot section. The analysis results are shown in figure 9.2.

In this case the decision was to stop the analysis at $\alpha=20^\circ$, because the obtained lift and drag coefficients, as figure 9.2(b) plots, are lower than the ones obtained on the previous geometry and the expected improvements in terms of driving force are not achieved.

Then, the twist distribution was incremented and the new analysed geometry presents a tip section value for the twist angle relative to the foot section equal to $\delta=20^\circ$.

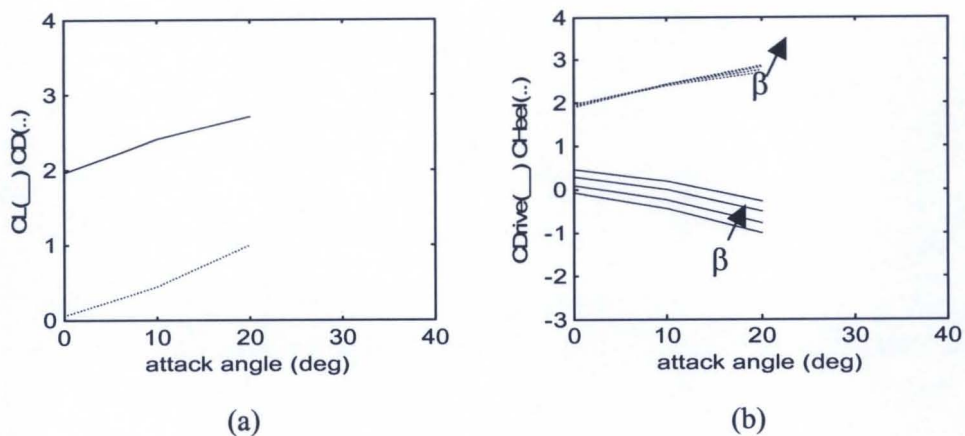


Figure 9.2: (a) Lift and induced drag coefficients, (b) drive and heel coefficient on the cylindrical surface with linear twist distribution $\delta=0^\circ$ to $\delta=8^\circ$.

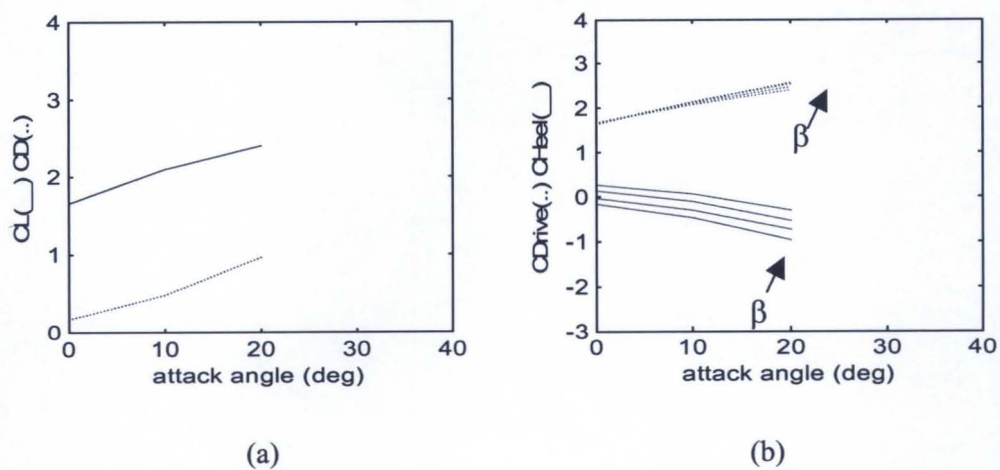


Figure 9.3: (a) Lift and induced drag coefficients (b) drive and heel coefficient on the cylindrical surface with linear twist distribution $\delta = 0^\circ$ to 20°

Figure 9.3 presents the results for this geometry. Observing these results, it is clear that both the lift and induced drag coefficients are smaller and that the sail can fly to windward for $\beta > 10^\circ$ and for a true attack angle $0^\circ < \alpha < 15^\circ$ maximum. Thus, the analysis stops at $\alpha < 20^\circ$. In addition, the behaviour of the curve suggests that within the observed shapes, the cylindrical surface with the bigger twist distribution can sail for a larger range of apparent wind angles, conserving a margin of lateral stability due to smaller values of the heel force coefficients.

Further consideration concerns what happens to the sailing forces in terms of drive force and heel force coefficients for the above-described sail surfaces in different trimmed configurations. In fact, considering the plots 9.1(b), 9.2(b) and 9.3(b), it is possible to note the trimming influences on the driving force and the heel force coefficients.

For a better reading of the above plots, it seems important to remember that the true attack angle is defined as:

$$\alpha = \beta - (\delta_m + \lambda) \quad (9.1)$$

where β is the apparent wind angle, δ_m the boom sheeting angle and λ the leeway angle.

Then, the sail-designer by reading those plots can establish, for example:

- the best twist distribution to adopt;
- for each configuration, a map of the driving force and the heeling force;
- the best configuration in terms of external loads acting on the sail and/or sailing boat stability for a required sailing velocity.

As mentioned above, the present section intends to simulate a sail design process. Therefore, in the following discussion, the behaviour of a sail designer is simulated. Of course, the following discussion is only valid in the view of the following restrictions:

- absence of unsteady force generated by changing configuration;
- known hydrodynamic forces generated by the hull, where the sail will be mounted;
- absence of the mast and boom influence.

Heretofore, thanks to the system design features, a previous sail-shape has been chosen.

At this stage, bearing in mind the limitations listed above, the sail designer can evaluate the sailing force coefficients and the performance of the designed sail.

The curves plotted in the above-mentioned figures can be read in two ways, both in the view of the formula 9.1. These curves plot the sailing force in all the steady equilibrated configurations for the sail:

- moving on a curve for a fixed apparent wind angle β , calculating the influence of the boom sheeting angle δ_m and the leeway λ ;
- for a fixed true attack angle α , calculating the influence of the trimming angles δ_m and λ jumping through the curve drawn for each apparent wind angle β .

The above readings include another kind of interpretation, in terms of manoeuvrability.

In the eventuality that the helmsman would like to accelerate the boat, maintaining the same sailing course, which means β and λ constant, the graph suggests incrementing the boom sheeting angle δ_m , which determines a decrement in the true attack angle α . Obviously, the increment of the driving force generates a decrement, even if it is smaller in absolute value, in the heel force. As a consequence, this induces a decrement of the leeway angle. In the eventuality that the wind intensity increases, the velocity triangle produces an increment in β . In fact, an increment in the velocity intensity results in an increment of lateral force, with an induced increment in the leeway angle.

In both above-mentioned cases, as a consequence of an induced lateral force, the boat will present a change in the sailing course, for the induced positive or negative variation in the leeway angle. For this reason, in the eventuality that the helmsman wants to keep the same sailing course, he has to make adjustments, being aware of the hydrodynamic characteristics of the hull.

Due to the fact that the present research refers to the steady configuration, then the transition phases of the adjustments for getting a new equilibrated configuration are not analysed. However, the present work can help the helmsman, as it can map the sail behaviour over all the possible sailing conditions.

Hence, in the eventuality of an apparent wind angle of $\beta=10^\circ$ (consider in the above plots the third curves in the direction of β increasing) and for a trimmed configuration,

described by boom sheeting angle $\delta_m=0^\circ$ and a leeway angle $\lambda=5^\circ$, the true attack angle, calculated by formula 9.1 is:

$$\alpha = 10^\circ - (0^\circ + 5^\circ), \quad \text{and consequently} \quad \alpha = 5^\circ.$$

The calculated values for the total driving and heeling force coefficients, evaluated as discussed in section 5.3.2, by using the formulas 5.20 and 5.21, inserting the total lift and induced drag coefficient evaluated by the formulas 5.16 and 5.17, are respectively:

- CDrives=0.19 and CHeels=2.41, on the cylindrical surface,
- CDrives=0.13 and CHeels=2.19, on the slight twisted cylindrical surface,
- CDrives=0.005 and CHeels=1.9, on the strong twisted cylindrical surface.

These coefficients indicate the following considerations:

- in terms of external load acting on the sail, the introduction of a twist distribution makes them lighter;
- when the twist is greater, the aerodynamic loads are higher at the tip sections;
- since the total force coefficients are evaluated for the same external pressure force $Q_\infty \text{AREA}_{\text{sail}}$ by formula 5.15, in order to increase the drive coefficients, which are too small in the third case, the next move is to decrease the sail area for the same external condition, introducing for example a no-zero taper ratio;
- by reading the coefficient values, the cylindrical surface with more twist permits sailing for larger values of apparent wind angle.

In accordance with the derived conclusion, figure 9.4 plots the results obtained in the same external conditions, when the sail surface has a taper ratio equal to:

$$\frac{C_{tip}}{C_{foot}} = \frac{0.6}{1} = 0.6; \quad (9.2)$$

As expected, the introduction of a taper ratio on the twisted cylindrical surface results in bigger values for both the lift and induced drag force coefficients. Considering the forces generated when sailing windward, for the same sail configuration of $\beta=10^\circ$ (look at third curve from the bottom of figure 9.4(b), in the direction of β increasing), boom sheeting angle $\delta_m=0^\circ$ and a leeway angle $\lambda=5^\circ$, which means $\alpha=5^\circ$, the obtained values are:

- CDrives_S=0.005 and CHeels=2.13.

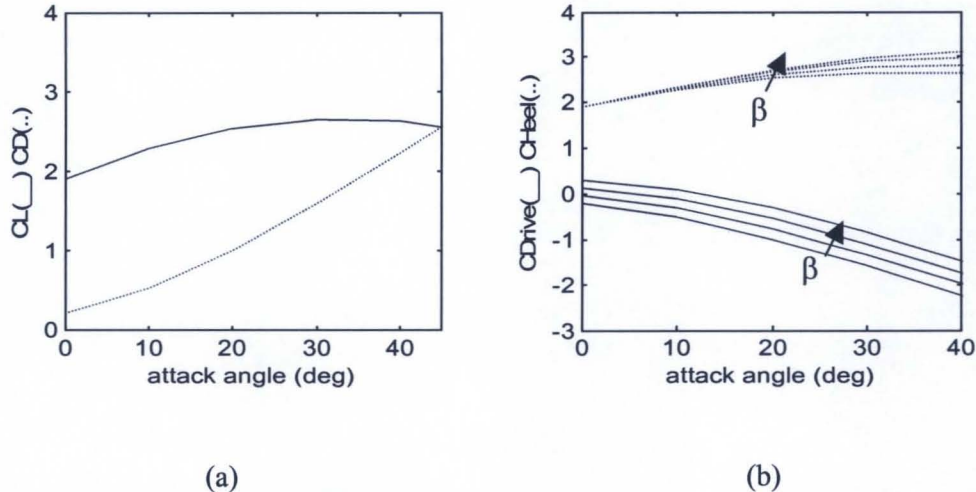


Figure 9.4: (a) Lift and induced drag coefficients, (b) drive and heel coefficients on the tapered surface ($c_t/c_f=0.6$), with linear twist distribution $\delta=0^\circ$ to $\delta=20^\circ$.

The drive force is smaller, while the heel force is bigger. Then the expected improvements have not been achieved. The reason is the high value of the twist angle at the tip, which, in this case, influences the force behaviour.

In the same conditions, if the boom sheeting angle is incremented until $\delta_m=5^\circ$ and consequently $\alpha=0^\circ$, then the coefficients are:

- CDrives_S = 0.125 and CHeels = 1.9,

which means that for an equal lateral force, in the same external wind condition and following the same sailed course, this sail shape enables the boat to go faster.

Further consideration derives from the observations of the behaviour of the curves calculated for bigger values of apparent wind angle: this shape appears to be more stable and faster than the twisted cylindrical surface.

However, since the range of possible angles for sailing is not incremented, rather it has shifted to another value, the same twisted cylindrical surface has been tapered more. The results of the analysis, in the case of a taper ratio equal to $c_t/c_f=0.4$ are shown in figure 9.5.

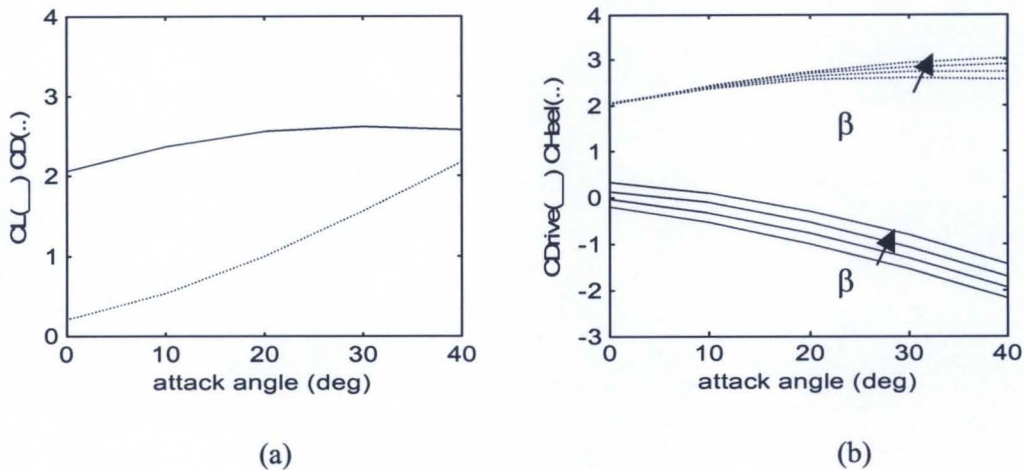


Figure 9.5: (a) Lift and induced drag coefficients (b) drive and heel coefficient on the tapered surface ($c_t/c_f=0.4$), with linear twist distribution $\delta=0^\circ$ to $\delta=20^\circ$.

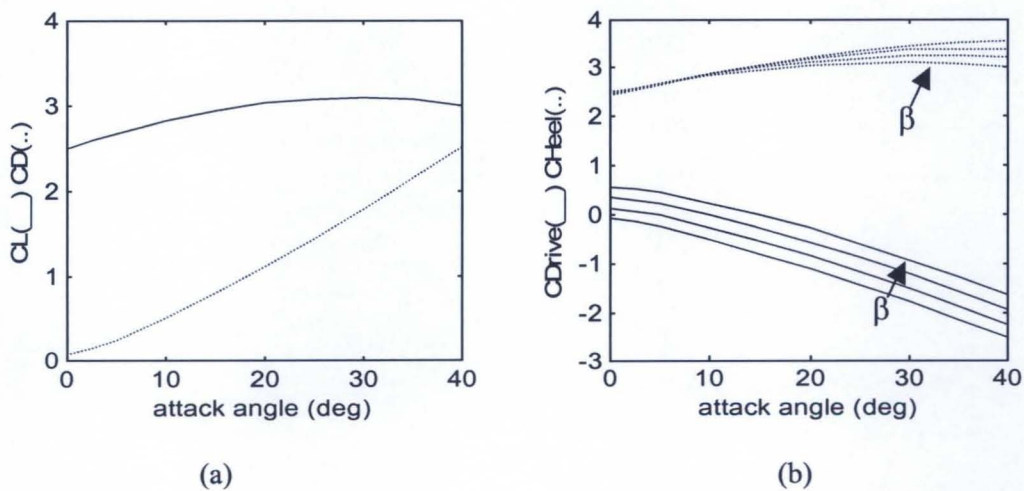


Figure 9.6: (a) Lift and induced drag coefficients (b) drive and heel coefficient on the tapered surface ($c_t/c_f=0.4$), with linear twist distribution $\delta=0^\circ$ to $\delta=8^\circ$.

Comparing what happens for the same sailing condition as above ($\beta=10^\circ$, boom sheeting angle $\delta_m=0^\circ$, leeway angle $\lambda=5^\circ$, being $\alpha=5^\circ$), the obtained values are:

- CDrives_S = 0.015 and CHeels_S = 2.24.

It is notable that the drive force has incremented, with only a small increment in the heel force. The improved values for the driving force coefficients are extended to almost the same range of angle as the less tapered surface. This is a consequence of the large twist presented, because the sail tip sections are less loaded.

For this reason, the same taper ratio ($c_t/c_f=0.4$) has been introduced to the slightly twisted cylindrical surface (tip twist angle $\delta = 8^\circ$), for which figure 9.6 presents the results.

The observations are:

- for each true attack angle the lift and the drag coefficients assume bigger values,
- the maximum efficiency is at $\alpha = 30^\circ$, where $CL_S = 3.1$ and $CD_S = 1.79$
- the range of true attack angle, for which it is possible to sail windward, is larger and the boat goes faster.

Considering the same sailing condition, the coefficients are:

- CDrives_S = 0.22 and CHeels_S = 2.68.

This means that this shape presents the biggest drive force coefficient obtained until now and it occurs for the entire range of possible sailing courses.

These results justify a more accurate analysis for an extended range of angles and furthermore suggest continuing in this direction in order to improve the results obtained. Repeating several times these tests produces a map, which provides an understanding of all-conceivable sailing conditions. If for example with this sail shape, the maximum curvature is moved ahead to 45% of the chord, the obtained results are plotted in figure 9.7.

From these results, it is evident that:

- the lift coefficients are bigger for each true attack angle;
- the maximum value is obtained at $\alpha=25^\circ$;
- the maximum efficiency is at $\alpha=22.5^\circ$, where $CL_S = 3.18$ and $CD_S 1.32$;
- the drive coefficients are the same for the same true attack angle, while the heel coefficients are bigger.

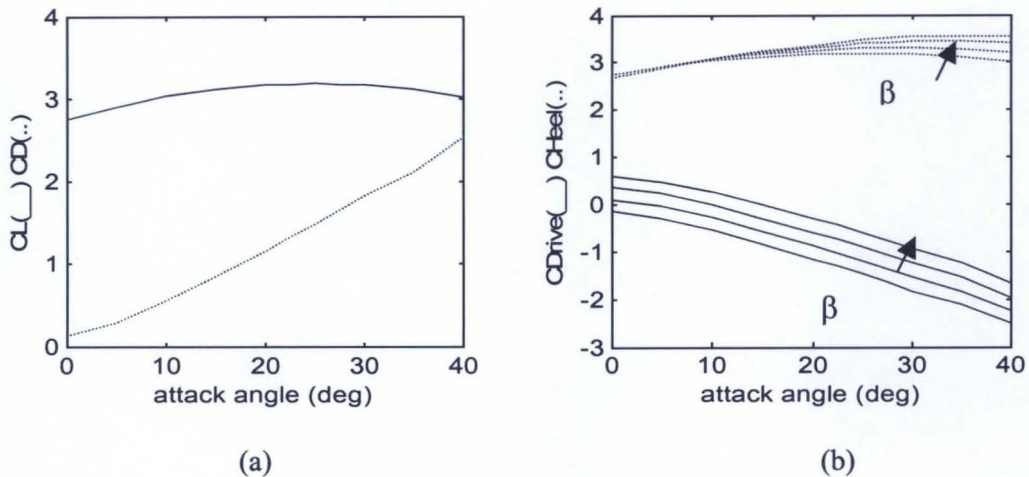


Figure 9.7: (a) Lift and induced drag coefficients (b) drive and heel coefficient on the tapered surface ($c_t/c_f=0.4$), with linear twist distribution $\delta=0^\circ$ to $\delta=8^\circ$ and max camber at 45% of the chord.

These above observations indicate that this configuration is unstable. However, the bigger values of heel coefficient help the helmsman, including the cases of changing the leeway angle and consequently the sailed course, even at slow velocities. Henceforth, this exercise might continue considering for example what happens if the maximum curvature is moved rearwards or by changing the value of the maximum curvature.

It has been decided to stop the present design example with the achievement of the above results, in accordance with the fact that the aim of illustrating the use of this system for aiding sail design has been achieved. Furthermore, the result of the design process, carried out in this section, ends up with a possible shape for a FINN Class sail and a complete map of its aerodynamic performance in different external conditions, without employing any model manufacture or experimental test costs. The only cost is the computational one, which can be reduced in the eventuality that a sail shape database is available. In this case, by manipulating a known sail shape in a similar process, the efficiency of the design process, defined by the ratio $\eta_{\text{design}} = \text{final shape/computational time}$ increases. In conclusion, table 9.2 summarises the results obtained in this design phase. This table shows only the sail shapes, which have shown effective possibilities of flying and the respective possible sailing courses.

Sail Shape	True attack angle	Apparent wind angle
Cylindrical surface	$0^\circ < \alpha < 5^\circ$	$\beta > 5^\circ$
	$0^\circ < \alpha < 17^\circ$	$\beta = 15^\circ$
Cylindrical surface + linear twist ($\delta=0^\circ$ to $\delta=20^\circ$)	$0^\circ < \alpha < 15^\circ$	$\beta = 20^\circ$

Table 9.2: Possible sail-shape and respective sailing courses

9.2.2 Sail design from a flat surface

This section approaches the design of a sail shape, starting from a flat trapezoidal shape. The aim of this design example is to demonstrate the possibility of using the system for finding the shape assumed by a flat sail, in several known external conditions. The final shape results in equilibrium with the corresponding distribution of loads, which are also calculated.

Before showing the results, it is important to clarify the reasons behind these tests and moreover the difference with the design example exposed in the preceding section. Since sail surfaces are built with an initial curvature, this kind of design procedure might appear worthless. However, as section 6.1.2 explains, the curvature is given by sewing together flat panels and, moreover, since large sail size utilises large sailcloth panels, this design process deepens the debate about the structural properties of particular sailcloth, naturally considered homogenous and isotropic.

Whereas the sail design example, shown in the previous section, builds up a final sail shape, without fixing the particular material used, henceforth the tests consider the design performance of a fixed shape, differentiating the structural properties of the used sailcloth.

Therefore, consider the case of a flat trapezoidal sail surface, characterised by the dimensions, shown in table 9.3. As usual, the data have been typed in the ‘Input Data’ G.U.I., displayed in figure 4.2, putting camber, twist and all the trimming angles, leeway, heel and boom sheeting equal to zero degrees. After improvements of the geometry made

by the appropriate G.U.I.s, shown in figure 4.5, 4.6 and 4.7, the 32-panel model has been obtained thanks to the ‘3D-Mesh’ interface, plotted in figure 4.9.

Foot chord length	1 metre
Luff length	2 metres
Head chord length	0.025 metre
Camber	0%
Gap	0.025 metre

Table 9.3: Trapezoidal sail section dimensions.

On completion of this geometry, the aeroelastic analysis has been carried out in the range of attack angle $\alpha=0^\circ$ to $\alpha=20^\circ$, considering the nodes along the luff and head sections blocked, whilst those along the foot have been able to slide along the boom-direction.

The analysis has been restricted to this small range of attack angle in the view of the fact that the system performs a potential aerodynamic analysis. In fact, as the initial surface is a flat plate, separations occur for higher attack angle values and results ought not to be reliable. Furthermore, as leeway angle is put equal to zero, and because the range of attack angle investigated produces small coefficients of induced drag, only an evaluation of the lateral stability of the sail is expected.

Henceforth, results have been analysed and the conclusions about the structural behaviour and the external loads obtained are exposed in the following paragraphs. In order to facilitate the understanding of the results consider figure 9.8 and 9.9. They plot the final results for the trapezoidal sail surface, as described above, in the event the flow velocity is 10m/sec and the sailcloth of thickness equal to 0.005m, is a type of Kevlar[®] (Poisson modulus $\nu=0.33$ and Young’s modulus $E = 7.39 \times 10^9$ Kgf/m²). The unique difference is the attack angle of the flow, which is respectively $\alpha=15^\circ$ and $\alpha=20^\circ$.

With regard to the deformed surface obtained, for the entire range of attack angle and for any type of sailcloth, three general characteristics have been demonstrated:

- resulting sail surfaces are twisted and curved,
- twist and curvature increases with the attack angle,

- maximum displacement is located between 50% and 80% of the local chord from the luff.

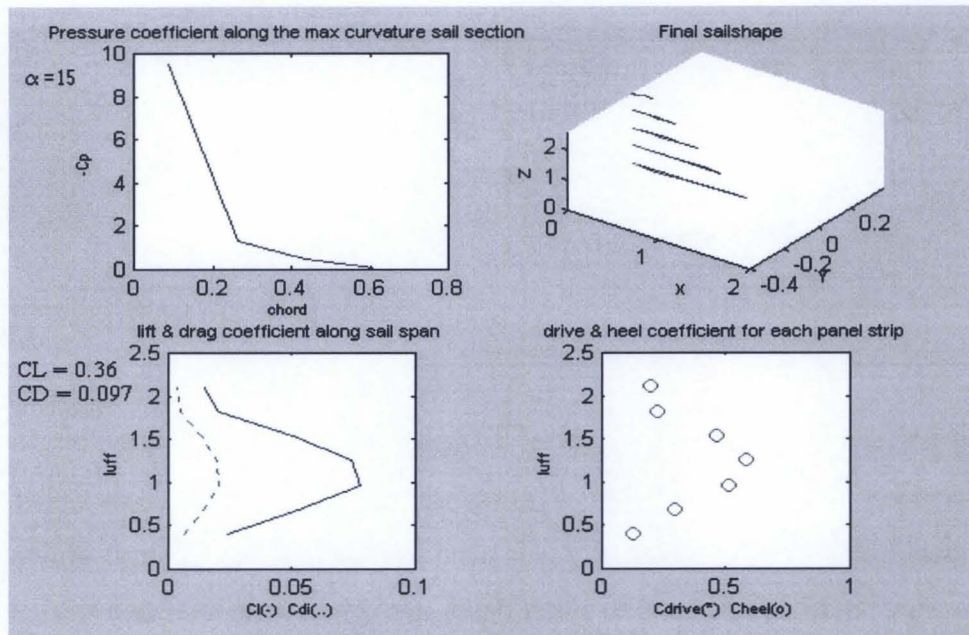


Figure 9.8: Final results for the flat sail at $\alpha=15^\circ$

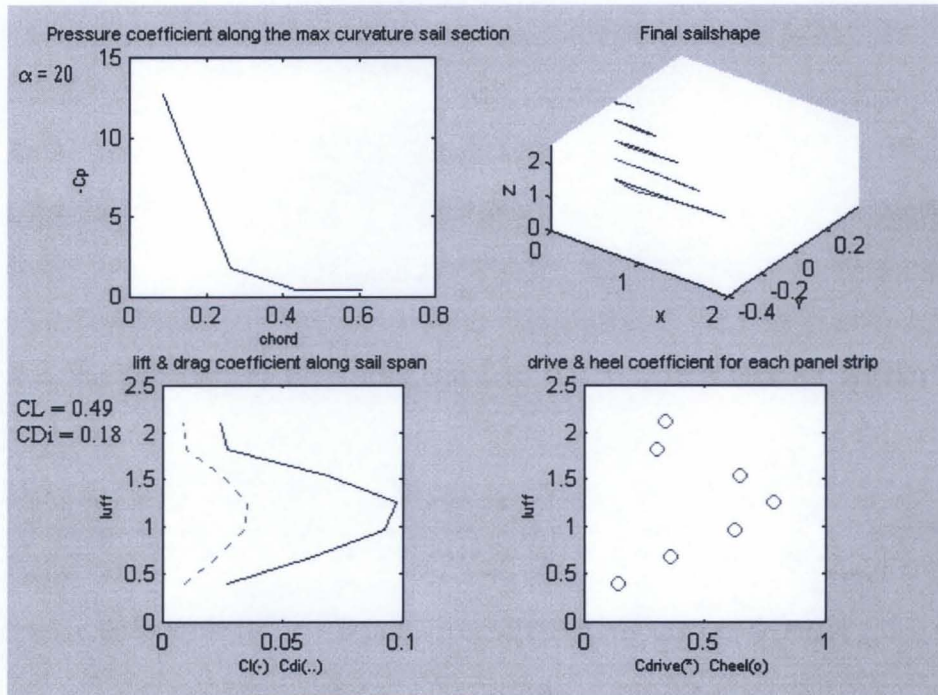


Figure 9.9: Final results for the flat sail at $\alpha=20^\circ$

In particular, with reference to the displacements along the x-direction U, generally:

- $U < 10^{-3}$ m, thus they are not appreciable with respect to the total displacement;
- their maximum values are concentrated at the bottom of the surface, between the lower and the middle section (which is between 25% and 50% of the luff curve);
- the distribution of the displacements stretches the sailcloth, as nodes closer to the luff have negative or zero displacement, whereas closer to the leech they are positive.

With reference to the displacements along the Y-direction V, mostly:

- in modulus, they are an order more than the component along X or Z direction,
- the node displacements along a section goes from zero at luff then increases until its maximum value and finally decreases at the leech,
- their maximum value is concentrated between 40% and 60% of the local chord from the luff,
- incrementing the attack angle increases the area of significant displacements, which produces more curvature.

Concluding, with reference to the displacements along the Z-direction, W, it has been noticed that they are:

- in modulus, $W \sim 10^{-3}$ m,
- concentrated behind 70% of the local chord,
- assuming the maximum values along the leech curve.

The particular deformed shape, assumed by combining the three displacements, is influenced by the particular set of constraints and total finite element number used. In fact, as the luff and the head nodes are blocked, the structure tends to assume the major displacements far from this constraint. Then, the maximum curvature and the twisted area are displaced after 40% of the local chord and around the middle sections (which means around 50% of the luff curve). The maximum values for both the characteristics depend upon material, thickness and attack angle.

Considering the external loads obtained, with attention to the figures 9.8 and 9.9, it has been observed that:

- pressure distribution along a section at about 30% of the luff, which corresponds to the maximum curvature according to the displacement distribution, assumes in both cases the typical shape of a plate pressure distribution, as expected;
- by looking at the force coefficient distributions along the luff, it is more evident that:
 - the most loaded section corresponds to that with maximum curvature,
 - the sail tip has the smallest loads;
- due to the fact that the leeway is zero, the drive force is not appreciable, while the heel coefficient distributions denote the tendency to create a non-zero leeway angle in order to drive the sail.

Several other tests have been carried out. The conclusions derived are that this system of analysis gives reliable results up to $\alpha=20^\circ$. In fact, the iterative solution for the case of $\alpha=25^\circ$ experiences a deformed shape characterised by a maximum displacement about 10^{-2} m at 50% of the chord, and a curvature displaced over the entire sail, including the tip, which determines load increments, causing an unstable sail shape.

However, the above limit is not absolute, but varies with the material properties and sailcloth thickness. Bearing in mind that these observed facts are the result of an aeroelastic analysis, sailcloth thickness affects structural deformation and at the same time load distribution. It has been proved that, by making the same test with a thinner sailcloth (thickness = 0.003m), the limit of applicability decreases to $\alpha=15^\circ$. Flow fields with bigger attack angle produce large deformations and mostly higher tip loads with respect to the lower sections, which makes the structure unstable.

According to the above facts, opposite behaviour has been observed in the eventuality that the thickness of the same sailcloth increases. For instance, analysing the results obtained for the thickness equal to 0.008m, the limit increases until $\alpha=35^\circ$, this increment producing a uniform deformed sail shape, likewise the distribution of the loads. Figure 9.10 corroborates these observations: the maximum curvature is displaced towards the middle section, where the loads assume their maximum, with respect to the previous examples.

Furthermore, figure 9.11 highlights the deformed shapes assumed by the 0.008m sailcloth through the iterative process. It is evident how the V displacement increments with further iterations, since during the first iteration, the calculated loads are related to the

flat sail, whereas after the second iteration the load increases are due to their curved shape. It is important to be precise that notwithstanding the coarse model, built with only 32 panels which has produced the deformed shape through only five nodal displacements for each section, important general design conclusions have been obtained.

In conclusion, this simple design example has demonstrated the feasibility of complete static aeroelastic analysis in order to find the final shape and the corresponding loads, starting from a flat sail shape.

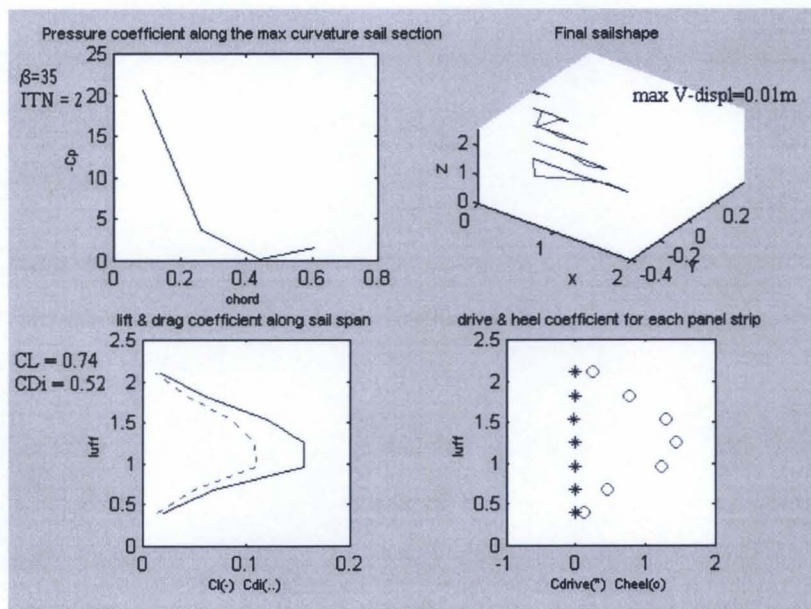


Figure 9.10: Final results for the flat sail with thickness = 0.008m at $\alpha=35^\circ$

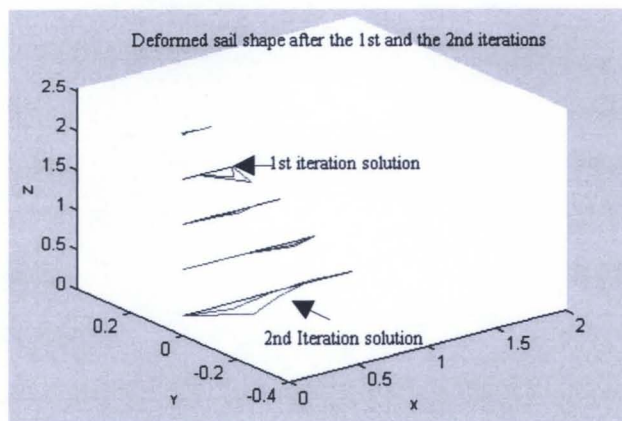


Figure 9.11: Particulars of the deformed shape assumed during the iterative process by the flat sail with thickness = 0.008m at $\alpha=35^\circ$

Summarising, it has been seen that this design system produces reliable results over the limited range of attack angle. High attack angle flow generates high loads, which ought to cause unstable thin sailcloth configurations. Indeed, this is not a limit for the solver, where it is a further indicator of the structural sail properties. Thin cloths undergo large deformation.

Higher attack angle flow deforms the sail more, due to higher loads developed, and displaces the maximum value for the curvature as well as the maximum load towards the middle sail section.

Furthermore, it is believed that despite the use of coarse numerical models, as in the case presented, complete analysis of the results allows establishing general comments and quantitative estimations for the structural behaviour as well as the load distribution. However, improved definition of novel shapes can be obtained by increasing the number of nodal points over the sail.

9.3 Mast Design example

In a generic sailing boat, either cruising or racing, the mast is an element of the rig. This structure holds the sails and drives the sailing boat, thanks to the combination of the boat's trimmed configuration and the particular required sail shapes, moulded using the rig's elements, [41].

Since the mast structure and its position on the deck affect the resistance and the driving force of a sailing boat, a poor mast design decreases the sailing performance particularly for racing boats. Properties such as low weight, high flexibility, high fracture loads are required from the structural point of view, whilst from the aerodynamic point of view, section shape is important for reducing the drag and the influence on the sails, [35], [63], [71].

As announced in chapter 2, before illustrating the results obtained for mast design, a brief review of the literature about mast design follows.

Inasmuch as the subject of this work is not mast design, henceforth the intent is to focus on the current need for improvements in sail loads calculations in order to make better masts and in evaluating the influence of the mast presence on the flow regime over the entire sail.

Modern yacht masts are flexible structures that allow controlling the sail shape by their bending. An efficient mast design achieves the highest values possible of the above structural and aerodynamic properties through a correct evaluation of the loads acting on it. Distinguishing three main categories, [55]: sail loads, tuning loads and dynamic loads, within the static analysis, the first two classes are considered. Due to certain external conditions, the crew decides to adopt a particular sail shape and rig configuration, in order to reach maximum sailing performance. Thus, the sail loads are properly due to the sail shape, whilst the tuning loads are developed for keeping the sail shape and consequently their value is influenced by the sail loads. Therefore, a realistic evaluation of the external loads acting on the sail is an important design factor [5], [8], [35].

It is important to report that the common habit is to fix a mast on a designed hull. Actually, there are several factories that produce and sell masts to other manufacturers, which provide hulls. Then, only when a customer buys a sail will usually the sail-makers care about which mast is going to sustain them. These facts corroborate that masts are designed without certainty about which boat is going to carry it and which sails it will carry. Despite this reality, improvements in mast design have been made. From the structural point of view, the requirements of flexibility, low weight and durability have brought the adoption of new materials. In order to improve the aerodynamic interaction with the sail behind, new elliptical section shapes have been experimented with, in order to minimise the flow separation behind it, which decreases sail performance. However, like sail design improvements, in mast design they are due in the majority to experience.

Thus, the next section deepens the debate about approaches to sail design, noting the importance covered by the interaction, both aerodynamic and structural, between mast, or rig, and sail for determining sailing performance. The following sections present the results of applying the developed system for aiding mast design and improving the actual techniques, as mentioned in section 1.4.3. In particular, firstly the explanation is given of

how the integrated design system is applied for evaluating mast loads due to the sail and secondly, the description of a FINN class sail-mast configuration analysis follows for showing the improvements obtained using the method.

9.3.1 Literature review

For determining sail loads, today, most of the mast designers are still using force coefficient tables extrapolated from wind tunnel tests or calculated by Milgram [44], as mentioned in chapter 2. Usually, as a project condition, the designer chooses the highest load condition from those tables. This procedure is approximate, because on one hand, it is assumed that the loaded sail is the one used in the wind tunnel tests and, on the other hand, it is accepted that the strongest external conditions possible for the mast are those for the reported case in the tables. This dual approximation requires the use of high values for the safety coefficient to the detriment of the mast design efficiency. Indeed, high safety coefficients for avoiding cracks, unexpected deformations or displacements and crew mistakes are required, which leads mostly to increments in the mast weight, [5].

Nowadays, mast design is one of the key focus areas for improvements in the total sailing performance. In view of this fact, scientific approaches are in development. It is possible to identify two ways of approaching mast design. There is a group of scientists, who are more interested in the structural analysis and design of the mast, such as Selness [55] and Boote [5]. They agree that mast analysis and design depend upon the assumed loads and the structural model. These authors have performed the structural analysis by applying the finite element method, considering the mast loaded by uniform loads calculated using empirical or experimental coefficients, available in the literature and based on the wind strength, as seen in chapter 2. The other group of scientists are more interested in the aerodynamic influence of mast design. Milgram, [44], extending to the three-dimensional case the results obtained in the wind tunnel on a two-dimensional mast-sail configuration, demonstrated the high influence on the flow around the sail behind the mast. Comparing with the case of a sail without mast, the total lift decreases whilst the total drag cannot be considered as the sum of the drag due to the sail and to the mast separately. Wilkinson, [64], in 1989 performed further wind tunnel tests on a two-dimensional sail-

mast configuration extending the flow data around the sail, as the pressure distribution shape along all sections were obtained. Later Boote and Caponnetto, [8], developed the first complete procedure for mast design, by applying loads obtained from a numerical evaluation of the flow around the sail configuration considered. Despite the poor numerical model and restrictions, the authors proved the importance of obtaining a correct sail load evaluation in improving mast design.

9.3.2 The application to mast design

This section outlines the phases of the method employed for estimating the loads along a sail mast and the influence of the mast presence on the flow regime over the sail. Therefore, as it has been necessary to implement the mast structural analysis according to the structural behaviour of a FINN class sailing boat mast, this is described below. Then, the concerns about the integration of the analysis system with the presence of the mast are addressed with the related results.

Mast Structural analysis

The required high performance for racing sailing boats in terms of velocity determines usually the utilisation of lighter masts with relatively low stiffness, which are able to work in a bent configuration and facilitate manoeuvring. Thus, especially for racing mast design, the use of force coefficient tables is very approximate. From these considerations, in order to optimise the performance of a particular sailing boat, it is believed that the design procedure should start with a previous study of the particular mast structural behaviour for the specific case and then to base the structural analysis on this.

FINN Class sail-mast system

Sections 1.3.1.1 and the related figures 1.2 and 1.3 furnish details about the FINN Class boat and typical sailing configuration characteristics. It is important to keep in mind that for this sailing boat, the mast is unstayed and the boom can be considered fixed to its end point. Practically, the sailing forces derive from the one sail, whose shape is formed from the combined action of the mast bend and the kicking strap forces. It has been seen that due to the overturning moments, keeping a stable sailing condition in strong wind conditions

requires a very flat sail shape, while in light wind it is preferable to make the sail fuller around the lower and the middle sections. Therefore, a flat sail shape is obtained by bending the mast and increasing the kicking strap tension, which decreases the camber and the sail twist. Thus, in these sailing conditions, the mast is designed for working in a bent configuration, under prevalently flexural loads due to the sail membrane forces along its length and due to the boom near its base. Therefore, in accordance with the above-described behaviour, in the present study, the structural analysis approximates the mast as a cantilevered beam working under flexural loads.

Therefore, a further code has been implemented in order to evaluate the mast structural behaviour. The structural analysis is accomplished by applying the method of ‘follower forces’. This method is a second order non-linear analysis. Thus, the loads are applied at the initial configuration and they are considered orthogonal to the mast in all the stages of the iteration process on the field of displacements. The method is implemented using the F.E. technique: the mast F.E. model is built using beam elements. Each node coincides with the node along the sail luff curve. Further, it has 4 degrees of freedom, 2 rotations and 2 displacements along the two directions in the plane orthogonal to the beam axes, since the forces applied act always in the orthogonal direction to the axis along the beam.

Integration of sail and mast analysis

The methodology elaborated for tackling the problem of the evaluation of the sail loads distribution along the mast is illustrated in figure 9.12.

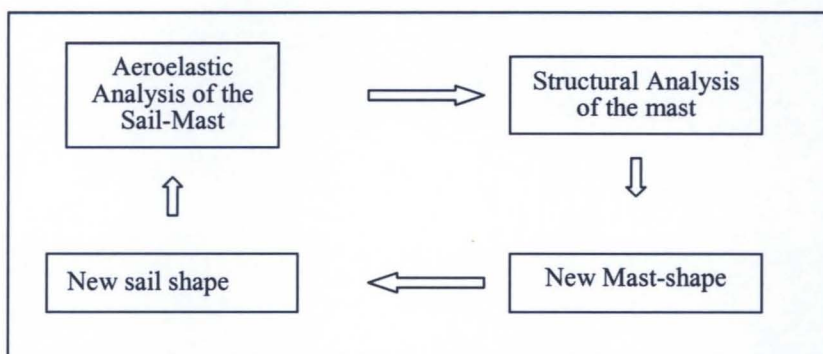


Figure 9.12: Analysis procedure

The adopted procedure goes through the following steps:

- 1) the aeroelastic analysis of the sail in real sailing conditions,
- 2) the successive structural analysis of the mast under the calculated loads, which provide the deformed mast shape,
- 3) adjustment of the sail luff curve, in the way it coincides with mast axes,
- 4) new evaluation of the sail loads until convergence.

Step 1) is carried out as explained in chapters 3, 4, 5 and 6, whilst the structural analysis of the mast, step 2), is accomplished as described in the previous subsection, considering it as a bending beam. The process is then reiterated until convergence is reached. Since the initial sail-mast configuration shape is in equilibrium, as it coincides with a sailing configuration under the described external conditions, the convergence procedure is fast.

Figure 9.13 describes better what an aeroelastic analysis of the sail-mast system entails. As mentioned several times, the method employed for this analysis is the one presented in this thesis. With this example, the versatility of the system is shown, demonstrating the possibility of interactive data exchange between the system and other codes. Thus, the approach employed for performing the above step 1) consists of generating an iterative calculation between:

- the aerodynamic analysis of the three-dimensional sail-shape, including the effects of the presence of the mast, which evaluates the pressure distribution for the given sail-mast configuration,
- the structural analysis of the sail under the evaluated pressure loads, which estimates the stress distribution for the equilibrium sail shape.

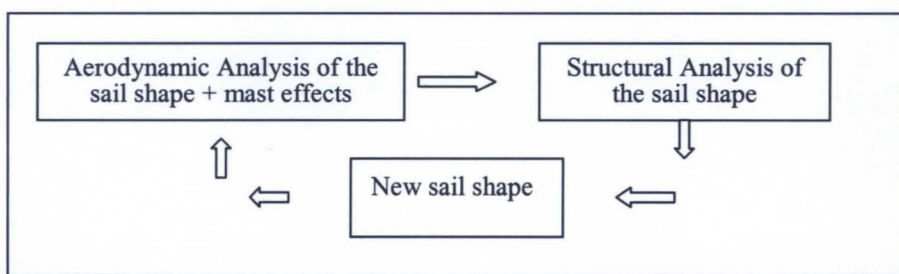


Figure 9.13: Aeroelastic Analysis of the SAIL-MAST system.

Figure 9.14 shows in detail how the aerodynamic analysis has been expanded to the mast analysis. This consists of an iterative procedure comprising two main steps.

In the first step, the sail-shape, considered as a rigid surface, affected only by the sea surface influence, is analysed for the known external conditions, using the method outlined in chapter 5. This gives the potential solution of the flow around the sail, without considering the presence of the mast.

In the second step, in order to take into account viscous effects, a 2D boundary layer analysis has been performed. The two-dimensional boundary layer solver is due to Coiro and Dini. This solves the integral laminar and turbulent boundary layer equations and it is capable of handling laminar separation bubbles. Further details about the solver are in the publications of the mentioned authors, and in a paper published with the present author, [38]. In the cases presented here only one inviscid/viscous interaction has been performed, called the weak interaction. The iterative procedure proceeds by taking into account the corrected pressures, which in turn will cause the new sail shape to be fed to the next aerodynamic analysis.

When the main loop, described in figure 9.14, converges, the structural analysis of the mast begins, as described in the previous section.

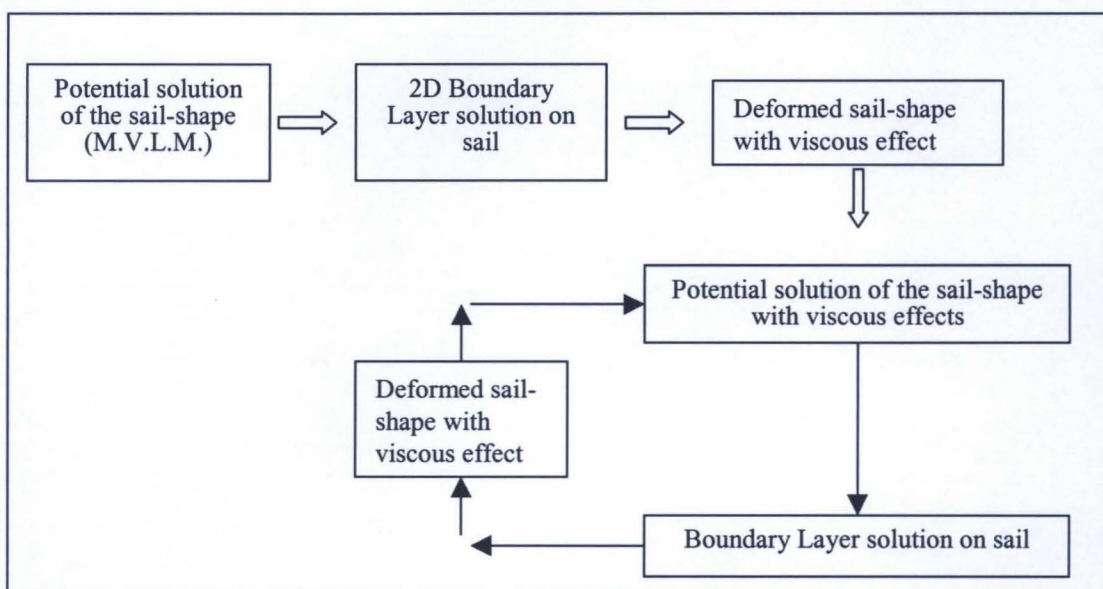


Figure 9.14: Aerodynamic analysis of the sail shape with the viscous effects.

9.3.3 Results and conclusions

In this section, the results obtained using the methodology discussed in the previous section are presented, utilising the features of the developed GUI.

As mentioned above, the chosen example considers a FINN Class sail-mast configuration, whose data are taken from the WB-Sail web-site and displayed in tables 4.1 and 4.2 and typed in the G.U.I. ‘Input interface’, as figure 9.15 shows. The difference between this example and the one used in chapter 4 is in the mast characteristics.

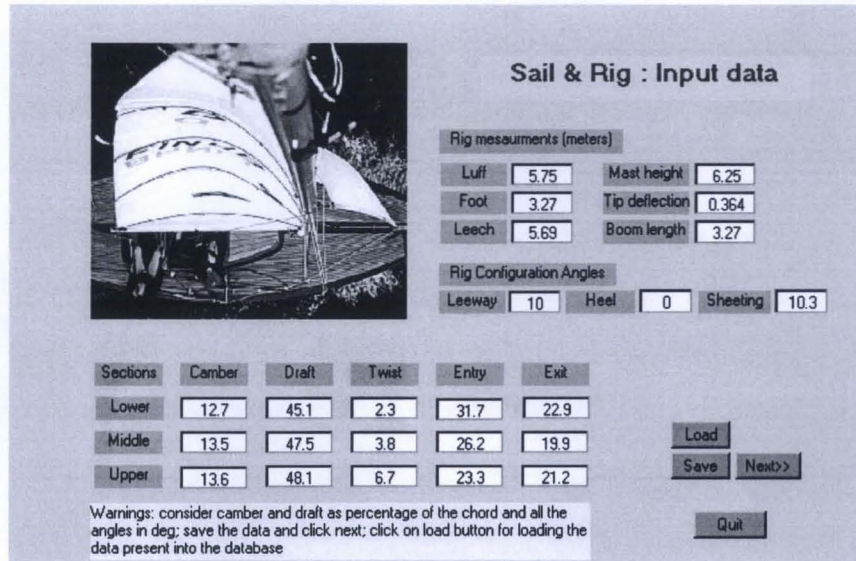


Figure 9.15: The ‘Input Data’ G.U.I. for the analysed sail-mast system.

Figure 9.16 plots the elaborated sail-mast geometry. It is evident that the geometric generation phase and the related G.U.I., as described in section 4.3 and 4.4, have been improved by adding the geometric definition and plot of the mast.

Then, following the methodology, the aerodynamic analysis is carried out. Figure 9.17 plots the panel model, the external conditions and the data related to the wake for the aerodynamic analysis performed as described in chapter 5. Once this phase converges, the structural analysis follows. Figure 9.18 shows the finite element model and the structural sailcloth properties used for this case.

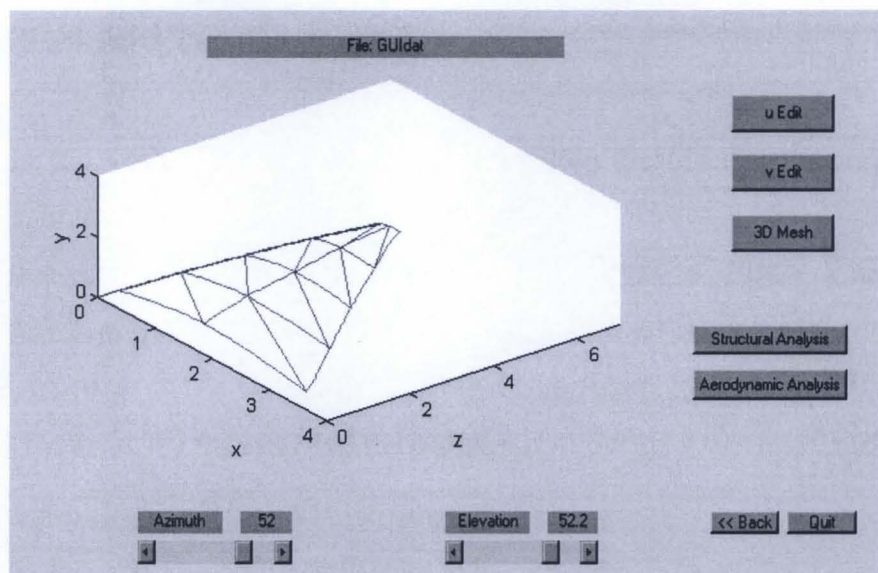


Figure 9.16: Elaborated geometry for the FINN class sail-mast system.

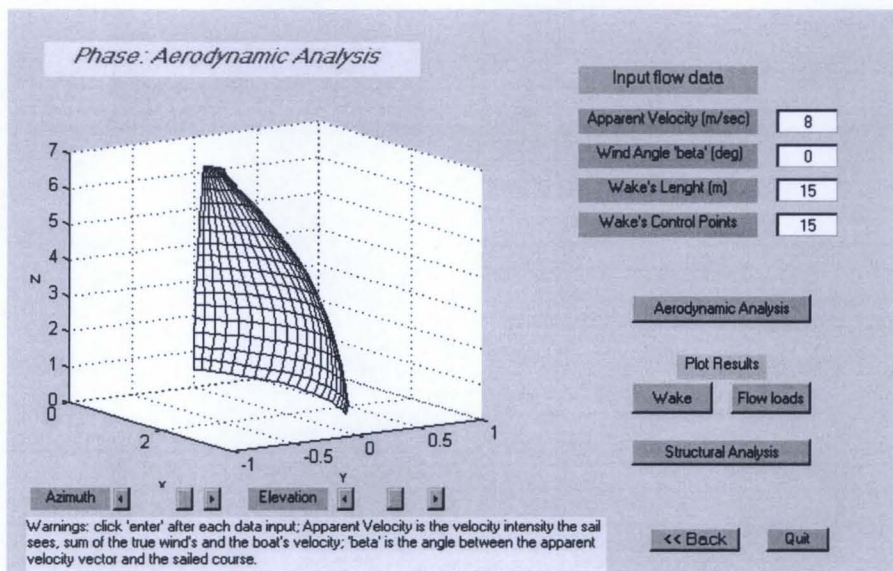


Figure 9.17: Sail panel model and external condition for the aerodynamic analysis

Figure 9.19 summarises the results obtained considering the boundary layer influence for the panel models shown in figure 9.17, focusing the attention on the load distribution close to the boom attached to the mast. Due to the high Reynolds number, in this case the force coefficients do not change. The same sail-shape has been analysed using just 64 panels for $\alpha=0^\circ$ and $\alpha=45^\circ$ for a $V=10\text{m/sec}$. Figure 9.20 shows the results for these tests.

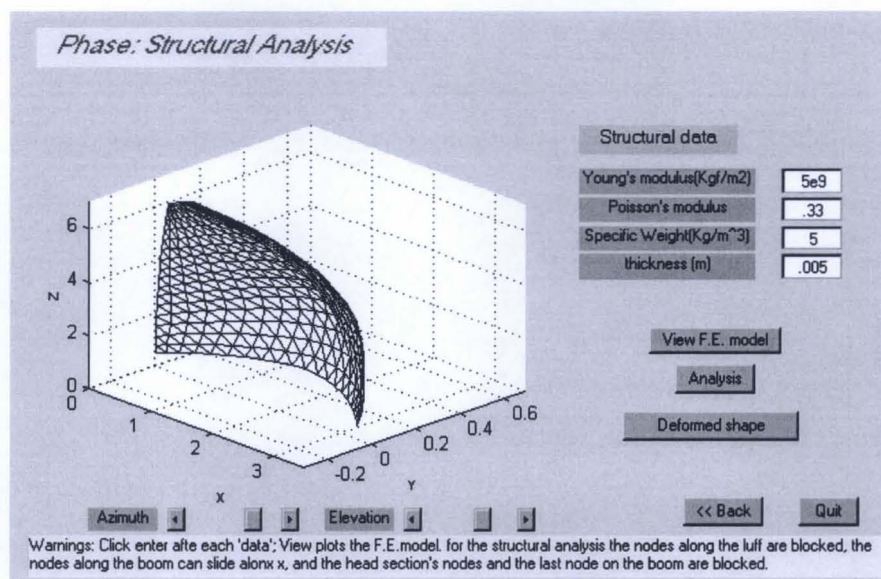


Figure 9.18: Sail finite element model and structural properties

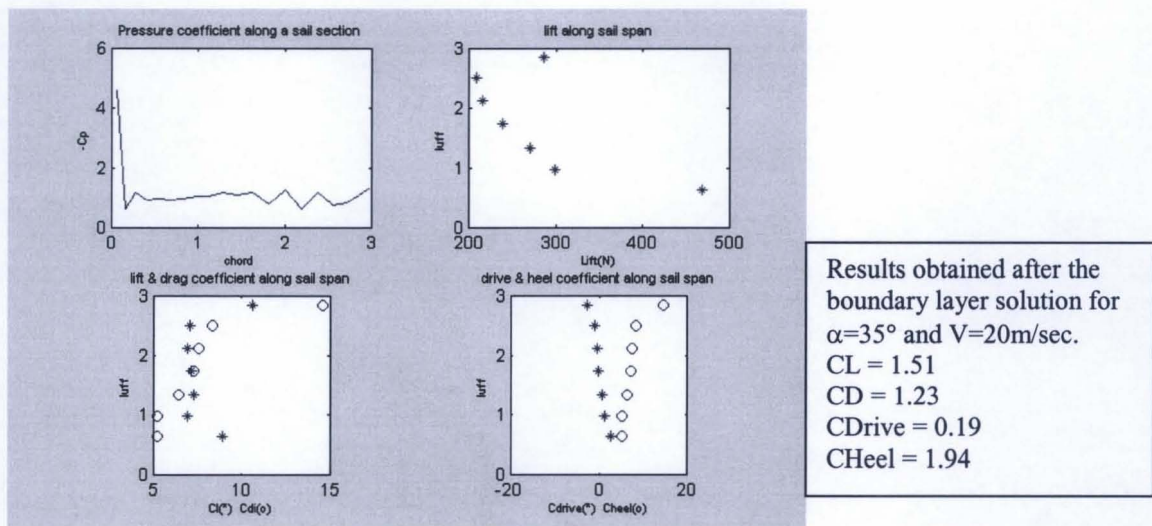


Figure 9.19: Results for the sail model with 320 panels.

These examples show that in both cases the values of the force coefficients drop 10%, when the sail is considered flexible, because of the changes of the sail shape. Furthermore, due to the limited panel number, the force coefficients are underestimated. Also, the boundary layer changes the force coefficients by a maximum of 4% of their values. This low effect is explained because the sail is considered without the mast. However, the

distribution along the sail luff curve is similar. These results are in accord with wind tunnel test data available in the references for similar FINN sails.

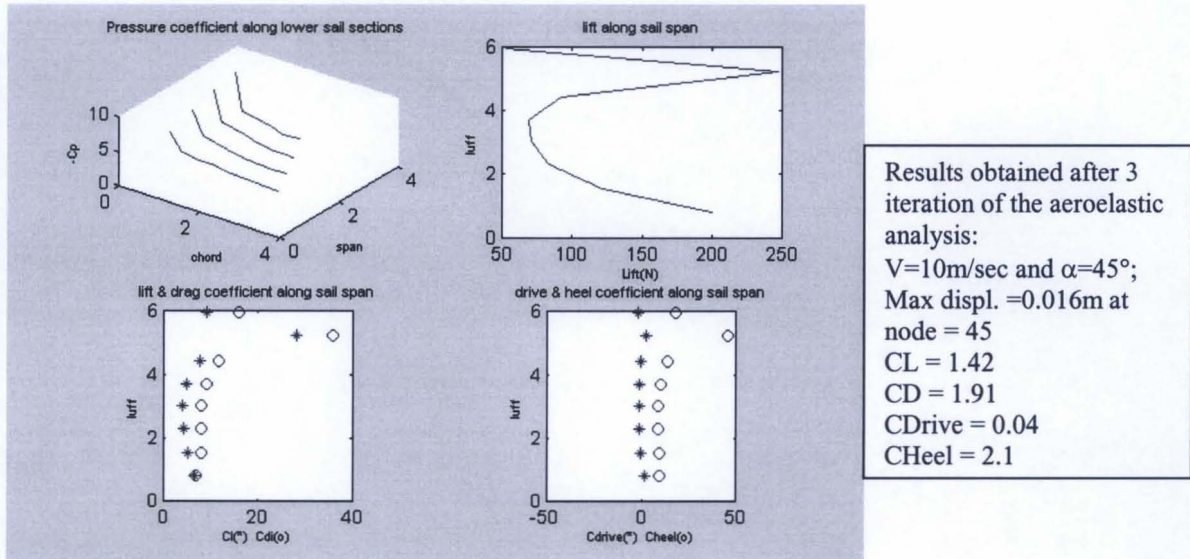


Figure 9.20: Results for the sail model with 64 panels

Analysing the results obtained, it is possible to conclude that:

- 1) the higher loads affect the base of the mast where the boom is attached
- 2) their distribution is not triangular;
- 3) viscous effects are not dominant on sail sections if the average Reynolds number is high and no separation is present;
- 4) the aerodynamic analysis of the mast-sail junction permits a better evaluation of the sail loads, thanks to a more accurate flow simulation.

Concluding, this section 9.3 has shown how the system can be interacting with other codes and the related modified G.U.I.s.

In particular, it has been shown how the system can be used for aiding mast design and construction methods, which constitute currently important key factors for improving sailing performance. It has been demonstrated that for every rig, an efficient mast design procedure must provide a realistic evaluation of the sail loads. It is believed that a prior

study of the particular mast structural behaviour is needed in order to develop an accurate structural analysis.

Summarising, despite the simplified structural model used in this example for the mast analysis, the results achieved show that the loads along the mast of a particular FINN Class sail depend on its particular shape and on the different external sailing conditions. Load distributions are not constant and uniform or triangular, as assumed by most of the mast designers, and are particularly dangerous where the boom is attached.

Therefore, it is believed that the obtained results are qualitatively reliable, whereas the accuracy of the quantitative values can be improved by developing a more accurate structural model and analysis of the mast. In addition, future examples of the implemented methodology will clarify the influence of the mast on the flow regime over the sail from the qualitative and quantitative points of view.

9.4 Conclusions

In this chapter, the design features and the versatility of the system, presented in this thesis, have been described and demonstrated, by performing design actions, namely:

- draw a FINN class sail shape, starting from few project data;
- define the final shape and mapping the behaviour of a flat sail shape in various external conditions;
- improve mast design and analyse the mast influence on the flow regime over the sail;
- hasten both sail and mast design;
- reduce costs of design actions due to the limited time consumed, computational power employed and people involved;
- reduce the number of possible design flaws, due to the accurate external loads and their distribution evaluation, as chapter 8 concludes;
- visualise the new and novel designed sail.

It is important to repeat here that the entirety of the presented design examples do not intend to exhaust the debate about sail or mast design nor the concerns of the design aims. The intent has been to describe possible approaches to this research field, which is young and in fast development, due to the use of powerful computational tools.

In addition, these examples do not end the possibilities of using the same system for other kinds of design approaches. Given these features, future examples will improve the results in the three areas approached here.

Chapter 10

Conclusions

The development of an integrated analysis and design system for a one-sail configuration has been presented. The focus of this research has responded to the current needs within the areas of analysis and design methodologies for sails, especially the one-sail configuration, in accordance with the stated research purpose, repeated here for clarity:

'To provide a full static aeroelastic method of analysis and design of a single-sail configuration supported by a user-friendly graphical interface. The emphasis shall be on providing a practical application of the sail analysis, which will allow further developments in sail design.'

In every respect, the development of the integrated sail analysis and design system has met the objectives within the mission statement, more specifically:

- The computational elements of the algorithms written for the different analysis phases have been developed to produce an efficient, flexible and user-friendly analysis method, which may be applied using personal computer capabilities.
- The analytic capabilities have allowed the enhancement of the design approach for one-sail configurations and masts.

- The development of test cases to assess the integrated system performance has allowed application to existent and novel sail configurations.
- The use of this system has simplified and speeded up the non-linear aeroelastic analysis of a membrane structure, such as a sail.

Considering the overall practicality of the system, current results are promising, especially when applied to FINN Class sails, or any other one-sail configuration.

In Chapter 8, the application of the analysis features to different sail shapes and in different sailing courses was shown to be successful. Two important results have arisen:

- the necessity of accurate performance analysis for each sail, for any given shape over all the possible sailing courses;
- the efficiency of knowing the load distribution.

With reference to necessity of accurate performance analysis, the reasons are in the demonstrated influence of the interaction between the aerodynamic loads and the structural properties of the sails. Therefore, the necessity of the aeroelastic static analysis is incontestable, notwithstanding general prediction of deformed sail shapes and load distributions. By testing a WB-Sails Finn Class sail, the performance analysis has demonstrated that a given sail maintains its shape and performance over a limited range of external conditions. Analysing the same sail over all the possible sailing courses produces a complete map of the sail behaviour, in terms of optimal shape for given external condition, total loads and their distribution.

With regard to the importance of knowing the load distribution over a sail shape, it has been shown how changing the amount and the distribution of camber and twist - the two geometrical parameters to transform a sail shape - influence the total force coefficient values but predominantly the load distribution. Beside this fact, the total force coefficient values do not guarantee that the given sail-shape can effectively sail and, moreover, do not ensure regard for the lateral sailboat stability nor the possible presence of separated flow.

Summarising, this analysis model does not achieve perfect numerical results, due to the limits it has, but gives nevertheless important information regarding the general sail shape behaviour and the load distributions for possible windward sailing courses.

The above observations and the results seen in chapter 8 corroborate the significant approximations made when the sail loads are assumed constant and uniform, or when loads evaluated by experiments on other sails are adapted to new sail designed shapes. This is the reason for most of the design flaws, which are reviewed after the construction and tests of a first shape. Knowledge of the behaviour is the only way to cut initial design flaws and related costs. In the light of the foregoing, the system has been created with appropriate design features and its versatile characteristics have been described and demonstrated, by performing design actions in chapter 9, namely:

- draw a FINN class sail shape, starting from few project data;
- define the final shape and mapping the behaviour of a flat sail shape in various external conditions;
- improve mast design and analyse the mast influence on the flow regime over the sail;
- hasten both sail and mast design;
- reduce costs of design actions due to the limited time consumed, computational power employed and people involved;
- reduce the number of possible design flaws;
- visualise the new and novel designed sail.

The entirety of the presented design examples do not intend to exhaust the debate about sail or mast design, nor the concerns of the design aims. The main intent has been the demonstration of the applicability and the reliability of the obtained results of the implemented system to these design fields, which are young and in fast development. In addition, these examples do not end the possibilities of using the same system for other kinds of design approaches. Given these features, further examples will improve the results in the three areas approached here.

Furthermore, it has been demonstrated that this system can interact with external codes in order to overtake its restrictions and enhance its capabilities in the following ways:

- its output in terms of external loads can be applied as input in a mast structural analysis solver, in order to evaluate the deformation of the mast;

- its output in terms of velocity distribution around the sail can be used as input by a boundary layer solver, in order to improve the flow field description around the sail and to introduce the mast presence effect on the loads distributions.

The implemented graphical user interface (G.U.I.) has been validated as being an easy tool for carrying out the analysis and design phases.

This thesis encloses a CD-ROM containing a video-demo of the integration of the design and analysis features into the Graphical User Interface, which explains and visualises the user-friendliness and some of the obtained results.

Recapitulating, the demonstrated versatility of the present system is believed be one of its most important worthiness. It is described and demonstrated by proper features, which from the analysis point of view enable the calculation of:

- the aerodynamic loads acting on a known sail shape in given external condition;
- the corresponding deformed sail shape.

The design features facilitate:

- development of novel sail shapes by using few initial design parameters;
- improvement of a designed sail-shape, by the easy review of results;
- tests of the structural sailcloth behaviour;
- easy and fast identification of possible design flaws;
- evaluation of whether the designed sail shape is maintained in prescribed conditions.

The possible applications are:

- prediction and improvement of sail performance,
- assistance of sail design and mast design.

In conclusion, it is important to state that the integrated sail analysis and design system presented has important margins of improvements and diversification.

Any future development can be divided into near term improvement of the current algorithms including the possibility of considering different typology of sail structural characteristics, and the long-term development of the analysis for two-sail configurations. Regarding the sail structural analysis, in the light of the fact that sails are usually built with neither homogeneous nor anisotropy materials, and usually different sailcloth are used for

the panels, near term improvements can be made by incorporating a detailed sail structural properties description. This includes the development of a selection phase of groups of finite elements and the associated structural properties.

Any future diversification could include application to windsurf sails, the integration of the mast, the development of a complete input customised for the Velocity Prediction Program (V.P.P.) for use in the performance prediction for the entire sailboat.

Appendix A

Aeroelastic Sail Behaviour

This appendix intends to complete the definition of the sail analysis as an aeroelastic problem, described in section 3.3, highlighting some useful aspects, which will ease the interpretation of chapters 3 to 7.

The science of aeroelasticity, [2], studies the reciprocal interactions between aerodynamic forces, elastic forces and inertial forces. Aeroelastic phenomenology does not exist in the case of a rigid structure and a flexible structure does not imply aeroelastic behaviour. Aeroelastic phenomena exist when the structural flexibility induces deformations, which cause a change in the aerodynamic forces. These different forces may produce different structural deformation, which will provoke still different aerodynamic forces. Such interactions may either tend to become smaller until a condition of stable equilibrium is reached or they may tend to diverge and destabilise the structure.

There are two important points to clarify. First of all, the sail analysis problem presented in this work is defined as static aeroelastic, because the influence of the inertial forces is excluded. Secondly, in the present study, the sail structural characteristics react to the aerodynamic forces with big displacements and small strain. Therefore, the structural flexibility causes displacements, which deform the sail-shape, inducing changes in the aerodynamic loads on it. Herewith, the meaning of deformation is clear, in this section.

With reference to the Collar triangle, plotted in figure A.1, the aeroelastic phenomena, which may occur in sailing in the light of the hypotheses considered in this thesis, are displayed in the upper-left side of the triangle, as they involve aerodynamic and elastic analysis. Brief descriptions follow.

Aeroelastic effects on static stability

This phenomenon considers the entirety of aeroelastic interactions due to the sail deformations, which influence the static stability of the sailboat. For example, in the event of a horizontal gust, the wind changes intensity and direction. This new external condition

might cause additional aerodynamic forces on the previous sail shape. As a consequence, these additional forces deform the sail-shape, and it is possible that there is no adaptation of the shape to this new set of forces, provoking the loss of static stability. In the case of a sail, if these events can be predicted and analysed in the design phase, the crew can change the shape to adapt to the new configuration, which will make the boat stable.

Load distribution

This phenomenon concerns the influence of the elastic deformation of the sail on the distribution of aerodynamic pressures over the sail itself. With reference to figure 5.4 and 5.7 in which are displayed the load distributions for the first and third step of the aeroelastic iterative process, the influence of the elastic deformation of the sail structure on the aerodynamic forces, in terms of intensity and luff-wise distribution is evident.

Control effectiveness.

This phenomenon concerns the influence of elastic deformations of the sail structure only on the controllability of the sailing boat. This phenomenon involves the sailboat controls, and appears when the sail elastic deformations provoke an increment of the heel force, which cannot be counteracted by the helmsman. In this event, there is a loss of equilibrium and the sailboat may turn upside down in the worst condition. This phenomenon is taken as one of the most important design parameters, which is verified in the sail design example proposed in paragraph 9.2.

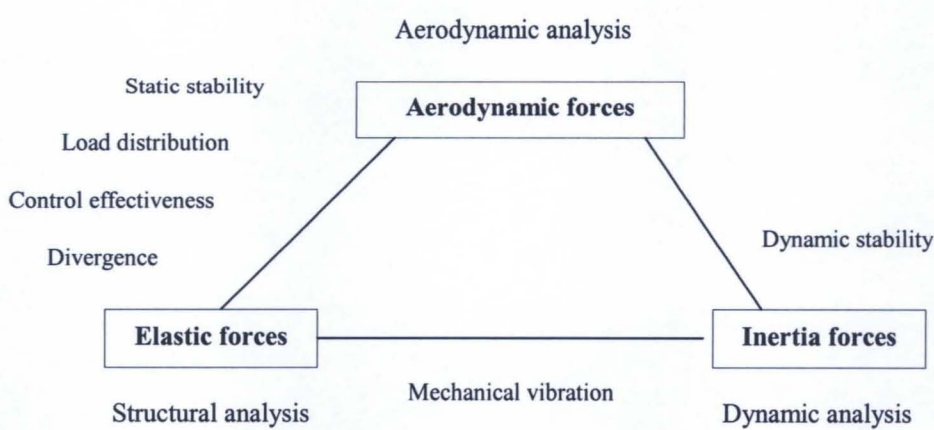


Figure A.1: Collar Triangle

Appendix B

Aerodynamic Analysis

This appendix illustrates physical explanations of some terms used for describing and carrying out the aerodynamic model and analysis, presented in chapter 5. It is for the sake of completeness and for easing the reading of the above-mentioned chapter.

B.1 Circulation, Vorticity and Potential Flows

The *circulation* contained within a closed contour in a body of fluid is defined as the integral around the contour of the component of the velocity vector that is locally tangent to the contour. That is, the *circulation* is defined as:

$$\Gamma = \oint \vec{u} \cdot d\vec{l} \quad (B.1)$$

where: \vec{u} is the velocity vector and $d\vec{l}$ is the element of contour.

The *vorticity* of an element of fluid is defined as the curl of its velocity vector. That is, the *vorticity* is defined by:

$$\omega = \vec{\nabla} \times \vec{u} \quad (B.2)$$

The vorticity vector is numerically twice the angular speed of rotation of the fluid element about its own axes. Hence, the vorticity is proportional to the angular velocity of a fluid element about its principal axes. Then, a particle, which is travelling on a circular streamline, will have no vorticity, provided that it does not revolve about its centre of gravity. The vorticity contained in a fluid element is related to the circulation around the element. By Stokes' theorem, the contour integral can be converted to a surface integral:

$$\Gamma = \oint \vec{u} \cdot d\vec{l} = \int_A (\vec{\nabla} \times \vec{u}) \cdot \vec{n} dA \quad (B.3)$$

where A is the area defined by the closed contour around which the circulation is calculated and \vec{n} is the unit vector to the surface.

Substituting the expression for the vorticity (B.2) into (B.3), the relation between the circulation and vorticity is the following:

$$\Gamma = \int_A (\vec{\omega} \cdot \vec{n}) dA \quad (B.4)$$

This equation (B.4) shows that, for arbitrary choices of contours and enclosing areas A, the two following implications are true:

$$\vec{\omega} = 0 \Leftrightarrow \Gamma = 0 \quad (B.5)$$

Flows, for which this relation (B.5) is true, are called *irrotational*; otherwise they are called *rotational*.

If the flow of an ideal fluid about a body originates in an irrotational flow, such as a uniform flow, the flow will remain irrotational even near the body. Therefore, the vorticity vector will be zero every where in the fluid.

Consequently, the following equation is true for every scalar function

$$\vec{\nabla} \times \vec{\nabla} \varphi = 0 \quad \forall \varphi \quad (B.6)$$

The condition of irrotationality (B.5) will be satisfied identically by choosing, for example:

$$\vec{u} = \vec{\nabla} \varphi \quad (B.7)$$

The scalar function is called velocity potential, and the flows are frequently referred as *potential flows*. For them, using the (B.2), the *continuity equation* is:

$$\vec{\nabla}^2 \varphi = 0 \quad (B.8)$$

B.2 Vortex Flow Theory

B.2.1 Two-dimensional flow field

Consider a flow where all the streamlines are concentric circles about a given point. If the velocity along any given circular streamline is constant, but the velocity is varying from one streamline to another inversely with distance from the common centre, the flow is called *vortex flow*.

This considered vortex flow belongs to a plane ($z = 0$), the velocity components in the radial and tangential direction to each circumference are:

$$V_r = 0; V_\theta = C / r \quad (\text{B.9})$$

C is a constant value to be determined.

The vortex flow has the following properties:

1. it is a physically possible incompressible flow, in fact at every point:

$$\vec{\nabla} \cdot \vec{V} = 0 \quad (\text{B.10})$$

2. it is irrotational: in fact, the condition

$$\vec{\nabla} \times \vec{V} = 0 \quad (\text{B.11})$$

is verified at each point of the flow field except at the origin.

To evaluate the constant C , take the circulation around a given circular streamline of radius r :

$$\Gamma = - \oint \vec{V} \cdot d\vec{s} = - V_\theta (2\pi r) \quad (\text{B.12})$$

From that, the two components of the velocity, expressed in (B.9) are:

$$V_\theta = \frac{C}{r} = - \frac{\Gamma}{2\pi r} \Rightarrow C = - \frac{\Gamma}{2\pi} \quad (\text{B.13})$$

Therefore, for a vortex flow, the equation (B.13) demonstrates that the circulation is constant and its value is called the *strength*.

To explain better the point 2, it is better to remember the relation between the circulation and the vorticity (equation (B.3)). Considering that the value of the circulation is constant whatever is the circular streamline, to understand what happens near the origin, it is better to look at the behaviour of the integral of circulation for $r \rightarrow 0$

$$\Gamma = - \oint \vec{V} \cdot d\vec{s} = - \iint_S (\vec{\nabla} \times \vec{V}) \cdot d\vec{S} \rightarrow |(\vec{\nabla} \times \vec{V})| ds \quad (\text{B.14})$$

Combining the equation (B.13) and (B.14), it is obtained:

$$r \rightarrow 0 \quad 2\pi C = |\vec{\nabla} \times \vec{V}| dS \rightarrow |\vec{\nabla} \times \vec{V}| = \frac{2\pi C}{dS}$$

However, the vorticity will be:

$$r \rightarrow 0 \Leftrightarrow dS \rightarrow 0 \quad |\vec{\nabla} \times \vec{V}| \rightarrow \infty$$

Concluding: the vortex flow is irrotational everywhere except at the point $r=0$, where the vorticity is infinite. Therefore, the origin, $r=0$, is a singular point in the flow field.

B.2.2 Infinite vortex filament flow field

In order to expand the concept of a point vortex consider a *straight vortex filament* of strength G . The flow induced in any plane perpendicular to the straight vortex filament by the filament itself is identical to that induced by a point vortex of the same strength. Indeed, the point vortex is simply a segment of a vortex filament and then the flow field generated by a vortex line in a perpendicular plane to this line is the same as that generated by a point vortex.

B.3.3 Biot - Savart Law

In general, a vortex filament can be curved. The filament induces a flow field in the surrounding space. If the circulation is taken about any path enclosing the filament, a constant value, G , is obtained. Hence, the strength of the vortex filament is defined as G . Consider a direct segment of the filament dl . The radius vector from dl to an arbitrary point P in space is r . The segment dl induces a velocity at P equal to:

$$d\vec{V} = \frac{\Gamma}{4\pi} \frac{dl \times \vec{r}}{|\vec{r}|^3} \quad (B.17)$$

Equation (B.17) is called the Biot-Savart law and is one of the most fundamental relations in the theory of inviscid, incompressible flow. In fact, the Biot-Savart law and the

vortex flow are simply aerodynamic tools. They are a solution of the governing equations for inviscid, incompressible flow.

B.3.4 Applications of the Biot-Savart law.

The velocity induced at point P by the directed segment of the vortex filament, dl , is given by eq. (B.17). Hence, the velocity induced at P by the entire vortex filament is

$$\vec{V} = \int_{-\infty}^{+\infty} \frac{\Gamma}{4\pi} \frac{dl \times \vec{r}}{|\vec{r}|^3} \quad (B.17)$$

From the definition of the cross product, the direction of V is orthogonal to the plane containing the vectors dl and r . The magnitude of the velocity is given by:

$$V = |V| \Rightarrow V = \frac{\Gamma}{4\pi} \int_{-\infty}^{+\infty} \frac{\sin \theta}{r^2} dl \quad (B.18)$$

Let h be the perpendicular distance from point P to the vortex filament.

By geometric consideration, the velocity (B.18) will be

$$V = \frac{\Gamma}{2\pi h} \quad (B.19)$$

The expression (B.19) is the *velocity induced at point P by an infinite, straight vortex filament at a perpendicular distance h from P*. It coincides with the velocity given by a point vortex in two-dimensional flow.

Consider a semi-infinite vortex filament: which extends from the point A to infinity. The point A can be considered a boundary of the flow. Let P be a point in the plane through A perpendicular to the filament. Then, by integrating formula B.18, the *velocity induced at point P by a semi-infinite straight vortex filament* is:

$$V = \frac{\Gamma}{4\pi h} \quad (B.20)$$

Appendix C

Structural Analysis

This appendix describes in detail some of the aspects related to the structural analysis, which chapter 6 avoided. The order of the presentation follows the basic steps for the derivation of the governing finite element equations described in section 6.2, in particular at points (i), (ii) and (iii), page 106.

C.1 Constitutive relations for the finite element adopted

Henceforth, analytical explanations amplify the formulation illustrated in section 6.2.1 related to the membrane element chosen.

With reference to the shape functions, formulated in 6.1, consider the displacement of an internal point in a membrane element, e.g. the r^{th} element plotted in figure 6.3, to be linear. Thus, the components of the displacement of a generic point $P(x,z)$ are linear functions:

$$\begin{cases} u(x, z) = \alpha_1 + \alpha_2 x + \alpha_3 z \\ v(x, z) = \alpha_4 + \alpha_5 x + \alpha_6 z \\ w(x, z) = \alpha_7 + \alpha_8 x + \alpha_9 z \end{cases} \quad (\text{C.1})$$

where $\alpha_i \quad \forall i = 1 \dots 9$ are unspecified coefficients.

In order to express the α_i coefficients in term of the 9 nodal displacement components:

$$U = [u_i, v_i, w_i, u_j, v_j, w_j, u_l, v_l, w_l] \quad (\text{C.2})$$

the displacements (C.1) are evaluated at the three element nodes. For instance, at node i :

$$\begin{cases} u_i = u(x_i, z_i) = \alpha_1 + \alpha_2 x_i + \alpha_3 z_i \\ v_i = v(x_i, z_i) = \alpha_4 + \alpha_5 x_i + \alpha_6 z_i \\ w_i = w(x_i, z_i) = \alpha_7 + \alpha_8 x_i + \alpha_9 z_i \end{cases} \quad (\text{C.3})$$

Likewise the equation system (C.3), if the expression (C.1) is written at node j and l , a system of 9 equations in 9 unknown coefficients α_i is obtained. Because the values of the nodal co-

ordinates (x_i, z_i) (x_j, z_j) (x_l, z_l) are known, it is possible to solve for α_i and the (C.1) become:

$$\begin{cases} u(x, z) = (a_1 + b_1 x + c_1 z)u_i + (a_2 + b_2 x + c_2 z)u_j + (a_3 + b_3 x + c_3 z)u_l \\ v(x, z) = (a_1 + b_1 x + c_1 z)v_i + (a_2 + b_2 x + c_2 z)v_j + (a_3 + b_3 x + c_3 z)v_l \\ w(x, z) = (a_1 + b_1 x + c_1 z)w_i + (a_2 + b_2 x + c_2 z)w_j + (a_3 + b_3 x + c_3 z)w_l \end{cases} \quad (C.4)$$

where:

$$\begin{aligned} a_1 &= (x_j z_l - x_l z_j)/2\Delta & b_1 &= (z_j - y_l)/2\Delta & c_1 &= (x_i - x_l)/2\Delta \\ a_2 &= (x_l z_i - x_i z_l)/2\Delta & b_2 &= (z_l - z_i)/2\Delta & c_2 &= (x_l - x_i)/2\Delta \\ a_3 &= (x_i z_j - x_j z_i)/2\Delta & b_3 &= (z_i - z_j)/2\Delta & c_3 &= (x_i - x_j)/2\Delta \end{aligned} \quad (C.5)$$

with

$$2\Delta = \det \begin{vmatrix} 1 & x_1 & z_i \\ 1 & x_j & z_j \\ 1 & x_l & z_l \end{vmatrix} = 2(\text{area of triangle}) \quad (C.6)$$

Then, if the element nodal co-ordinates and their displacements in the element coordinate system are known, the displacement components of a generic point P(x, z) internal to this element will be known. For this reason, the equations are called "element shape functions"(C.4). For clarity, the system (C.4) coincides with the system (6.1), where the coefficients $\alpha_{1,2,3}$ are the expressions in brackets in (C.4).

With regard to the relation between displacement and deformation, expressed by formula (6.3), they are not linear due to the fact that displacements and rotations of the fibres are large. In the view of the fact that the membrane element is incapable of sustaining flexural stresses, the stress components, at each point, are tangent to the curved surface of the membrane to equilibrate normal loads. Significant displacements and rotations of the surface accompany load changes, then stresses and the local curvature change to maintain equilibrium and those changes.

The non-linear displacement-strain relations are, for a typical element in the element coordinate system:

$$\left\{ \begin{array}{l} \varepsilon_x = \frac{\partial u}{\partial x} + \frac{1}{2} \left[\left(\frac{\partial u}{\partial x} \right)^2 + \left(\frac{\partial v}{\partial x} \right)^2 + \left(\frac{\partial w}{\partial x} \right)^2 \right] \\ \varepsilon_z = \frac{\partial w}{\partial z} + \frac{1}{2} \left[\left(\frac{\partial u}{\partial z} \right)^2 + \left(\frac{\partial v}{\partial z} \right)^2 + \left(\frac{\partial w}{\partial z} \right)^2 \right] \\ \gamma_{xz} = \frac{\partial u}{\partial z} + \frac{\partial w}{\partial x} + \frac{1}{2} \left[\left(\frac{\partial u}{\partial x} \frac{\partial u}{\partial z} \right) + \left(\frac{\partial v}{\partial x} \frac{\partial v}{\partial z} \right) + \left(\frac{\partial w}{\partial x} \frac{\partial w}{\partial z} \right) \right] \end{array} \right. \quad (C.7)$$

where the derivatives of element shape functions, will be obtained from the original function. For example, for the first strain component, the first derivative will be:

$$\frac{\partial u}{\partial x} = b_1 u_1 + b_2 u_2 + b_3 u_3 \quad \text{and so on.}$$

Then, the complete expression for the same strain component will be:

$$\varepsilon_x = b_1 u_1 + b_2 u_2 + b_3 u_3 + \frac{1}{2} \left[(b_1 u_1 + b_2 u_2 + b_3 u_3)^2 + (b_1 v_1 + b_2 v_2 + b_3 v_3)^2 + (b_1 w_1 + b_2 w_2 + b_3 w_3)^2 \right]$$

and so on for the other components. In matrix form:

$$\left\{ \begin{array}{l} \varepsilon_x \\ \varepsilon_z \\ \gamma_{xz} \end{array} \right\} = \left[\begin{array}{ccccccc} b_1 & 0 & 0 & b_2 & 0 & 0 & b_3 \\ 0 & c_1 & 0 & 0 & c_2 & 0 & 0 \\ c_1 & b_1 & 0 & c_2 & b_2 & 0 & c_3 \end{array} \right] \left\{ \begin{array}{l} u_i \\ v_i \\ w_i \\ u_j \\ v_j \\ w_j \\ u_l \\ v_l \\ w_l \end{array} \right\} + \frac{1}{2} \left[\begin{array}{ccccccc} \frac{\partial u}{\partial x} & \frac{\partial v}{\partial x} & \frac{\partial w}{\partial x} & 0 & 0 & 0 \\ 0 & 0 & 0 & \frac{\partial u}{\partial z} & \frac{\partial v}{\partial z} & \frac{\partial w}{\partial z} \\ \frac{\partial u}{\partial z} & \frac{\partial v}{\partial z} & \frac{\partial w}{\partial z} & \frac{\partial u}{\partial x} & \frac{\partial v}{\partial x} & \frac{\partial w}{\partial x} \end{array} \right] \left\{ \begin{array}{l} \frac{\partial u}{\partial x} \\ \frac{\partial v}{\partial x} \\ \frac{\partial w}{\partial x} \\ \frac{\partial u}{\partial z} \\ \frac{\partial v}{\partial z} \\ \frac{\partial w}{\partial z} \\ \frac{\partial u}{\partial x} \\ \frac{\partial v}{\partial x} \\ \frac{\partial w}{\partial x} \end{array} \right\} \quad (C.8)$$

or either in symbolic form the (C.8) is written as:

$$\boldsymbol{\varepsilon} = \boldsymbol{B} \boldsymbol{u} + \frac{1}{2} \boldsymbol{A} \boldsymbol{\theta} \quad (C.9)$$

where:

$$A = \begin{bmatrix} \frac{\partial u}{\partial x} & \frac{\partial v}{\partial x} & \frac{\partial w}{\partial x} & 0 & 0 & 0 \\ 0 & 0 & 0 & \frac{\partial u}{\partial z} & \frac{\partial v}{\partial z} & \frac{\partial w}{\partial z} \\ \frac{\partial u}{\partial z} & \frac{\partial v}{\partial z} & \frac{\partial w}{\partial z} & \frac{\partial u}{\partial x} & \frac{\partial v}{\partial x} & \frac{\partial w}{\partial x} \end{bmatrix}$$

$$\vartheta = \begin{Bmatrix} \frac{\partial u}{\partial x} \\ \frac{\partial v}{\partial x} \\ \frac{\partial w}{\partial x} \\ \frac{\partial u}{\partial z} \\ \frac{\partial v}{\partial z} \\ \frac{\partial w}{\partial z} \end{Bmatrix} = \begin{bmatrix} b_1 & 0 & 0 & b_2 & 0 & 0 & b_3 & 0 & 0 \\ 0 & b_1 & 0 & 0 & b_2 & 0 & 0 & b_3 & 0 \\ 0 & 0 & b_1 & 0 & 0 & b_2 & 0 & 0 & b_3 \\ c_1 & 0 & 0 & c_2 & 0 & 0 & c_3 & 0 & 0 \\ 0 & c_1 & 0 & 0 & c_2 & 0 & 0 & c_3 & 0 \\ 0 & 0 & c_1 & 0 & 0 & c_2 & 0 & 0 & c_3 \end{bmatrix} \begin{Bmatrix} u_i \\ v_i \\ w_i \\ u_j \\ v_j \\ w_j \\ u_l \\ v_l \\ w_l \end{Bmatrix}$$

or in symbolic form $\vartheta = Gu$

Substituting these definitions into the symbolic expressions for the strain (C.11), the resulting expression is:

$$\varepsilon = \left(B + \frac{1}{2} AG \right) u \quad (\text{C.10})$$

As discussed in section 6.1.1, sailcloth properties enable considering the description of the constitutive relations between stress and strain as ‘linear elastic plane stress’ (formula (6.4)). Then, considering formula (6.4), here reported for easiness:

$$\sigma = D\varepsilon + \sigma_0 \quad (6.4)$$

where: σ_0 is the initial stress vector;

D is the elastic matrix defined as:

$$D = \frac{E}{1-\nu^2} \begin{bmatrix} 1 & \nu & 0 \\ \nu & 1 & 0 \\ 0 & 0 & \frac{1-\nu^2}{2} \end{bmatrix}$$

and E is the Young's modulus and ν the Poisson's ratio.

C.2 Governing F.E. equations through the Principle of virtual work

The basic problem in a general non-linear structural analysis is to find the state of the equilibrium of a body corresponding to the applied loads, [53], [57], [66].

The equilibrium condition of a system of finite elements representing the body under applied load can be expressed as:

$${}^t R + {}^t F = 0 \quad (\text{C.11})$$

where the vector ${}^t R$ lists the externally applied nodal point forces in the configuration at the same time t , and the vector ${}^t F$ lists the nodal point forces that corresponds to the element stresses in the equilibrium configuration. The equation (C.11) must express the equilibrium of the system in the current deformed geometry taking due account of all non-linearity. This equilibrium equation must be satisfied throughout the complete history of a load application. Because the strain-displacement relations are non-linear, the relation cannot be solved directly; however, an approximate solution can be obtained by referring all variables to a previously calculated known equilibrium configuration and linearising the resulting equations. This solution can be improved by iteration.

To develop the governing equations for the approximate solutions obtained by linearisation, we recall that the solutions for times $0, \Delta t, 2\Delta t, \dots, t$ have already been calculated and that we can refer the stresses and the strains to one of these known equilibrium configurations.

Hence, in principle, any one of the already calculated equilibrium configurations could be used. In practice, however, the choice lies essentially between two formulations, which have been termed Total Lagrangian formulation (T.L.) and Updated Lagrangian formulation (U.L.).

Both the above formulations include all non-linear kinematic effects. The main difference is the reference configuration. In the former all variables are referred to the initial configurations at the time $t=0$, while in the latter to the configuration at the time t . Since the difference is in the reference configuration, indeed the numerical solution will give the same result. In the present formulation, the Total Lagrangian Formulation is used as it is assumed that the sail shape and the trimmed configuration at the time $t=0$, which corresponds to the loaded configuration.

The structural problem defined by the formula (C.11), can be expressed by the principle of the virtual work, as follow:

$$\exists U : F_{\text{int}}(U) = F_{\text{ext}} \quad (\text{C.12})$$

or, in words, find the displacement node vector U , corresponding to an equilibrium and compatible system configuration, such that the calculated internal forces at each node, which balance the internal stresses, are equal to the external forces (or applied forces).

C.2.1 Principle of the virtual work

The principle of virtual work relates to two distinct and separate systems in which the first is a set of forces in equilibrium (P and σ as the external forces and internal stresses, respectively), and the second is a set of geometrically compatible deformations (U and ε as the displacements and strains, respectively).

The principle of virtual work states that for any system in equilibrium, the external virtual work must be equal to the internal virtual work. In practice, one of the systems always relates to a real or actual structure, in which some sort of solution is required, while the other is an imaginary or virtual system. Therefore, it is possible to have the option of establishing:

- *theorem of virtual forces* in which a real system of displacements and strains is coupled to a virtual system of forces and stresses
- *theorem of virtual displacements* in which a real system of forces and stresses is coupled to a virtual system of displacements and strains.

The object of this part is to write the equations of equilibrium for a single element in the local coordinate system via '*principle of the virtual work*', as in formula (6.5) and (6.6). Thus, recalling the Lagrangian approach of the finite virtual displacement theory and assuming that an infinitesimal virtual displacement δu is executed from an equilibrium configuration of the sail and a virtual strain $\delta \varepsilon$ results from the displacement, the equation (C.12) for such an element becomes:

$$\int_{V_e} \delta \varepsilon^T \sigma dV = \int_{V_e} \delta u^T F_V dV + \int_{S_e} \delta u^T F_S dS \quad (\text{C.13})$$

where V_e is the element volume and S_e the element surface. The term on the left side represents the virtual work due to the internal force. The term on the right side represents the virtual work due to the external loads: F_V is the body force vector, while F_S is the nodal force vector acting

on the element surface. Considering both the external nodal force vectors known, it is possible to re-write the principle (C.12) as follow:

$$\int_{V_e} \delta \varepsilon^T \sigma dV - \delta u^T p = 0 \quad (C.14)$$

Considering the r^{th} element, the (C.14) coincides with the formula (6.5), when $V_e = V_r^{\text{th}}$.

Using the strain symbolic expression (C.10), the strain increment is

$$\delta \varepsilon = [B + AG] \delta u \quad (C.15)$$

and substituting this expression into equation (C.14), the result is:

$$\int_{V_e} [(B + AG) \delta u]^T \sigma dV - \delta u^T p = 0 \quad (C.16)$$

and if the expression for stress (C.11) is substituted, the (C.16) becomes:

$$\int_{V_e} [(B + AG) \delta u]^T \left[D \left(B + \frac{1}{2} AG \right) + \sigma_0 \right] dV - \delta u^T p = 0 \quad (C.17)$$

This is the equation of element equilibrium, which coincide with the seen expression (6.6).

C.2.2 Assemblment of the F.E. equations and solutions.

The equations (C.17) must be transformed to the global coordinate system and finally assembled to obtain the "global equilibrium equations". These equations are non-linear and they will be solved iteratively by the Newton-Raphson method.

To this end, the governing equations for each element must be linearized. Thus, taken:

$$\varphi_i = \int_{V_e} (B + A^i G)^T \left[D \left(Bu^i + \frac{1}{2} A^i g^i \right) + \sigma_0 \right] dV - p \quad (C.18)$$

which is called the residual term after the i^{th} iteration. The next step is obtained from:

$$\varphi^{(i+1)} = \varphi^i + \frac{\partial \varphi^i}{\partial u} \Delta u^i = 0 \quad (C.19)$$

or

$$\frac{\partial \varphi^i}{\partial u} \Delta u^i = -\varphi^i \quad (\text{C.20})$$

From this equation the incremental displacements may be computed and the displacements after the $(i+1)^{\text{th}}$ iteration can be expressed as

$$u^{i+1} = u^i + \Delta u^i \quad (\text{C.21})$$

In equation (C.20), the derivative $\frac{\partial \varphi^i}{\partial u}$ is the element stiffness matrix and it consists of two parts, as follows:

$$\begin{aligned} K_m^i &= \frac{\partial \varphi_i}{\partial u} = \int_{V_e} (B + A^i G)^T \frac{\partial}{\partial u} \left[D \left(B u^i + \frac{1}{2} A^i g^i \right) \right] dV + \\ &\int_{V_e} \frac{\partial}{\partial u} \left[(B + A^i G^i)^T \right] \times \left[D(B u^i + A^i g^i) + \sigma_0 \right] dV = \\ &K_e^i + K_g^i \end{aligned} \quad (\text{C.22})$$

where K_e^i is the elastic stiffness matrix, defined as follows:

$$K_e^i = \frac{\partial \varphi_i}{\partial u} = \int_{V_e} (B + A^i G)^T [D(B + A^i G^i)] dV \quad (\text{C.23})$$

and K_g^i is the geometric stiffness matrix:

$$K_g^i = \int_{V_e} G^T \frac{\partial (A^i)}{\partial u} \sigma dV = \int_{V_e} G^T M^i G dV \quad (\text{C.24})$$

$$\text{where: } M^i = \begin{bmatrix} \sigma_x & 0 & 0 & \tau_{xy} & 0 & 0 \\ 0 & \sigma_x & 0 & 0 & \tau_{xy} & 0 \\ 0 & 0 & \sigma_x & 0 & 0 & \tau_{xy} \\ \tau_{xy} & 0 & 0 & \sigma_y & 0 & 0 \\ 0 & \tau_{xy} & 0 & 0 & \sigma_y & 0 \\ 0 & 0 & \tau_{xy} & 0 & 0 & \sigma_y \end{bmatrix}$$

Both element stiffness matrices could be computed only if the displacements u, v, w are known. To start the iterative solution, a compatible but not necessarily equilibrating displacement

field is needed. Once the element matrices are assembled in the global equations, new displacement fields will be computed. Using these displacements, new element matrices will be established and the process will be repeated until the computed global displacements agree with the displacements used to compute the element matrices. Then the displacements will be both compatible and equilibrating.

Summarising, the structural analysis problem, identified with formula (C.11), has been re-written by the principle of virtual work in formulae (C.19) and (C.20). It has seen how the stiffness matrix for each finite element is derived. Henceforth, it is shown the method of the solution.

In addition, a difficult task is the implementation of the software to compute the vectors:

$F_{\text{int}}(U)$, $F_{\text{ext}}(U)$, $\frac{dF_{\text{int}}}{dU}(U)$, particularly for the first iteration, because the stiffness matrix is singular if it is evaluated for the displacement vector $U^0 = 0$. For this reason the following structural analysis adopts a strategy of performing an initial linear analysis, to find an equilibrium and compatible configuration for the system, after which a non-linear solution is obtained using the displacement vector from the previous linear solution U^0 . In this way, for the first iteration the stiffness matrix will be not singular, because the vector $U^0 \neq 0$.

The non-linear system of equations (C.12) or in the formulation (C.9) is solved by the standard Newton-Raphson method. The iterate (U^i) is constructed by:

$$U^0 = 0;$$

$$\forall i \geq 1, \left[\frac{dF_{\text{int}}}{dU}(U^{i-1}) \right] \cdot \{U^i - U^{i-1}\} = -\{F_{\text{int}}(U^{i-1}) - F_{\text{ext}}\};$$

where $\frac{dF_{\text{int}}}{dU}(U^{i-1})$ is the stiffness operator of the finite element system when the displacement of the free nodes is U^{i-1} .

Another problem concerns the velocity of the convergence of the iteration method adopted, because large displacement components are obtained from the first iteration, due to the ill conditioned stiffness matrix.

To improve convergence the procedure outlined below is employed. For any small scalar ΔU_{\max} positive, the Newton-Raphson procedure will be modified in the following way:

$$U^0 = U^l;$$

$\forall i \geq 1$

$$\Delta U^i : \left[\frac{dF_{\text{int}}}{dU}(U^{i-1}) \right] \cdot \{\Delta U^i\} = -\{F_{\text{int}}(U^{i-1}) - F_{\text{ext}}\};$$

$$U^i = U^{i-1} + \min\left(\frac{\Delta U_{\max}}{\|\Delta U^i\|}, 1\right) \cdot \Delta U^i$$

In this way the difference between two consecutive evaluated displacement components cannot be greater than the limited ΔU_{\max} . Convergence will be got when

$$\frac{|F_{\text{int}}(U^i) - F_{\text{ext}}|}{\|F_{\text{ext}}\|} \text{ and } \frac{|U^i - U^{i-1}|}{|U_{\max}^{i-1}|}$$

are smaller than a predetermined value.

The final configuration for the system is dependent on the displacement vector U^i .

Appendix D

A Scottish sailmaker outlook

The interview was conducted by telephone on the 12th December 2000 by myself with John Highcock, who is the co-founder of Saturn Sails Limited, sited in Largs Yacht Haven, Largs, KA30 8EZ, Scotland.

John Highcock established Saturn Sails originally in Ayr, in 1979, with Colin McKenzie and another friend. The three co-founders, who were working in different medium-size English sailmaker factories, through market research, recognised that there were no sailmaker factories in Scotland and consequently the Scottish yachtsmen were used to buying sails in England, but were not satisfied as the customer service was expensive and poor. Therefore, despite the fact that the market comprised a small number of dissatisfied Scottish yachtsmen, they believed that starting a sailmaker factory was a good business opportunity.

The initial strategy planned to reach the sailors, their customers, by establishing themselves in the coastal town of Ayr and making contacts with the local sailing club.

In order to convince potential clients to buy one of their sails instead of a ‘popular brand’ sail, they proposed a full service to the customer from the personalised sail design, the choice of the material and the manufacture up to the moment of fitting onto the boat.

In order to always ensure a competitive product, from the start they paid attention to all the new sailmaking technologies, new materials and new trends, selecting and buying what was of worth for their business by using their experience. Customer satisfaction combined with the experience and knowledge in sailmaking has driven the story of Saturn Sails and has brought a gradual increment of customers throughout the years.

In 1979 there were no technologies available in sailmaking. Thus, the initial product was completely handcrafted and any single step was based on their experience and knowledge. They selected and used, prevalently, Dacrons and Nylon, refusing initially the new fibre Mylar.

Later, Colin and John decided to move to Largs. They contacted local sailing clubs and factories producing fibres. Nowadays, their main furnishes are Contender, Dimension and Bainbridge. When in 1982 the computer package CAD/CAM was on the market, John attended a course and studied a way to adapt this tool's features for designing sails. At the start of the 90s, they bought 'Relax' which allows structural analysis of the sail designed by CAD/CAM and afterwards, a technology for cutting sail panels using a laser.

Briefly, in his sailmaker factory, the available technology consists of a CAD/CAM system for designing sails and producing panel shapes to cut and a commercial package for structural analysis. The aerodynamic loads applied in their designing phases are evaluated by their experience, as there is not commercial package in the market, which is suitable for them and wind tunnel tests are very poor and expensive for them.

With this technology they produce a customised product, which results in a more expensive compared with a sail from a massive production as they buy sailcloth from suppliers. However, customers buy their sails, since they are attracted by the experience, a well-proven and reliable product and popularity. Their success is characterised by the constant attention paid to the new available technologies and analysis system in sailmaking and the result is a continuing increment of the number of customers and popularity. Therefore, John Highcock will buy an integrated design system, which goes through all the sail design phases, permitting the visualisation of the geometry and results. He believes that if the cost of this system is sustainable and it is not very difficult to use, this system will make an important step ahead in sail design techniques currently used in the majority of the sailmaker companies.

Glossary

America's Cup is the world's most prestigious sailboat race since the Victorian-era. The event began with the historic 1851 race around England's Isle of Wight, which was won by the New York Yacht Club's schooner America.

Boom is the pole or spar attached to the mast to which the foot (lower edge) of the sail is fastened.

Conditions generally refer to the weather conditions at a given time.

Crew is the group of people who assist the skipper in sailing a yacht. Strict rules determine the number of people in a race, for example an America's Cup crew is comprised of 16 people.

Cruiser-boat is designed with overnight accommodations.

Draft is the curve built joining the points of maximum curvatures of the five sail sections.

Dinghy is a small rowing boat, sometimes rigged with a sail and often raced. Also a tender, either rowed or equipped with power, used to go to and from a larger vessel.

Downwind is the way of sailing when the wind comes from the aft of the boat.

Genoa is a large foresail that overlaps the shroud base and used for sailing upwind and when reaching.

Helm is the area of a boat where operational controls are located. In the case of the Finn, the helm is the tiller. Thus, the helms-person is the person, who controls and hence steers the boat.

Helmsman is the crewmember who steers the yacht; usually also called skipper or driver.

Hiking is the name of this position. The helmsman must create an overturning moment exploiting his weight and his position. Therefore, the hiking posture consists in extending more or less all the body over the water, flexing the spine so that it is still possible to use the tiller and look around freely. In the event of severe wind condition, this is a very difficult manoeuvre for the sailor. Thus, there are rigid rules about the minimum sailor weight (which can be 90 Kg) and the technical equipment used for making hiking easier. Recently, it has been fixed by the rules that a boat shall use no device other than hiking straps to project a competitor's body outboard.

Hull is the actual body or shell of the boat that rests in the water

I.M.S: International Measurement System enables to evaluation of the performance of a sailing boat through powerful software. The main performance considered is the maximum speed achievable. The Massachusetts Institute of Technology (MIT) developed it with immediate fortune at the end of the 1970s.

ISAF: International Sailing Federation - ISAF Secretariat (Sailing International Ltd.) - Ariadne House, Town Quay, Southampton, Hampshire, SO14 2AQ, U.K. - Telephone: +44 23 80 635111; Fax: +44 23 80 635789 The main contact email is: sail@isaf.co.uk

Jib is the smaller version of a genoa that doesn't overlap the shroud base and is used for sailing upwind in heavy winds.

Keel is a fixed bottom-most portion or longitudinal centerline of a hull (see footnote 11), usually found on larger sailboats. Its surface is generally bigger than the rudder (see footnote 13), in order to generate the hydrodynamic force necessary to balance the aerodynamic force.

Knot is the velocity unit and corresponds to one nautical mile per hour.

Leech is the sail trailing edge.

Leeward means away from the wind, downwind, the side of a boat on which the mainsail lies. *Lee-side* is the side of an object that is sheltered from the wind. Thus, the side of the sail not in front of the wind is called leeward side (figure 1.4). It is the opposite of windward

Low weight allows sailing boats to go faster because they carry smaller loads. Then, in the event of light air it increases its stability. In fact, it is easier to maintain the stability, because the rolling moment as well as the pitching moment, generated by the presence of the weight, is lower.

Luff curve is the sail leading edge. In the case of a FINN class sail or a mainsail, the luff coincides with the sail edge attached to the mast. To optimise its design, in working conditions its shape is required to follow the mast bent configuration.

Mast is the spar that holds up the sails and supports the boom and sails.

Nautical Mile is the unit of geographical distance used on salt-water charts where: 1 nautical mile is 6076 feet or 1.15 statute miles. Therefore 1 statute mile = 0.87 nautical mile.

Racer-boat is designed primarily for speed and competition with a minimum of built-in creature comforts. There is also a class of boats named *racer/cruiser*, which are fast and designed with comfortable accommodation.

Reaching is the sailing course taken when the apparent wind angle is between 45 and 135 degrees.

Rig is a common term, which refers to the lines used for hoisting and controlling the sails directly or indirectly, such as through control of the mast, booms and spars in general. The lines are usually made from rope. Once the rope becomes operational in the boat, it is then referred to as a “line”. Most lines on small sailboats are made from synthetic twisted or braided rope, such as polyester or polypropylene. Nylon is usually not a good line because it stretches too much. Nowadays, ropes of natural materials such as hemp are rarely used. Wire rope is sometimes used for some rigs, but must be connected to rope at the moving ends that must be handled.

Rigging is the entirety of wires, lines, halyards and other items used to attach the sails and the spars to the boat. The lines that do not have to be adjusted often are known as standing rigging. The lines that are adjusted to raise, lower and trim the sails are known as running rigging.

Rudder is a movable blade-surface (underwater fin) hinged vertically below the hull (see footnote 11) near the stern that controls boat steering. A tiller or a wheel controls it. The *tiller* is a bar connected to the rudder and used to steer the boat. Usually keel, rudder and trim-tab are united in one piece (see footnote 12 an 14). However, in all set configurations, they are like symmetric wings.

Running Rigging is the entirety of moving rods and lines that support and control the mast and sails.

Sailing course is the direction in which a boat is steered (see figure 1.7).

Spar is a basic term for a mast, boom or yard.

Stretch is a structural property of sailcloth. It depends upon the material and construction methods. These above characteristics determine different value for the stretch even between two sails, constructed with the same material. In fact, stretch can assume different values for the same direction, when a different way is used to seam together the panels. Furthermore, loads application time influences stretch value. Some materials, when initially loaded, respond with a little stretch, which increases, showing great elongation if the loads are maintained for long. Once loads are removed, some material will recover or return to their original dimensions. *Recovery* is the name of this property. Some cloth will never recover its initial dimensions, and in this case the material shows a *creep*. Many factors determinate the value of the stretch: some are geometrical and some are due to the fibres’ elongation. However, a low value for the stretch is required, because sailing the sailcloth experience large displacements and variable loads.

*Telltale*s are streamers attached to the sail to indicate wind flow.

Trim tab is a hydraulically adjusted horizontal plate located on the bottom, usually on the back of the rudder, that controls the trim angle of a boat at speed.

Velocity Made Good (vmg) is the velocity of a yacht relative to its progress directly towards or away from the wind.

Windward means towards the wind, upwind, the side of a boat toward the wind. *Windward* is the direction from which the wind is coming. Thus, the side of the sail facing the wind is called windward side (figure 4.1).

Sources:

www.americascup.org

www.ukhamble.com

www.hoofers.org

References

- [1] Anderson J.D. jr., (1991) ‘Fundamentals of Aerodynamics’, 2nd ed., McGraw-Hill International Edition
- [2] Bisplinghoff R.L., Ashley H. & Halfman R.L., (1996) ‘Aeroelasticity’, DOVER PUBLICATION, MINEOLA, New York.
- [3] Byoung K.C., Ha-Yong S. & Woo S.Y., (1993) ‘Visually smooth composite surfaces for an unevenly spaced 3D data array’, Computer Aided Geometric Design, Vol. 10,
- [4] Bojsen-Møller F. & Bojsen-Møller J., (1999) ‘ Biomechanics of sailing’, Sailing and Science – in an Interdisciplinary Perspective, Editor Gisela Sjøgaard, Institute of Exercise and Sport Sciences, University of Copenhagen, 77-93
- [5] Boote D., (1990) ‘Some considerations about the structural design of sailing masts’, Proceeding of ATMA Congress, 451-483
- [6] Bosset N. & Mutnick I., (1997) ‘An Investigation of full scale force produced by a sail, The 13th Chesapeake Sailing Yacht Symposium, 37-47
- [7] Campbell I., (1998) ‘The performance of offwind sails obtained from wind tunnel tests’, Proceedings of RINA International Conference on Modern Yacht, 1-14
- [8] Caponetto M. & Boote D., (1991) ‘A numerical approach to the design of sailing yacht masts’, The 10th Chesapeake Sailing Yacht Symposium, 59-81
- [9] Caponetto M., Castelli A., Dupont P., Bonjour B., Mathey P.-L., Sanchi S. & Sawaley M.L., (1999) ‘Sailing yacht design using advanced numerical flow techniques’, The 14th Chesapeake Sailing Yacht Symposium, 97-104
- [10] Charvet T. & Huberson S., (1992) ‘Numerical calculation of the flow around sails’, European Journal of Mechanics, B/Fluids, Vol. 11, N° 5, 599-610
- [11] Cyr S. & Newman B.G., (1996) ‘Flow past two-dimensional membrane airfoils with rear separation’, Journal of Wind Engineering and Industrial Aerodynamics, Vol. 63, 1-16
- [12] Claughton A., (1999) ‘Developments in the IMS VPP formulation’, The 14th Chesapeake Sailing Yacht Symposium, 1-21
- [13] Clemmer G., (1985), ‘The calculation of sail panels using developed surfaces’, The 7th Chesapeake Sailing Yacht Symposium, 51-58

- [14] Couser P., (1998) 'Computational methods for investigating sail forces –A case study' presented at Yacht Vision 1998, New Zealand.
- [15] Couser P. and Deane N., (1999) 'Use of CFD techniques in the preliminary design of upwind sails', The 14th Chesapeake Sailing Yacht Symposium, 143-155
- [16] Dal Monte A., Gallozzi C. & Dalla Vedova D., (1999) 'Boat construction – drag and aerodynamics, Sailing and Science – in an Interdisciplinary Perspective, Editor Gisela Sjøgaard, Institute of Exercise and Sport Sciences, University of Copenhagen, 35-51
- [17] Day S., (1991) 'The optimisation of aerodynamic lift distribution for a heeled yacht in a wind gradient', Royal Institution of Naval Architects Meeting, 91-100
- [18] Day S., (1995) 'The Design of Yacht Sailplans for Maximal Upwind Speed' The 12th Chesapeake Sailing Yacht Symposium, 97-116
- [19] Day S., (1996) 'Sail optimisation for maximal speed', Journal of Wind Engineering and Industrial Aerodynamic, 63, 131-154
- [20] Doyle B.P. & Mahr P.F., (1995) 'Yacht sails – Flexible fiber composite membrane' Proceedings of the 40th International SAMPE Symposium, 232-241
- [21] Haarstick S., (1977) 'Principles of Sail Design', SNAME Transaction, 73-95
- [22] Heinemann K., (1999) 'Socio-economic factors in the development of sailing sport technology', Sailing and Science – in an Interdisciplinary Perspective, Editor Gisela Sjøgaard, Institute of Exercise and Sport Sciences, University of Copenhagen, 53-75
- [23] Holla V.S., Rao K.P., Asthana C.B. & Arokiaswamy A., (1994) 'Aerodynamic characteristics of pretensioned elastic membrane rectangular sailwings', Computer Methods in Applied Mechanics and Engineering, vol 44, 1-16
- [24] Euerle S.E. & Greeley D.S., (1993) 'Towards a rational upwind sail force model for VPPs', The 11th Chesapeake Sailing Yacht Symposium, 75-86
- [25] Fallow B., (1996) 'America's Cup Sail Design', Journal of Wind Engineering and Industrial Aerodynamics, Vol. 63, 183-192
- [26] Faux I.D. and Pratt M.J., (1978) 'Computational Geometry for Design and Manufacture', Ellis Horwood Limited Publishing,
- [27] Fukasawa T. & Katori M., (1993) 'Numerical approach to the aeroelastic responses of three-dimensional flexible sails', The 11th Chesapeake Sailing Yacht Symposium, 87-105
- [28] Fujino M., Fukasawa T., Kagemoto H. & Katori M., (1992) 'Aerodynamic Characteristics of Elastically Deformed 3-Dimensional Membrane Sail', J.S.N.A. Japan, Vol. 172, 49-58

- [29] Garret R. (1996), 'The symmetry of Sailing', Sheridan House, NY.
- [30] Greeley D.S., Kirkman K.L., Drew A.L., Cross-Whiter J., (1989) 'Scientific sail shape design', the 9th Chesapeake Sailing Yacht Symposium, 33-80
- [31] Jackson P. S., (1982) 'A 3-D aeroelastic sail model', Proceeding of Science of Sail Design, 55-66
- [32] Jackson P. S., (1985) 'The analysis of the three-dimensional sails', Proceeding of the 10th Canadian Congress of Applied Mechanics, 59-67
- [33] Jackson P. S. & Christie G.W., (1987) 'Numerical analysis of three-dimensional elastic membrane wings', AIAA Journal, Vol. 25, N° 5, 676-682
- [34] Larsson L., (1990) 'Scientific methods in yacht design', Annual Review of Fluid Mechanics, Vol. 22, 349- 385
- [35] Linskey T., (1996) 'Design cruising rig', Sail, Unite Marine publishing, Boston, Vol. 27, N° 2, 49-53
- [36] Lombardi G. & Tonelli A., (1994) 'Experimental pressure evaluation near a sail leading edge under real conditions', Aeronautical Journal, 319-322
- [37] Malpede S.M. & Vezza M., (2000) 'Developments of an interactive sail design method', Acta Polytechnica, Journal of Advanced Engineering Design, Vol. 40, N°1/2000, 66-74
- [38] Malpede S.M., Vezza M. & Coiro D.P., (2000), 'Loads distribution along sail-mast', The Engineering of Sport, edited by Subic A.J. & Haake S.J., Blackwell Science, 441-449
- [39] Masuyama Y & Fukasawa T., (1997) 'Full scale measurement of sail force and the validation of Numerical Calculation method', The 13th Chesapeake Sailing Yacht Symposium, 23-36
- [40] Marchaj C.A., (1964) 'Sailing theory and practice', Dodd, Mead & Co., N.Y.
- [41] Marchaj C.A. (1993) AERO-HIDRODYNAMICS OF SAILING, 2nd edn., Adlard Coles Nautical, London
- [42] McCormick B.W., 'Aerodynamics, Aeronautics, and Flight Mechanics', John Wiley & Sons, 1979
- [43] Milgram J.H., (1968) 'The analytical design of yacht sails', Annual Meeting of the Society of Naval Architects and Marine Engineers, Vol. 76, 118-160
- [44] Milgram J.H., (1978) 'Effects of Masts on the aerodynamics of Sail Sections', Marine Technology, Vol. 15, N° 1, 35-42

- [45] Milgram J.H., (1993) 'Naval Architecture Technology Used in Winning The 1992 America's Cup Match', SNAME Transactions, Vol.101, 399-436
- [46] Milgram J.H., (1998) 'Fluid mechanics for sailing vessel design', Annual Review Fluid Mechanics, Vol. 30, 613-653
- [47] Moore G., (1997) 'Mastering the mainsail', Sail, Vol. 28, No 8, 20-23
- [48] Muttin F., (1991) 'Structural analysis of sails', European Journal of Mechanics, A/Solids, Vol. 10, N° 5, 517-534.
- [49] van Oossanen P., (1993) 'Predicting the Speed of Sailing yacht', SNAME Transaction, Vol. 11, 337-397
- [50] Pallis J.M., Banks D.W. & Okamoto K., (2000) '3D computational fluid dynamics in competitive sail, yacht and windsurf design', The Engineering of Sport, edited by Subic A.J. & Haake S.J., Blackwell Science, 361-365
- [51] Ranzenbach R.C., Andersson P. & Flynn D., (1999) 'A 1997-1998 Whitbread Sail Program – Lesson learned', The 14th Chesapeake Sailing Yacht Symposium, 87-96
- [52] Ranzenbach R.C., Mairs C., (1999) 'Wind tunnel testing of offwind sails', The 14th Chesapeake Sailing Yacht Symposium, 171-179
- [53] Rao S.S., 'The finite element method in engineering', 2nd Ed., Pergamon Press, Oxford.
- [54] Schoop H. & Hänsel M., (1997) 'Structural and Aerodynamic Calculation of Sails as Flexible Membranes', Ship Technology Research, Vol. 44, 88-97
- [55] Selness J. N. (1980) 'The finite element method (FEM) of structural analysis applied to mast rigs', Proceedings of the 10th AIAA Symposium, Oxwarn California, 44-53
- [56] Spurway N. (1999) 'Sailing Physiology', Sailing and Science – in an Interdisciplinary Perspective, Editor Gisela Sjøgaard, Institute of Exercise and Sport Sciences, University of Copenhagen, 95-117
- [57] Stasa F.L., 'Applied finite element analysis for engineers', HRW, N.Y., 1985
- [58] Sugimoto T., (1992) 'A first course in optimum design of yacht sails', Proceeding of the 11th Australasian Fluid Mechanics Conference, 1209-1212
- [59] Tabarrok B. & Qin Z., (1992) 'Non linear analysis of tension structures', Computers & Structures, Vol. 45, No 5/6, 973-984
- [60] Thrasher D.F., Mook D.T. & Nayfeh A.H., (1979) 'A computer-based method for analysing the flow over sails', Proc. SNAME at the 4th Chesapeake Sailing Yacht Symposium, 119-127#

- [61] Tunstall-Behrens H., (1959) 'Instructions in sailing', The Brompton Library, Museum Press Limited, London
- [62] Whidden T. & Levitt M., (1990) 'The art and science of sails', published by Adlard Coles, London
- [63] Whidden T., (1997), 'Considering Curves', Yachting, 32
- [64] Wilkinson S., (1989), 'Static pressure distributions over 2D mast/sail geometries', Marine Technology, Vol. 26, N° 4, 333-337
- [65] Wood C.J. & Tan S.H., (1978) 'Towards an optimum yacht sail', Journal of Fluid-Mechanics, Vol. 85, part 3, 459-477
- [66] Zienkiewicz O.C., (1971) 'The finite element method in Engineering science', McGraw Hill, London
- [67] Ansys53 Manuals
- [68] <http://www.doylesails.com/designinfo-process.htm>
- [69] <http://www.eclipse.co.uk>
- [70] <http://www.finnclass.org>
- [71] <http://www.48north/aug98/carbmast.htm>
- [72] <http://www.hood-sails.com/fr>
- [73] <http://www.northsails.co.uk/articles/fast/up-tech.htm>
- [74] <http://www.paw.com/sail/neilpride/manual>
- [75] <http://www.sailnet.com/>
- [76] <http://www.shoresails.com/performance>
- [77] <http://www.velanet.it/>
- [78] <http://www.wb-sails.fi/news/>
- [79] <http://uksailmakers.com>
- [80] Davidson K. S. M., (1936) 'Some experimental studies of the sailing yacht', Transaction of the Society of Naval Architects and Marine Engineers, Vol. 44.

